THÈSE EN COTUTELLE PRÉSENTÉE

POUR OBTENIR LE GRADE DE

DOCTEUR DE

L'UNIVERSITÉ DE BORDEAUX

ET DE L'UNIVERSITÉ DU PAYS BASQUE

Spécialité : électronique

Préparée à ESTIA RECHERCHE

ÉCOLE DOCTORALE Sciences Physique et de l'Ingénieur

ÉCOLE DOCTORALE de l'UPV/EHU

Par Samuel JUPIN

Advanced Control of Multilevel Power Converters for Weak Grid Applications

Sous la direction de Ionel VECHIU
et de Gerardo TAPIA OTAEGUI

Soutenue le 4 décembre 2020

Membres du jury :

M. SOLSONA, Jorge	Professeur, Universidad Nacional del Sur	Rapporteur
M. IOV, Florin	Professeur Associé, Aalborg Universitet	Rapporteur
M. XU, Lie	Professeur, University of Stralthclyde	Examinateur
M. ZUBIZARRETA, Asier	Maître de Conférence, UPV/EHU	Examinateur
M. BRIAT, Olivier	Maître de Conférence, Université de Bordeaux	Examinateur
M. BACHA, Seddik	Professeur, Université Grenoble Alpes	Examinateur

(cc)2020 SAMUEL JUPIN (cc by-nc-nd 4.0)

Titre : Contrôle avancé des convertisseurs de puissance multi-niveaux pour applications sur réseaux faibles.

Résumé :

Avec l'avènement progressif des micros-réseaux incorporant les sources d'énergie renouvelable, un nouveau paradigme apparait dans la distribution de l'électricité. Ces nouvelles architectures interfacent des consommateurs non contrôlés à des sources d'énergie intermittentes, plaçant d'importantes contraintes sur les étapes de conversion, stockage et gestion de l'énergie.

Les convertisseurs de puissance s'adaptent en conséquence avec en particulier le développement des convertisseurs multi-niveaux, qui supportent à composants égaux des puissances plus importantes que leurs prédécesseurs et assurent une meilleure qualité de l'énergie, mais dont le contrôle gagne en complexité.

Du fait de leur nature hybride, le contrôle des convertisseurs de puissance est traditionnellement scindé en deux parties. D'un côté les objectifs continus liés à la fonction principale d'interfaçage des convertisseurs, de l'autre le pilotage des interrupteurs quantifiés qui le forment, la modulation.

Dans ce contexte, les exigences croissantes en rendement, fiabilité, polyvalence et performance imposent un gain conséquent d'intelligence de l'ensemble de l'architecture de contrôle. Pour répondre à ces exigences, nous proposons de traiter à la fois les objectifs liés à la fonction d'interface des convertisseurs et ceux rattachés à leur nature avec un unique contrôleur. Cette décision implique d'incorporer la non-linéarité des convertisseurs de puissance au contrôleur, ce qui revient à supprimer le bloc de modulation. La modulation est la solution habituelle pour linéariser le comportement interne des convertisseurs. Une approche de Contrôle à Modèle Prédictif (MPC) a été retenue pour traiter cette non-linéarité ainsi que la grande diversité d'objectifs de contrôle qui accompagne les convertisseurs de puissance.

L'algorithme développé combine la théorie des graphes, avec différents algorithmes comme ceux de Dijkstra et A* à un modèle d'état spécialisé pour les systèmes à commutation, formant ainsi un outil puissant et universel capable de manipuler simultanément la nature discrète des interrupteurs de puissance et celle continue de son environnement. L'étude du modèle d'état utilisé pour les convertisseurs de puissance comme systèmes commutants conduit à des résultats concernant la stabilité et la contrôlabilité de ces systèmes

Le contrôleur ainsi obtenu est ensuite éprouvé en simulation, face à des cas d'applications variés : onduleur isolé ou connecté à un réseau, redresseur et convertisseur bidirectionnel. La même structure de contrôle est confrontée à chacune de ces situations pour trois topologies multi-niveaux : Neutral Point-Clamped, Flying Capacitor et Cascaded H-Bridge. La capacité d'adaptation du contrôleur est regroupée dans deux étapes fondamentales : la prédiction, qui utilise le modèle du convertisseur, et la fonction de coût, qui traduit le cahier des charges en un problème d'optimisation résolu par l'algorithme. Changer de topologie implique de modifier le modèle, sans

impact sur la fonction de coût, tandis que modifier cette fonction suffit à s'adapter aux différentes applications.

Les résultats montrent que le contrôleur pilote directement les interrupteurs de puissance en fonction des objectifs. Les performances générales de cette structure unique sont comparables à celles des structures multiples utilisées pour chacun des cas étudiés, à l'exception notable du fonctionnement redresseur, où la rapidité et l'étendue des possibilités sont tout particulièrement intéressants.

En conclusion, le contrôleur développé est capable de traiter un grand nombre d'applications, topologies, objectifs et contraintes. Alors que les modifications du cahier des charges ou des conditions de fonctionnement impactent souvent profondément les structures traditionnelles de contrôle linéaire, ces altérations ne modifient pas l'architecture du contrôleur MPC développé. Cela illustre la polyvalence de la solution proposée ainsi que son universalité, démontrée davantage par la capacité à s'adapter à des convertisseurs de puissance différents et sans modifications. Finalement, la complexité de la modulation est pleinement incluse dans la structure, offrant un gain de simplicité et de flexibilité au design du contrôle.

Mots clés :

Electronique de puissance; réseau faible; MPC

Title: Advanced Control of Multilevel Power Converters for Weak Grid Applications

Abstract :

With the progressive rise of the micro-grids incorporating renewable energy sources, a new electricity distribution paradigm is emerging. These new architectures interface uncontrolled consumers with intermittent energy sources, therefore imposing more stress on the conversion, storage and management of the energy.

Power converters are adapting accordingly, in particular, with the development of multi-level converters, which allow higher power rates and better power quality than their predecessors with similar components, but whose control is becoming increasingly complex.

Due to their hybrid nature, the control of power converters is traditionally split into two parts: on the one side, the continuous objectives related to the main interfacing function of the power converters, and, on the other side, the driving of their quantized power switches, known as the modulation strategy.

In this context, the growing demands in efficiency, reliability, versatility and performance require a high level of intelligence of the complete control structure. To meet these requirements, the objectives of this research work are to address both the interfacing objectives and the inner driving of the converter into a single controller. This decision implies incorporating the non-linearity of power converters into the controller, equivalent to suppressing the traditional modulation block. Modulation is the traditional solution to linearize the inner operation of the converters. The Model Predictive Control (MPC) approach was chosen to handle the non-linearity and the diversity of control objectives that accompany power converters.

The developed control algorithm combines graph theory, with Dijkstra, A* and other algorithms, with a special state-space model designed for switching systems to form a powerful universal tool capable of simultaneously manipulating the discrete and continuous nature of the converter and its environment. Switched state-space models are studied, leading to interesting results on stability and controllability concerning their application on power converters.

The obtained controller is then tested in simulation, with various case studies: grid-connected and standalone inverter, rectifier and bidirectional operation. These situations are studied for three common multi-level topologies: Neutral Point-Clamped, Flying Capacitor and Cascaded H-Bridge. The exact same MPC structure is used for each and every one of the case studies, with adaptations of its internal behavior. This behavior is agglomerated in two functions: the prediction, containing the model of the converter, and the cost function, which translates the control requirements into the optimal problem solved by the algorithm. Changing the topology implies adjusting the model, without impacting the cost function, while modifying this function is sufficient to adapt to the different applications.

The results show that the controller manages to directly drive the power switches according to the application, demonstrating a large variety of considerations and objectives. The overall performance of this unique structure is comparable to that of the multiple structures used for each of the studied cases, with the notable exception of rectifier operation mode, where the speed and range of possibilities are particularly interesting.

In conclusion, the developed controller manages miscellaneous applications, topologies, objectives and constraints. While the traditional linear control structures

have to change, often deeply, for different operation modes and control requirements, such modifications do not affect the control architecture of the designed MPC controller. This shows the versatility of the proposed solution and its universality, further demonstrated by its ability to adapt to different power converters without modifications. Finally, the complexity of the modulation is fully included in the structure, offering simplicity and flexibility to the control design.

Keywords:

Power electronics; weak grid; MPC

ESTIA Recherche

201420655V

n°97, allée Théodore Monod, ESTIA 2, Technopole Izarbel
64210 BIDART

Abstract

With the progressive rise of the micro-grids incorporating renewable energy sources, a new electricity distribution paradigm is emerging. These new architectures interface uncontrolled consumers with intermittent energy sources, therefore imposing more stress on the conversion, storage and management of the energy.

Power converters are adapting accordingly, in particular, with the development of multi-level converters, which allow higher power rates and better power quality than their predecessors with similar components, but whose control is becoming increasingly complex.

Due to their hybrid nature, the control of power converters is traditionally split into two parts: on the one side, the continuous objectives related to the main interfacing function of the power converters, and, on the other side, the driving of their quantized power switches, known as the modulation strategy.

In this context, the growing demands in efficiency, reliability, versatility and performance require a high level of intelligence of the complete control structure. To meet these requirements, the objectives of this research work are to address both the interfacing objectives and the inner driving of the converter into a single controller. This decision implies incorporating the non-linearity of power converters into the controller, equivalent to suppressing the traditional modulation block. Modulation is the traditional solution to linearize the inner operation of the converters. The Model Predictive Control (MPC) approach was chosen to handle the non-linearity and the diversity of control objectives that accompany power converters.

The developed control algorithm combines graph theory, with Dijkstra, A* and other algorithms, with a special state-space model designed for switching systems to form a powerful universal tool capable of simultaneously manipulating the discrete and continuous nature of the converter and its environment. Switched state-space models are studied, leading to interesting results on stability and controllability concerning their application on power converters.

The obtained controller is then tested in simulation, with various case studies: grid-connected and standalone inverter, rectifier and bidirectional operation. These situations are studied for three common multi-level topologies: Neutral Point-Clamped, Flying Capacitor and Cascaded H-Bridge. The exact same MPC structure is used for each and every one of the case studies, with adaptations of its internal behavior. This behavior is agglomerated in two functions: the prediction, containing the model of the converter, and the cost function, which translates the control requirements into the optimal problem solved by the algorithm. Changing the topology implies adjusting the model, without impacting the cost function, while modifying this function is sufficient to adapt to the different applications.

The results show that the controller manages to directly drive the power switches according to the application, demonstrating a large variety of considerations and objectives. The overall performance of this unique structure is comparable to that of the multiple structures used for each of the studied cases, with the notable exception of rectifier operation mode, where the speed and range of possibilities are particularly interesting.

In conclusion, the developed controller manages miscellaneous applications, topologies, objectives and constraints. While the traditional linear control structures have to change, often deeply, for different operation modes and control requirements, such modifications do not affect the control architecture of the designed MPC controller. This shows the versatility of the proposed solution and

its universality, further demonstrated by its ability to adapt to different power converters without modifications. Finally, the complexity of the modulation is fully included in the structure, offering simplicity and flexibility to the control design.

Résumé

Avec l'avènement progressif des micros-réseaux incorporant les sources d'énergie renouvelable, un nouveau paradigme apparait dans la distribution de l'électricité. Ces nouvelles architectures interfacent des consommateurs non contrôlés à des sources d'énergie intermittentes, plaçant d'importantes contraintes sur les étapes de conversion, stockage et gestion de l'énergie.

Les convertisseurs de puissance s'adaptent en conséquence avec en particulier le développement des convertisseurs multi-niveaux, qui supportent à composants égaux des puissances plus importantes que leurs prédécesseurs et assurent une meilleure qualité de l'énergie, mais dont le contrôle gagne en complexité.

Du fait de leur nature hybride, le contrôle des convertisseurs de puissance est traditionnellement scindé en deux parties. D'un côté les objectifs continus liés à la fonction principale d'interfaçage des convertisseurs, de l'autre le pilotage des interrupteurs quantifiés qui le forment, la modulation.

Dans ce contexte, les exigences croissantes en rendement, fiabilité, polyvalence et performance imposent un gain conséquent d'intelligence de l'ensemble de l'architecture de contrôle. Pour répondre à ces exigences, nous proposons de traiter à la fois les objectifs liés à la fonction d'interface des convertisseurs et ceux rattachés à leur nature avec un unique contrôleur. Cette décision implique d'incorporer la non-linéarité des convertisseurs de puissance au contrôleur, ce qui revient à supprimer le bloc de modulation. La modulation est la solution habituelle pour linéariser le comportement interne des convertisseurs. Une approche de Contrôle à Modèle Prédictif (MPC) a été retenue pour traiter cette non-linéarité ainsi que la grande diversité d'objectifs de contrôle qui accompagne les convertisseurs de puissance.

L'algorithme développé combine la théorie des graphes, avec différents algorithmes comme ceux de Dijkstra et A* à un modèle d'état spécialisé pour les systèmes à commutation, formant ainsi un outil puissant et universel capable de manipuler simultanément la nature discrète des interrupteurs de puissance et celle continue de son environnement. L'étude du modèle d'état utilisé pour les convertisseurs de puissance comme systèmes commutants conduit à des résultats concernant la stabilité et la contrôlabilité de ces systèmes

Le contrôleur ainsi obtenu est ensuite éprouvé en simulation, face à des cas d'applications variés : onduleur isolé ou connecté à un réseau, redresseur et convertisseur bidirectionnel. La même structure de contrôle est confrontée à chacune de ces situations pour trois topologies multi-niveaux : Neutral Point-Clamped, Flying Capacitor et Cascaded H-Bridge. La capacité d'adaptation du contrôleur est regroupée dans deux étapes fondamentales : la prédiction, qui utilise le modèle du convertisseur, et la fonction de coût, qui traduit le cahier des charges en un problème d'optimisation résolu par l'algorithme. Changer de topologie implique de modifier le modèle, sans impact sur la fonction de coût, tandis que modifier cette fonction suffit à s'adapter aux différentes applications.

Les résultats montrent que le contrôleur pilote directement les interrupteurs de puissance en fonction des objectifs. Les performances générales de cette structure unique sont comparables à celles des structures multiples utilisées pour chacun des cas étudiés, à l'exception notable du fonctionnement redresseur, où la rapidité et l'étendue des possibilités sont tout particulièrement intéressants.

En conclusion, le contrôleur développé est capable de traiter un grand nombre d'applications, topologies, objectifs et contraintes. Alors que les modifications du cahier des charges ou des conditions de fonctionnement impactent souvent profondément les structures traditionnelles de contrôle linéaire, ces altérations ne modifient pas l'architecture du contrôleur MPC développé. Cela illustre la

polyvalence de la solution proposée ainsi que son universalité, démontrée davantage par la capacité à s'adapter à des convertisseurs de puissance différents et sans modifications. Finalement, la complexité de la modulation est pleinement incluse dans la structure, offrant un gain de simplicité et de flexibilité au design du contrôle.

Resumen

El advenimiento progresivo de las microrredes que incorporan fuentes de energía renovable está dando lugar a un nuevo paradigma de distribución de la electricidad. Este nuevo planteamiento sirve de interfaz entre consumidores no controlados y fuentes intermitentes, implicando desafíos adicionales en materia de conversión, almacenamiento y gestión de la energía.

Los convertidores de potencia se adaptan en consecuencia, en particular con el desarrollo de los convertidores multinivel, que integrando los mismos componentes que sus predecesores y un control más complejo, soportan potencias más altas y aseguran una mejor calidad de la energía.

Debido al carácter híbrido de los convertidores de potencia, su control se divide comúnmente en dos partes: por un lado, el control de los objetivos continuos vinculados a la función principal de los convertidores de servir de interfaz, y, por otro, el control discreto de los interruptores de potencia, conocido con el nombre de modulación.

En este contexto, las exigencias crecientes en términos de eficiencia, fiabilidad, versatilidad y rendimiento hacen necesaria una mejora de la inteligencia de la estructura de control. Para cumplir con estos requisitos, se propone tratar mediante un solo controlador ambas problemáticas, la vinculada a la función de interfaz de los convertidores y la relacionada con su naturaleza discreta. Esta decisión implica incorporar la no-linealidad de los convertidores de potencia en el controlador, lo que equivale a suprimir el bloque de modulación, que constituye la solución tradicional para linealizar el comportamiento interno de los convertidores. Se adopta un planteamiento de Control Predictivo basado en Modelos (MPC) para abordar la no-linealidad y la gran diversidad de objetivos de control que acompañan a los convertidores de potencia.

El algoritmo desarrollado combina teoría de grafos —con algoritmos de Dijkstra, A* y otros— con un modelo de estado especial para sistemas conmutados al objeto de proporcionar una herramienta potente y universal, capaz de manipular simultáneamente el carácter cuantificado de los interruptores de potencia y el continuo de las entidades interconectadas por el convertidor. Se han obtenido resultados sobre la estabilidad y la controlabilidad de los modelos de estado conmutados aplicados al caso particular de los convertidores de potencia.

El controlador así desarrollado y descrito se ha examinado en simulación frente a varios casos y aplicaciones: inversor aislado o conectado a la red, rectificador y convertidor bidireccional. Se ha empleado la misma estructura de control para tres topologías de convertidor multinivel: Neutral-Point Clamped, Flying Capacitor y Cascaded H-Bridge. Al objeto de adaptarse a los cambios citados, lo único que varía en el controlador es el modelo del convertidor adoptado para la predicción, así como la función de coste, que traduce los requisitos de control en un problema de optimización a solucionar por el algoritmo. Un cambio de topología resulta en una modificación del modelo interno, sin impacto sobre la función de coste, mientras que variaciones de esta función son suficientes para adaptarse a la aplicación.

Los resultados muestran que el controlador logra actuar directamente sobre los interruptores de potencia en función de diversos requisitos. Los desempeños de la estructura de control propuesta son similares a los de las numerosas estructuras dedicadas a cada uno de los casos estudiados, excepto en el caso de operación en modo rectificador, en el que la versatilidad y rapidez de control obtenidos son particularmente interesantes.

En definitiva, el controlador planteado puede emplearse para diferentes aplicaciones, topologías, objetivos y limitaciones. Si bien las estructuras de control lineal tradicionales han de modificarse, a

menudo en profundidad, para afrontar diferentes modos de operación o requisitos de control, dichas alteraciones no tienen ningún impacto sobre la arquitectura del controlador MPC obtenido, lo que pone de manifiesto su versatilidad, así como su universalidad, también demostrada por su capacidad para adaptarse a diferentes convertidores de potencia sin modificaciones importantes. Finalmente, la solución propuesta elude por completo la complejidad de la modulación, ofreciendo simplicidad y flexibilidad al diseño del control.

Contrôle avancé des convertisseurs de puissance multi-niveaux pour applications sur réseaux faibles

Avec l'avènement progressif des micros-réseaux incorporant les sources d'énergie renouvelable, un nouveau paradigme apparait dans la distribution de l'électricité. De fait, la nécessité de produire de l'énergie électrique à partir de ressources moins polluantes et moins limitées en quantité que le charbon, le gaz et le pétrole est à l'origine du développement d'alternatives reposant sur l'exploitation du vent, du soleil, des marées et autres ressources renouvelables. Ces ressources ne sont pas contrôlées, ce qui implique d'abord d'établir les centrales de production là où ces ressources sont situées mais aussi de devoir adapter en permanence la chaîne de distribution de l'énergie à une production variable et décorrélée des besoins en énergie réels du réseau.

Le réseau électrique traditionnel de distribution ne convient pas à une trop forte présence de ses sources d'énergie renouvelables. En réponse, d'autres modèles sont développés, avec une forte présence des micro-réseaux. Les micro-réseaux sont une approche à la fois plus restreinte et plus répartie, c'est à dire qu'ils couvrent généralement un territoire de plus petite taille que les réseaux électriques globaux présentement majoritaires, mais aussi qu'ils reposent davantage sur une pluralité de sources plutôt que sur un nombre réduit de centrales produisant suffisamment d'énergie pour tout le reste du réseau et fonctionnent alternativement connectés ou non à celui-ci. De même, ces réseaux pratiquent souvent un flux bidirectionnel de l'énergie, grâce à une forte présence d'éléments de stockage.

Ainsi, ces nouvelles architectures interfacent des consommateurs non contrôlés à des sources d'énergie intermittentes. Ce transfert d'énergie est effectué à travers des réseaux généralement faibles, ce qui signifie que leurs propriétés de tension et de fréquence dépendent de l'injection et la consommation d'énergie. Ces réseaux reposent sur des systèmes de stockage et de gestion de l'énergie avancés pour fonctionner. De ces deux thématiques découle aussi une contrainte toute particulière sur les différentes étapes de conversion de l'énergie électrique.

Les convertisseurs de puissance sont un élément critique de cette chaîne de conversion. En conséquence, leur bonne performance est essentielle au fonctionnement des micro-réseaux, et donc à l'intégration des sources d'énergie renouvelable. Afin d'améliorer les performances générales des convertisseurs, des topologies dites multi-niveaux sont développées. Ces structures proposent plus de deux possibilités pour relier leur entrée à leur sortie. Le nombre de façons d'effectuer la liaison détermine le nombre de niveaux,

avec Fig. 1 un exemple des trois chemins possibles pour un convertisseur Neutral Point Clamped (NPC) à trois niveaux (3L-NPC).

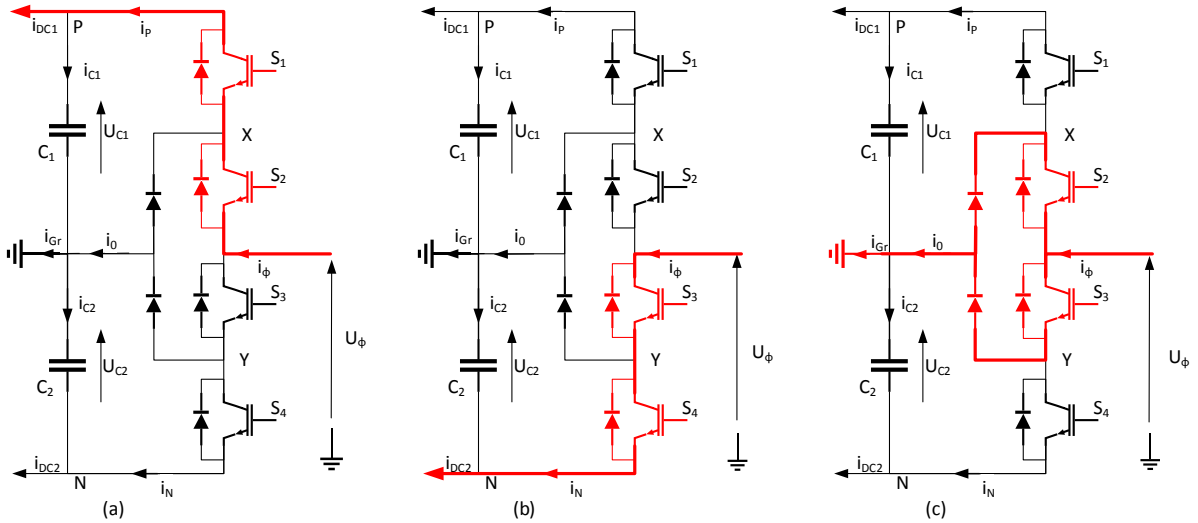

Fig. 1 Différentes positions de commutation pour un convertisseur 3L-NPC

Cette famille de convertisseurs de puissance comporte plusieurs membres, définis par le nombre de niveaux et par la topologie des différents composants utilisés. Les plus courantes sont le NPC, le Flying Capacitor (FC) et le Cascaded H-bridge (CHB) illustrées Fig. 1 et Fig. 2, mais une multitude d'autres versions existe pour diverses applications. Les convertisseurs multi-niveaux supportent de plus hautes puissances à composants égaux que leurs équivalents à deux niveaux, ce qui permet de les utiliser sur des applications de moyenne voire haute puissance. De plus, ils facilitent le contrôle des harmoniques et donc de la qualité de l'énergie. En contrepartie, le nombre de composants augmente et le contrôle de ces architectures de convertisseurs est plus complexe.

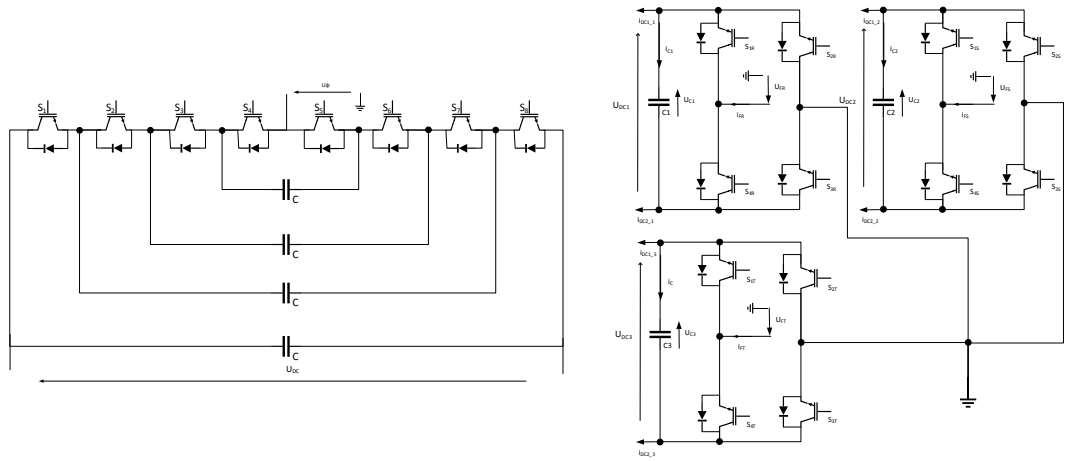

(a) (b)

Fig. 2 Exemples de topologies de convertisseurs multi-niveaux (a) FC cinq niveaux (b) CHB trois niveaux

Les convertisseurs de puissance interfacent des grandeurs électriques continues à l'aide d'interrupteurs de puissance discrets par nature. Chacun d'entre eux ne possède que deux états possibles et

c'est la combinaison des états des différents interrupteurs qui permet de contrôler les grandeurs électriques. Cette nature hybride, qui sépare le fonctionnement interne booléen du convertisseur des dynamiques continues de ce qu'il interface entraîne des complications en termes de contrôle. La première conséquence est la non-linéarité. Pour y pallier, la méthode la plus courante se repose sur des stratégies de modulation, séparant le contrôle en deux parties. D'un côté tout ce qui concerne les objectifs liés à la fonction d'interface des convertisseurs, où sont regroupés les différents objectifs de qualité de l'énergie et ceux rattachés aux systèmes connectés aux convertisseurs. De l'autre, la communication avec la nature discrète du convertisseur.

Ainsi, traditionnellement, le contrôle des convertisseurs de puissance est scindé en deux parties distinctes, chacune s'occupant de ses propres objectifs. Cependant, les contraintes croissantes sur la chaîne de conversion se font aussi sentir sur les objectifs de contrôle, qui ne peuvent plus simplement être traités séparément. L'une des pistes pour aborder ce problème, est de développer un contrôleur capable de traiter simultanément cette ambiguïté. Les deux approches sont synthétisées Fig. 3.

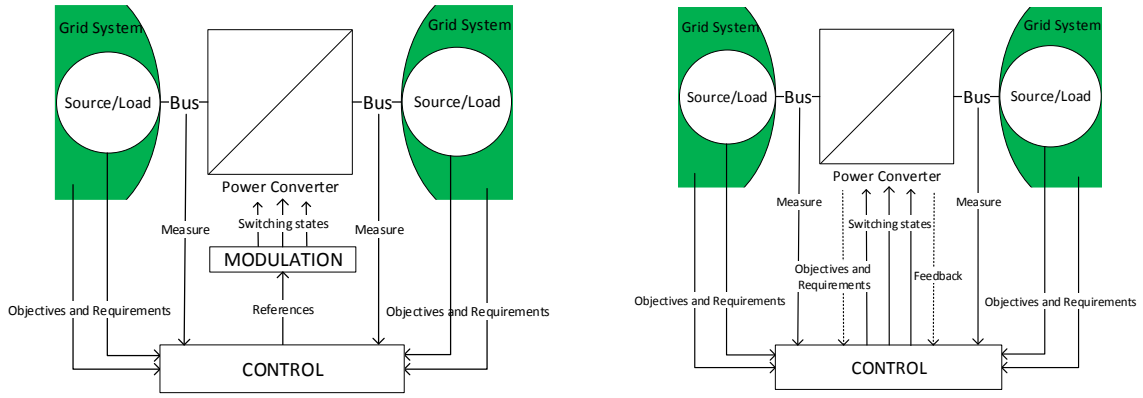

Fig. 3 Schémas de principe de contrôle des convertisseurs de puissance. (a) avec modulation, (b) sans modulation.

Afin de développer un contrôleur capable de traiter à la fois la non-linéarité des convertisseurs mais aussi le nombre important d'entrées et de sorties qu'ils impliquent ainsi que la complexité des objectifs à atteindre, le choix s'est porté vers les algorithmes Model Predictive Control (MPC). Ces stratégies de contrôle associent une méthode de modélisation et de prédiction à la résolution d'un problème d'optimisation. Le type de modèle et le type d'algorithme optimal sont variables mais la version la plus courante, qui associe des modèles d'états linéaires à des algorithmes quadratiques, n'est pas adaptée au cas des convertisseurs de puissance. En particulier parce qu'elle ne peut pas traiter la non-linéarité qui pose un problème ici.

Deux étapes interdépendantes sont donc nécessaires pour développer un contrôleur MPC capable de traiter le cas des convertisseurs de puissance : établir un système de modélisation et sélectionner l'outil mathématique pour poser et résoudre le problème d'optimisation. Une approche basée sur des modèles d'états commutants a été choisie. Cette méthode définit un modèle paramétrisé par les états ouvert ou fermé

des interrupteurs, ou de façon bijective par les options de connexion que ceux-ci proposent. Ce modèle, nommé Switched State Space Representation (SSSR), prend la forme d'une matrice d'état fonction des positions de connexion du convertisseur.

La SSSR permet donc de formaliser le comportement de tout convertisseur de puissance à l'aide de modèles linéaires par morceaux : tant que l'état de connexion du convertisseur ne change pas, son comportement peut être modélisé par une représentation d'état linéaire. Il est impossible de conclure sur la stabilité ou la contrôlabilité d'un système décrit par une SSSR seulement en étudiant séparément chacun des sous-systèmes. Il est toutefois possible de définir la stabilisabilité comme l'existence d'une séquence d'ordres de commutations qui stabilise le système.

Trouver une combinaison linéaire stable des sous-systèmes qui composent une SSSR suffit pour démontrer qu'elle est stabilisable. La réciproque est fausse : l'existence d'une combinaison des sous-systèmes formant un système équivalent instable ne garantit pas que le système global soit instable. Concernant la contrôlabilité, il est possible de définir une matrice de contrôlabilité en concaténant celles des différents sous-systèmes et d'étudier ensuite son rang, mais cette solution est difficile à appliquer pour des systèmes de grande taille.

Les modèles SSSR permettent de modéliser les convertisseurs de puissance à l'aide d'arbres de possibilités, comme présenté Fig. 4. Il devient possible d'assigner un poids à la transition d'un nœud de cet arbre à un autre en utilisant le sous-système associé et les objectifs du cahier des charges. Finalement, la SSSR permet de définir le problème d'optimisation comme la recherche d'un chemin le plus court dans un graphe. Plusieurs algorithmes traitent de tels problèmes et l'algorithme A* a été choisi ici dans un souci de vitesse de navigation dans l'arbre des possibilités.

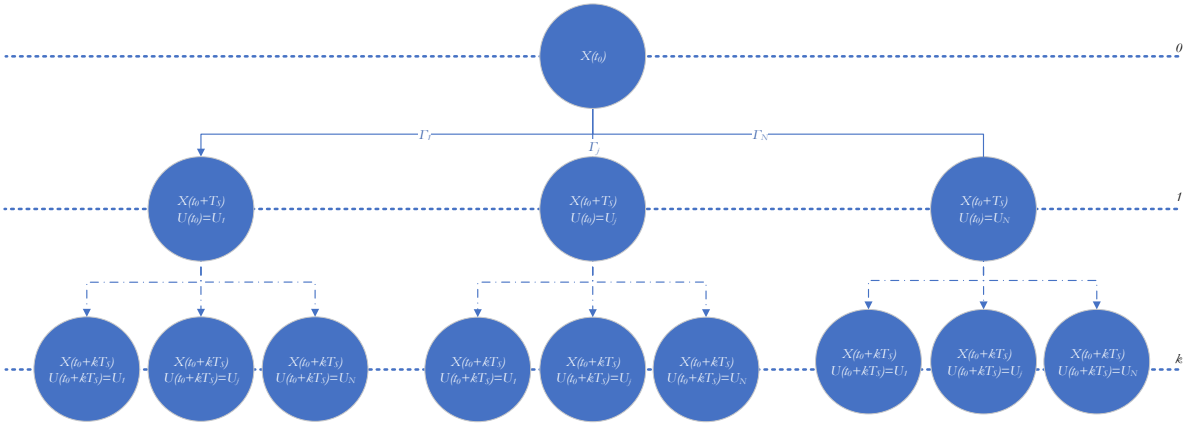

Fig. 4 Arbre des possibilités type pour un convertisseur de puissance modélisé à travers une SSSR

Le contrôleur final associe donc la SSSR à un algorithme A* en un formalisme qui permet à cette structure de traiter n'importe quel convertisseur de puissance sans modifications profondes, là où des convertisseurs différents impliquent généralement une stratégie de modulation différente et donc des

réglages des contrôleurs supplémentaires. La fonction à optimiser est définie librement selon l'application et le cahier des charges, sans se soucier de la linéarité.

Des critères de réglage et d'évaluation des performances du contrôleur ont été définis. Un résultat intéressant indique que le choix des normes pour le calcul de la fonction d'optimisation n'a aucune signifiance sur les performances finales. Des tests de sensibilité et de robustesse ont été menés, mettant en exergue l'importance de la définition de la fonction de coût utilisée. Plusieurs expressions et sous-expressions de cette fonction ont été étudiées et formalisées afin de traiter une grande variété d'objectifs de contrôle, tels que le suivi de référence sur un état, sur une variable de sortie, sur une variation des différentes grandeurs du système ou le respect de contraintes. D'autre part, les modèles SSSR utilisés pour modéliser les topologies NPC, FC et CHB à trois niveaux ont été vérifiés en simulation. Finalement, le contrôleur MPC développé a été mis à l'épreuve en simulation.

En ce qui concerne le contrôleur, plusieurs cas simples ont été traités pour commencer : un fonctionnement en onduleur autonome avec des charges équilibrées puis déséquilibrées, en onduleur connecté au réseau puis en redresseur connecté au réseau. Les trois situations impliquent des objectifs différents, traduits chaque fois par une expression différente de la fonction objectif. Chacune de ces études a été menée avec les trois topologies évoquées précédemment, ce qui demande de modifier le modèle interne utilisé dans la SSSR mais pas la fonction de coût.

Les résultats de ces études de cas montrent que le contrôleur MPC développé est universel : à condition que les modèles SSSR soient bons, le contrôleur fonctionne avec n'importe quelle topologie sans aucun besoin de modifier autrement sa structure. De même, modifier l'expression de la fonction de coût suffit à s'adapter aux différents objectifs de contrôle, sans impacter l'architecture ni les algorithmes employés. Le contrôleur est également robuste et propose des performances similaires en tout point à celles obtenues avec les autres structures de contrôle, voire légèrement supérieures tant en précision qu'en rapidité dans le cas précis du fonctionnement redresseur.

Ensuite, une application de convertisseur servant d'interface entre un système de stockage hybride et un réseau de charges comme présenté Fig. 5 fut simulée pour explorer davantage les possibilités du contrôleur. Le convertisseur contrôlé doit assurer l'échange de puissance dans les deux sens sous les meilleures conditions de tension et de fréquence. Plusieurs évènements liés aux connexions des différentes charges interviennent, venant perturber ces grandeurs, selon la Table 1.

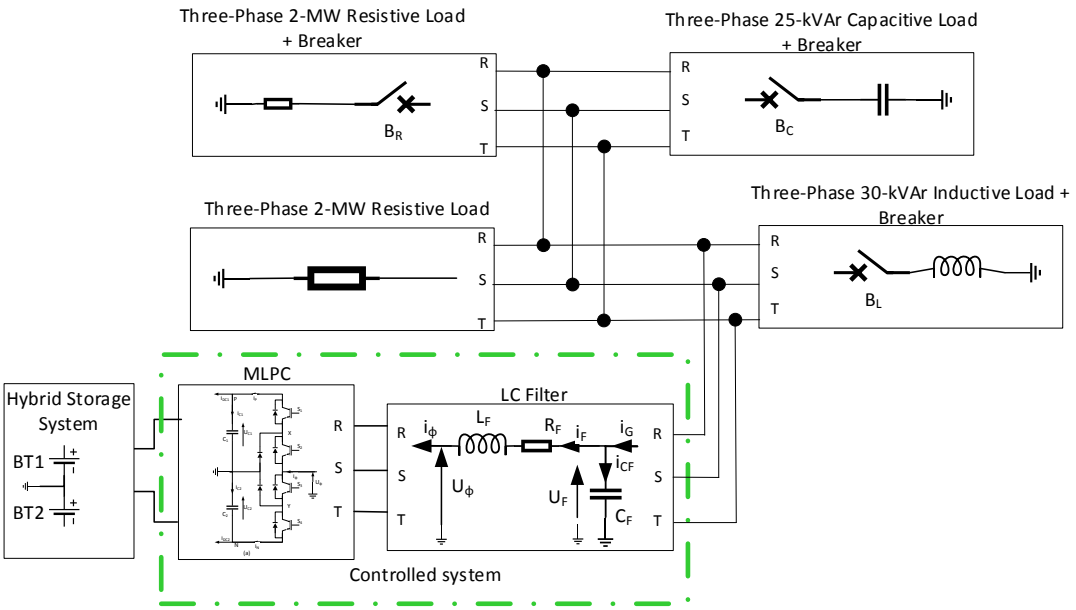

Fig. 5 Application sur un réseau isolé.

TABLE 1
ÉVENEMENTS ET TABLE DES CONNEXIONS

t (s)	0.2		0.3	0.4	0.6	0.8	0.9	1	1.2	1.3
B_R	0	1	1	1	1	0	0	0	0	0
B_C	0	0	0	1	1	1	1	0	0	1
B_L	0	0	0	0	1	1	1	1	0	0
P^*(MW)	2	4	4	4	4	2	2	2	2	2
β	0.5	0.5	0.515	0.515	0.515	0.515	0.475	0.475	0.475	0.5

Les résultats, illustrés Fig. 6 et Fig. 7, corroborent les résultats attendus : le contrôleur MPC développé manipule précisément les interrupteurs du convertisseur pour répondre intelligemment à des situations et des consignes variables. Ces conclusions encouragent une poursuite des recherches pour améliorer les algorithmes utilisés, dans le but d'accélérer les calculs et étendre la force de prédiction et d'optimisation du contrôler, et pour mettre le contrôleur ainsi que les modèles utilisés à l'épreuve de l'expérimentation.

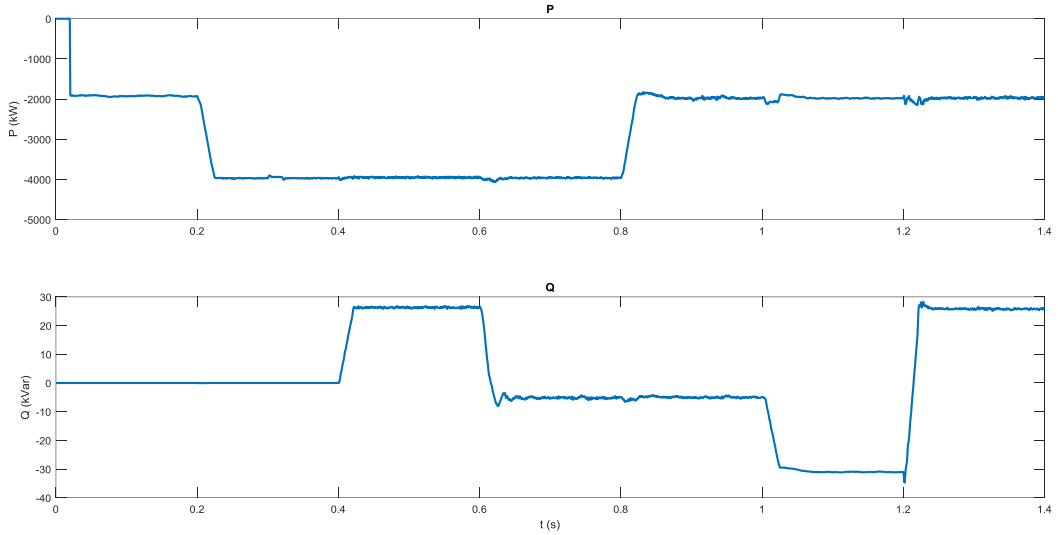

Fig. 6 Contrôle des puissances actives (en haut) et réactives (en bas)

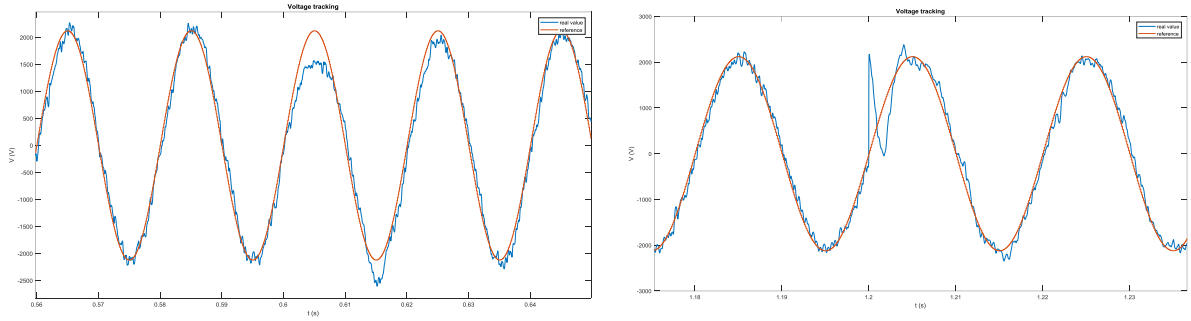

(a) (b)

Fig. 7 Tension sur la phase R. (a) : ajout de la charge inductive, (b) ajout de la charge capacitive

Control avanzado de convertidores de potencia multiniveles para aplicaciones en redes débiles

El advenimiento progresivo de las microrredes que incorporan fuentes de energía renovable está dando lugar a un nuevo paradigma de distribución de la electricidad. Emanciparse de los recursos contaminantes y limitados como el carbón, el gas o el petróleo para producir energía eléctrica requiere desarrollar alternativas basadas en la explotación del viento, el sol, las mareas y otros fenómenos físicos. Estos recursos no son controlados, lo que implica no solo establecer centrales de producción en los emplazamientos donde se localizan dichos recursos, sino también adaptar permanentemente la cadena de distribución de la energía a una producción variable y sin correlación con las necesidades de energía de la red.

La red eléctrica tradicional, centralizada, no cuenta con una fuerte presencia de los citados recursos de energía renovable. En contraposición, se están desarrollando otros modelos con gran cantidad microrredes. Estas constituyen una solución más restringida y distribuida, puesto que generalmente cubren un territorio de menor amplitud que las redes eléctricas globales actualmente mayoritarias y, además, se apoyan sobre una multitud de fuentes en lugar de sobre un número limitado de centrales que producen energía para todo el resto de la red, a la que pueden conectar y desconectar alternativamente. Del mismo modo, estas redes favorecen a menudo un flujo bidireccional de la energía, gracias a una fuerte presencia de elementos de almacenamiento.

Así, estas nuevas arquitecturas permiten conectar consumidores no controlados a fuentes de energías intermitentes. Esta transferencia de energía se materializa a través de redes frecuentemente débiles, lo que significa que sus características de tensión y de frecuencia dependen de la inyección y el consumo de energía. El funcionamiento de tales redes se fundamenta en sistemas avanzados de almacenamiento y de gestión de la energía. De estos dos últimos aspectos se derivan también restricciones particulares sobre las diferentes etapas de conversión de la energía eléctrica.

Los convertidores de potencia son un elemento crítico de esta cadena de conversión. En consecuencia, sus desempeños son esenciales para el funcionamiento de las microrredes y, por consiguiente, para la integración de fuentes de energía renovable. Con el fin de mejorar el desempeño general de los convertidores, se desarrollan topologías multinivel. Dichas estructuras proporcionan más de dos posibilidades para conectar su entrada con su salida. La cantidad de formas de realizar tal conexión determina el número de niveles. A modo de ejemplo, la Fig. 1 muestra los tres conexionados posibles para cualquiera de las ramas de un convertidor Neutral-Point Clamped (NPC) de tres niveles (3L-NPC).

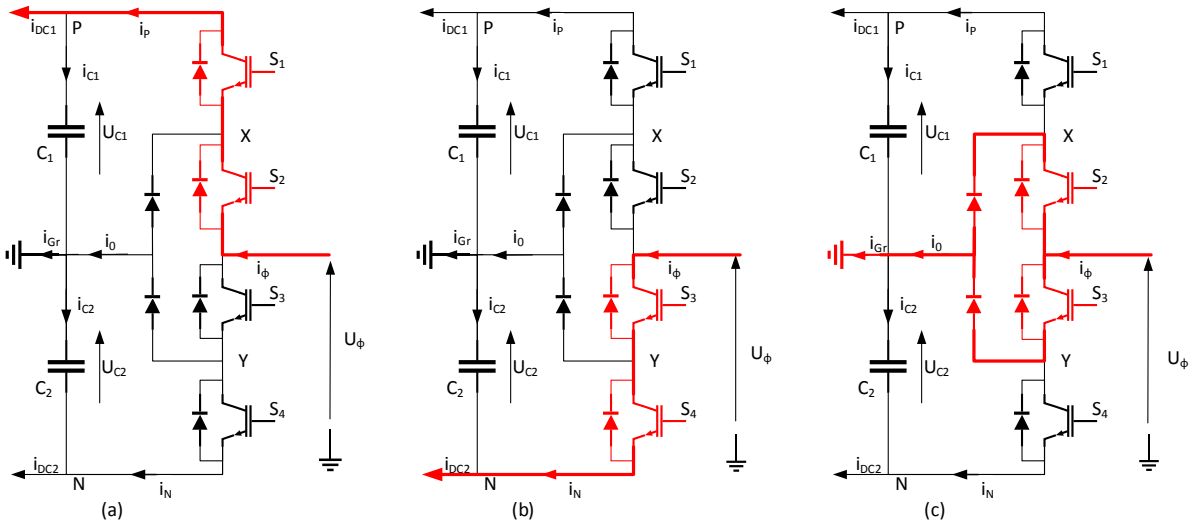

Fig. 1. Diferentes posiciones de conmutación para un convertidor 3L-NPC

Esta familia de convertidores de potencia contiene gran cantidad de miembros, definidos por el número de niveles y el reparto de los diferentes componentes utilizados. Los más comunes son el NPC, el Flying Capacitor (FC) y el Cascaded H-Bridge (CHB), ilustradas, respectivamente, en las Figs. 1 y 2, si bien existe una multitud de otras versiones para diversas aplicaciones. Los convertidores multinivel soportan potencias más altas que sus predecesores con idénticos componentes, lo que permite utilizarlos en aplicaciones de media o alta potencia. Además, facilitan el control de los armónicos y, en consecuencia, de la calidad de la energía. Como contrapartida, la cantidad de componentes aumenta y el control de estas arquitecturas de convertidor se torna más compleja.

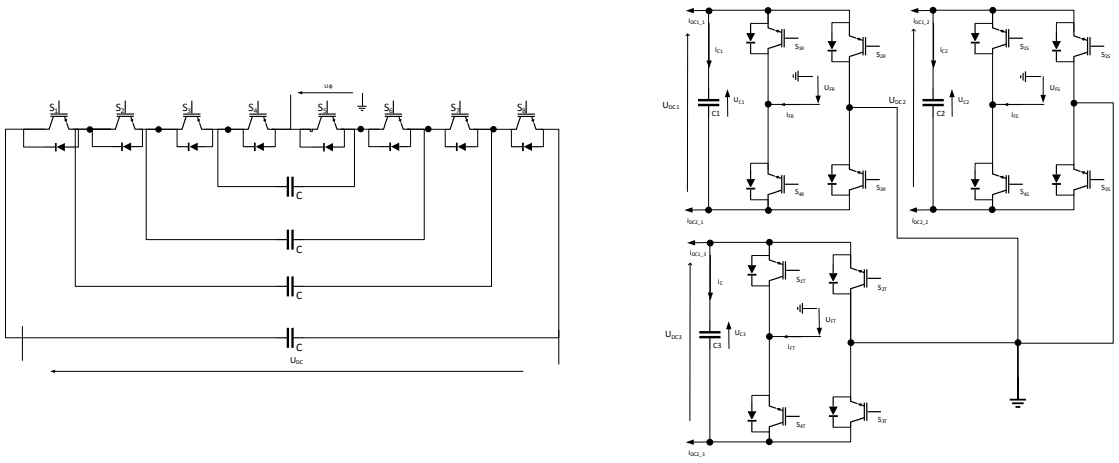

(a) (b)

Fig. 2. Ejemplos de convertidores multinivel (a) FC de cinco niveles (b) CHB de tres niveles

Los convertidores de potencia conectan magnitudes eléctricas continuas con la ayuda de interruptores de potencia discretos por naturaleza. Cada uno posee solo dos estados posibles, y es la combinación de los estados de los diferentes interruptores lo que permite controlar las variables eléctricas. Esta naturaleza híbrida, que separa el comportamiento interno booleano del convertidor de las dinámicas continuas de los elementos que conecta, implica complicaciones para el control. La primera consecuencia de la misma es la no-linealidad. El método más común para resolverla consiste en hacer uso de estrategias de modulación, separando el control en dos partes: por un lado, todo lo concerniente a los objetivos vinculados a la función de interfaz de los convertidores, entre los que se encuentran los asociados a la calidad de la energía y los relativos a los sistemas interconectados por el convertidor, y, por otro, el enlace con la naturaleza discreta del convertidor.

Así, tradicionalmente, el control de los convertidores de potencia se escinde en dos partes distintas, cada una de las cuales prioriza sus propios objetivos. Sin embargo, las exigencias crecientes sobre la cadena de conversión de la energía pesan también sobre los objetivos de control, que no pueden continuar tratándose separadamente. Una posible solución consiste en desarrollar un controlador que trate simultáneamente esta ambigüedad. Los dos métodos se resumen en la Fig. 3.

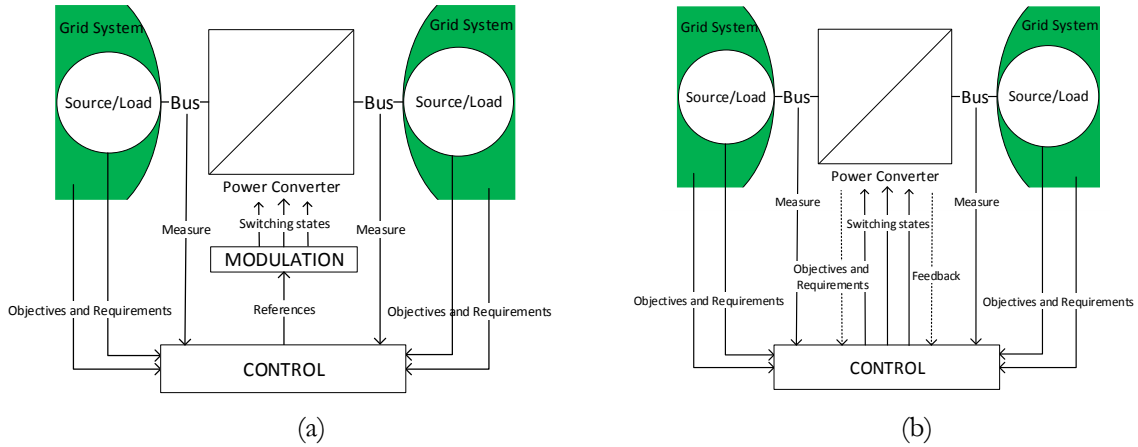

Fig. 3. Esquemas de principio del control de convertidores, (a) con modulación, (b) sin modulación

Con el fin de desarrollar un controlador que trate la no-linealidad de los convertidores y el elevado número de entradas y salidas que implican, así como la complejidad de los objetivos a satisfacer, se adoptan algoritmos de Control Predictivo basado en Modelos —Model Predictive Control (MPC)—. Dichas estrategias de control asocian un método de modelado y de predicción con la resolución de un problema de optimización. Los tipos de modelo y de algoritmo de optimización varían, pero la combinación más común, que relaciona modelos de estado lineales con algoritmos cuadráticos, no permite tratar los convertidores de potencia, fundamentalmente a causa de su no-linealidad.

Se precisan dos etapas interdependientes para construir un controlador MPC que posibilite abordar el caso de los convertidores de potencia: establecer un sistema de modelado y seleccionar la herramienta matemática para definir y resolver el problema de optimización. Se adopta un enfoque basado en modelos

de estado conmutados. Este método define un modelo parametrizado por los estados de los interruptores de potencia, o, de forma biyectiva, las opciones de conexión que estos implican. Este modelo, denominado Switched State-Space Representation (SSSR), da lugar a una matriz del sistema función de las posiciones de conexión de los interruptores de potencia del convertidor.

La SSSR permite formalizar el comportamiento de cualquier convertidor de potencia mediante modelos lineales por partes: siempre y cuando el estado de conexión del convertidor no varíe, su comportamiento puede ser modelado como una representación de estado lineal. Sin embargo, resulta imposible concluir nada acerca de la estabilidad o la controlabilidad de un sistema descrito por una SSSR únicamente estudiando, de forma separada, todos y cada uno de los subsistemas lineales resultantes. No obstante, se puede definir su estabilizabilidad como la existencia de una secuencia de órdenes que estabiliza el sistema.

Hallar una combinación lineal estable de los subsistemas que constituyen una SSSR es suficiente para demostrar la estabilizabilidad del sistema global. Lo contrario es falso: la existencia de una combinación lineal de dichos subsistemas que resulta en un sistema equivalente instable no garantiza que el sistema global sea instable. En lo concerniente a la controlabilidad, es posible definir una matriz de controlabilidad concatenando las de los diferentes subsistemas lineales para, posteriormente, analizar su rango, si bien este método es muy difícilmente implementable en sistemas de gran tamaño.

Los modelos SSSR representan los convertidores de potencia en forma de árboles de posibilidades, como se ilustra en la Fig. 4. Puede asignarse un peso a la transición de un nodo de tal árbol a otro utilizando el subsistema asociado a la transición y los objetivos de control. Finalmente, la SSSR permite definir el problema de optimización como la búsqueda del camino más corto en un grafo. Son varios los algoritmos concebidos para abordar este tipo de problema, habiéndose elegido el conocido como A* por conducir a una rápida navegación por el árbol de posibilidades.

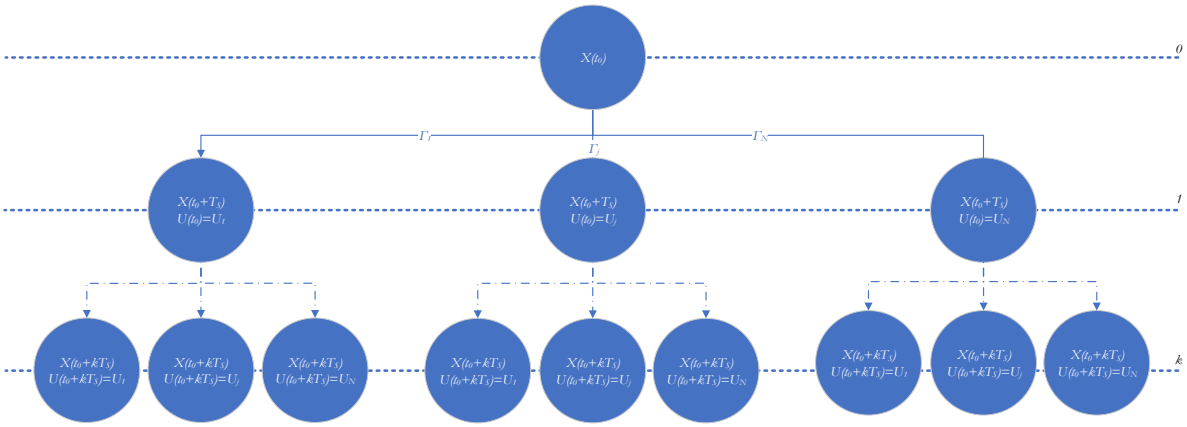

Fig. 4. Árbol de posibilidades para un convertidor de potencia modelado por una SSSR

Por tanto, el controlador final asocia la SSSR a un algoritmo A* mediante un formalismo, otorgando a la estructura resultante la capacidad de tratar con cualquier convertidor de potencia sin modificaciones importantes, cuando convertidores diferentes requieren generalmente de estrategias de modulación diferentes, así como de ajustes suplementarios para los controladores. Además, la función a optimizar se define libremente según la aplicación y las exigencias, sin preocuparse de la linealidad.

Se definen criterios de sintonía y de evaluación del rendimiento del controlador. Una conclusión interesante indica que la selección de las normas para el cálculo de la función de coste tiene muy poca influencia sobre los resultados finales por lo que respecta al tiempo de cómputo o al cumplimiento de los objetivos. Pruebas de sensibilidad y de robustez subrayan la importancia de definir correctamente la función de coste. Se estudian y formalizan varias expresiones de dicha función y de las subfunciones que la integran para una variedad de objetivos de control, como el seguimiento de referencias de estados, de variables de salida, de variaciones de las diferentes magnitudes del sistema o el respeto de restricciones. Asimismo, se evalúan en simulación las representaciones SSSR utilizadas para modelar las topologías NPC, FC y CHB de tres niveles. Finalmente, el controlador MPC desarrollado se somete a prueba en simulación.

En lo referente al citado controlador, se tratan varios casos simples en primer lugar: un inversor autónomo con cargas equilibradas y, posteriormente, desequilibradas, un inversor conectado a la red y, a continuación, un rectificador conectado a la red. Los tres escenarios implican objetivos diferentes, traducidos cada vez mediante una expresión diferente de la función de coste. Cada uno de dichos estudios se lleva a cabo con las tres topologías evocadas anteriormente, modificando el modelo SSSR, pero sin retocar la función de coste.

Los resultados de tales casos de estudio muestran que el controlador MPC es universal: a condición de que los modelos SSSR sean los adecuados, el controlador opera con cualquier topología sin requerir ninguna modificación de su estructura. Del mismo modo, cambiar la función de coste es suficiente para adaptarse a los diversos objetivos de control sin afectar ni a la arquitectura de control ni a los algoritmos empleados. El controlador MPC es también robusto y confiere características similares o ligeramente superiores a las obtenidas con otras estructuras de controladores, especialmente en el caso rectificador, tanto en cuanto a rapidez como a precisión.

Para concluir, se simula una aplicación en la que el convertidor actúa como interfaz entre un sistema de almacenamiento y una red de cargas, tal y como se presenta en la Fig. 5, al objeto de profundizar en la exploración de las posibilidades del controlador. El convertidor controlado debe garantizar el intercambio de potencia en las dos direcciones, preservando las mejores condiciones posibles de tensión y frecuencia. Varios eventos resultan de la conexión de las diferentes cargas, según la Tabla 1.

TABLA 1
TABLA DE EVENTOS Y CONEXIÓN

t (s)	0.2	0.3	0.4	0.6	0.8	0.9	1	1.2	1.3
B_R	0	1	1	1	1	0	0	0	0	0
B_C	0	0	0	1	1	1	1	0	0	1
B_L	0	0	0	0	1	1	1	1	0	0
P^*(MW)	2	4	4	4	4	2	2	2	2	2

Los resultados, ilustrados en las Figs. 6 y 7, corroboran los obtenidos anteriormente: el controlador MPC desarrollado manipula con precisión los interruptores de potencia del convertidor para responder inteligentemente a situaciones y demandas variables. Estas conclusiones alientan a proseguir la investigación con el propósito de perfeccionar los algoritmos empleados, acelerando los cálculos y aumentando la capacidad de predicción y de optimización del controlador, así como de evaluar experimentalmente los modelos y el controlador desarrollados.

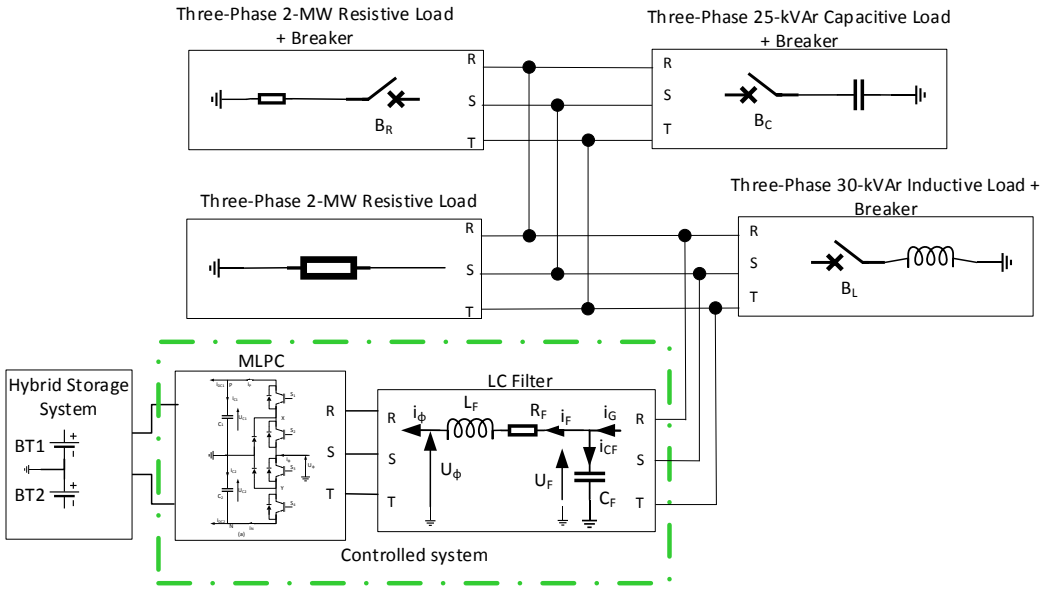

Fig. 5. Aplicación con una red aislada.

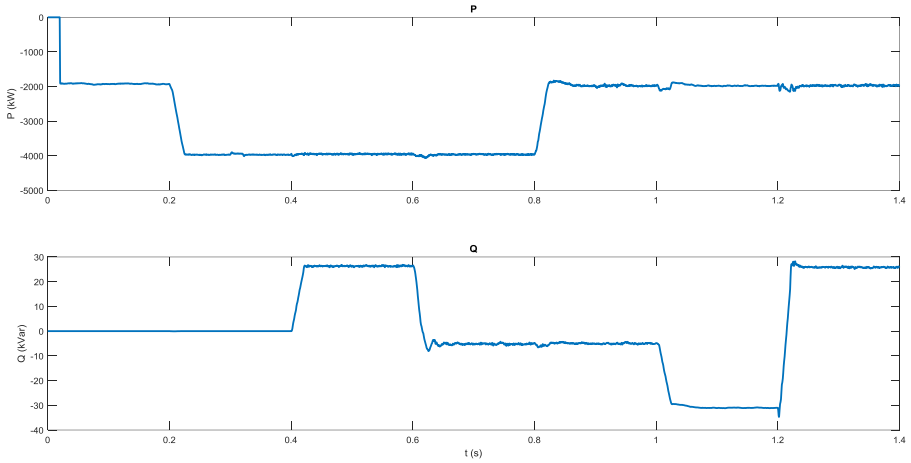

Fig. 6. Control de la potencias activa (arriba) y reactiva (abajo)

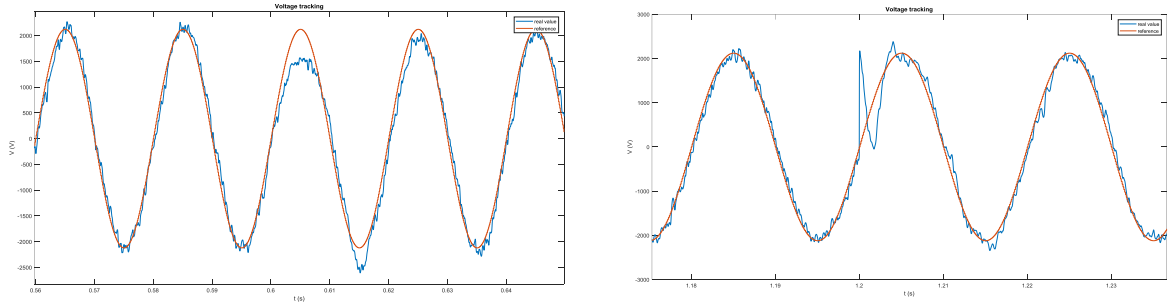

(a) (b)

Fig. 7. Tensión de la fase R, (a) inclusión de la carga inductiva, (b) adición de la carga capacitiva

Table of contents

Glossary

3L-NPC: 3 Level Neutral-Point Clamped

3L-FC: 3 Level Flying Capacitor

3L-CHB: 3 Level Cascaded H-Bridge

CSSSR: Continuous Switched State-Space Representation

DSSSR: Discrete Switched State-Space Representation

EMPC: Explicit MPC

FCS-MPC: Finite Control Set MPC

GPC: General Prediction Control

HVDC: High Voltage Direct Control

LQ: Linear Quadratic

LTI: Linear Time Invariant

MG: MicroGrids

MIMO: Multiple Input Multiple Output

ML-PC: Multi-level Power Converter

MMC: Modular Multi-level Converter

MPC: Model Predictive Control

OSS: Optimal Switching Sequence

OSV: optimal Switching Vector

PCC: Point of Common Coupling

PLL: Phase-Locked Loop

PWM: PulseWidth Modulation

RES: Renewable Energy Sources

SISO: Single Input Single Output

SMC: Sliding Mode Control

SPSM: Simscape Power System Model

SPWM: Sinusoidal PWM

SSSR: Switched State-Space Representation

SVM: Space Vector Modulation

THD: Total Harmonic Distortion

ZOH: Zero-Order Hold

Introduction

1. Presentation of the thesis

The present thesis work has been prepared in the context of a cotutelle between the ESTIA-Recherche laboratory from ESTIA Institute of Technology, France associated to Bordeaux University and the Department of Automatic Control and Systems Engineering from the University of the Basque Country UPV/EHU (Spain). The main research interests of this collaboration are related to the power electronics and automation applied to Renewable Energy Sources (RES) and MicroGrids (MG). This work was supported by the Nouvelle Aquitaine Region (Insu'Grid FUI project), the Spanish Ministry of Economy and Business (research project DPI2015-64985-R), the UPV/EHU (research grant GIU16/54), as well as the Basque Government (research grant IT1256-19).

2. Context

Ever since the domestication of electric energy, one of the most prevalent priorities has been its transportation and distribution from the various energy producers to the consumers. Along with this history, starting at the end of the XIXth century, many discoveries, trials and modifications led to the centralised AC grid that now dominates and connects the world [1]. This grid can be described as the sum of three components [2]. First, power plants generate extensive amounts of electricity from various energy sources such as coal, gas, nuclear, fuel or water potential. These sources are chosen for the amount of energy they can produce and for their —relative— accessibility. Then, the energy is transmitted via electric lines interspersed with power conversion stations, whose crucial purpose is to modify the characteristics of the energy carried to minimise losses and to interface the different elements of the grid. Finally, the consumers, of various sizes, needs and consumptions stand at the end of this unidirectional chain [3]. In this disposition, the management of the grid is achieved by fitting the energy produced to the consumption, thanks to the control over the production of the different source plants.

The maturation of the distribution and conversion technologies continuously brings new, more rigorous operational criteria to the table. These requirements include efficiency and reliability of the power converters, whose roles and missions in the distribution chain are already multiple. Indeed, they have an interfacing role, enabling and managing the connection of sources and consumers to the gris, but they also perform precise functionalities aiming at optimising the global operation of the elements they are connecting together [4], [5].

Environmental issues surround the fossil energy sources, as the process transforming their thermodynamic energy into an electric one generates generous amounts of greenhouse gases and other contaminants, participating strongly to the current pollution situation. Aggregated to the depletion of these fossil energy resources, this motivates the necessity to find other cleaner sources, such as renewable energy

sources. As a result, these sources and the plants associated have been massively integrated into the grid for the past two decades [6].

Renewable resources include wind, hydroelectricity, solar irradiance and tides, amongst others. Most of these resources share two negative properties: first of all, they require specific topological and climatic conditions to be harnessed. The geographic implantation is essential in a centralised grid, as its stability and its stiffness are obtained thanks to a dense meshing that cannot be attained with isolated sources located far from the rest of the grid. This distance critically affects the grid, making it weaker. The weakness or stiffness of a grid evaluates the consequences of power injection or consumption on its properties, such as the frequency and the voltage of the electric signal carried. If injecting power has no impact on these properties, then the grid is considered stiff. Otherwise, it is said to be weak. This trait is deeply related to the physical implementation of the grid and related to the impedance of its lines, and specifically the ratio between the resistive part, R, and the reactive part, X. If X/R is lower than 0.5, the grid is considered to be weak [7].

The second shared property is the uncontrollability of the RES. As it is impossible to control the energy carried from the wind or solar irradiance, it is impossible for wind turbines and solar plants to deliver the specific quantity of energy required to feed the consumers. Consumption is not constant, and production has to adjust itself to ensure the power balance. To compensate for this lack of controllability, most renewable power plants are accompanied by storage systems. To summarise, the connection of RES to the grid with high penetration is subject to several operational problems, such as voltage inconsistency, frequency instability and discontinuity of service [8]. The aggregation of these characteristics calls for a different approach to the distribution of renewably generated electricity, such as distributed generation and microgrids.

The centralised grid already relies heavily on power conversion to maintain power quality, stability, and to provide various ancillary services, for overall reliability. The massive integration of RES in this grid is made possible by the power converters, and the distributed generation grids rely even more on them: the power conversion is a critical link of the chain that brings electricity to the world. In this context, power converters —through advanced control strategies— could play an essential role in order to improve power quality and grid stability [9]. The grid and the power converters have always been evolving together, and as such, the implementation of power conversion in electric grids is currently changing. To increase the efficiency, the range of applications and the power capacity of converters, several tracks to progress are investigated. A major proposition concerns the topology of the converters.

Power converters are hybrid systems: they act discreetly on continuous values through their power semiconductor switching devices. Depending on the arrangement of the power switches, the properties change. In particular, the levels of a converter qualify the possible connections it can put into action. The most common forms have two levels, meaning that the AC side can be connected to the DC in two different ways. Usually , the configurations lead to a positive potential or a negative potential. Over the past years,

various topologies with more than two levels have been emerging, especially for high power applications. These are called Multi-Level Power Converters (ML-PCs). Such topologies offer a solution to the efficiency and power rate of the converters, against a gained complexity and price. Their implementation into the grid has been raising ever since their introduction, especially with RES applications.

The hybrid nature of power converters leads to control difficulties usually bypassed thanks to the modulation strategies [10], [11]. The main point of this method is to address the non-linearity of the power conversion and to provide an equivalent average system that can then be treated by conventional control structures. An important number of the previously evoked control objectives is related to the exact command of the switching devices and are therefore undertaken by the modulation block [4][12]. It is then a critical element of the control chain which impacts the control objectives and requirements, as well as the models used to develop the different control structures.

In order to further improve efficiency and reliability of power converters without recurring to profound modifications of the control architectures, it is important to provide additional intelligence to their control, down to the level of power switches. This idea is particularly interesting for ML-PCs, as the modulation strategies and their impacts on the control design are heightened by these topologies. Recently, a variety of advanced controls has been developed to improve the operation of power converters, such as sliding-mode control [13]–[15] or Model Predictive Control (MPC) [16]–[18]. Both methods offer the capacity to directly overcome the obstacle attributable to the hybrid nature of converters by means of the controller, therefore enabling a deeper control of the system. Nevertheless, they strongly depend on the definition of models and equations of the systems to perform optimally. This dependency has to be seen in the light of the numerous types of power converters designed for a proportional number of different applications and specificities [19], [20].

3. Objectives

The objective of this thesis work is to provide a universal control solution to directly manipulate all power converters down to their power switches, while considering a variety of control objectives, including efficiency and reliability issues. In order to satisfy this objective, the following intermediate goals were fixed:

- Analysis of the most common power converters in the family of multi-level technologies, Neutral Point Clamped (NPC), Flying Capacitor (FC) and Cascaded H-Bridge (CHB) to understand their limits, purposes and uses.
- Analysis of the existing control strategies associated with these power converters in the context of grid connection and RES integration.
- Description of a modelling tool, Switched State-Space Representation (SSSR), for all power converters down to their switches, expression and validation of this SSSR for the three topologies

mentioned above.

- Design of an advanced MPC algorithm able to eliminate the modulation control stage, to operate with any SSSR of any power converter, regardless of the topology, the application or the number of levels, and to integrate as many control requirements as possible.
- Characterisation of the developed control strategy: Stability and stabilisability, controllability, robustness and sensitivity, together with the evaluation of the algorithm performance.
- Validation of the control method in simulation on a representative sample of applications: stand-alone operation with a balanced and unbalanced load, rectifier, grid-connected and grid-forming operation mode.

4. Organisation of the document

The present essay is divided into five chapters. This section details the composition of each chapter.

The first chapter reviews the different existing multi-level power converter technologies and the most common associated control methods. Three main topologies are retained and described in detail, namely NPC, FC and CHB. Among the control strategies cited, special care is paid to MPC, as it holds high interest for the control of power converters without modulation.

The second chapter focuses on proposing and formalising a modelling method applicable to all power converters, describing their behaviour down to their power switches. The technique used is a non-linear modelling strategy commonly applied to other hybrid systems, mechanical or chemical, for example, chosen for its compatibility with the MPC strategy. The model is first described theoretically, then applied to three topologies outlined in the first chapter, before validation in simulation.

The third chapter details the algorithms developed to perform the optimisation aspect of the MPC controller. A thorough description of the different steps and tasks of the optimisation function is complemented by a discussion about possible variants. To conclude, different criteria of performance are selected and applied to the final algorithm.

The fourth chapter explores the theoretical consequences of the association of the modelling method described in Chapter II with the algorithms presented in Chapter III. Conclusions are drawn concerning the stability and controllability of the models defined in the second chapter, concerning the integration of the control objectives into the controller and the rules surrounding the construction of the cost function representing them, as well as concerning the robustness and sensitivity of the resulting controller.

The fifth chapter collects and illustrates the simulation results of four case of study, designed to challenge the developed solution and to emphasise the compliance to the initial objectives of universality, versatility and performance. The case studies consist of a stand-alone inverter operation, a grid-connected

inverter application, a rectifier case and, finally, a study of a converter controlled to perform the four-quadrant operation with both DC- and AC-related objectives in an isolated grid. The four cases lead to a complete array of applications, with many combinations of topologies and filters, further demonstrating the capabilities of the controller proposed.

Finally, the last part of this thesis dissertation summarises the presented work and its main conclusions. Future research lines and perspectives are also provided.

5. Bibliography

[1] H. B. Puttgen, P. R. MacGregor, and F. C. Lambert, "Distributed generation: Semantic hype or the dawn of a new era?," *IEEE Power Energy Mag.*, vol. 1, no. 1, pp. 22–29, Feb. 2003, doi: 10.1109/MPAE.2003.1180357.

[2] S. M. Kaplan, "Electric power transmission: Background and policy issues," pp. 47–85, Jan. 2011.

[3] A. A. Bayod-Rújula, "Future development of the electricity systems with distributed generation," *WESC 2006*, vol. 34, no. 3, pp. 377–383, Mar. 2009, doi: 10.1016/j.energy.2008.12.008.

[4] S. Ceballos *et al.*, "Efficient Modulation Technique for a Four-Leg Fault-Tolerant Neutral-Point-Clamped Inverter," *IEEE Trans. Ind. Electron.*, vol. 55, no. 3, pp. 1067–1074, Mar. 2008, doi: 10.1109/TIE.2008.917098.

[5] H. Wang, M. Liserre, and F. Blaabjerg, "Toward Reliable Power Electronics: Challenges, Design Tools, and Opportunities," *IEEE Ind. Electron. Mag.*, vol. 7, no. 2, pp. 17–26, Jun. 2013, doi: 10.1109/MIE.2013.2252958.

[6] F. Blaabjerg and K. Ma, "Future on Power Electronics for Wind Turbine Systems," *IEEE J. Emerg. Sel. Top. Power Electron.*, vol. 1, no. 3, pp. 139–152, Sep. 2013, doi: 10.1109/JESTPE.2013.2275978.

[7] S. Grunau and F. W. Fuchs, "Effect of Wind-Energy Power Injection into Weak Grids," p. 7.

[8] M. Tsili and S. Papathanassiou, "A review of grid code technical requirements for wind farms," *IET Renew. Power Gener.*, vol. 3, no. 3, pp. 308–332, Sep. 2009, doi: 10.1049/iet-rpg.2008.0070.

[9] K. Katsavounis, P. Hou, W. Hu, and Z. Chen, "Optimal energy flow in islanded integrated energy systems," in *IECON 2017 - 43rd Annual Conference of the IEEE Industrial Electronics Society*, Oct. 2017, pp. 369–374, doi: 10.1109/IECON.2017.8216066.

[10] B. P. McGrath and D. G. Holmes, "Multicarrier PWM strategies for multi-level inverters," *IEEE Trans. Ind. Electron.*, vol. 49, no. 4, pp. 858–867, 2002.

[11] J. Zaragoza, J. Pou, S. Ceballos, E. Robles, P. Ibanez, and J. L. Villate, "A Comprehensive Study of a Hybrid Modulation Technique for the Neutral-Point-Clamped Converter," *IEEE Trans. Ind. Electron.*, vol. 56, no. 2, pp. 294–304, Feb. 2009, doi: 10.1109/TIE.2008.2005132.

[12] Bum-Seok Suh, Gautam Sinha, M. D. Manjrekar, and T. A. Lipo, "Multilevel Power Conversion - An Overview Of Topologies And Modulation Strategies," in *Proceedings of the 6th International Conference on Optimization of Electrical and Electronic Equipments*, May 1998, vol. 2, p. AD-AD, doi: 10.1109/OPTIM.1998.708006.

[13] A. Susperregui, J. Jugo, I. Lizarraga, and G. Tapia, "Automated control of doubly fed induction generator integrating sensorless parameter estimation and grid synchronisation," *IET Renew. Power Gener.*, vol. 8, no. 1, pp. 76–89, Jan. 2014, doi: 10.1049/iet-rpg.2013.0045.

[14] M. I. Martinez, A. Susperregui, and G. Tapia, "Second-order sliding-mode-based global control scheme for wind turbine-driven DFIGs subject to unbalanced and distorted grid voltage," *IET Electr. Power Appl.*, vol. 11, no. 6, pp. 1013–1022, 2017, doi: 10.1049/iet-epa.2016.0711.

[15] S. Tan, Y. M. Lai, and C. K. Tse, "Indirect Sliding Mode Control of Power Converters Via Double Integral Sliding Surface," *IEEE Trans. Power Electron.*, vol. 23, no. 2, pp. 600–611, Mar. 2008, doi: 10.1109/TPEL.2007.915624.

[16] P. Cortes, J. Rodriguez, D. E. Quevedo, and C. Silva, "Predictive Current Control Strategy With Imposed Load Current Spectrum," *IEEE Trans. Power Electron.*, vol. 23, no. 2, pp. 612–618, Mar. 2008, doi: 10.1109/TPEL.2007.915605.

[17] S. Kouro, P. Cortes, R. Vargas, U. Ammann, and J. Rodriguez, "Model Predictive Control—A Simple and Powerful Method to Control Power Converters," *IEEE Trans. Ind. Electron.*, vol. 56, no. 6, pp.

1826–1838, Jun. 2009, doi: 10.1109/TIE.2008.2008349.
[18] M. Pereira, D. Limon, T. Alamo, and L. Valverde, "Application of Periodic Economic MPC to a Grid-Connected Micro-Grid**The financial support from Ministerio de EconomÍa y Competitividad (Project No. DPI2013-48243-C2-2-R) is gratefully acknowledged.," *IFAC-Pap.*, vol. 48, no. 23, pp. 513–518, 2015, doi: 10.1016/j.ifacol.2015.11.330.
[19] P. Cortes, A. Wilson, S. Kouro, J. Rodriguez, and H. Abu-Rub, "Model Predictive Control of Multilevel Cascaded H-Bridge Inverters," *IEEE Trans. Ind. Electron.*, vol. 57, no. 8, pp. 2691–2699, Aug. 2010, doi: 10.1109/TIE.2010.2041733.
[20] S. Vazquez *et al.*, "Model Predictive Control: A Review of Its Applications in Power Electronics," *IEEE Ind. Electron. Mag.*, vol. 8, no. 1, pp. 16–31, Mar. 2014, doi: 10.1109/MIE.2013.2290138.

Chapter I: State of the art

1. Multi-level power converters

1.1 Definition and advantages

Multi-level power converters (ML-PCs) are a development of the power conversion technology, based on power electronics and controlled converters. The term "multi-level" refers to the different energy paths that can be created by the converter. For example, considering a two-level voltage source inverter, it can bind its DC and AC sides two ways: connecting the AC load to a positive potential V or its negative version $-V$. By extension, with three levels, an intermediary point is created, often 0, and so on for higher values. With this definition, it appears that the typical power converters are two-level converters and that single-level conversion is nonsense. Both odd and even number of levels are found, with different consequences on the operation and characteristics of the converter. Theoretically, this number can reach high values [1], [2].

Generally speaking, adding levels to a power converter leads to higher voltage levels with lower voltage ratings, therefore reducing the strain on the components and allowing higher energy trades with the same components. Another welcome feature is the induced enhanced waveforms: increasing the number of levels amounts to diminishing the quantisation step of the converter, automatically implying an improved precision when generating signals. Additionally, multi-level converters present reduced electromagnetic interference [3]–[5].

Nevertheless, this approach also has inconveniences, amongst which some of the most notables are the necessity to balance the levels introduced and the repartition of the energy between the components. It is also worth noting that the multi-level topologies have an increased number of components, leading to a high cost in comparison to converters with fewer levels, along with a higher strain on the control algorithms employed to manage all the different combinations permitted. Finally, a large variety of ML-PCs can be found, with critical structural modifications, leading to personalised control structures [6], [7]. This variety is of course also seen as an asset, since the numerous forms are meant to address the many miscellaneous issues coming along with power conversion and its many applications. These advantages and disadvantages are summed up in Table 1.1.

TABLE 1.1
MAIN INTERESTS AND DISADVANTAGES OF ML-PCS

Main advantages	Main limitations
Higher power transfer capability with the same switching technology	Variety of forms entailing a variety of control structures
Reduced harmonic distortion	Energy repartition needs to be controlled to prevent heterogenous aging
Reduced electromagnetic interference	Higher cost, growing with the number of levels
Variety of topologies to handle many applications	Control burden

Because of their improved power rates, ML-PCs are often found in high power applications [4] such as grid connection and industrial driving. Still, thanks to their superior waveforms, they also prove useful as active filters and for applications with lower powers. Going on, the main focus of this thesis is the applications of ML-PCs in the renewable energy and storage integration field.

1.2 Classification of ML-PCs

Multi-level converters can be classified according to the technological solution they employ. There are four main approaches, each leading to subdivisions when specific needs or applications are met. The first method relies on diodes to clamp the different levels from each other. The second method uses capacitors to constrain the voltage across open switches. The third method is an adaptation of the full-bridge, stacking piles of bridges to generate a proportional number of levels. Finally, the fourth method is a general approach combining different commutation topologies to reach higher levels. The two latest ways are similar in their stacking mentality and are clustered in the wider family of the multi-cell multilevel converters[3], [4]. On the opposite side, the first two methods form the integrated multilevel converters, as summed up in Fig. 1.1.

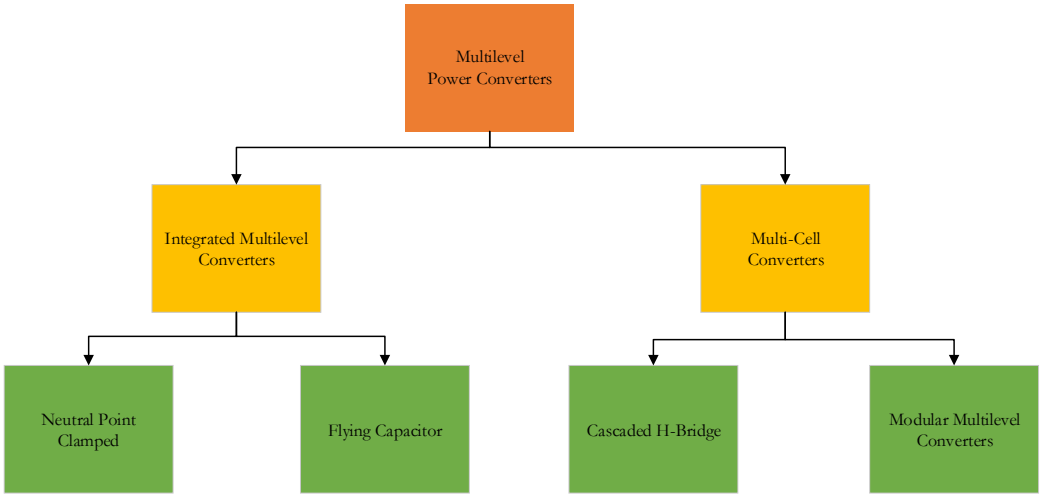

Fig. 1.1. Simplified classification of high-power ML-PCs

The multicell topologies are highly modulable, reaching high levels and offering a variety of adaptations to their context. They are often designed and used for complex or specific applications. For example, their first documented utilisation was dedicated to plasma stabilisation, which required particular harmonics content and precision, only accessible with an important number of levels [8]. Similarly, they are found in High Voltage Direct Current (HVDC) systems [9], operating as a STATCOM [10], or forming DC microgrids [11].

The integrated multilevel topologies are more difficult to modulate, but they were the first multilevel topologies introduced [12] and have since been heavily implemented in a multitude of industrial applications. The possibility to couple such topologies back-to-back enables all conversion directions, leading to easy implementations on drive applications [13] and grid connection. The integrated multilevel converters are often designed for drive applications and grid connection but show limitations when considering applications where spectral requirements or power distribution and quality through the plant can be critical. In these cases, Multi-Cell Inverters are preferred [14].

The classification proposed here can be extended to further specify and explore the ramifications of each branch, especially concerning the Modular Multilevel [15]. However, the principles stay the same, and there is no explicit reason to develop these families any further in this thesis.

1.3 Common topologies

1.3.1 Neutral-Point Clamped

The first integrated multi-level converters subfamily leads to Neutral Point Clamped (NPC) topologies. These topologies can be found under different forms depending on the way the connection is made (active, nested, stacked, active stacked) and on the number of levels[16]–[19]. This topology is the first multi-level topology considered in 1980 [12], and as such is very well documented. This structure can be extended to any number of levels [20], but odd numbers are preferred for utility applications, as even numbers prevent neutral clamping. Thanks to the neutral clamping, combining rectifiers and inverters is simple, leading to further applications on AC drives. However, this topology inherently poses a problem of unbalanced capacitor voltages. This is the main drawback of this structure, as it requires special attention when designing the control architecture and the modulation strategies [21]–[23]. Another inconvenience comes from the voltage blocking capability of the diodes. Indeed, it compulsorily grows with the number of levels, which in turns implies diodes in series, adding components to the structure[24], [25]. These two obstacles explain why NPCs are mostly found for 3 or 5 levels, which automatically reduces the spectrum of applications, especially when aiming at utility grid applications. The electrical scheme of the elementary cell of the 3 Level NPC (3L-NPC) is presented in Fig. 1.2, its global implementation in Fig. 1.3 and the 5 Level one is displayed in Fig. 1.4.

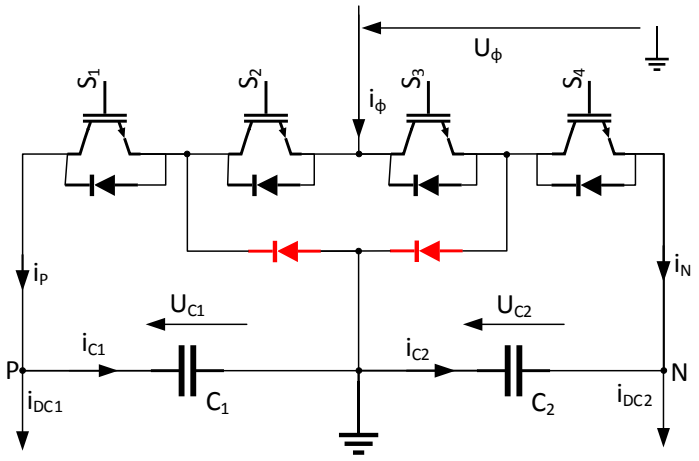

Fig. 1.2. 3L NPC Commutation leg

The cells, or legs, are usually three, or four in certain applications relying, for example, on control of the neutral [26]–[28]. These legs are connected to a common DC-link, as presented in Fig. 1.3. The DC-link is then connected to the DC source or load. The structure of this link requires applying caution to ensure the balance of its two capacitors. The precise combinations of the states of the power switches will be further discussed and described in Chapter II. The multi-level structures displayed here have a lot of potential for power interfacing [29], and even though these are the most mature multi-level topologies, there still are future investigations and many evolutions for the use of NPC converters.

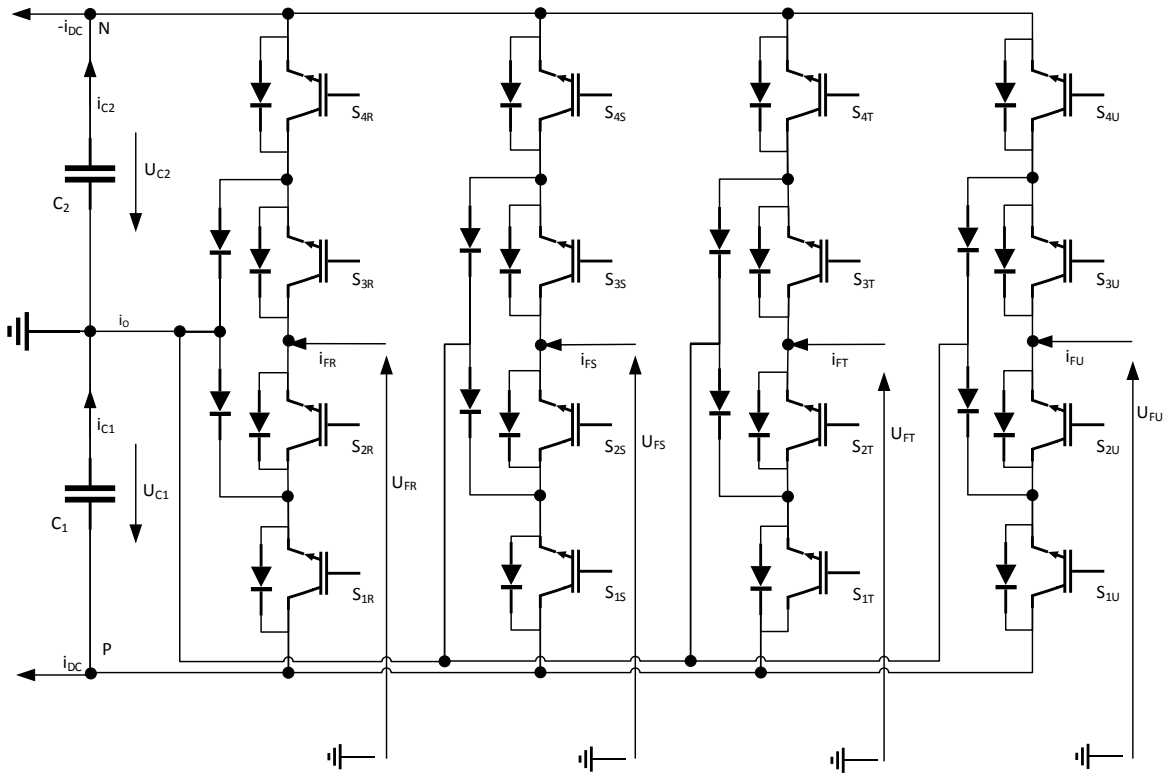

Fig. 1.3. 3L NPC with four legs

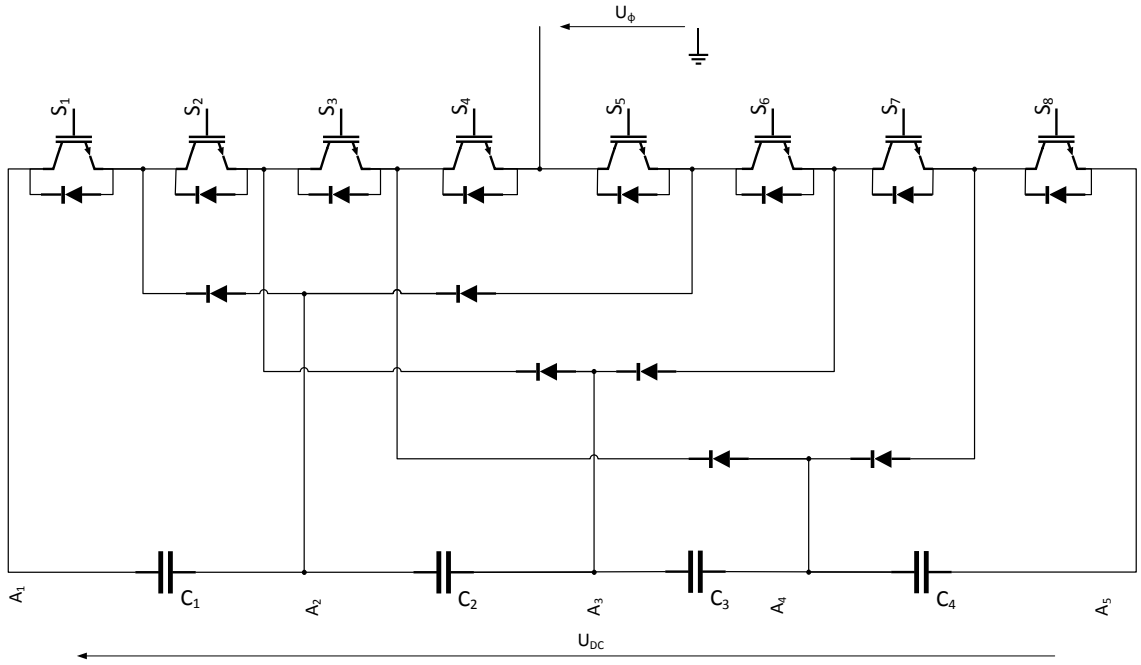

Fig. 1.4. Elementary leg of 5-level NPC

The 5-level topology presented in Fig. 1.4 perfectly illustrates the concept of levels for converters and some of its consequences: the 5 levels, $A_{1...5}$ give more flexibility to the control, and for a given application with fixed power exchange, the capacitors, diodes and power switches see less power flowing through them individually [30]–[32]. However, compared to the three-level topology, the number of diodes tripled, and the number of capacitors and power switches doubled, consequently increasing the overall price of the topology.

1.3.2Flying Capacitor

The Flying Capacitor (FC) topology addresses the diode proliferation issue by using capacitors to block the voltage. Introduced in 1992 [33], this multilevel structure shows independent voltage sources, which solves the unbalanced voltage issue raised by NPC. The capacitors are initially planned to have a fixed voltage, but they are fully controllable, thanks to the distribution of the switches around them. This way, they can be considered as additional inertia for the converter, and it is unique among power converters [3], [34]. The presence of the capacitors can theoretically bring interesting properties, especially when considering faults or designing higher-level topologies. However, the scale of this inertia is often tiny compared to the powers considered. It cannot be treated as a solution to irregular energy production by itself. This topology shares many similarities and advantages with NPC while solving two of its limitations cited earlier. However, other issues arise: the capacitors have to be controlled and managed accurately, which proves difficult for conventional control structures, and they increase the overall cost of the converter considerably [35], [36].

Fig. 1.5 presents the basic switching cell for 3-Level Flying Capacitors (3L-FC), while Fig. 1.6 illustrates the 5-Level topology (5L-FC). The inner capacitor is highlighted in red in Fig. 1.5. Similar to the NPC topology, all legs ultimately connect to the same DC interface, as presented in Fig. 1.7, illustrating the case with 3 phases/legs. The effect of the switches' states will be described further in Chapter II.

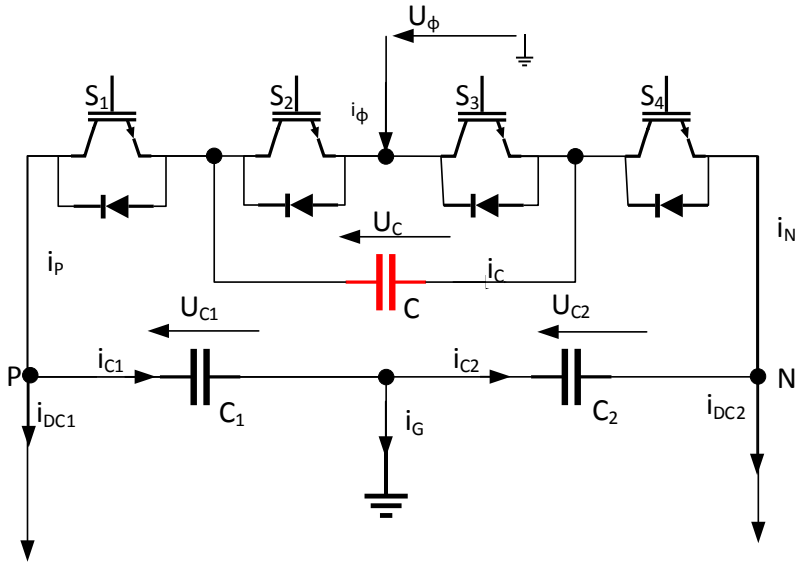

Fig. 1.5. Elementary 3L FC commutation cell

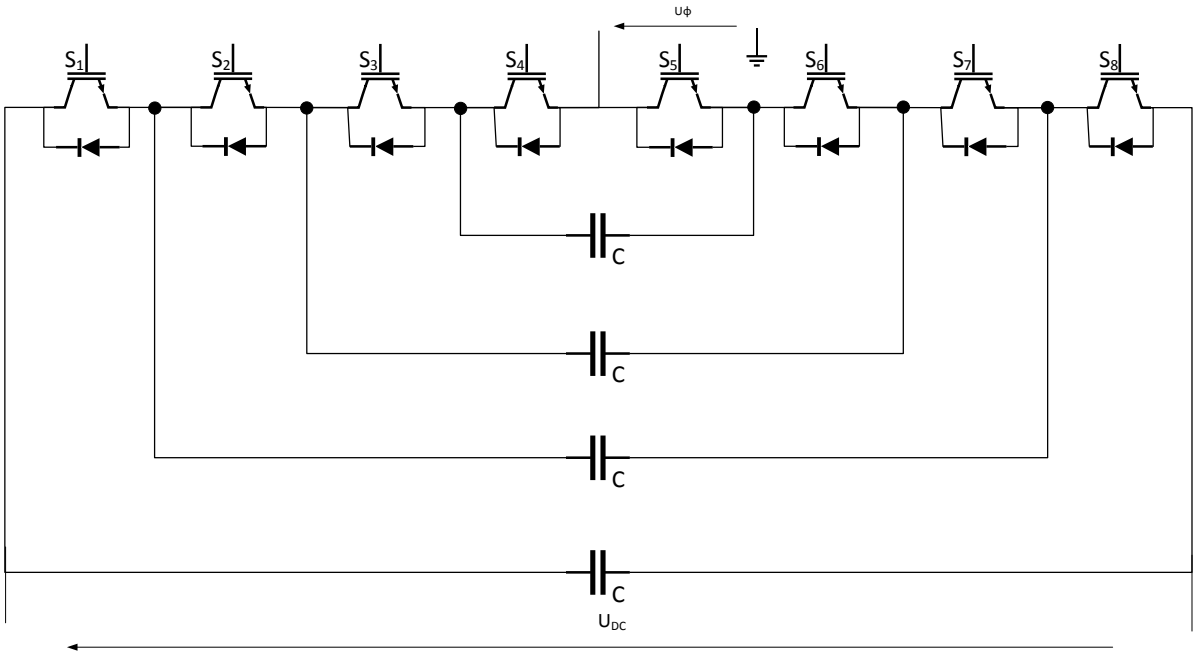

Fig. 1.6. Elementary leg of 5L-FC

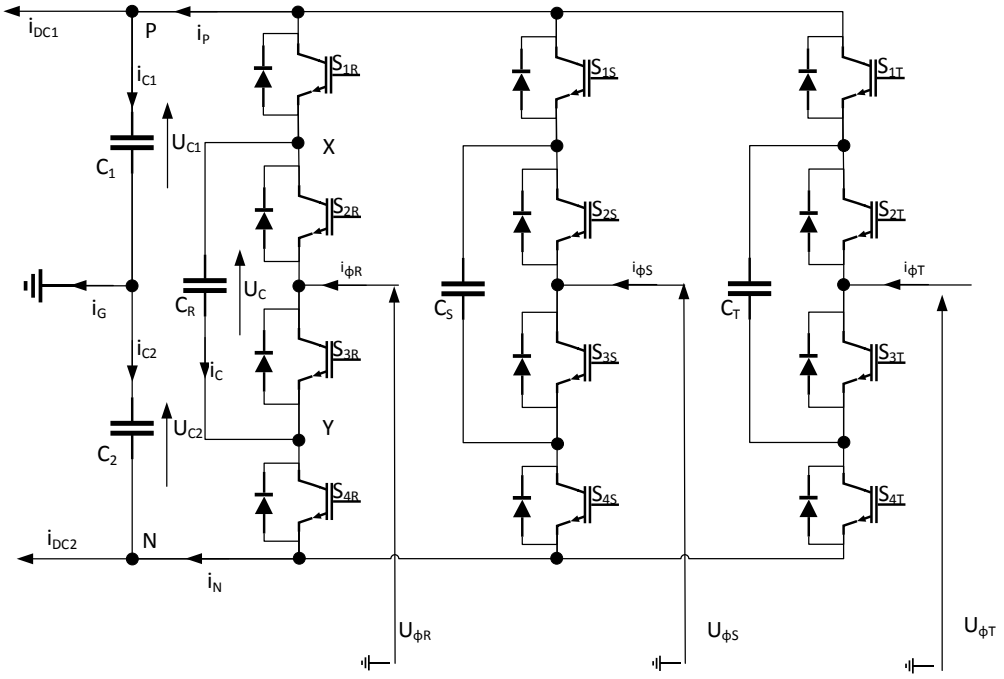

Fig. 1.7. Electrical scheme of 3L-FC with 3-legs

Similar to the situation presented for NPC topologies, raising the number of levels increases the number of components drastically compared to the three-level topology, though a bit less in the case of FC compared to the previous NPC one [37], [38]. The control of the inner capacitors' voltages is managed through redundant connection possibilities: different ways to connect the AC phase to a given point exist, with a capital difference being whether capacitors are being charged or discharged [39]. This means that different power paths connect the same two points, binding the AC and the DC sides identically but impacting the inner components of the converter differently. This redundancy is the base of power balance amongst the components and voltage control of the capacitors. It is especially welcome in case of failure of inner components and for maintenance related issues [40].

1.3.3Cascaded H-Bridge

The Cascaded H-Bridge (CHB) topology was first introduced in 1988 for plasma stabilisation [8]. This structure significantly differs from the two previous ones, with multiple dedicated DC buses. It consists of half of the full-bridges stacked -cascaded- together. The full-bridge structure is displayed in Fig. 1.8. The entanglement generates different voltage levels. This architecture is highly modulable, enabling a very high number of levels. However, its DC sources are all separated, limiting the possibility to be used back-to-back. This topology also shows reliability and fault function as the switches are disposed in such a way that several different switching orders produce identical voltage levels. Finally, this structure is designed for applications bent on accuracy and quality but is not necessarily adapted for bulkier or simpler industrial applications [41]. Because the DC sources/loads are separated, it is fit for interfacing with solar panels: a single multi-level cascaded H-bridge converter can interface several solar panels to the grid alone: in the case of 3 levels, 3

panels, or 3 storage units can connect separately, as shown in Fig. 1.9 [42]–[45]. A 5-level case accommodates double this number, as highlighted by Fig. 1.10, and it keeps growing when accumulating levels.

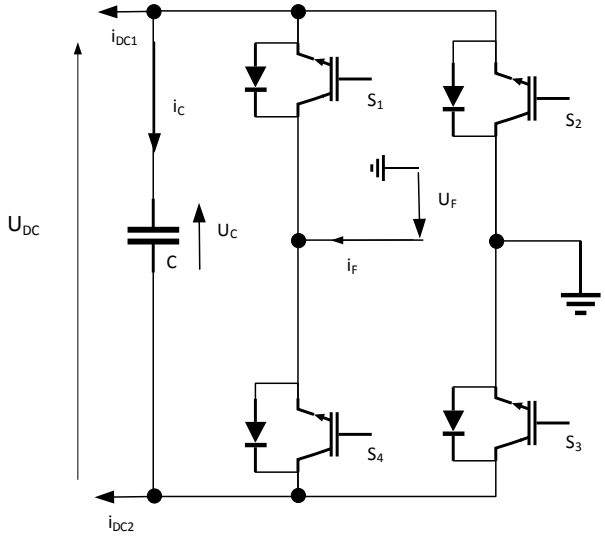

Fig. 1.8. 3L CHB commutation cell

Fig. 1.8 presents the elementary switching leg of 3L-CHB, while Fig. 1.9 illustrates the separated DC links property on a 3 phases case. The extension to 5-level CHB displayed in Fig. 1.10 is extended itself for any number of levels. The 5-level leg is, in fact, the superposition of two 3-level legs, illustrating the modulable aspect of this topology.

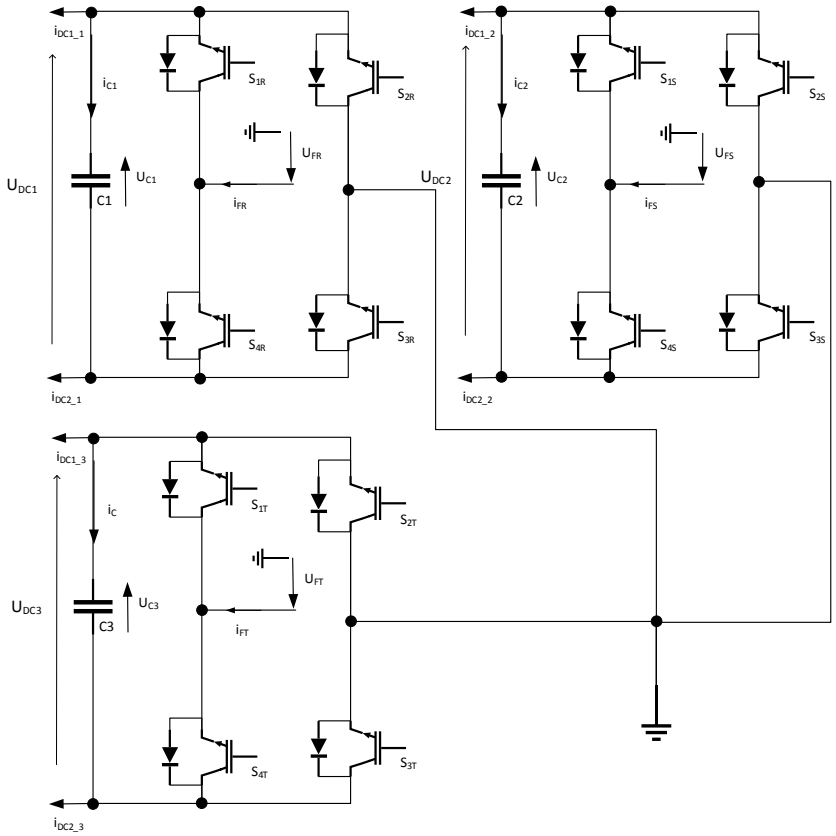

Fig. 1.9. Electrical scheme of 3L-CHB with 3 phases

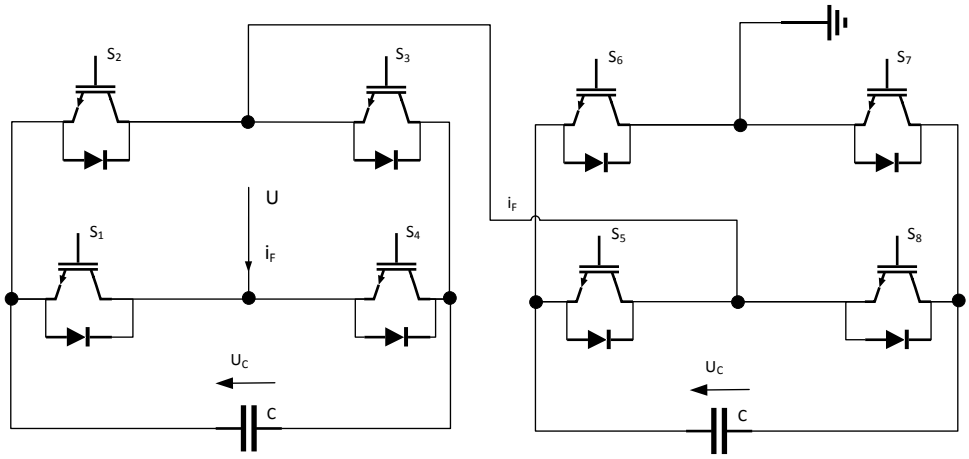

Fig. 1.10. Elementary 5L-CHB leg

1.3.4 Modular Multilevel Converters

Modular Multilevel Converters (MMC) were first introduced in 2001 [46] to address AC-AC conversion for electrical traction. They were later also used for motor drives, high voltage direct current transmission and power quality improvement. They are built by cascading commuting submodules, of which they share the properties. Two dimensions are explored: the layout of the structure and the choice of the submodules [15]. Depending on the choices made, different properties can be extracted or eliminated to generate an application adapted converter. Similar to CHB, MMC is easily deduced for higher levels, which in turn leads to a large variety of applications. An important matter concerning this topology is the ability to perform AC-AC conversion or DC-DC conversion, therefore erasing the need to combine rectifiers and inverters back-to-back [48]. The complexity of the control strategies increases rapidly for these topologies with consequences on computational effort and prices [9].

As the definition is permissive and the research domain still rather recent, new ML-PCs topologies are created and developed for various applications [11], [15], [49], [50], to improve previous results or to reach otherwise impossible objectives. Nevertheless, the industrial sector mostly uses NPC topologies, with 3 levels, and the inclusion of other topologies is bound to happen with time.

2 Power conversion and modulation

2.1 General operation

All ML-PCs, as well as the other power converters, show a hybrid behaviour: they aim to control continuous variables such as the currents and voltages on both sides of the converter, but they act on discrete elements: the states of the power switches. When confronted with this difficulty, the most common

solution is to add an intermediary, charged with translating the continuous considerations in discrete terms. This interface role is addressed by the modulation strategies. The resulting generic control structure is presented in Fig. 1.11. In this figure, a colour code is applied to distinguish the continuous and discrete elements, properly underlining the translation role of the modulation.

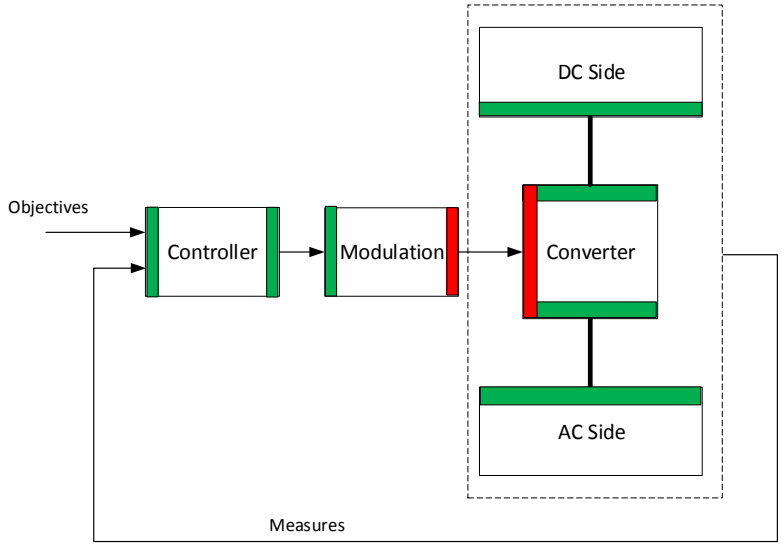

Fig. 1.11. Conventional control structure of power converters, discrete signals in red, continuous in green.

This structure is widely found and well developed, a prime example is that most of the numerous previously cited articles when introducing the different topologies used it. The controller block used here hides a vast range of architectures and objectives, while the modulation block saw various improvements and derivation with time [51]–[54]. This structure underlines the necessary joint progress of the modulation and the control. For instance, the best controller conceivable is pointless when paired with an inappropriate modulation strategy, and vice-versa. Finally, this coupling also enables a separation of objectives: some operating goals are assigned to the control section, while the modulation tackles others.

Typically, the performance of a modulation strategy is established based on efficiency, reliability and signal quality, from an internal point of view.[55], [56] Efficiency is related to minimising the losses, and especially the switching losses, occurring at each power switch action. Reliability is linked to the repartition of the stress on the components and the management of inner values. Finally, the quality of the signal refers to the harmonics contained inferred by the switching actions on the final signal.

Meanwhile, the controller's objectives are oriented towards the external aspects of the conversion, such as the power exchange, the quality of the signals received and delivered, and the tracking of different specific goals related to either the DC or AC side. There is a multitude of such aims, considering the many applications of power converters: the purposes may be different for use in grid-connected or isolated situations when driving a motor or managing a storage system and so on.

2.2 Modulation strategies

As shown in Fig. 1.12, various modulation strategies have been designed to generate acceptable waveforms. The simplest one, staircase modulation, quantises the desired waveform according to the voltage levels brought by the converter [57]. This was the first strategy used due to its easy implementation and low switching frequency. However, the spectral performance is unsurprisingly low [3]. To compensate this weakness, offline adjustments can be computed, giving birth to Pre-Calculated PWM methods [58]. These two strategies compare the desired signal to a horizontal grid constructed from the levels of the converter. Other plans of action are enhanced versions of this quantisation, like Sigma Delta Modulation [59]. It is important to note that these modulation strategies were often devised for GTO thyristors, as they support higher voltages but require a lower switching frequency than their IGBT counterparts, faster but supporting lesser voltages. When considering this other case, other strategies are developed [60].

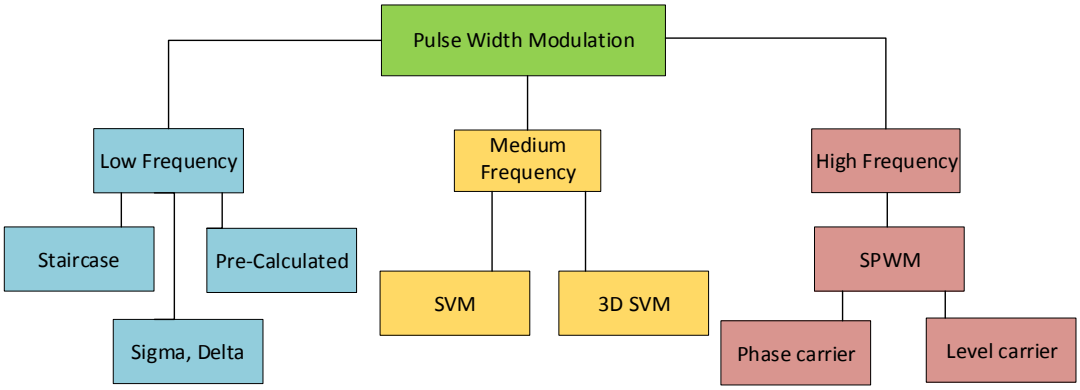

Fig. 1.12. Classification of modulation strategies

The first of these strategies was introduced early for industrial applications and has now been reviewed thoroughly, leading to extensive documentation and variations[61]–[63]. The family born from this technique forms the Sub-harmonic Pulse Width Modulation, also known as Sinusoidal Pulse Width Modulation (SPWM). The technic consists of comparing the desired reference signal with carriers and deciding on the switching events accordingly. The carriers are triangular signals of fixed amplitude and frequency. The frequency of the carrier signal is expectedly far higher than the frequency of the modulating signal, generally by several orders of magnitude. In two-level applications, it is possible and common to use only one carrier, as the switching elements of a phase are complementary. Because the number of switching elements increases with the number of levels, the number of necessary carriers has to follow the trend [64]–[67]. Defining N_{level} the number of levels of a multilevel power converter, the number of carriers used to generate the modulation signals has to be $N_{level} - 1$. Depending on the number of carriers, their form, polarity and respective phase, the harmonic content changes [51], [68]. It is also possible to change the number of references to handle low modulation depths. The modulating signal is generated by a controller, usually designed in the rotating reference frame, meaning that conversions have to be introduced in between the control and modulation steps [69].

The second modulation strategy is cited as early as 1988 [70]. It maps the different voltage positions to create a space vector. The desired voltage is synthesised based on the different switching vectors of the converter. The vectors can be represented in a 3D diagram in its more direct form or a 2D plane when the Clarke transform, and other modelling tools are applied. This modulation technique is well known as Space Vector Modulation (SVM). The space chosen is usually a rotating *d-q* plan, as illustrated in Fig. 1.13. The images are extracted from [29], [71]. The objective of a modulation strategy is to select the bests of these vectors to generate the desired signal properly. Different strategies to choose the switching positions when the point reference is located between different voltage vectors have been studied, with varying results in terms of stress reduction, harmonics suppression or voltage balance [22], [72]–[74]. The 3D-SVM strategy is used when the hypothesis leading to a reduction of the space by Clarke's transform are not met, for example, when the system is unbalanced [75]. This method is an extension of the 2D-SVM, with identical approaches, similar properties and a slightly increased difficulty caused by the additional dimension and the entailing complexity of the vectors.

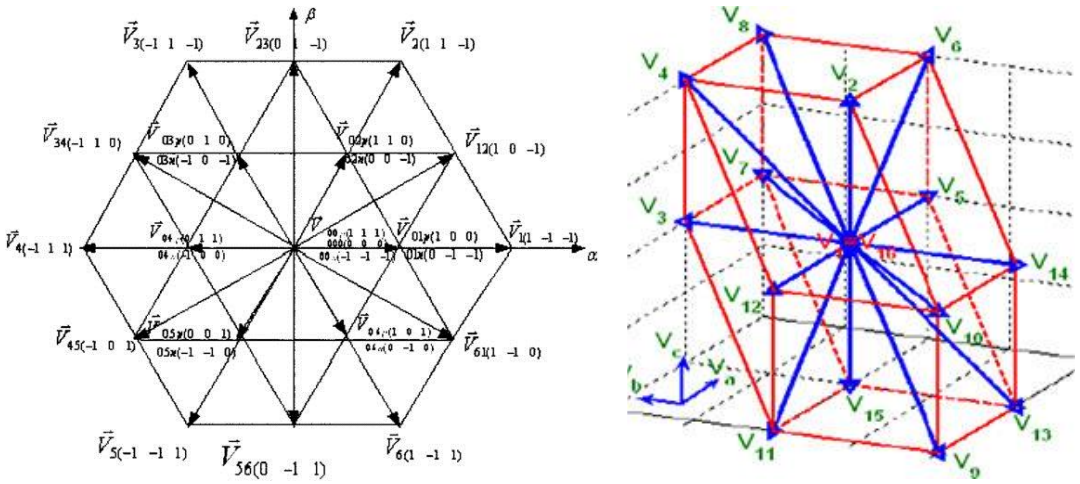

(a) (b)

Fig. 1.13. Space vector representation of a three-level inverter, (a)2d-SVM, (b) 3d-SVM

Overall, the modulation strategies and algorithms have profoundly evolved with time, as the technologies and the requirements evolved as well. New modulation strategies arose to satisfy new or more demanding control objectives and applications[76], [77], [77]–[79]. They present many variations and adaptations, with the 3D-SVM being the most potent and versatile as of now. It is essential to plan the controller and the modulation together, as the models and the inputs change according to the strategy employed, leading to an adaptation of the controller.

3 Control architectures

Power converters are elements found in close to all applications in the electric grid, at every level: the power conversion is necessary for almost all power levels and modes. They are always associated with other elements, which determine the function of the power converters: their role is to interface two electric components, themselves often part of an ensemble of electric components. Control objectives derive from

that function, leading to a variety of control requirements proportional to the diversity of applications. This property is illustrated in Fig. 1.14, where each element generates control requirements that can concern a large array of problems, from the energy flow of a grid to the switching losses of the converter. The resulting architectures are therefore numerous as well. Power conversion and power electronics are a rather mature technology, and their control is similarly advanced. As a consequence, the control of power converters is subjected to issues such as reliability, robustness, efficacity and many other performance criteria [80]–[82].

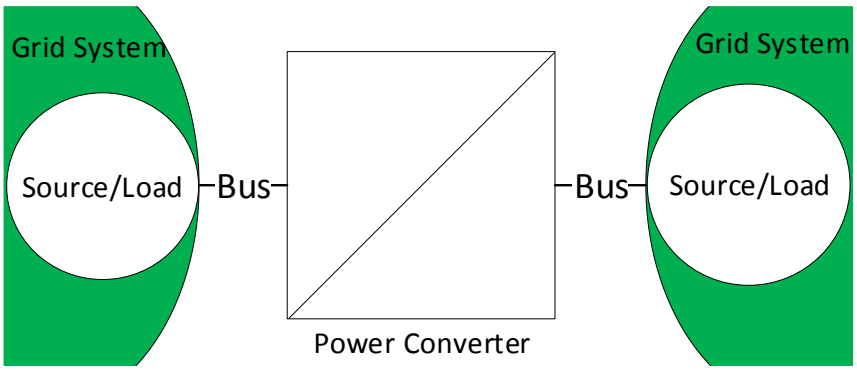

Fig. 1.14. General context of power conversion.

The way power converters operate lead to a separation of the control objectives in two parts. On one side, the objectives related only to the converter itself, and on the other side, the ones linked to the elements connected to the converter. These control requirements have different timescales and rely on different modelling methods. It is often possible to cleanly separate them and to treat them separately. This differentiation is accentuated by the previously stated hybrid nature of power converters: they naturally lead to non-linear control. To recapitulate, the main issues that control architectures for power converters have to face are as follow. First, the control requirements and constraints are numerous and vary with the applications. Second, power converters are non-linear by nature. Third, the demands regarding the quality of the control are always stricter, as they reflect the maturation of the technology [83], [84].

3.1 Modulation-based control

3.1.1 Linear control

The very first consideration, the most limiting one, is with no doubt the non-linearity ensuing from the switching nature of power converters. In order to bypass this difficulty, modulation strategies have been, and are still being, developed to serve as an intermediary between the general control structure and the converter. The general, or upper, structure can then ignore the non-linear aspect of the control problem and focus on other priorities. The control problem is very different when considering the addition of the power converter and its modulation block instead of the power converter alone. In particular, the model of

the controlled plant changes drastically: the high switching frequency and the modulation strategy lead to the removal of several dynamics of the converter, and to the establishment of averaged models of the system formed by the power converter plus its modulation strategy [15], [85]. These dynamics are considered as handled by the modulation block and therefore require no care from the other controllers, which can then consider the dynamics of the connected electric components and simply transmit the necessary references to the modulation block. The general scheme resulting from this repartition of the tasks is given in Fig. 1.15. This scheme is very general and summarises the approach of every modulation-based control structure. Very often, the control is distributed hierarchically, where different objectives are separated from each other according to their importance and their dynamics, and different controllers are allocated to them. In this thesis, only levels of control close to the converter are studied.

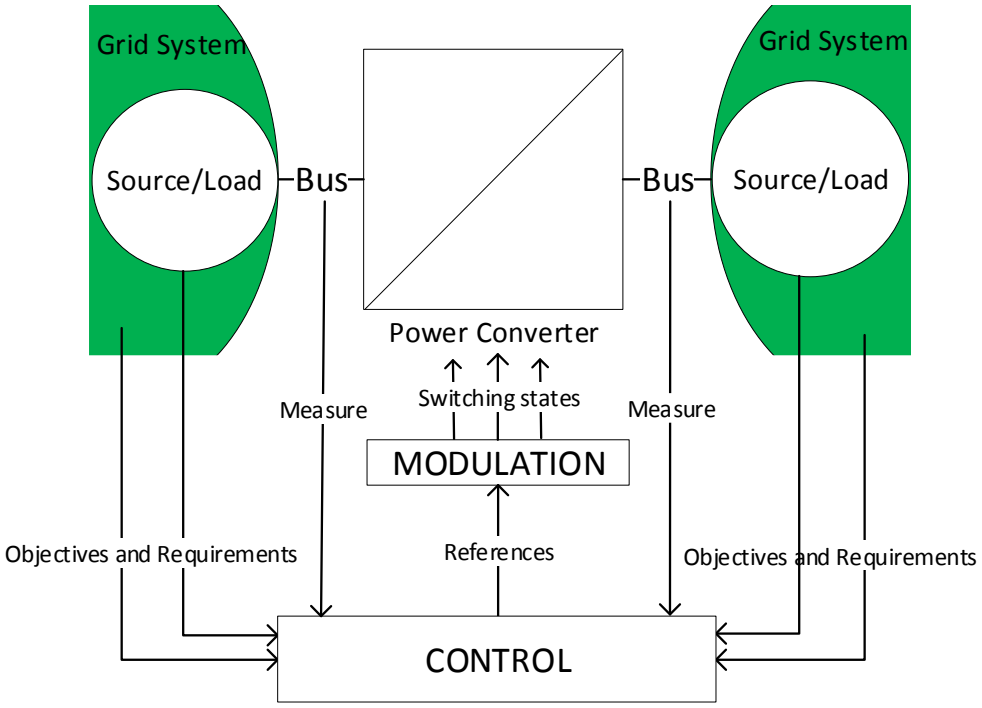

Fig. 1.15. General control structure of a modulation-based architecture

The resulting architectures rely on the modulation block, whose complexity and importance has been stated in I.2, to accurately transmit their orders to the converter. The main question is then to express the miscellaneous control requirements arising from the many possible applications and situations. For linear controllers, it is necessary to have linearly independent objectives. The power flow is a very common objective, separated with two different methods. The power is related to the product of the voltage and the current, which have very different time responses. As a consequence, it is possible to cascade their respective control loops and consider the two control problems separately. Another method relies on transformations and is particularly well adapted to simplify AC systems. These transformations are based on a vector approach of the sinusoidal signals to express them in a different plane. [86]

Typically, electrical and mechanical behaviours and dynamics are expressed for generators and most rotating machines, but chemical modelling could also be implied when considering storage systems or any other necessary method. The resulting control structure then possesses requirements on the electric components connected to the power converter. These elements are therefore modelled and added to the averaged model of the modulation-controlled power converter. The phenomena considered and studied deeply modify the control structure, as a typical example is the application of transforms to simplify the situation [83]. These include the Park, Clarke, Concordia and Fortescue transforms, used to express the three-phase problem in a more comfortable form. They rely on a space-vector approach and are used to make a continuous system out of alternative signals. This way, it becomes easier to tackle the different issues of power and to express the control problem with a linear approach.

The Clarke transform is used to reduce the number of dimensions of the signals: under the condition that it is balanced, applying this transformation to a three-phase system outputs a two-phase one. The Clarke transform conserves the amplitude of the signal, but not the powers. The Concordia transformation is similar; only it conserves the power instead of the amplitudes [87]. These two operations are equivalent to observing the system from the point of view of the stator of a rotating generator, and they reduce the size of the problem –for balanced systems– but they do not simplify the oscillating aspect of the signals. The Park's transform goes further and introduces a rotation of the base expressed by Clarke's transform. This requires information on the angle of rotation of the signals, retrieved via a Phase Lock Loop (PLL) block. This rotation frame is used to stick the new base on the rotor instead of on the stator: the signals are oscillating at the same frequency as the base, which eliminates their alternative nature [88]. With this method, three-phased balanced oscillating signals are transformed into two continuous signals, which considerably simplifies the expression of the control of the system. The Fortescue transform is used to decompose an unbalanced three-phased system into three balanced systems, called zero, positive and negative. The method is also known as the symmetrical component's method, and it leads to mutually linearly independent components, which can be exploited for linear control [89].

Overall, the main idea concerning the control of power converters is that this area actually does not focus on the converters but on the elements they interface. Even if the same converter is used, its control structure will change whether it operates with a solar plant, a rotating machine, a DC grid or any other application. Depending on the models and the different transformations used to express the control problem, the structure itself can change. However, the objective of this operation is to cull linearly independent or dynamically independent objectives, which in turn makes it possible to apply all the theoretical PID and linear control architectures on power converters, as long as the modulation is performed smoothly.

The control of the relative objectives of each side of the converter is also often separated, with cascading loops of linear control dedicated to their own goal and dynamics. These objectives can also impact differently the modulation itself, depending on the algorithms it uses, leading to intertwined loops of control

routing to different elements of the modulation function. For example, the control of the DC link of 3-Level NPC converters can be separated from the AC power exchange control when using SVM strategy [29]. The control of the DC voltage is done by playing with the redundancy offered by the topology: several vectors have the same impact on the AC signals, but they present different consequences on the DC part. Incorporating this property in the control structure is possible when knowing the behavior of the modulation strategy. Consequently, instead of solely feeding the modulation strategy a voltage and frequency reference —which is preferable when using SPWM strategies— it is possible to provide more information with the SVM method, which further enriches the control structure. The choice of the modulation strategy is fundamental to the design of the control structure behind [29], [76]. The ensuing general control architecture is presented in Fig. 1.16. The controlled system and the control objectives concern the addition of the power converter with the electrical components connected to it. The transformations, and other operations used for example to uncouple some bound variables, help to express a linear control problem and a linearised controlled system. Then, the linear control adopted can take any of the forms of linear control in its entirety, with PID loops, sometimes in cascade, representing the majority of the cases.

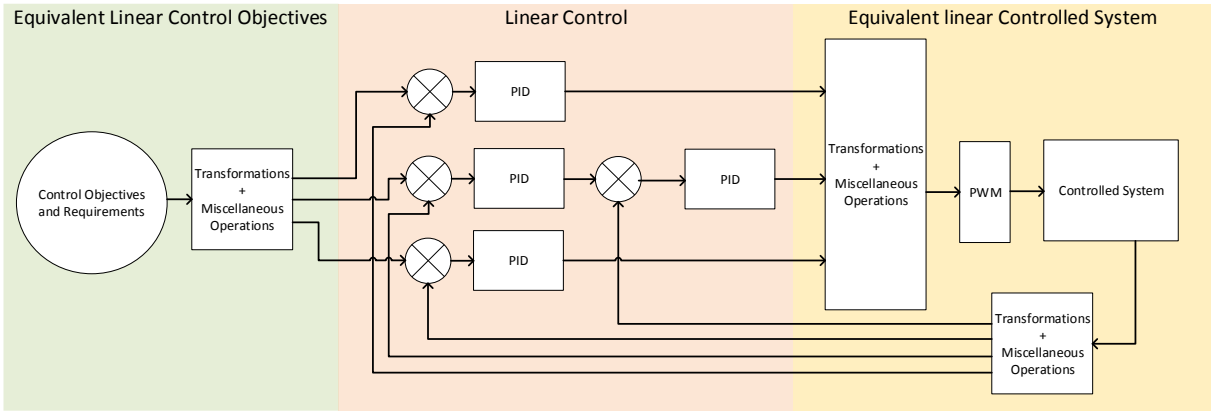

Fig. 1.16. General structure of linear control for power converters

3.1.2Other advanced controllers

All the control problems resulting from the different applications of power conversion are expressed independently thanks to various transformations and modeling methods. This enables the development of linear control loops, but also to try and apply more advanced controllers, at different levels. Advanced strategies are found at three different levels of control: the modulation level, the interfacing level and a more general, higher level. This thesis will not dwell on this last part. However, both the modulation and interfacing control are prone to optimisation and other advanced strategies.

To begin with, the modulation aspect sees implementations of optimisation methods such as machine-learning based strategies. The objectives are to improve the Total Harmonic Distortion (THD) of the obtained signal, to maximise the efficiency of the converter and to ensure robustness of the modulation

block. Genetic algorithms are found, as well as neural networks, to explore ways to better the modulation algorithms [90]–[92].

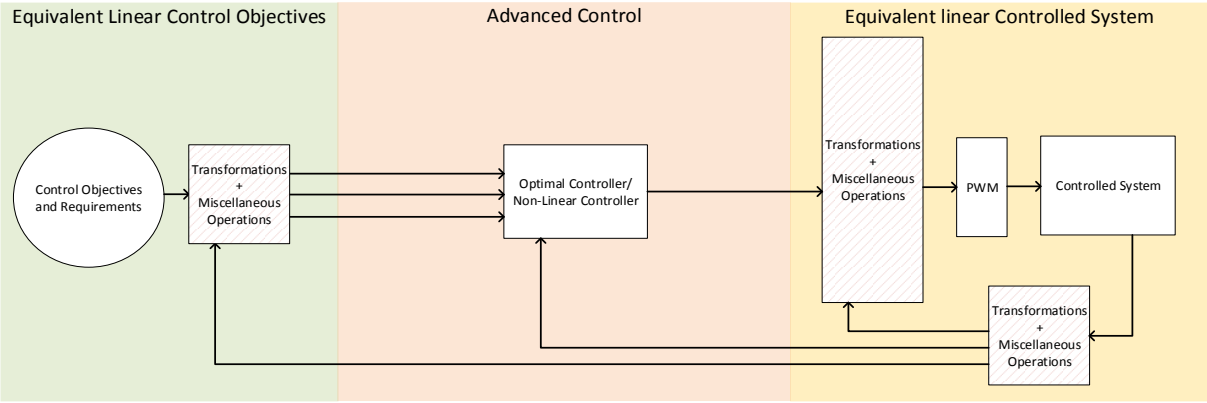

Fig. 1.17. General structure of advanced control architectures with modulation. The striped blocks are sometimes either not necessary or included in the controller.

Otherwise, the control structure related to the function of the power converters sees a lot of possible advanced algorithms. The resulting general architecture is displayed in Fig. 1.17, which highlights one of the advantages of these methods: the control algorithms are often advanced enough to handle a part of the non-linearity and to simplify the integration of the different objectives and requirements omnipresent when considering power converters and their applications. Among those algorithms, Sliding Mode Control (SMC) and Model Predictive Control (MPC) are two families that have been implemented to control power converters. Sliding Mode Control (SMC) is a non-linear control method using a discontinuous control signal that influences a non-linear system to move along a crossed section defined by a function called sliding or switching function. This technique has gained constant interest thanks to its superior robustness, which makes SMC scheme particularly adapted to the power converter field because of the variable conditions in which it operates. SMC is a robust control strategy that shows great versatility and many various forms, depending on the choice of the switching variables, of the control variables or the control order. SMC can be associated with power electronics to propose advanced performances overall [93]–[96].

MPC is an optimisation algorithm that also defines a function to operate. Called the cost function, this key element is designed to represent the control objectives of the system. The algorithm uses an inner model to perform a closed-loop optimisation based on prediction. For linear systems, MPC is equivalent to a closed-loop Linear Quadratic Regulator (LQR) [97], [98]. One strength of MPC relies on its definition: even though its most common form is based on linear optimisation, it is possible to change both the prediction model and the optimisation algorithm to adapt to other situations. Another asset of MPC is its ability to handle both Multi Input Multi Output (MIMO) systems and constraints intrinsically [98]. This property is welcomed for power converters, as the control requirements they have to meet are often strict and as they usually are confronted with MIMO applications. Two MPC algorithms are found in control architectures relying on modulation, such as General Prediction Control (GPC) which applies the most

classical linear quadratic MPC form, [99], [100], and the Explicit MPC (EMPC) which operates with offline parametric optimisation to gain time when running [101].

3.2 Modulation-less structures

The previous architectures always separated the nature and the function of power converters: the control of the switches is done separately from the control of the flows traded through the converter. The reasons for this segregation are two. The first one is the high non-linearity that results from the hybrid dynamics emerging from the very definition of power conversion methods. The second reason is the difference in time dynamics of the two domains: the switching frequency of power converters is very high, which demands fast-paced control, while the dynamics of the electric phenomena can be much slower, in particular when considering the grid, storage or RES applications, which suggests lesser time constraints on the control. The use of modulation then enables the development of controllers subjected to the latter lenient time requirements [85], [102].

These two issues sum up perfectly the difficulty of designing a controller meant to manage the switching operations and the power flow of the converter directly. However, the separation of the control objectives into two sides is not as clear as expected: with the need for efficiency and reliability, it becomes interesting to add intelligence to the commutation. This wisdom can be attained by closing the loop of modulation: so far, the modulation block receives order and translates those to the converter's switches, it is operating in open loop. One of the ideas motivating modulation-based structures is to reconciliate the different dynamics of power conversion to close the control loop, as presented in Fig. 1.18: the control structure receives feedback and control objectives directly related to the nature of the power converter and adds them to the ones extracted from the application [103]–[105].

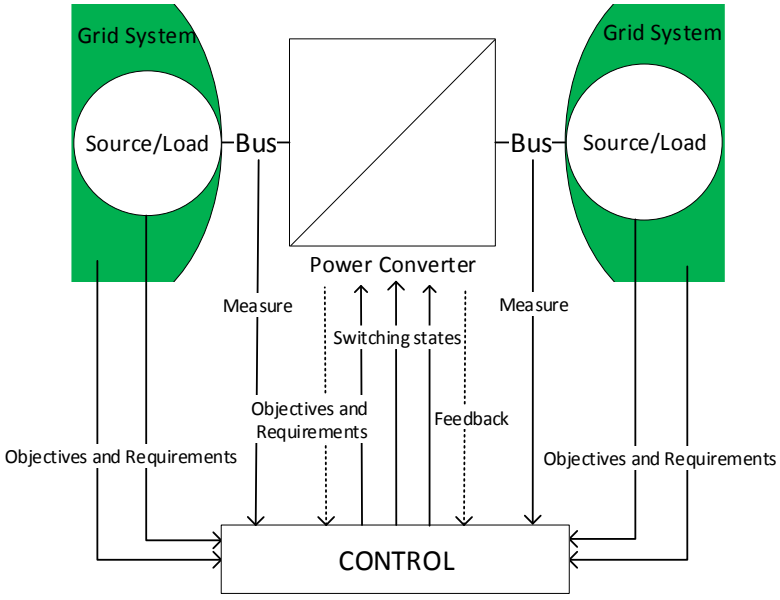

Fig. 1.18. General control structure of a modulation-less architecture

Another motivation for modulation-less structures is related to the dependence between the different levels of control: the developments of modulation and control have to be performed simultaneously to ensure better performances. In consequence, control architecture and its tuning are designed for a specific modulation strategy, for a particular power converter and a particular application. This ends up diminishing the universality and the flexibility of these global control structures strongly. Hence the interest of devising a control architecture more polyvalent and more adaptative, which can be done by directly incorporating the nature and the function of the power converters altogether.

The number of algorithms able to handle this ambivalence is limited, as addressing both the non-linearity and the humongous computational stress is extremely difficult. However, thanks to the exponential growth of computational power, made possible by advances in informatics, the calculation pressure is greatly reduced, which opens the door to computationally heavy algorithms, minding adaptations. So far, two main approaches dominate can be considered to control power converters without modulation. The SMC algorithms introduced earlier are initially designed to operate with switching elements, which makes them particularly adapted to the situation. However, the application of these algorithms on power converters without modulation is only possible up to 2-level power converters: the relations between the switching states and the control objectives are too intricated, numerous and complex to use these two in conjunction [106].

The other prospective family of controllers for modulation-less structures is MPC. In fact, as long as a model and an optimisation algorithm are found, a MPC controller can be developed. The branch of MPC for power converters without modulation is called Finite Control Set MPC (FCS MPC) and leads to two subfamilies: the Optimal Switching Vector MPC (OSV MPC) and the Optimal Switching Sequence MPC (OSS MPC). The main difference between these algorithms is the attention given to the switching frequency. In the case of OSV MPC, this frequency is not fixed: the algorithm finds an optimal vector of switching status with no cares given to the ensuing frequency, while the OSS MPC algorithm selects a sequence of changes. In this case, the number of commutations is already decided for the duration of the sequence, which permits managing the switching frequency [102], [107]–[109].

The FCS MPC algorithms define and model the power converter with the different possible switching positions it can exhibit. They use these models to evaluate the available future systems depending on the switching states. Next, they compare these possible predicted futures according to a cost function and finally elect the optimal one. This method evolves with the depth of the prediction, the type of model and the type of optimisation algorithm used. The limits to the definition of the cost function are virtually inexistent, but the computational cost is explosive. Indeed, MLPCs offer a large number of possible switching states and increasing the depth of prediction and optimisation only leads to an exponential number of potentialities considered to solve the optimisation problem. For this reason, the FCS MPC algorithms for MLPCs often have one step of optimisation, or use commercial optimisers [103], [110], [111].

FCS MPC shows a high potential for the control of MLPCs, especially concerning the ease of use and implementation. Indeed, the controller's structure does not change with the different hypothesis applied on the system, and a low number of elements need to be tuned, especially when compared to the PID structures where at least one controller is assigned to each objective [112]. Many control requirements can be put into action, even non-linear ones or constraints, without modifying the algorithms of control. This polyvalence and this flexibility come along the universality of the approach: the methods employed to build the FCS-MPC algorithms can be applied to all power converters with no exception. The properties of the four MPC algorithms encountered earlier are collected in Table 1.2.

TABLE 1.2
MOST USED MPC STRATEGIES FOR POWER ELECTRONICS

MPC Strategy	GPC	EMPC	OSV-MPC	OSS-MPC
Modulation	Yes	Yes	Not required	Not required
Switching frequency	Fixed	Fixed	Not fixed	Fixed
Optimisation	Online	Offline	Online	Online
Constraints	No	Yes	Yes	Yes
Horizon	Long	Long	Short	Short
Formulation	Complex	Complex	Intuitive	Intuitive
References	[99], [100]	[101]	[102], [107]	[108], [109]

The different algorithms and approaches introduced earlier are compiled in Table 1.3. Their comparison is based on different criteria such as the ability to handle the MIMO problems naturally generated by power converters and their applications, the possibility to add constraints and the need for additional transforms to express the objectives. The robustness and the number of different elements needing tuning are also considered. This analysis shows that the main solution to handle the non-linearity of power converters to design a flexible and universal controller seems to be the FCS-MPC.

TABLE 1.3
CONTROL STRUCTURES FOR ML-PCS

Control Structure	Linear Control	CCS-MPC	FCS-MPC	SMC
Modulation	Yes	Yes	No	Yes, for MLPCs
MIMO management	No	Yes	Yes	Yes
Optimisation	No	Yes	Yes	Yes
Constraints	No	Yes	Yes	Yes
Tuning necessary	High	Low	Low	Low
Formulation	Complex	Complex	Intuitive	Complex
Robustness	Low	High	High	High
Dependency on transformations	Yes	Yes	No/Limited	No/Limited

4 Conclusion

Throughout this chapter, the technology of multi-level power converters has been discussed, highlighting their high potential for medium to high power applications. Some typical topologies were presented, including the Neutral-Point Clamped, the Flying Capacitor and the Cascaded H-Bridge, whose 3 level forms will be the centre of the study in the following chapters. The potential for these three ML-PCs is very high and promising for future micro-grid applications. The complexity of the control of such converters has also been underlined, with the need for an intermediary between the controller and the plant: the modulation. This block has been presented and some of its implementations described.

A certain distribution of the control objectives and requirements has been underlined, with the modulation strategy tackling most of the inner goals while the control is designed to manage the interfacing aspects and the specificity of the applications. It has been shown that linear controllers are the most common approach concerning this second side of the control, but also that advanced control strategies are being developed and implemented as the complexity of the control system and the control requirements keeps growing with the maturity of power converters and the novelty of their applications. Examples of such advanced control include genetic algorithms (used in the modulation block), SMC and MPC. With the motivation to conciliate the non-linearity of MLPCs and their MIMO aspect with a single, polyvalent and universal control structure, MPC algorithms emerge as particularly interesting

5 Bibliography

[1] N. Mohan, T. M. Undeland, and W. P. Robbins, *Power electronics: converters, applications, and design*, 3rd ed. Hoboken, NJ: John Wiley & Sons, 2003.

[2] B. M. Bird and K. G. King, *An introduction to power electronics*. United States: John Wiley and Sons, Inc.,New York, NY, USA, 1983.

[3] and, 'Multilevel converters-a new breed of power converters', *IEEE Trans. Ind. Appl.*, vol. 32, no. 3, pp. 509–517, May 1996, doi: 10.1109/28.502161.

[4] Bum-Seok Suh, Gautam Sinha, M. D. Manjrekar, and T. A. Lipo, 'Multilevel Power Conversion - An Overview Of Topologies And Modulation Strategies', in *Proceedings of the 6th International Conference on Optimization of Electrical and Electronic Equipments*, May 1998, vol. 2, p. AD-AD, doi: 10.1109/OPTIM.1998.708006.

[5] S. Khomfoi and L. M. Tolbert, '17 - Multilevel Power Converters', in *Power Electronics Handbook (Third Edition)*, M. H. Rashid, Ed. Boston: Butterworth-Heinemann, 2011, pp. 455–486.

[6] Remus Teodorescu, Marco Liserre, and Pedro Rodriguez, 'Grid Converter Structures for Wind Turbine Systems', in *Grid Converters for Photovoltaic and Wind Power Systems*, IEEE, 2007, pp. 123–143.

[7] Mahinda Vilathgamuwa, Dulika Nayanasiri, and Shantha Gamini, *Power Electronics for Photovoltaic Power Systems*. Morgan & Claypool, 2015.

[8] M. Marchesoni, M. Mazzucchelli, and S. Tenconi, 'A non conventional power converter for plasma stabilization', in *PESC '88 Record., 19th Annual IEEE Power Electronics Specialists Conference*, Apr. 1988, pp. 122–129 vol.1, doi: 10.1109/PESC.1988.18125.

[9] R. Marquardt, 'Modular Multilevel Converter: An universal concept for HVDC-Networks and extended DC-Bus-applications', in *The 2010 International Power Electronics Conference - ECCE ASIA -*, Jun. 2010, pp. 502–507, doi: 10.1109/IPEC.2010.5544594.

[10] H. M. P and M. T. Bina, 'A Transformerless Medium-Voltage STATCOM Topology Based on Extended Modular Multilevel Converters', *IEEE Trans. Power Electron.*, vol. 26, no. 5, pp. 1534–1545, May 2011, doi: 10.1109/TPEL.2010.2085088.

[11] M. A. Perez, D. Arancibia, S. Kouro, and J. Rodriguez, 'Modular multilevel converter with integrated storage for solar photovoltaic applications', in *IECON 2013 - 39th Annual Conference of the IEEE Industrial Electronics Society*, Nov. 2013, pp. 6993–6998, doi: 10.1109/IECON.2013.6700292.

[12] A. Nabae, I. Takahashi, and H. Akagi, 'A New Neutral-Point-Clamped PWM Inverter', *IEEE Trans. Ind. Appl.*, vol. IA-17, no. 5, pp. 518–523, Sep. 1981, doi: 10.1109/TIA.1981.4503992.

[13] T. Salzmann, G. Kratz, and C. Daubler, 'High-power drive system with advanced power circuitry and improved digital control', in *Conference Record of the 1991 IEEE Industry Applications Society Annual Meeting*, Sep. 1991, pp. 272–278 vol.1, doi: 10.1109/IAS.1991.178166.

[14] A. Krishna R and L. P. Suresh, 'A brief review on multi level inverter topologies', in *2016 International Conference on Circuit, Power and Computing Technologies (ICCPCT)*, Mar. 2016, pp. 1–6, doi: 10.1109/ICCPCT.2016.7530373.

[15] A. Dekka, B. Wu, R. L. Fuentes, M. Perez, and N. R. Zargari, 'Evolution of Topologies, Modeling, Control Schemes, and Applications of Modular Multilevel Converters', *IEEE J. Emerg. Sel. Top. Power Electron.*, vol. 5, no. 4, pp. 1631–1656, Dec. 2017, doi: 10.1109/JESTPE.2017.2742938.

[16] Y. P. Siwakoti, S. Liese, A. Mahajan, A. Palanisamy, D. Rogers, and F. Blaabjerg, 'A New Seven-Level Active Boost Neutral Point Clamped (7L-ABNPC) Inverter', in *2018 IEEE Energy Conversion Congress and Exposition (ECCE)*, Sep. 2018, pp. 5636–5642, doi: 10.1109/ECCE.2018.8558067.

[17] M. Narimani, B. Wu, G. Cheng, and N. Zargari, 'A new nested neutral point clamped (NNPC) converter for medium-voltage (MV) power conversion', in *2014 IEEE Applied Power Electronics Conference and Exposition - APEC 2014*, Mar. 2014, pp. 2372–2377, doi: 10.1109/APEC.2014.6803635.

[18] G. B. Lee, F. Engelbrecht, and H. J. Beukes, 'Series-stacked and neutral point clamped multilevel converter topologies for MVDC transmission', in *IEEE AFRICON. 6th Africon Conference in Africa,* Oct. 2002, vol. 2, pp. 735–741 vol.2, doi: 10.1109/AFRCON.2002.1160005.

[19] D. Floricau, E. Floricau, L. Parvulescu, and G. Gateau, 'Loss balancing for Active-NPC and Active-Stacked-NPC multilevel converters', in *2010 12th International Conference on Optimization of Electrical and Electronic Equipment*, May 2010, pp. 625–630, doi: 10.1109/OPTIM.2010.5510438.

[20] N. S. Choi, J. G. Cho, and G. H. Cho, 'A general circuit topology of multilevel inverter', in *PESC '91 Record 22nd Annual IEEE Power Electronics Specialists Conference*, Jun. 1991, pp. 96–103, doi: 10.1109/PESC.1991.162660.

[21] B. Fan, W. Zhao, W. Yang, and R. Li, 'A simplified SVPWM algorithm research based on the neutral-point voltage balance for NPC three-level inverter', in *2012 IEEE International Conference on Automation and Logistics*, Aug. 2012, pp. 150–154, doi: 10.1109/ICAL.2012.6308188.

[22] F. Guo, T. Yang, S. Bozhko, and P. Wheeler, 'A Novel Virtual Space Vector Modulation Scheme for Three-Level NPC Power Converter with Neutral-Point Voltage Balancing and Common-Mode Voltage Reduction for Electric Starter/Generator System in More-Electric-Aircraft', in *2019 IEEE Energy Conversion Congress and Exposition (ECCE)*, Oct. 2019, pp. 1852–1858, doi: 10.1109/ECCE.2019.8913186.

[23] X. Lin, S. Gao, J. Li, H. Lei, and Y. Kang, 'A new control strategy to balance neutral-point voltage in three-level NPC inverter', in *8th International Conference on Power Electronics - ECCE Asia*, Jun. 2011, pp. 2593–2597, doi: 10.1109/ICPE.2011.5944742.

[24] J. Ewanchuk, J. Salmon, and B. Vafakhah, 'A Five-/Nine-Level Twelve-Switch Neutral-Point-Clamped Inverter for High-Speed Electric Drives', *IEEE Trans. Ind. Appl.*, vol. 47, no. 5, pp. 2145–2153, Oct. 2011, doi: 10.1109/TIA.2011.2161857.

[25] T. Heinzel, K. Komatsu, M. Kakefu, S. Okita, Y. Kobayashi, and O. Ikawa, 'Three-phase Advanced Neutral-Point-Clamped IGBT module', in *2012 15th International Power Electronics and Motion Control Conference (EPE/PEMC)*, Sep. 2012, p. LS2a.4-1, doi: 10.1109/EPEPEMC.2012.6397406.

[26] M. Sharifzade, H. Vahedi, A. Sheikholeslami, H. Ghoreyshi, and K. Al-Haddad, 'Modified selective harmonic elimination employed in four-leg NPC inverters', in *IECON 2014 - 40th Annual Conference of the IEEE Industrial Electronics Society*, Nov. 2014, pp. 5196–5201, doi: 10.1109/IECON.2014.7049291.

[27] M. Rivera, J. Rodriguez, V. Yaramasu, and B. Wu, 'Predictive load voltage and capacitor balancing control for a four-leg NPC inverter', in *2012 15th International Power Electronics and Motion Control Conference (EPE/PEMC)*, Sep. 2012, p. DS3c.8-1, doi: 10.1109/EPEPEMC.2012.6397344.

[28] M. Sharifzadeh, H. Vahedi, A. Sheikholeslami, P. Labbé, and K. Al-Haddad, 'Hybrid SHM–SHE Modulation Technique for a Four-Leg NPC Inverter With DC Capacitor Self-Voltage Balancing', *IEEE Trans. Ind. Electron.*, vol. 62, no. 8, pp. 4890–4899, Aug. 2015, doi: 10.1109/TIE.2015.2405059.

[29] Q. Tabart, I. Vechiu, A. Etxeberria, and S. Bacha, 'Hybrid Energy Storage System Microgrids Integration for Power Quality Improvement Using Four-Leg Three-Level NPC Inverter and Second-Order Sliding Mode Control', *IEEE Trans. Ind. Electron.*, vol. 65, no. 1, pp. 424–435, Jan. 2018, doi: 10.1109/TIE.2017.2723863.

[30] H. Chang, R. Wei, Q. Ge, X. Wang, and H. Zhu, 'Comparison of SVPWM for five level NPC H-bridge inverter and traditional five level NPC inverter based on line-voltage coordinate system', in *2015 18th International Conference on Electrical Machines and Systems (ICEMS)*, Oct. 2015, pp. 574–577, doi: 10.1109/ICEMS.2015.7385100.

[31] J. A. F. Neto, R. P. T. Bascopé, and R. G. A. Cacau, 'A five-level stacked neutral point clamped converter based on multi-state switching cell', in *2017 Brazilian Power Electronics Conference (COBEP)*, Nov. 2017, pp. 1–6, doi: 10.1109/COBEP.2017.8257281.

[32] H. Dallagi, 'Modelling, simulation and analysis of three phase five level NPC inverter for induction motor drive', in *2015 16th International Conference on Sciences and Techniques of Automatic Control and Computer Engineering (STA)*, Dec. 2015, pp. 562–569, doi: 10.1109/STA.2015.7505196.

[33] T. A. Meynard and H. Foch, 'Multi-level conversion: high voltage choppers and voltage-source inverters', in *PESC '92 Record. 23rd Annual IEEE Power Electronics Specialists Conference*, Jun. 1992, pp. 397–403 vol.1, doi: 10.1109/PESC.1992.254717.

[34] M. O. Bilgic and M. Ehsani, 'Analysis of single flying capacitor converter by the state-space averaging technique', in *1988., IEEE International Symposium on Circuits and Systems*, Jun. 1988, pp. 1151–1154 vol.2, doi: 10.1109/ISCAS.1988.15130.

[35] S. K. Chattopadhyay and C. Chakraborty, 'A new technique for capacitor balancing of three-level flying-capacitor multilevel inverter', in *IECON 2017 - 43rd Annual Conference of the IEEE Industrial Electronics Society*, Nov. 2017, pp. 6357–6362, doi: 10.1109/IECON.2017.8217107.

[36] V. Dargahi and A. Shoulaie, 'Capacitors voltage balancing modeling in three phase flying capacitor converters with booster', in *2012 3rd Power Electronics and Drive Systems Technology (PEDSTC)*, Feb. 2012, pp. 103–108, doi: 10.1109/PEDSTC.2012.6183306.

[37] C. Cheng and L. He, 'Flying-capacitor-clamped five-level inverter based on switched-capacitor topology', in *2016 IEEE Energy Conversion Congress and Exposition (ECCE)*, Sep. 2016, pp. 1–5, doi: 10.1109/ECCE.2016.7855123.

[38] T. Abhilash, A. Kirubakaran, and V. T. Somasekhar, 'A Seven-Level Hybrid Inverter with DC-Link and Flying Capacitor Voltage Balancing', in *2019 IEEE International Conference on Environment and Electrical Engineering and 2019 IEEE Industrial and Commercial Power Systems Europe (EEEIC / I&CPS Europe)*, Jun. 2019, pp. 1–5, doi: 10.1109/EEEIC.2019.8783553.

[39] Z. Oudjebour, E. M. Berkouk, and M. O. Mahmoudi, 'Modelling, control and feedback control of the multilevel flying capacitors rectifier. Application to double star induction machine', in *2010 IEEE International Energy Conference*, Dec. 2010, pp. 507–512, doi: 10.1109/ENERGYCON.2010.5771734.

[40] B. S. Kumar and A. Kirubakaran, 'A Complete Fault-Tolerant Solution For A Single-Phase Five-Level Hybrid Flying Capacitor Inverter', in *2019 Innovations in Power and Advanced Computing Technologies (i-PACT)*, Mar. 2019, vol. 1, pp. 1–5, doi: 10.1109/i-PACT44901.2019.8960006.

[41] L. Stefanski, D. Bernet, M. Schnarrenberger, C. Rollbühler, A. Liske, and M. Hiller, 'Cascaded H-Bridge based Parallel Hybrid Converter — A novel Topology for perfectly sinusoidal high power Voltage Sources', in *IECON 2019 - 45th Annual Conference of the IEEE Industrial Electronics Society*, Oct. 2019, vol. 1, pp. 1639–1646, doi: 10.1109/IECON.2019.8927740.

[42] A. Chitra and S. Himavathi, 'Modeling and experimental validation of solar PV system for cascade H-bridge multilevel inverter', in *2013 International Conference on Power, Energy and Control (ICPEC)*, Feb. 2013, pp. 260–265, doi: 10.1109/ICPEC.2013.6527662.

[43] M. S. B. Ranjana, P. S. Wankhade, and N. D. Gondhalekar, 'A modified cascaded H-bridge multilevel inverter for solar applications', in *2014 International Conference on Green Computing Communication and Electrical Engineering (ICGCCEE)*, Mar. 2014, pp. 1–7, doi: 10.1109/ICGCCEE.2014.6922468.

[44] K. Anand, S. N. Ahamad Faruqui, and A. Ali, 'Three Phase Transformerless Cascaded H- Bridge Solar PV Multilevel Inverter', in *2019 International Conference on Computing, Power and Communication Technologies (GUCON)*, Sep. 2019, pp. 876–879.

[45] X. Yan and A. Hamza, 'Control strategy of cascaded H-Bridge inverter for grid connected with Solar Photovoltaic conversion systems', in *2014 IEEE Conference and Expo Transportation Electrification Asia-Pacific (ITEC Asia-Pacific)*, Sep. 2014, pp. 1–5, doi: 10.1109/ITEC-AP.2014.6941206.

[46] M. Glinka and R. Marquardt, 'A New AC/AC Multilevel Converter Family', *IEEE Trans. Ind. Electron.*, vol. 52, no. 3, pp. 662–669, Jun. 2005, doi: 10.1109/TIE.2005.843973.

[47] S. Jupin, I. Vechiu, and G. Tapia, 'Direct state-space model for model predictive control of multi-level power converters', in *IECON 2017-43rd Annual Conference of the IEEE Industrial Electronics Society*, 2017, pp. 7759–7764.

[48] J. A. Ferreira, 'The Multilevel Modular DC Converter', *IEEE Trans. Power Electron.*, vol. 28, no. 10, pp. 4460–4465, Oct. 2013, doi: 10.1109/TPEL.2012.2237413.

[49] G. Bergna *et al.*, 'A Generalized Power Control Approach in ABC Frame for Modular Multilevel Converter HVDC Links Based on Mathematical Optimization', *IEEE Trans. Power Deliv.*, vol. 29, no. 1, pp. 386–394, Feb. 2014, doi: 10.1109/TPWRD.2013.2279300.

[50] Q. Xu, F. Ma, A. Luo, Y. Chen, and Z. He, 'Hierarchical Direct Power Control of Modular Multilevel Converter for Tundish Heating', *IEEE Trans. Ind. Electron.*, vol. 63, no. 12, pp. 7919–7929, Dec. 2016, doi: 10.1109/TIE.2016.2542159.

[51] S. Fukuda and K. Suzuki, 'Harmonic evaluation of carrier-based PWM methods using harmonic distortion determining factor', in *Proceedings of Power Conversion Conference-PCC'97*, 1997, vol. 1, pp. 259–264.

[52] Gang Zhang, Zhigang Liu, Lei Wang, and Hengli Quan, 'An optimized PWM modulation scheme for high power three-level converter', in *2009 International Conference on Mechatronics and Automation*, Aug. 2009, pp. 5008–5013, doi: 10.1109/ICMA.2009.5246084.

[53] Y. Long, X. Xiao, Y. Xu, Y. Xu, and B. Yu, 'A hybrid Modulation method for improved modular multilevel converter applied for power quality compensation in medium voltage', in *2013 1st International Future Energy Electronics Conference (IFEEC)*, Nov. 2013, pp. 789–793, doi: 10.1109/IFEEC.2013.6687609.

[54] Shuhuai Shi, Yan Yang, Tianhua Zhu, Feng Wang, and Fang Zhuo, 'High power DC/AC/DC converter based on different modulation strategies', in *2016 IEEE 8th International Power Electronics and Motion Control Conference (IPEMC-ECCE Asia)*, May 2016, pp. 315–320, doi: 10.1109/IPEMC.2016.7512305.

[55] A. H. Bhat and P. Agarwal, 'A Three-Phase Neutral-Point Clamped AC/DC Converter Based On Modified Space Vector Modulation for Power Quality Improvement', in *2006 IEEE International Conference on Industrial Technology*, Dec. 2006, pp. 1380–1385, doi: 10.1109/ICIT.2006.372397.

[56] X. Du, G. Li, P. Sun, L. Zhou, and H. Tai, 'A hybrid modulation method for lifetime extension of power semiconductors in wind power converters', in *2015 IEEE Applied Power Electronics Conference and Exposition (APEC)*, Mar. 2015, pp. 2565–2570, doi: 10.1109/APEC.2015.7104712.

[57] E. Barbie, R. Rabinovici, and A. Kuperman, 'Analytic formulation and optimization of weighted total harmonic distortion in single-phase staircase modulated multilevel inverters', *Energy*, vol. 199, p. 117470, May 2020, doi: 10.1016/j.energy.2020.117470.

[58] P. N. Enjeti and R. Jakkli, 'Optimal power control strategies for neutral point clamped (NPC) inverter topology', *IEEE Trans. Ind. Appl.*, vol. 28, no. 3, pp. 558–566, May 1992, doi: 10.1109/28.137436.
[59] A. Hirota, B. Saha, S. Mun, and M. Nakaoka, 'An Advanced Simple Configuration Delta-Sigma Modulation Three-Phase Inverter Implementing Space Voltage Vector Approach', in *2007 IEEE Power Electronics Specialists Conference*, Jun. 2007, pp. 453–457, doi: 10.1109/PESC.2007.4342030.
[60] N. S. Hasan, N. Rosmin, Dygku. A. Awg. Osman, and A. H. Musta'amal@Jamal, 'Reviews on multilevel converter and modulation techniques', *Renew. Sustain. Energy Rev.*, vol. 80, pp. 163–174, Dec. 2017, doi: 10.1016/j.rser.2017.05.163.
[61] I. Colak and E. Kabalci, 'Developing a novel sinusoidal pulse width modulation (SPWM) technique to eliminate side band harmonics', *Int. J. Electr. Power Energy Syst.*, vol. 44, no. 1, pp. 861–871, Jan. 2013, doi: 10.1016/j.ijepes.2012.08.024.
[62] Haitao Zhang *et al.*, 'An improved CPS-SPWM and unified modulation strategy for multilevel converter', in *2016 IEEE PES Asia-Pacific Power and Energy Engineering Conference (APPEEC)*, Oct. 2016, pp. 1306–1310, doi: 10.1109/APPEEC.2016.7779705.
[63] P. S. Sanjay, P. R. Tanaji, and S. K. Patil, 'Symmetrical Multilevel Cascaded H-Bridge Inverter Using Multicarrier SPWM Technique', in *2018 3rd International Conference for Convergence in Technology (I2CT)*, Apr. 2018, pp. 1–4, doi: 10.1109/I2CT.2018.8529331.
[64] R. Petrella and A. Pevere, 'Interleaved carrier-based modulations for reducing low-frequency neutral point voltage ripple in the three-phase neutral point clamped inverter', in *2014 IEEE Applied Power Electronics Conference and Exposition - APEC 2014*, Mar. 2014, pp. 2386–2393, doi: 10.1109/APEC.2014.6803637.
[65] Su Zhonglai, Zeng Guang, and Zhang Jinggang, 'Research on optimization Carrier Phase-Shifted SPWM of cascaded STATCOM', in *2011 2nd International Conference on Artificial Intelligence, Management Science and Electronic Commerce (AIMSEC)*, Aug. 2011, pp. 4252–4255, doi: 10.1109/AIMSEC.2011.6010151.
[66] Yu Xiong, Yinhai Zhang, Kun Wei, and Zhongchao Zhang, 'Carrier phase-shifted SPWM based current-source multi-converter', in *Eighteenth Annual IEEE Applied Power Electronics Conference and Exposition, 2003. APEC '03.*, Feb. 2003, vol. 1, pp. 89–93 vol.1, doi: 10.1109/APEC.2003.1179181.
[67] Chumei Feng and V. G. Agelidis, 'On the comparison of fundamental and high frequency carrier-based PWM techniques for multilevel NPC inverters', in *2002 IEEE 33rd Annual IEEE Power Electronics Specialists Conference. Proceedings (Cat. No.02CH37289)*, Jun. 2002, vol. 2, pp. 520–525 vol.2, doi: 10.1109/PSEC.2002.1022506.
[68] B. P. McGrath and D. G. Holmes, 'Multicarrier PWM strategies for multi-level inverters', *IEEE Trans. Ind. Electron.*, vol. 49, no. 4, pp. 858–867, 2002.
[69] P. Chaturvedi, 'Chapter Three - Conventional Multilevel Inverter: Topologies and Control Strategies', in *Modeling and Control of Power Electronics Converter System for Power Quality Improvements*, S. K. Dwivedi, S. Jain, K. K. Gupta, and P. Chaturvedi, Eds. Academic Press, 2018, pp. 85–120.
[70] J. K. Steinke, 'Control of a neutral-point-clamped PWM inverter for high power AC traction drives', in *Third International Conference on Power Electronics and Variable-Speed Drives*, Jul. 1988, pp. 214–217.
[71] Ning-Yi Dai, Man-Chung Wong, and Ying-Duo Han, 'Application of a three-level NPC inverter as a three-phase four-wire power quality compensator by generalized 3DSVM', *IEEE Trans. Power Electron.*, vol. 21, no. 2, pp. 440–449, Mar. 2006, doi: 10.1109/TPEL.2005.869755.
[72] L. G. Franquelo, J. I. León, M. M. Prats, and R. Portillo, 'Space vector modulation techniques formultilevel converters - a survey', *Przeglad Elektrotchniczny*, pp. 56–61, 2006.
[73] L. Saribulut, A. Teke, and M. Tümay, 'Vector-based reference location estimating for space vector modulation technique', *Electr. Power Syst. Res.*, vol. 86, pp. 51–60, May 2012, doi: 10.1016/j.epsr.2011.12.004.
[74] M. Verij Kazemi, A. Sadeghi Yazdankhah, and H. Madadi Kojabadi, 'Direct power control of DFIG based on discrete space vector modulation', *Renew. Energy*, vol. 35, no. 5, pp. 1033–1042, May 2010, doi: 10.1016/j.renene.2009.09.008.
[75] L. Saribulut and M. Tümay, 'Robust space vector modulation technique for unbalance voltage disturbances', *Electr. Power Syst. Res.*, vol. 80, no. 11, pp. 1364–1374, Nov. 2010, doi: 10.1016/j.epsr.2010.05.009.
[76] P. Frutos, E. Christopher, and A. Sánchez, 'On the Implementation of a 3D Space Vector Modulation Algorithm', in *2018 IEEE International Autumn Meeting on Power, Electronics and Computing (ROPEC)*, Nov. 2018, pp. 1–6, doi: 10.1109/ROPEC.2018.8661390.

[77] M. M. Renge and H. M. Suryawanshi, 'Three-Dimensional Space-Vector Modulation to Reduce Common-Mode Voltage for Multilevel Inverter', *IEEE Trans. Ind. Electron.*, vol. 57, no. 7, pp. 2324–2331, Jul. 2010, doi: 10.1109/TIE.2009.2027247.
[78] M. G. Villalva, M. E. de Oliveira Filho, and E. R. Filho, 'Detailed implementation of a current controller with 3D space vectors for four wire active filters', in *The Fifth International Conference on Power Electronics and Drive Systems, 2003. PEDS 2003.*, Nov. 2003, vol. 1, pp. 536-541 Vol.1, doi: 10.1109/PEDS.2003.1282896.
[79] C. Zhang, Q. Yang, Y. Li, and J. Lu, 'A novel 3D space vector PWM control method for 3D magnetic property measurement apparatus', in *2014 17th International Conference on Electrical Machines and Systems (ICEMS)*, Oct. 2014, pp. 1892–1897, doi: 10.1109/ICEMS.2014.7013805.
[80] A. Renault, J. Rodas, L. Comparatore, J. Pacher, and R. Gregor, 'Modulated Predictive Current Control Technique for a Three-Phase Four-Wire Active Power Filter based on H-bridge Two-Level Converter', in *2018 53rd International Universities Power Engineering Conference (UPEC)*, Sep. 2018, pp. 1–6, doi: 10.1109/UPEC.2018.8542044.
[81] X. Zhou, T. Pan, and Z. Ji, 'Comparison on control strategies of the grid-side converter of variable speed constant frequency doubly-fed wind power generation system', in *2009 Chinese Control and Decision Conference*, Jun. 2009, pp. 3082–3085, doi: 10.1109/CCDC.2009.5192828.
[82] K. Wang, Y. Wang, Z. Cheng, L. Liu, L. Jia, and Y. Liang, 'Research on Reactive Power Control of the Grid-Side Converter of DFIG Based Wind Farm', in *2018 2nd IEEE Conference on Energy Internet and Energy System Integration (EI2)*, Oct. 2018, pp. 1–4, doi: 10.1109/EI2.2018.8582077.
[83] Sixing Du, Apparao Dekka, Bin Wu, and Navid Zargari, 'Classical Control of Modular Multilevel Converter', in *Modular Multilevel Converters: Analysis, Control, and Applications*, IEEE, 2018, pp. 79–102.
[84] Farzin Asadi, Kei Eguchi, and Jerry Hudgins, *Dynamics and Control of DC-DC Converters*. Morgan & Claypool, 2018.
[85] J. Rodriguez *et al.*, 'State of the Art of Finite Control Set Model Predictive Control in Power Electronics', *IEEE Trans. Ind. Inform.*, vol. 9, no. 2, pp. 1003–1016, May 2013, doi: 10.1109/TII.2012.2221469.
[86] J. Rocabert, A. Luna, F. Blaabjerg, and P. Rodríguez, 'Control of Power Converters in AC Microgrids', *IEEE Trans. Power Electron.*, vol. 27, no. 11, pp. 4734–4749, Nov. 2012, doi: 10.1109/TPEL.2012.2199334.
[87] Fabio Saccomanno, 'Appendix 1: Transformation to Symmetrical Components', in *Electric Power Systems: Analysis and Control*, IEEE, 2003, pp. 676–679.
[88] Fabio Saccomanno, 'Appendix 2: Park's Transformation', in *Electric Power Systems: Analysis and Control*, IEEE, 2003, pp. 680–687.
[89] Q. Tabart, 'Modélisation et commande d'une interface à base d'un convertisseur NPC pour système de stockage hybride dédié micro-réseau', Université de Grenoble Alpes, 2019.
[90] G. Durgasukumar and M. K. Pathak, 'Comparison of adaptive Neuro-Fuzzy-based space-vector modulation for two-level inverter', *Int. J. Electr. Power Energy Syst.*, vol. 38, no. 1, pp. 9–19, Jun. 2012, doi: 10.1016/j.ijepes.2011.10.017.
[91] Z. Liu, G. Fei, and Z. Chen, 'Simulation Study of Double Closed-loop SPWM Inverter Based on Fuzzy Neural Network', in *2018 IEEE 3rd Advanced Information Technology, Electronic and Automation Control Conference (IAEAC)*, Oct. 2018, pp. 241–245, doi: 10.1109/IAEAC.2018.8577665.
[92] S. Ravikumar, H. Vennila, and R. Deepak, 'Hybrid power generation system with Total Harmonic Distortion minimization using improved Rider Optimization Algorithm: Analysis on converters', *J. Power Sources*, vol. 459, p. 228025, May 2020, doi: 10.1016/j.jpowsour.2020.228025.
[93] M. I. Martinez, A. Susperregui, and G. Tapia, 'Second-order sliding-mode-based global control scheme for wind turbine-driven DFIGs subject to unbalanced and distorted grid voltage', *IET Electr. Power Appl.*, vol. 11, no. 6, pp. 1013–1022, 2017, doi: 10.1049/iet-epa.2016.0711.
[94] A. Susperregui, M. I. Martinez, G. Tapia, and I. Vechiu, 'Second-order sliding-mode controller design and tuning for grid synchronisation and power control of a wind turbine-driven doubly fed induction generator', *IET Renew. Power Gener.*, vol. 7, no. 5, pp. 540–551, Sep. 2013, doi: 10.1049/iet-rpg.2012.0026.
[95] N. Swain, S. M. Ali, C. K. Panigrahi, D. P. Kumar, and 2018 2nd International Conference on Trends in Electronics and Informatics (ICOEI), 'Sliding Mode Controller-A Nonlinear Approach to Non-Isolated Cuk Converter for Constant Voltage Application', pp. 288–292, 2018.

[96] A. Susperregui, J. M. Herrero, M. I. Martinez, G. Tapia-Otaegui, and X. Blasco, 'Multi-Objective Optimisation-Based Tuning of Two Second-Order Sliding-Mode Controller Variants for DFIGs Connected to Non-Ideal Grid Voltage', *Energies*, vol. 12, no. 19, p. 3782, Oct. 2019, doi: 10.3390/en12193782.
[97] A. K. Singh and B. C. Pal, 'Chapter 7 - Control Based on Dynamic Estimation: Linear and Nonlinear Theories', in *Dynamic Estimation and Control of Power Systems*, A. K. Singh and B. C. Pal, Eds. Academic Press, 2019, pp. 121–140.
[98] E. F. Camacho and C. Bordons, *Model predictive control*. London ; New York: Springer, 2004.
[99] R. Kennel, A. Linder, and M. Linke, 'Generalized predictive control (GPC)-ready for use in drive applications?', in *2001 IEEE 32nd Annual Power Electronics Specialists Conference (IEEE Cat. No.01CH37230)*, Jun. 2001, vol. 4, pp. 1839–1844 vol. 4, doi: 10.1109/PESC.2001.954389.
[100] M. G. Judewicz, S. A. González, N. I. Echeverría, J. R. Fischer, and D. O. Carrica, 'Generalized Predictive Current Control (GPCC) for Grid-Tie Three-Phase Inverters', *IEEE Trans. Ind. Electron.*, vol. 63, no. 7, pp. 4475–4484, Jul. 2016, doi: 10.1109/TIE.2015.2508934.
[101] S. Mariethoz and M. Morari, 'Explicit Model-Predictive Control of a PWM Inverter With an LCL Filter', *IEEE Trans. Ind. Electron.*, vol. 56, no. 2, pp. 389–399, Feb. 2009, doi: 10.1109/TIE.2008.2008793.
[102] T. Geyer and D. E. Quevedo, 'Multistep Finite Control Set Model Predictive Control for Power Electronics', *IEEE Trans. Power Electron.*, vol. 29, no. 12, pp. 6836–6846, Dec. 2014, doi: 10.1109/TPEL.2014.2306939.
[103] C. Xia, T. Liu, T. Shi, and Z. Song, 'A Simplified Finite-Control-Set Model-Predictive Control for Power Converters', *IEEE Trans. Ind. Inform.*, vol. 10, no. 2, pp. 991–1002, May 2014, doi: 10.1109/TII.2013.2284558.
[104] A. Kanaan, F. Sebaaly, and H. Y. Kanaan, 'FCS-MPC with PNSC reference generation method for a 3L-NPC inverter under grid faults', in *2017 11th IEEE International Conference on Compatibility, Power Electronics and Power Engineering (CPE-POWERENG)*, Apr. 2017, pp. 223–228, doi: 10.1109/CPE.2017.7915173.
[105] J. Michalík, Z. Peroutka, and V. Šmídl, 'Finite control set MPC of active current-source rectifier with full state space model', in *IECON 2015 - 41st Annual Conference of the IEEE Industrial Electronics Society*, Nov. 2015, pp. 004121–004126, doi: 10.1109/IECON.2015.7392743.
[106] V. Utkin, J. Guldner, and J. Shi, *Sliding Mode Control in Electromechanical Systems*. London, UK: Taylor&Francis, 1999.
[107] J. Rodriguez *et al.*, 'Predictive Current Control of a Voltage Source Inverter', *IEEE Trans. Ind. Electron.*, vol. 54, no. 1, pp. 495–503, Feb. 2007, doi: 10.1109/TIE.2006.888802.
[108] S. A. Larrinaga, M. A. R. Vidal, E. Oyarbide, and J. R. T. Apraiz, 'Predictive Control Strategy for DC/AC Converters Based on Direct Power Control', *IEEE Trans. Ind. Electron.*, vol. 54, no. 3, pp. 1261–1271, Jun. 2007, doi: 10.1109/TIE.2007.893162.
[109] S. Vazquez, A. Marquez, R. Aguilera, D. Quevedo, J. I. Leon, and L. G. Franquelo, 'Predictive Optimal Switching Sequence Direct Power Control for Grid-Connected Power Converters', *IEEE Trans. Ind. Electron.*, vol. 62, no. 4, pp. 2010–2020, Apr. 2015, doi: 10.1109/TIE.2014.2351378.
[110] R. Mendez, D. Sbarbaro, and J. Espinoza, 'High dynamic and static performance FCS-MPC strategy for static power converters', in *2016 IEEE Energy Conversion Congress and Exposition (ECCE)*, Sep. 2016, pp. 1–7, doi: 10.1109/ECCE.2016.7855146.
[111] X. Liu, D. Wang, and Z. Peng, 'An improved finite control-set model predictive control for nested neutral point-clamped converters under both balanced and unbalanced grid conditions', *Int. J. Electr. Power Energy Syst.*, vol. 104, pp. 910–923, Jan. 2019, doi: 10.1016/j.ijepes.2018.07.046.
[112] R. P. Aguilera and D. E. Quevedo, 'On stability and performance of finite control set MPC for power converters', in *2011 Workshop on Predictive Control of Electrical Drives and Power Electronics*, Oct. 2011, pp. 55–62, doi: 10.1109/PRECEDE.2011.6078688.

Chapter II: Switched State-Space Representation for MPC

1. Interest and limitation of MPC

Model Predictive Control (MPC) is a control method that combines optimization and prediction to provide intelligent control [1]. Miscellaneous variations are found, depending on the optimization method and on the means of prediction. The most general form is portrayed in Fig.2.1. The most common case integrates quadratic programming with linear state-space representation and is deployed in a large variety of industrial or research applications, such as energy management, varied chemical processes, mechatronics, … However, MPC does not represent a single model/optimizer set but defines all possible combinations.

Because it relies on optimization, MPC requires more computational effort than more common control methods, such as PID or Linear Quadratic (LQ) controllers. As a matter of fact, the MPC algorithms based on quadratic programming consist in looping such a LQ regulator. Aside from this computational stress, the method can handle complex system definitions and constraints. This explains why it is mostly found in applications, industrial or academic, with large systems with multiple inputs and outputs (MIMO), physical constraints and multiple objectives, but above all long sample periods. The constraints aspect is significant, as they are rarely managed intrinsically and usually have to be implemented outside of the controller, often leading to design issues. On Single Input Single Output (SISO) systems, MPC is usually not a cost effective solution, as its design complexity outweighs the improvements it can bring. Quite often, complex systems and control specifications are approached by multiplying the low-intelligence controllers. This is seldom as efficient as desired.

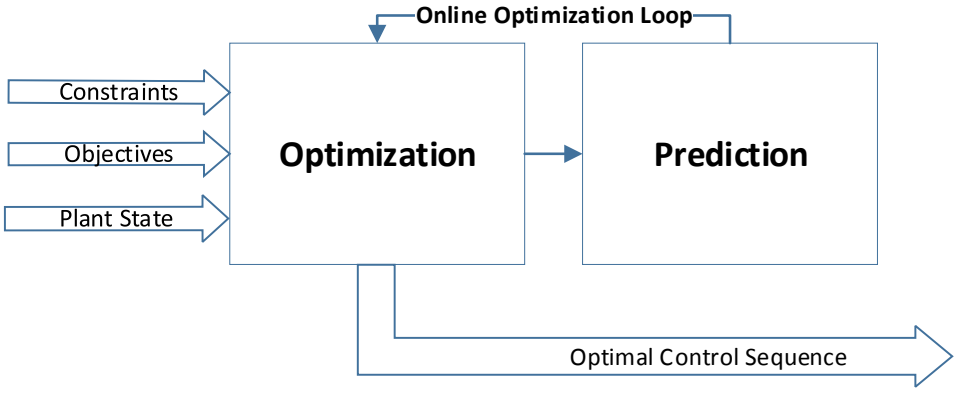

Fig. 2.1. General operation of MPC algorithms

To summarize, Model Predictive Control is a strategy particularly well adapted to MIMO plants where various physical or behavior constraints and miscellaneous requirements coexist. The case of multi-level power converters absolutely pertains to this category, especially when considering the converter without any modulation block, as explained in the previous chapter. This leads to a variety of MPC applications for power converters in the past few years [2], [3]. However, it is not a common domain for

MPC, as the models are not linear, therefore banishing the use of conventional state-space representations and quadratic optimizers. Furthermore, the time constraints are extremely strong for power converters. Indeed, since it performs looped optimization, Model Predictive Control ends up computationally heavy and requires efficient and fast processors. The permanent progress of computing power abates this issue, without entirely solving it. MPC can be applied to ever faster dynamics, but the case of power converters is particularly extreme. Indeed, their switching frequency could be very high (up to several dozen of kHz), which implies a very short time allotted to compute the optimal control to apply. Furthermore, the typical control architecture implies the deduction and transfer of said input being carried out in the lapse of only a fraction of the sample time. The assets and inconveniences of MPC for multi-level power converters direct switch control are summarized in the following table.

TABLE 2.1
MAIN INTERESTS AND DISADVANTAGES OF MPC

Main advantages	Main limitations
Handles MIMO systems	Algorithm complexity
Incorporates constraints	Computational burden
Incorporates prediction	
Optimal definition of the control problem	
Robustness	
Very large variety of applications and versions	

Many parameters are driving the performance of the control. In particular, the cost function and the prediction horizon play crucial roles in the computation stress: they are intertwined with the quality of the control and thereupon with the depth of calculation, hence the general time cost. All these factors imply that for implementation, the algorithm can neither consider overly complicated objectives nor envision elongated periods. Overall, two main issues have been brought up. First, the need to develop a fast enough algorithm to be implemented on a real power converter. Second, the impossibility to rely on the most wide-spread algorithms based on quadratic programming, because of the non-linear nature of the power converters. These problems form a couple: prediction and optimization, evolving together. In this situation, we propose to first address the issue of modeling, which has to describe accurately enough the behavior of all power converters for the final algorithm to be universal to all such applications and practical enough to develop an optimization algorithm treating that model.

2. Switched State-Space Representation

Switched State Space Representation (SSSR) is a modeling method used when considering hybrid systems combining a discrete definition with continuous quantities [4]. Typical examples include chemical processes [5], plants with several points of operation (this is common with motors with gears for example)[6], parameter-varying systems [7], etc. The overall system is described by a set of continuous subsystems, associated with the various events σ affecting the system. This means that instead of the ordinary dynamics, as presented in (2.1), the SSSR model is portrayed by (2.2).

$$\dot{\boldsymbol{x}}(t) = \boldsymbol{A}\boldsymbol{x}(t) + \boldsymbol{B}\boldsymbol{u}(t) + \boldsymbol{E}\boldsymbol{d}(t) \tag{2.1}$$

$$\dot{\boldsymbol{x}}(t) = \boldsymbol{A}_{\sigma(t)}\boldsymbol{x}(t) + \boldsymbol{E}_{\sigma(t)}\boldsymbol{d}(t) \tag{2.2}$$

Therefore, the global "power converter" system can be described as a combination of the "power converter in position σ" subsystems. In the case of power converters, the position is dictated by control $\boldsymbol{u}$, which leads to

$$\dot{\boldsymbol{x}}(t) = \boldsymbol{A}\big(\boldsymbol{u}(t)\big)\boldsymbol{x}(t) + \boldsymbol{E}\big(\boldsymbol{u}(t)\big)\boldsymbol{d}(t). \tag{2.3}$$

This equation highlights the subsystem definition: for each possible control $\boldsymbol{u}$, the $\boldsymbol{A}(\boldsymbol{u})$ and $\boldsymbol{E}(\boldsymbol{u})$ matrices are constant and lead to a usual linear state-space representation as in (2.1). This allows prediction and modeling as usual and can be associated to an optimal graph navigation algorithm aiming at developing a general MPC scheme therefore adapted to any power converter topology.

3. Adaptation to Multi-Level Power Converters

As can be seen from Fig. 2.2, the most general presentation of power converters shows five aspects. First, the two outer buses, whose behaviors are considered external to the converter itself: their dynamics are not the object of this study, and their respective actions on the converter are regarded as uncontrolled inputs. Then, the corresponding filters or links, containing several capacitors and inductors, to which the state variables are associated. The bridge between the two groups of state variables is made through the switching cells, which for some topologies may add state variables. The control is performed by the open/close orders transmitted to each transistor of the switching cells.

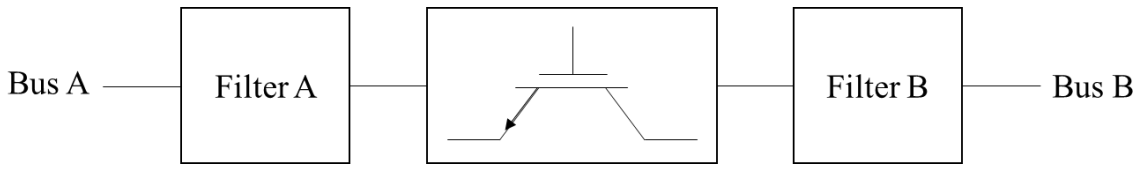

Fig. 2.2. General context of power conversion. Two buses, A and B, are connected through a filter + commutation cell system.

Therefore, the state vector is divided into three parts: the $\boldsymbol{x}_A$ states corresponding to the A side filter, the $\boldsymbol{x}_{con}$ ones related to the internal components of the converter, and the $\boldsymbol{x}_B$ states are coming from the other side's filter. Similarly, the uncontrolled input vector is formed by the $\boldsymbol{d}_A$ inputs generated by the

A side and the $\boldsymbol{d_B}$ ones spawned by the B side. The control vector $\boldsymbol{u}$ is an image of the switches' positions. The input, control and state vectors are presented in (2.4). By construction, it is possible for some of these sub-vectors to be empty, depending on the topology and on the context.

$$\boldsymbol{d} = \begin{bmatrix} \boldsymbol{d_A} \\ \boldsymbol{d_B} \end{bmatrix}; \quad \boldsymbol{u} = \boldsymbol{f}(\boldsymbol{switch}); \quad \boldsymbol{x} = \begin{bmatrix} \boldsymbol{x_A} \\ \boldsymbol{x_{con}} \\ \boldsymbol{x_B} \end{bmatrix} \tag{2.4}$$

The $\boldsymbol{f}$ function is chosen to accurately depict the impact of the switching states on the connection between the A and B sides. For energy management applications, which need to perceive the quantity of energy passing through every switch precisely, $\boldsymbol{f}$ can be specified as bijective. Nevertheless, though surjective, this function is not necessarily injective, as distinct switching positions can lead to the same link.

With this definition of the state variables, the $\boldsymbol{A}$ matrix can be divided in blocks as shown in (2.5).

$$\boldsymbol{A(u)} = \begin{bmatrix} \boldsymbol{A_{AA}} & \boldsymbol{A_{Acon}(u)} & \boldsymbol{A_{AB}(u)} \\ \boldsymbol{A_{conA}(u)} & \boldsymbol{A_{concon}} & \boldsymbol{A_{conB}(u)} \\ \boldsymbol{A_{BA}(u)} & \boldsymbol{A_{Bcon}(u)} & \boldsymbol{A_{BB}} \end{bmatrix} \tag{2.5}$$

Particularly, the diagonal blocks do not depend on the switching orders, while all the remaining submatrices are defined as functions of the switching control. The $\boldsymbol{A_{AA}}$ and $\boldsymbol{A_{BB}}$ blocks represent the dynamics of the filters, while all the other blocks contain the converter's proper behavior. It is interesting to note that with this approach the $\boldsymbol{E}$ input matrix in (2.6) does not depend on the switching positions.

$$\dot{\boldsymbol{x}} = \boldsymbol{A(u)x} + \boldsymbol{Ed} \tag{2.6}$$

In effect, fixing the position of the switches contained within a power converter switching cell leads to an electrical circuit that can be linearly modeled using its elementary equations components and Kirchhoff's laws. Therefore, given a position k, a specific $\boldsymbol{A_k}$ matrix is defined leading to subsystem (2.7):

$$\dot{\boldsymbol{x}} = \boldsymbol{A_k x} + \boldsymbol{Ed}. \tag{2.7}$$

Then, all sets (2.7) are assembled according to the theorem of superposition. This method calls for combinatory logic. Indeed, considering that all possible controls for each switching cell are mutually exclusive, the command can be expressed through logic binary variables obeying elementary logic laws . In particular, assuming that U_{cell} is the set of the N_{poss} possible switching states for a switching cell, it turns out that

$$\boldsymbol{u_k} \in U_{cell}; \ \sum_{k=1}^{N_{poss}} \boldsymbol{u_k} = 1. \tag{2.8}$$

From there on, all the subsystems represented by (2.7) can be added up as follows:

$$\sum_{k=1}^{N_{poss}} \boldsymbol{u_k \dot{x}} = \sum_{k=1}^{N_{poss}} \boldsymbol{u_k} \, (\boldsymbol{A_k x} + \boldsymbol{Ed}), \tag{2.9}$$

which, by virtue of (2.8), turns into

$$\dot{\boldsymbol{x}} = \left(\sum_{k=1}^{N_{poss}} \boldsymbol{u_k A_k} \right) \boldsymbol{x} + \boldsymbol{Ed}. \tag{2.10}$$

Given that equations (2.8)–(2.10) are representative of a single cell, Kirchhoff's current law is thus applied to link all the converter switching cells to one another. Indeed, once equations are established for one cell, bounding them together is done by applying the adequate current or voltage laws, resulting in sums of the previous equations . The resulting system is of the form

$$\dot{\boldsymbol{x}}(t) = \boldsymbol{A}\big(\boldsymbol{u}(t)\big)\boldsymbol{x}(t) + \boldsymbol{E}\boldsymbol{d}(t). \tag{2.11}$$

Consequently, the $\boldsymbol{A}(\boldsymbol{u})$ matrix, formed from the different $\boldsymbol{A}_k$, depicts the dynamics of power converters using a SSSR. This method relies only on the laws of electricity and is suitable for any power converter application. It is interesting to note that two-level power converters can be expressed with (2.1), but that it is impossible to do so for multi-level power converters, rendering the discussed method imperative for them.

All the previous definitions are expressed in continuous time. However, since the control is exerted discretely, a controller designed to deal with power converters without modulation has to be discrete. Therefore, such a controller requires a discrete model to operate. Application of the zero-order hold (ZOH) discretization method results in an equivalent discrete-time model of the form

$$\boldsymbol{x}(n+1) = \boldsymbol{A}_d\big(\boldsymbol{u}(n)\big)\boldsymbol{x}(n) + \boldsymbol{E}_d\big(\boldsymbol{u}(n)\big)\boldsymbol{d}(n), \tag{2.12}$$

where n refers to the n^{th} sampling instant and

$$\boldsymbol{A}_d\big(\boldsymbol{u}(n)\big) = e^{\boldsymbol{A}(\boldsymbol{u}(n))T};\ \boldsymbol{E}_d\big(\boldsymbol{u}(n)\big) = \int_0^T e^{\boldsymbol{A}(\boldsymbol{u}(n))t}\boldsymbol{E}dt, \tag{2.13}$$

with $\boldsymbol{T}$ being the sample time.

The ZOH discretization method is preferred, as it leads to an equivalent discrete-time model representing the original continuous-time system exactly as perceived by a discrete controller. Thus, (2.13) reveals that matrix $\boldsymbol{E}_d$ can no longer be considered control independent. As a matter of fact, both $\boldsymbol{A}_d$ and $\boldsymbol{E}_d$ are functions of control $\boldsymbol{u}$, thus implying that the number of matrices to be computed in the discrete case is roughly twice that of the continuous one. However, this additional computational burden is necessary when discrete-time control is to be implemented.

4. Electrical equations for each topology

To properly define the matrices previously described in Section 3, the first step is to establish the electrical laws of the different topologies. Even though these equations fully describe the power converters, they are not sufficient to define a state-space representation and have to be associated to the dynamics of the accumulative components of the filters and the links, as well as those inside the converter. This dependence on the filters together with the final state space representation matrices will be explained in Section 5.

4.1 Neutral-Point Clamped

Fig. 2.3 represents the three different switching positions for the Three Level Neutral Point Clamped topology (3L-NPC):

(a) S_P: the phase is bound to the P node of the DC-link,

(b) S_N: the phase is bound to the N node of the DC-link,

(c) S_0: the phase is bound to the neutral point of the DC-link.

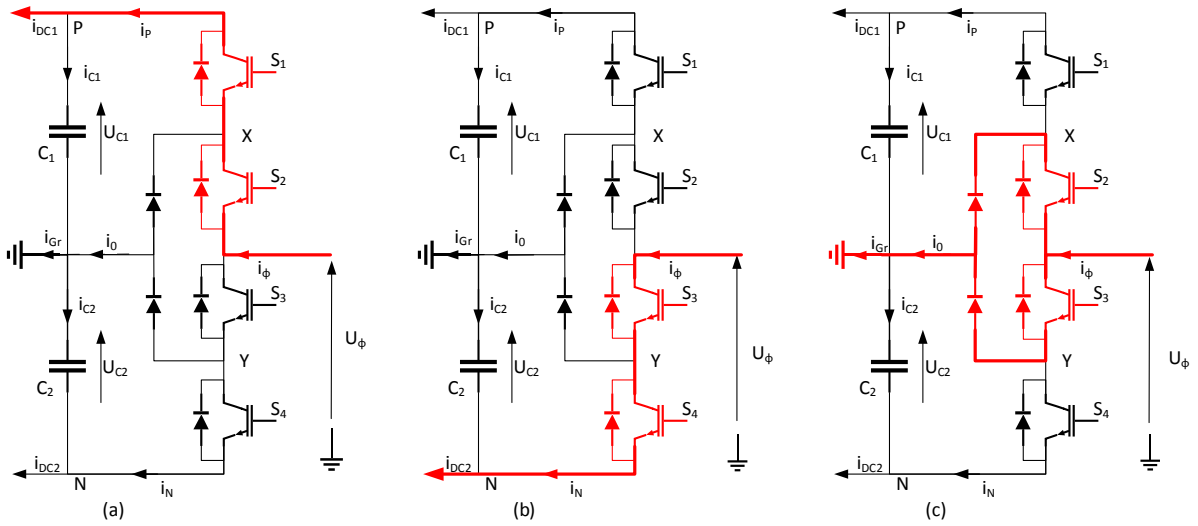

Fig. 2.3. Switching positions for one phase of the 3L NPC

Therefore, the set of accessible positions for any commutation cell is given by

$$U_{cell} = \{S_P, S_0, S_N\}.$$

The concordance between the previous set and the open/close state of the switches of the associated cells is summed up in Table 2.2, where 1 represents a closed state and 0 an open state.Crucially, $S_j$designates the switching state of the leg j, where j covers Ψ the set of all the legs of the power converter. More often than not, N_{legs} the cardinal of this set is either 3 or 4. The switching position of a leg can be

any member of U_{cell}. The notation S_{jP} translates the case where $S_j = S_P$ and so on for all elements of U_{cell}. The notations introduced in this subsection are applied onward.

TABLE 2.2
RELATION BETWEEN THE SWITCHES STATE AND THE CONNECTION VARIABLE FOR 3L-NPC

S_j	S_1	S_2	S_3	S_4	Connection
S_P	1	1	0	0	P
S_N	0	0	1	1	N
S_0	0	1	1	0	0

Considering the case of a single leg and applying the Kirchhoff's laws on the adequate meshes and nodes of the circuit in Fig. 2.3, as well as the notations described in said figure, the following equations are derived:

$$U_\phi = S_P U_{C1} - S_N U_{C2} \tag{2.14}$$

$$i_{C1} = i_P - i_{DC1}; \quad i_P = S_P i_\phi \tag{2.15}$$

$$i_{C2} = -i_N + i_{DC2}; \quad i_N = S_N i_\phi, \tag{2.16}$$

$$i_0 = S_0 i_\phi \tag{2.17}$$

where all four possible switching states are handled together, as suggested for the general case in (2.10)–(2.12). Furthermore, by virtue of (2.15), (2.16), (2.17) and (2.8), it is found that

$$i_{Gr} = i_{C1} - i_{C2} + i_0 = (S_P + S_N + S_0) i_\phi - i_{DC1} - i_{DC2} = i_\phi - i_{DC1} - i_{DC2}. \tag{2.18}$$

The currents i_{DC1} and i_{DC2} are often the opposite of one another and thus cancel themselves in the previous equation. How frequent the case may be, the hypothesis is strong and does not bring much value to the modeling process, which is why it was preferred to separate these two currents and consider them as independent. The same decision is reciprocated onward.

As pointed out in Section 3, extending this analysis to a 3L-NPC converter of any number of legs N_{legs} is performed by application of the theorem of superposition and (2.10). A variable, for example U_ϕ, of a leg j is noted $U_{\phi j}$. This notation differs from the one concerning the switching positions, as the message is different. Indeed, in one case the variable is defined by the leg, while in the other case the variable of the

leg is defined by its value. The (2.14)–(2.18) set turns, equation by equation, into the (2.19)–(2.23) set given next:

$$U_{\phi j} = S_{jP}U_{C1} - S_{jN}U_{C2};\ \ \forall\, j \in \Psi \tag{2.19}$$

$$i_{C1} = i_P - i_{DC1};\ \ \ i_P = \sum_{j\in\Psi} S_{jP} i_{\phi j} \tag{2.20}$$

$$i_{C2} = -i_N + i_{DC2};\ \ \ i_N = \sum_{j\in\Psi} S_{jN} i_{\phi j} \tag{2.21}$$

$$i_0 = \sum_{j\in\Psi} S_{j0} i_{\phi j} \tag{2.22}$$

$$i_{Gr} = \sum_{j\in\Psi}\ i_{\phi j} - i_{DC1} - i_{DC2}. \tag{2.23}$$

4.2 Flying Capacitor

The four distinct ways in which the Three-Level Flying Capacitor (3L-FC) topology allows connecting each AC phase to the DC side are illustrated Fig. 2.4:

(a) S_P: the phase is bound to the P node of the DC-link,

(b) S_N: the phase is bound to the N node of the DC-link,

(c) S_{CN}: the phase is bound to N through the inner capacitor, passing by the X point before Y,

(d) S_{CP}: the phase is bound to P through the inner capacitor, first passing by Y then X.

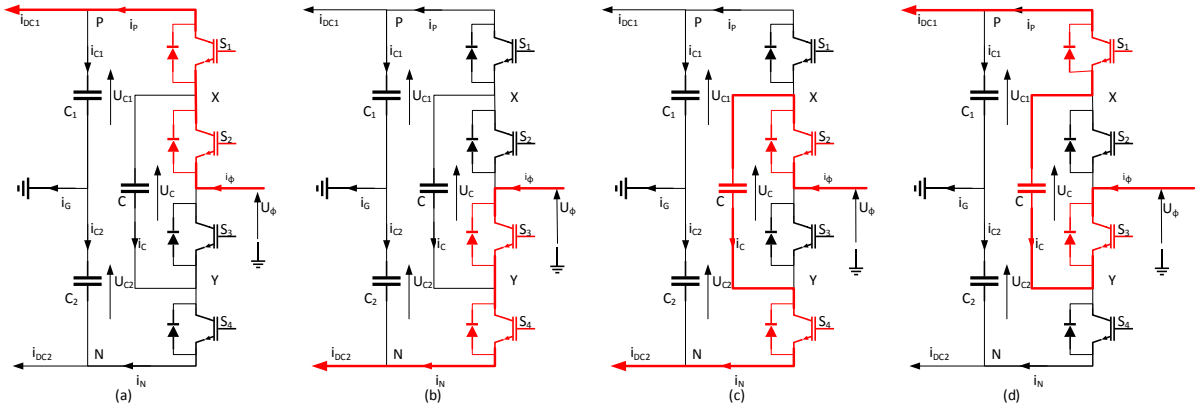

Fig. 2.4. Switching positions for one leg of 3L-FC

Accordingly, the set of possible switching states for any commutation cell U_{cell}, is given by

$$U_{cell} = \{S_P, S_N, S_{CP}, S_{CN}\}. \tag{2.24}$$

The correspondence between the open/closed state of the switches constituting the converter leg, and the previous values are summed up in Table 2.3.

TABLE 2.3
RELATION BETWEEN THE SWITCHES STATE AND THE CONNECTION VARIABLE FOR 3L-FC

S_j	S_1	S_2	S_3	S_4	Connection
S_P	1	1	0	0	X→P
S_N	0	0	1	1	Y→N
S_{CP}	1	0	1	0	Y→X→P
S_{CN}	0	1	0	1	X→Y→N

In the equations provided hereafter, the first switching state of the switches displayed in Table 2.3 will be represented by considering that $S_P = 1$ and $S_N = S_{CP} = S_{CN} = 0$, while the second one will be denoted by $S_N = 1$ and $S_P = S_{CP} = S_{CN} = 0$, and so on. As noticed for the generic case in (2.10), this implies that (2.25) is valid at any time, hence explicitly stating that the $N_{poss} = 4$ possible controls for the commutation cell are mutually exclusive.

$$S_P + S_N + S_{CP} + S_{CN} = 1 \tag{2.25}$$

Considering the case of a single leg, the following equations are derived by applying Kirchhoff's laws on the adequate meshes and nodes of the circuit in Fig. 2.4:

$$U_\phi = (S_{CN} - S_{CP})U_C + (S_P + S_{CP})U_{C1} - (S_N + S_{CN})U_{C2} \tag{2.26}$$

$$i_C = (S_{CN} - S_{CP})i_\phi \tag{2.27}$$

$$i_{C1} = i_P - i_{DC1}; \quad i_P = (S_P + S_{CP})i_\phi \tag{2.28}$$

$$i_{C2} = -i_N + i_{DC2}; \quad i_N = (S_N + S_{CN})i_\phi, \tag{2.29}$$

where all four possible switching states are handled together, as suggested for the general case in (2.10)–(2.12). Furthermore, using (2.28), (2.29) and (2.25), it is found that

$$i_G = i_{C1} - i_{C2} = (S_P + S_N + S_{CP} + S_{CN})i_\phi - i_{DC1} - i_{DC2} = i_\phi - i_{DC1} - i_{DC2}. \tag{2.30}$$

As pointed out in Section 3, extending this analysis to a 3L FC converter of any number of legs, N_{legs}, requires applying the theorem of superposition. Similarly to the Subsection 4.1 the (2.26)–(2.30) set turns, equation by equation, into the (2.31)–(2.35) set given next:

$$U_{\phi j} = \left(S_{jCN} - S_{jCP}\right)U_{Cj} + \left(S_{jP} + S_{jCP}\right)U_{C1} - \left(S_{jN} + S_{jCN}\right)U_{C2}; \quad \forall j \in \Psi \tag{2.31}$$

$$i_{Cj} = \left(S_{jCN} - S_{jCP}\right)i_{\phi j}; \quad \forall j \in \Psi \tag{2.32}$$

$$i_{C1} = i_P - i_{DC1}; \quad i_P = \sum_{j\in\Psi} \left(S_{jP} + S_{jCP}\right)i_{\phi j} \tag{2.33}$$

$$i_{C2} = -i_N - i_{DC2}; \quad i_N = \sum_{j\in\Psi} \left(S_{jN} + S_{jCN}\right) i_{\phi j} \tag{2.34}$$

$$i_G = \sum_{j\in\Psi} i_{Fj} - i_{DC1} - i_{DC2}. \tag{2.35}$$

4.3 Cascaded H-Bridge

From Fig. 2.5, the Three-Level Cascaded H-Bridge (3L-CHB) topology offers four different connection possibilities to bound the AC phases to the DC side. It is interesting to note that two distinct switching states lead to the same switching position:

(a) S_P: the phase is bound to the ground through the DC-link's capacitor, passing first by the P node

(b) S_N: the phase is bound to the ground through the DC-link's capacitor, passing first by the N node

(c) S_0: the phase is bound to the ground avoiding the DC-link

(d) S_0: the phase is directly connected to the ground, not to the DC-link.

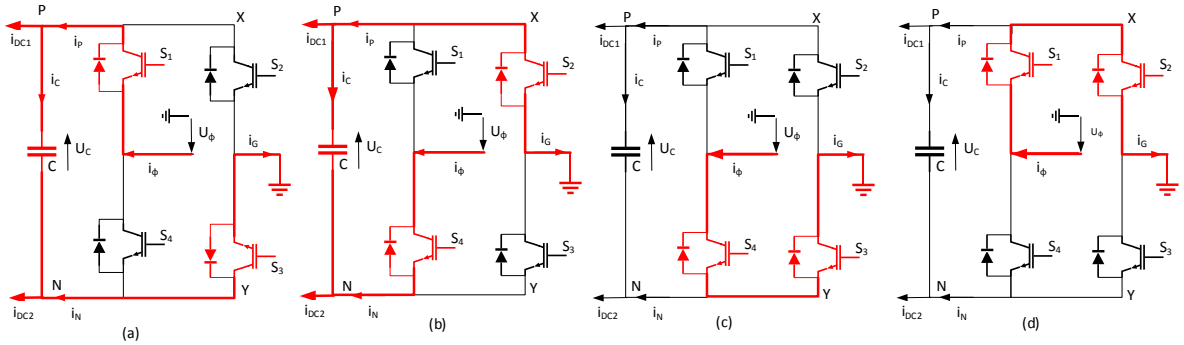

Fig. 2.5. Switching positions for one phase of 3L-CHB

In this specific case, the set of possible switching states for any commutation cell U_{cell}, is given by

$$U_{cell} = \{S_P, S_N, S_0\}. \tag{2.36}$$

The correspondence between the open/closed state of the switches constituting the switching cells of the converter leg and the previous values summed up in Table 2.4, where 1 represents the closed state and 0 the open state, and $\overline{\text{X}}$ stands for all points except X.

TABLE 2.4
RELATION BETWEEN THE SWITCHES STATE AND THE CONNECTION VARIABLE FOR 3L-CHB

S_j	S_1	S_2	S_3	S_4	Connection
S_P	1	0	1	0	$\overline{\text{X}}$
S_N	0	1	0	1	$\overline{\text{Y}}$
S_0	1	1	0	0	Y
S_0	0	0	1	1	X

In the equations provided hereafter, the first switching state of the switches displayed in Table 2.4 will be represented considering that $S_P = 1$ and $S_N = S_0 = 0$, while the second one will be denoted by $S_N = 1$ and $S_P = S_0 = 0$, and so on. As noticed for the generic case in (2.8), this implies that (2.37) is valid at any time, hence explicitly stating that the $N_{poss} = 3$ possible controls for the commutation cell are mutually exclusive. In this situation, the relation between the states of the switches and the connection variables is not bijective: four possible open/closed combinations are relevant but only three connection possibilities stand out, as two of the switch positions are equivalent in terms of routing.

$$S_P + S_N + S_0 = 1 \tag{2.37}$$

Considering the case of a single leg, the following equations are derived by applying Kirchhoff's laws on the adequate meshes and nodes of the circuit in Fig. 2.5:

$$U_\phi = (S_P - S_N)U_C \tag{2.38}$$

$$i_C = i_P - i_{DC1}; \quad i_P = S_P i_\phi \tag{2.39}$$

$$i_C = i_{DC2} - i_N; \; i_N = S_N i_\phi \tag{2.40}$$

where all four possible switching states are handled together, as suggested for the general case in (2.10)–(2.12). Furthermore, the combination of (2.39) and (2.40), minding the combinatory logic of the connection variables, and the application of the Kirchhoff's current law on the connection point to the ground and (2.17) lead respectively to (2.41) and (2.42).

$$2i_C = i_P - i_N + i_{DC1} - i_{DC2} \tag{2.41}$$

$$i_{Gr} = (S_P + S_N + S_0)\big(i_\phi - i_{DC1} - i_{DC2}\big) = i_\phi - i_{DC1} - i_{DC2}. \tag{2.42}$$

Adopting the notations and methods previously used in Subsections 4.1 and 4.2, the (2.38), (2.41)–(2.42) set turns, equation by equation, into the (2.43)–(2.45) set given next:

$$U_{\phi j} = \big(S_{jP} - S_{jN}\big)U_{Cj}; \quad \forall j \in \Psi \tag{2.43}$$

$$i_{Cj} = \big(S_{jP} - S_{jN}\big)\frac{\mathrm{i_{\phi j}}}{2} + \frac{i_{DC1j}}{2} - \frac{i_{DC2j}}{2} \quad \forall j \in \Psi \tag{2.44}$$

$$i_G = \textstyle\sum_{j\in\Psi} i_{\phi j} - i_{DC1j} - i_{DC2j}. \tag{2.45}$$

Contrarily to the FC and NPC topologies where the DC-link is shared, implicating only one DC source/load for the converter, the CHB topology has isolated DC loads/sources, as stated in Chapter 1.

Consequently, while in Subsections 4.1 and 4.2 the extension to multiple legs meant their was only one i_{DC1} and one i_{DC2}, there are as many pairs of those as there are legs for the CHB case, hence (2.44).

5 Switched-State Space Matrices

5.1 Different filters

Fig. 2.6 illustrates the three filters studied in this chapter. The L filter is the simplest one and is sufficient to establish a state-space representation of the converter when combined with the previously stated equation sets. Its schematic is represented into the green frame, considering all the other components shown on the figure as inexistent. However, it is common to employ LC and LCL filters as they offer better performances, such as concerning the current ripples or the suppression of undesired harmonics.

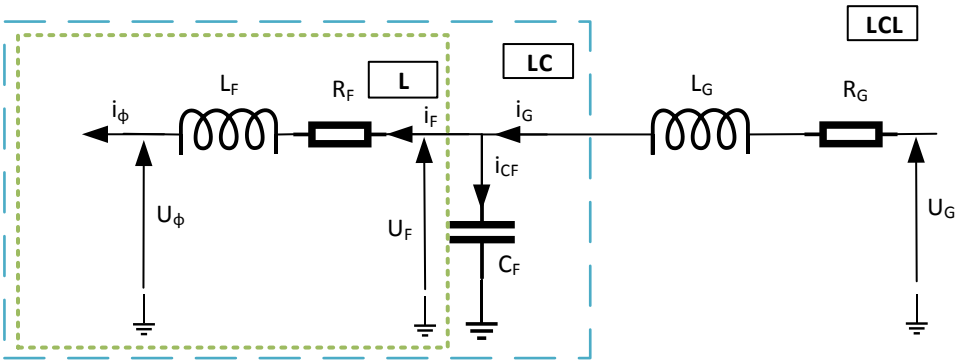

Fig. 2.6. Filters considered: L, LC and LCL

Similarly to the L filter, the LC one is shown in the blue casing. It is important to note that the state-space representation and its various describing vectors are determined not by the purpose of the plant, but by its nature. For instance, capacitors entail the presence of currents in the input vector, while inductances involve voltages, regardless of the current input to the system. Consequently, the AC-related input for L and LCL filters is a voltage and, for the LC case, it is a current, even though the overall situation may not change: for example, the grid could be considered as a voltage generator for all three filters. It may seem counter intuitive not to acknowledge the real behavior of the system as it is implemented in reality. However, the explanation comes from the definition of the system: as explained in Fig. 2.6, only the inside of the boxes belongs to the modeled system. An alternative formulation would be that everything outside of the filters themselves is not taken into account: the information about whether the plant is connected to a current or voltage generator is not accessible to the model.

The L filter equations are given by:

$$U_F - L_F \frac{di_F}{dt} - R_F i_F - U_\phi = 0 \tag{2.46}$$

$$i_\phi = i_F. \tag{2.47}$$

Equation (2.47) is applicable to all three topologies and all three filters. The equations describing the LC filter are given next:

$$U_F - L_F \frac{di_F}{dt} - R_F i_F - U_\phi = 0 \tag{2.48}$$

$$i_G - C_F \frac{dU_F}{dt} - i_F = 0. \tag{2.49}$$

Equations (2.46) and (2.48) are virtually identical. Indeed, the application of the mesh law on LC filter is the same as the one on L filter, as the voltage across the terminals of the C_F capacitor is the equal to the U_F voltage, since they are in parallel. Finally, the following expressions fully describe the LCL filter:

$$U_G - L_G \frac{di_G}{dt} - R_G i_G - U_F = 0 \tag{2.50}$$

$$U_F - L_F \frac{di_F}{dt} - R_F i_F - U_\phi = 0 \tag{2.51}$$

$$i_G - i_F - C_F \frac{dU_F}{dt} = 0. \tag{2.52}$$

These equations are combined with the equation sets of the previous subsections to form state-space representations of the converters. Considering the filters independently, equations (2.46)–(2.52) can be expressed for any $j \in \Psi$.

5.2 Detailed modeling of 3L-FC with LCL filter

Combining the equation sets from Section 4 and Subsection 0.1 for each converter topology and each filter, it becomes possible to establish the SSSR models of the 9 combinations of converter topology and filter. Each one of the three converter topologies can be associated to any of the three filters, leading to 9 potentialities. The reasoning leading to the state-space matrices will be developed for 3L-FC topology associated to LCL filter, which is the complete application discussed here in the following, but it is identically applied to the other cases in Annex 1 and Annex 2, respectively for 3L-NPC and 3L-CHB with LCL filter.

Some useful intermediate parameters and variables can be created to lighten the equations. Let us define (2.53) for all topologies, (2.54) for 3L-FC and (2.55) for 3L-CHB.

$$\left.\begin{aligned} \tau_{Gj} &= \frac{R_{Gj}}{L_{Gj}} \\ \tau_{Fj} &= \frac{R_{Fj}}{L_{Fj}} \end{aligned}\right\}; \quad \forall j \in \Psi \tag{2.53}$$

$$\Delta_j = S_{jCN} - S_{jCP}; \quad \Sigma_j = S_{jP} + S_{jCP}; \quad \Gamma_j = S_{jN} + S_{jCN} \tag{2.54}$$

$$\Delta_j = S_{jP} - S_{jN} \tag{2.55}$$

The definitions of (2.54) and (2.55) imply that Δ_j, Σ_j and Γ_j are functions of the control $\boldsymbol{u}$ applied to the system.

From Subsection 4.2, as far as the capacitors of the converter and the DC-link are concerned, their corresponding dynamics are modeled as

$$C_j \frac{dU_{Cj}}{dt} = i_{Cj}; \quad \forall j \in \Psi \tag{2.56}$$

$$C_1 \frac{dU_{c1}}{dt} = i_{c1} \tag{2.57}$$

$$C_2 \frac{dU_{c2}}{dt} = i_{c2}. \tag{2.58}$$

Solving the di_{Gj}/dt in (2.50) gives rise to the following first set of four state equations:

$$\frac{di_{Gj}}{dt} = -\tau_{Gj} i_{Gj} - \frac{1}{L_{Gj}} U_{Fj} + \frac{1}{L_{Gj}} U_{Gj}; \quad \forall j \in \Psi. \tag{2.59}$$

Moreover, replacing (2.31) into (2.51), and subsequently solving for di_{Fj}/dt, produces

$$\frac{di_{Fj}}{dt} = -\tau_{Fj} i_{Fj} + \frac{1}{L_{Fj}} U_{Fj} - \frac{1}{L_{Fj}} \Delta_j U_{Cj} - \frac{1}{L_{Fj}} \Sigma_j U_{C1} + \frac{1}{L_{Fj}} \Gamma_j U_{C2}; \quad \forall j \in \Psi. \tag{2.60}$$

The last set of four state equations arising from the LCL filter is derived from (2.52) as follows:

$$\frac{dU_{Fj}}{dt} = \frac{1}{C_{Fj}} i_{Gj} - \frac{1}{C_{Fj}} i_{Fj}; \quad \forall j \in \Psi. \tag{2.61}$$

On the other hand, after replacing (2.32) into (2.56), consideration of (2.47) leads to

$$\frac{dU_{Cj}}{dt} = \frac{1}{C_j} \Delta_j i_{Fj}; \quad \forall j \in \Psi. \tag{2.62}$$

Finally, taking (2.47) into account, the last two state equations provided next are derived by substituting (2.33) and (2.34) into, respectively, (2.57) and (2.58):

$$\frac{dU_{c1}}{dt} = \frac{1}{C_1} \sum_{j \in \Psi} \Sigma_j i_{Fj} - \frac{1}{C_1} i_{DC1} \tag{2.63}$$

$$\frac{dU_{c2}}{dt} = -\frac{1}{C_2} \sum_{j \in \Psi} \Gamma_j i_{Fj} + \frac{1}{C_2} i_{DC2}. \tag{2.64}$$

From (2.59)–(2.64), the adequate state vector as described in (2.4) is

$$\boldsymbol{x}_A^T = \left[i_{G\Psi_1} \dots i_{G\Psi_{Nlegs}} i_{F\Psi_1} \dots i_{F\Psi_{Nlegs}} U_{F\Psi_1} \dots U_{F\Psi_{Nlegs}} \right] \tag{2.65}$$

$$\boldsymbol{x}_{con}^{T} = \left[U_{C\Psi_1} \dots U_{C\Psi_{Nlegs}}\right];\ \ \boldsymbol{x}_{B}^{T} = [U_{C1}\ U_{C2}], \tag{2.66}$$

and the input vector, also from (2.4), is given by

$$\boldsymbol{d}_{A}^{T} = \left[U_{G\Psi_1} \dots U_{G\Psi_{Nlegs}}\right];\ \ \boldsymbol{d}_{B} = [i_{DC}]. \tag{2.67}$$

For any topology and for any phase-repeated parameter or variable, $\lambda_j; j \in \Psi$, let us also define

$$\boldsymbol{\lambda} = \begin{bmatrix} \lambda_{\Psi_1} \\ \vdots \\ \lambda_{\Psi_{N_{legs}}} \end{bmatrix};\ \ diag(\boldsymbol{\lambda}) = \begin{bmatrix} \lambda_{\Psi_1} & \cdots & 0 \\ \vdots & \ddots & \vdots \\ 0 & \cdots & \lambda_{\Psi_{N_{legs}}} \end{bmatrix}. \tag{2.68}$$

From there on, the submatrices defined in (2.5) can be deduced for the 3L-FC case associated to an LCL filter as follows:

$$\boldsymbol{A}_{AA} = \begin{bmatrix} diag(-\boldsymbol{\tau}_G) & \mathbb{O}_{\mathrm{N_{legs}}\times\mathrm{N_{legs}}} & diag\left(-\frac{1}{\boldsymbol{L}_G}\right) \\ \mathbb{O}_{\mathrm{N_{legs}}\times\mathrm{N_{legs}}} & diag(-\boldsymbol{\tau}_F) & diag\left(\frac{1}{\boldsymbol{L}_F}\right) \\ diag\left(\frac{1}{\boldsymbol{C}_F}\right) & diag\left(-\frac{1}{\boldsymbol{C}_F}\right) & \mathbb{O}_{\mathrm{N_{legs}}\times\mathrm{N_{legs}}} \end{bmatrix} \tag{2.69}$$

$$\boldsymbol{A}_{AB} = \begin{bmatrix} \mathbb{O}_{\mathrm{N_{legs}}\times 1} & \mathbb{O}_{\mathrm{N_{legs}}\times 1} \\ -\boldsymbol{\Sigma}/\boldsymbol{L}_F & \boldsymbol{\Gamma}/\boldsymbol{L}_F \\ \mathbb{O}_{\mathrm{N_{legs}}\times 1} & \mathbb{O}_{\mathrm{N_{legs}}\times 1} \end{bmatrix};\ \ \boldsymbol{A}_{Acon} = \begin{bmatrix} \mathbb{O}_{\mathrm{N_{legs}}\times\mathrm{N_{legs}}} \\ diag\left(-\frac{\boldsymbol{\Delta}}{\boldsymbol{L}_F}\right) \\ \mathbb{O}_{\mathrm{N_{legs}}\times\mathrm{N_{legs}}} \end{bmatrix} \tag{2.70}$$

$$\boldsymbol{A}_{BA} = \begin{bmatrix} \mathbb{O}_{1\times\mathrm{N_{legs}}} & \boldsymbol{\Sigma}^T/C_1 & \mathbb{O}_{1\times\mathrm{N_{legs}}} \\ \mathbb{O}_{1\times\mathrm{N_{legs}}} & -\boldsymbol{\Gamma}^T/C_2 & \mathbb{O}_{1\times\mathrm{N_{legs}}} \end{bmatrix} \tag{2.71}$$

$$\boldsymbol{A}_{BB} = \mathbb{O}_{2\times 2};\ \ \boldsymbol{A}_{Bcon} = \mathbb{O}_{2\times\mathrm{N_{legs}}};\ \ \boldsymbol{A}_{conB} = \mathbb{O}_{\mathrm{N_{legs}}\times 2};\ \ \boldsymbol{A}_{concon} = \mathbb{O}_{\mathrm{N_{legs}}\times\mathrm{N_{legs}}} \tag{2.72}$$

$$\boldsymbol{A}_{conA} = \begin{bmatrix} \mathbb{O}_{\mathrm{N_{legs}}\times\mathrm{N_{legs}}} & diag\left(\frac{\boldsymbol{\Delta}}{\boldsymbol{C}}\right) & \mathbb{O}_{\mathrm{N_{legs}}\times\mathrm{N_{legs}}} \end{bmatrix} \tag{2.73}$$

Similarly, the $\boldsymbol{E}$ matrix is stated thereafter:

$$\boldsymbol{E} = \begin{bmatrix} diag\left(\frac{1}{\boldsymbol{L}_G}\right) & \mathbb{O}_{\mathrm{N_{legs}}\times 1} & \mathbb{O}_{\mathrm{N_{legs}}\times 1} \\ \mathbb{O}_{3\mathrm{N_{legs}}\times\mathrm{N_{legs}}} & \mathbb{O}_{3\mathrm{N_{legs}}\times 1} & \mathbb{O}_{3\mathrm{N_{legs}}\times 1} \\ \mathbb{O}_{1\times\mathrm{N_{legs}}} & -1/C_1 & 0 \\ \mathbb{O}_{1\times\mathrm{N_{legs}}} & 0 & 1/C_2 \end{bmatrix} \tag{2.74}$$

5.3 SSSR of all topologies

Following the methodology described previously and applying it to the different cases precedingly evoked, the state and input vectors for the three topologies and the three filters are summed up in Table 2.5:

TABLE 2.5
STATE AND DISTURBANCE VECTORS

Filter	Topology	$\boldsymbol{x}_A$	$\boldsymbol{x}_{con}$	$\boldsymbol{x}_B$	$\boldsymbol{d}_A$	$\boldsymbol{d}_B$
L	NPC	$\boldsymbol{i}_F$	$\emptyset$	$\begin{bmatrix} U_{C1} \\ U_{C2} \end{bmatrix}$	$\boldsymbol{U}_F$	$\begin{bmatrix} i_{DC1} \\ i_{DC2} \end{bmatrix}$
	FC		$\boldsymbol{U}_C$			
	CHB		$\emptyset$	$\boldsymbol{U}_C$		$\begin{bmatrix} \boldsymbol{i}_{DC1} \\ \boldsymbol{i}_{DC2} \end{bmatrix}$
LC	NPC	$\begin{bmatrix} \boldsymbol{i}_F \\ \boldsymbol{U}_F \end{bmatrix}$	$\emptyset$	$\begin{bmatrix} U_{C1} \\ U_{C2} \end{bmatrix}$	$\boldsymbol{i}_G$	$\begin{bmatrix} i_{DC1} \\ i_{DC2} \end{bmatrix}$
	FC		$\boldsymbol{U}_C$			
	CHB		$\emptyset$	$\boldsymbol{U}_C$		$\begin{bmatrix} \boldsymbol{i}_{DC1} \\ \boldsymbol{i}_{DC2} \end{bmatrix}$
LCL	NPC	$\begin{bmatrix} \boldsymbol{i}_G \\ \boldsymbol{i}_F \\ \boldsymbol{U}_F \end{bmatrix}$	$\emptyset$	$\begin{bmatrix} U_{C1} \\ U_{C2} \end{bmatrix}$	$\boldsymbol{U}_G$	$\begin{bmatrix} i_{DC1} \\ i_{DC2} \end{bmatrix}$
	FC		$\boldsymbol{U}_C$			
	CHB		$\emptyset$	$\boldsymbol{U}_C$		$\begin{bmatrix} \boldsymbol{i}_{DC1} \\ \boldsymbol{i}_{DC2} \end{bmatrix}$

Considering the above notations, the submatrices forming the A matrix of (2.3) according to (2.5) are given in the following tables for the three topologies and the three filters.

TABLE 2.6
SUBMATRICES FOR SSSR OF 3L-NPC

sub-matrix	L	LC	LCL
$\boldsymbol{A}_{AA}$	$diag(-\boldsymbol{\tau}_F)$	$\begin{bmatrix} diag(-\boldsymbol{\tau}_F) & diag(\frac{1}{\boldsymbol{L}_F}) \\ diag\left(-\frac{1}{\boldsymbol{C}_F}\right) & \mathbb{O}_{\mathrm{N_{legs}}\times\mathrm{N_{legs}}} \end{bmatrix}$	$\begin{bmatrix} diag(-\boldsymbol{\tau}_G) & \mathbb{O}_{\mathrm{N_{legs}}\times\mathrm{N_{legs}}} & diag(-\frac{1}{\boldsymbol{L}_G}) \\ \mathbb{O}_{\mathrm{N_{legs}}\times\mathrm{N_{legs}}} & diag(-\boldsymbol{\tau}_F) & diag(\frac{1}{\boldsymbol{L}_F}) \\ diag(\frac{1}{\boldsymbol{C}_F}) & diag\left(-\frac{1}{\boldsymbol{C}_F}\right) & \mathbb{O}_{\mathrm{N_{legs}}\times\mathrm{N_{legs}}} \end{bmatrix}$
$\boldsymbol{A}_{AB}$	$\begin{bmatrix} -\frac{\boldsymbol{S}_P}{\boldsymbol{L}_F} & \frac{\boldsymbol{S}_N}{\boldsymbol{L}_F} \end{bmatrix}$	$\begin{bmatrix} \frac{-\boldsymbol{S}_P}{\boldsymbol{L}_F} & \frac{\boldsymbol{S}_N}{\boldsymbol{L}_F} \\ \mathbb{O}_{\mathrm{N_{legs}}\times 1} & \mathbb{O}_{\mathrm{N_{legs}}\times 1} \end{bmatrix}$	$\begin{bmatrix} \mathbb{O}_{\mathrm{N_{legs}}\times 1} & \mathbb{O}_{\mathrm{N_{legs}}\times 1} \\ \frac{-\boldsymbol{S}_P}{\boldsymbol{L}_F} & \frac{\boldsymbol{S}_N}{\boldsymbol{L}_F} \\ \mathbb{O}_{\mathrm{N_{legs}}\times 1} & \mathbb{O}_{\mathrm{N_{legs}}\times 1} \end{bmatrix}$

$\boldsymbol{A}_{Acon}$	$\emptyset$	$\emptyset$	$\emptyset$
$\boldsymbol{A}_{BA}$	$\begin{bmatrix} \boldsymbol{S}_P^T/C_1 \\ -\boldsymbol{S}_N^T/C_2 \end{bmatrix}$	$\begin{bmatrix} \boldsymbol{S}_P^T/C_1 & \mathbb{O}_{1\times \mathrm{N_{legs}}} \\ -\boldsymbol{S}_N^T/C_2 & \mathbb{O}_{1\times \mathrm{N_{legs}}} \end{bmatrix}$	$\begin{bmatrix} \mathbb{O}_{1\times \mathrm{N_{legs}}} & \boldsymbol{S}_P^T/C_1 & \mathbb{O}_{1\times \mathrm{N_{legs}}} \\ \mathbb{O}_{1\times \mathrm{N_{legs}}} & -\boldsymbol{S}_N^T/C_2 & \mathbb{O}_{1\times \mathrm{N_{legs}}} \end{bmatrix}$
$\boldsymbol{A}_{BB}$	$\mathbb{O}_{2\times 2}$	$\mathbb{O}_{2\times 2}$	$\mathbb{O}_{2\times 2}$
$\boldsymbol{A}_{Bcon}$	$\emptyset$	$\emptyset$	$\emptyset$
$\boldsymbol{A}_{CA}$	$\emptyset$	$\emptyset$	$\emptyset$
$\boldsymbol{A}_{conB}$	$\emptyset$	$\emptyset$	$\emptyset$
$\boldsymbol{A}_{concon}$	$\emptyset$	$\emptyset$	$\emptyset$

TABLE 2.7
SUBMATRICES FOR SSSR OF 3L-FC

sub-matrix	L	LC	LCL
$\boldsymbol{A}_{AA}$	$[diag(-\boldsymbol{\tau}_F)]$	$\begin{bmatrix} diag(-\boldsymbol{\tau}_F) & diag(\frac{1}{\boldsymbol{L}_F}) \\ diag(-\frac{1}{\boldsymbol{C}_F}) & \mathbb{O}_{\mathrm{N_{legs}}\times \mathrm{N_{legs}}} \end{bmatrix}$	$\begin{bmatrix} diag(-\boldsymbol{\tau}_G) & \mathbb{O}_{\mathrm{N_{legs}}\times \mathrm{N_{legs}}} & diag\left(-\frac{1}{\boldsymbol{L}_G}\right) \\ \mathbb{O}_{\mathrm{N_{legs}}\times \mathrm{N_{legs}}} & diag(-\boldsymbol{\tau}_F) & diag\left(\frac{1}{\boldsymbol{L}_F}\right) \\ diag\left(\frac{1}{\boldsymbol{C}_F}\right) & diag\left(-\frac{1}{\boldsymbol{C}_F}\right) & \mathbb{O}_{\mathrm{N_{legs}}\times \mathrm{N_{legs}}} \end{bmatrix}$
$\boldsymbol{A}_{AB}$	$[-\boldsymbol{\Sigma}/\boldsymbol{L}_F \quad \boldsymbol{\Gamma}/\boldsymbol{L}_F]$	$\begin{bmatrix} -\boldsymbol{\Sigma}/\boldsymbol{L}_F & \boldsymbol{\Gamma}/\boldsymbol{L}_F \\ \mathbb{O}_{\mathrm{N_{legs}}\times 1} & \mathbb{O}_{\mathrm{N_{legs}}\times 1} \end{bmatrix}$	$\begin{bmatrix} \mathbb{O}_{\mathrm{N_{legs}}\times 1} & \mathbb{O}_{\mathrm{N_{legs}}\times 1} \\ -\boldsymbol{\Sigma}/\boldsymbol{L}_F & \boldsymbol{\Gamma}/\boldsymbol{L}_F \\ \mathbb{O}_{\mathrm{N_{legs}}\times 1} & \mathbb{O}_{\mathrm{N_{legs}}\times 1} \end{bmatrix}$
$\boldsymbol{A}_{Acon}$	$\left[diag(-\frac{\boldsymbol{\Delta}}{\boldsymbol{L}_F})\right]$	$\begin{bmatrix} diag(-\frac{\boldsymbol{\Delta}}{\boldsymbol{L}_F}) \\ \mathbb{O}_{\mathrm{N_{legs}}\times \mathrm{N_{legs}}} \end{bmatrix}$	$\begin{bmatrix} \mathbb{O}_{\mathrm{N_{legs}}\times \mathrm{N_{legs}}} \\ diag\left(-\frac{\boldsymbol{\Delta}}{\boldsymbol{L}_F}\right) \\ \mathbb{O}_{\mathrm{N_{legs}}\times \mathrm{N_{legs}}} \end{bmatrix}$
$\boldsymbol{A}_{BA}$	$\begin{bmatrix} \boldsymbol{\Sigma}^T/C_1 \\ -\boldsymbol{\Gamma}^T/C_2 \end{bmatrix}$	$\begin{bmatrix} \boldsymbol{\Sigma}^T/C_1 & \mathbb{O}_{1\times \mathrm{N_{legs}}} \\ -\boldsymbol{\Gamma}^T/C_2 & \mathbb{O}_{1\times \mathrm{N_{legs}}} \end{bmatrix}$	$\begin{bmatrix} \mathbb{O}_{1\times \mathrm{N_{legs}}} & \boldsymbol{\Sigma}^T/C_1 & \mathbb{O}_{1\times \mathrm{N_{legs}}} \\ \mathbb{O}_{1\times \mathrm{N_{legs}}} & -\boldsymbol{\Gamma}^T/C_2 & \mathbb{O}_{1\times \mathrm{N_{legs}}} \end{bmatrix}$
$\boldsymbol{A}_{BB}$	$\mathbb{O}_{2\times 2}$	$\mathbb{O}_{2\times 2}$	$\mathbb{O}_{2\times 2}$
$\boldsymbol{A}_{Bcon}$	$\mathbb{O}_{2\times \mathrm{N_{legs}}}$	$\mathbb{O}_{2\times \mathrm{N_{legs}}}$	$\mathbb{O}_{2\times \mathrm{N_{legs}}}$
$\boldsymbol{A}_{conA}$	$\left[diag(\frac{\boldsymbol{\Delta}}{\boldsymbol{C}_\phi})\right]$	$\left[diag(\frac{\boldsymbol{\Delta}}{\boldsymbol{C}_\phi}) \quad \mathbb{O}_{\mathrm{N_{legs}}\times \mathrm{N_{legs}}}\right]$	$\left[\mathbb{O}_{\mathrm{N_{legs}}\times \mathrm{N_{legs}}} \quad diag\left(\frac{\boldsymbol{\Delta}}{\boldsymbol{C}_\phi}\right) \quad \mathbb{O}_{\mathrm{N_{legs}}\times \mathrm{N_{legs}}}\right]$
$\boldsymbol{A}_{conB}$	$\mathbb{O}_{\mathrm{N_{legs}}\times 2}$	$\mathbb{O}_{\mathrm{N_{legs}}\times 2}$	$\mathbb{O}_{\mathrm{N_{legs}}\times 2}$
$\boldsymbol{A}_{concon}$	$\mathbb{O}_{\mathrm{N_{legs}}\times \mathrm{N_{legs}}}$	$\mathbb{O}_{\mathrm{N_{legs}}\times \mathrm{N_{legs}}}$	$\mathbb{O}_{\mathrm{N_{legs}}\times \mathrm{N_{legs}}}$

TABLE 2.8
SUBMATRICES FOR SSSR OF 3L-CHB

sub-matrix	L	LC	LCL
$\boldsymbol{A_{AA}}$	$[diag(-\boldsymbol{\tau}_F)]$	$\begin{bmatrix} diag(-\boldsymbol{\tau}_F) & diag\left(\frac{1}{\boldsymbol{L}_F}\right) \\ diag\left(-\frac{1}{\boldsymbol{C}_F}\right) & \mathbb{O}_{\mathrm{N_{legs}}\times\mathrm{N_{legs}}} \end{bmatrix}$	$\begin{bmatrix} diag(-\boldsymbol{\tau}_G) & \mathbb{O}_{\mathrm{N_{legs}}\times\mathrm{N_{legs}}} & diag\left(-\frac{1}{\boldsymbol{L}_G}\right) \\ \mathbb{O}_{\mathrm{N_{legs}}\times\mathrm{N_{legs}}} & diag(-\boldsymbol{\tau}_F) & diag\left(\frac{1}{\boldsymbol{L}_F}\right) \\ diag\left(\frac{1}{\boldsymbol{C}_F}\right) & diag\left(-\frac{1}{\boldsymbol{C}_F}\right) & \mathbb{O}_{\mathrm{N_{legs}}\times\mathrm{N_{legs}}} \end{bmatrix}$
$\boldsymbol{A_{AB}}$	$\left[\mathrm{diag}(\frac{\boldsymbol{\Delta}}{\boldsymbol{L}_F})\right]$	$\begin{bmatrix} \mathrm{diag}\left(\frac{\boldsymbol{\Delta}}{\boldsymbol{L}_F}\right) \\ \mathbb{O}_{N_{legs}\times\mathrm{N_{legs}}} \end{bmatrix}$	$\begin{bmatrix} \mathbb{O}_{\mathrm{N_{legs}}\times\mathrm{N_{legs}}} \\ \mathrm{diag}\left(\frac{\boldsymbol{\Delta}}{\boldsymbol{L}_F}\right) \\ \mathbb{O}_{\mathrm{N_{legs}}\times\mathrm{N_{legs}}} \end{bmatrix}$
$\boldsymbol{A_{Acon}}$	$\emptyset$	$\emptyset$	$\emptyset$
$\boldsymbol{A_{BA}}$	$\left[diag(-\frac{\boldsymbol{\Delta}^T}{2\boldsymbol{C}})\right]$	$\left[diag(-\frac{\boldsymbol{\Delta}^T}{2\boldsymbol{C}}) \quad \mathbb{O}_{\mathrm{N_{legs}}\times\mathrm{N_{legs}}}\right]$	$\left[\mathbb{O}_{\mathrm{N_{legs}}\times\mathrm{N_{legs}}} \quad diag(-\frac{\boldsymbol{\Delta}^T}{2\boldsymbol{C}}) \quad \mathbb{O}_{\mathrm{N_{legs}}\times\mathrm{N_{legs}}}\right]$
$\boldsymbol{A_{BB}}$	$\mathbb{O}_{\mathrm{N_{legs}}\times\mathrm{N_{legs}}}$	$\mathbb{O}_{\mathrm{N_{legs}}\times\mathrm{N_{legs}}}$	$\mathbb{O}_{\mathrm{N_{legs}}\times\mathrm{N_{legs}}}$
$\boldsymbol{A_{Bcon}}$	$\emptyset$	$\emptyset$	$\emptyset$
$\boldsymbol{A_{conA}}$	$\emptyset$	$\emptyset$	$\emptyset$
$\boldsymbol{A_{conB}}$	$\emptyset$	$\emptyset$	$\emptyset$
$\boldsymbol{A_{concon}}$	$\emptyset$	$\emptyset$	$\emptyset$

The only missing part allowing to fully define the power converter is the E matrices. Keeping in mind the state vectors given in Table 2.4, the E matrices are deduced from Subsection 4 and summed up in Table 2.9.

TABLE 2.9
E MATRICES FOR EVERY TOPOLOGY AND FILTER

Filter / Topology	L	LC	LCL
3L-NPC	$\begin{bmatrix} diag(\frac{1}{\boldsymbol{L}_F}) & \mathbb{O}_{\mathrm{N_{legs}}\times 1} & \mathbb{O}_{\mathrm{N_{legs}}\times 1} \\ \mathbb{O}_{1\times\mathrm{N_{legs}}} & \frac{1}{C_1} & 0 \\ \mathbb{O}_{1\times\mathrm{N_{legs}}} & 0 & -\frac{1}{C_2} \end{bmatrix}$	$\begin{bmatrix} \mathbb{O}_{\mathrm{N_{legs}}\times\mathrm{N_{legs}}} & \mathbb{O}_{\mathrm{N_{legs}}\times 1} & \mathbb{O}_{\mathrm{N_{legs}}\times 1} \\ diag(\frac{1}{\boldsymbol{C}_F}) & \mathbb{O}_{\mathrm{N_{legs}}\times 1} & \mathbb{O}_{\mathrm{N_{legs}}\times 1} \\ \mathbb{O}_{1\times\mathrm{N_{legs}}} & \frac{1}{C_1} & 0 \\ \mathbb{O}_{1\times\mathrm{N_{legs}}} & 0 & -\frac{1}{C_2} \end{bmatrix}$	$\begin{bmatrix} diag(\frac{1}{\boldsymbol{L}_G}) & \mathbb{O}_{\mathrm{N_{legs}}\times 1} & \mathbb{O}_{\mathrm{N_{legs}}\times 1} \\ \mathbb{O}_{2\mathrm{N_{legs}}\times\mathrm{N_{legs}}} & \mathbb{O}_{2\mathrm{N_{legs}}\times 1} & \mathbb{O}_{2\mathrm{N_{legs}}\times 1} \\ \mathbb{O}_{1\times\mathrm{N_{legs}}} & \frac{1}{C_1} & 0 \\ \mathbb{O}_{1\times\mathrm{N_{legs}}} & 0 & -\frac{1}{C_2} \end{bmatrix}$
3L-FC	$\begin{bmatrix} diag(\frac{1}{\boldsymbol{L}_F}) & \mathbb{O}_{\mathrm{N_{legs}}\times 1} & \mathbb{O}_{\mathrm{N_{legs}}\times 1} \\ \mathbb{O}_{\mathrm{N_{legs}}\times\mathrm{N_{legs}}} & \mathbb{O}_{\mathrm{N_{legs}}\times 1} & \mathbb{O}_{\mathrm{N_{legs}}\times 1} \\ \mathbb{O}_{1\times\mathrm{N_{legs}}} & \frac{1}{C_1} & 0 \\ \mathbb{O}_{1\times\mathrm{N_{legs}}} & 0 & -\frac{1}{C_2} \end{bmatrix}$	$\begin{bmatrix} \mathbb{O}_{\mathrm{N_{legs}}\times\mathrm{N_{legs}}} & \mathbb{O}_{\mathrm{N_{legs}}\times 1} & \mathbb{O}_{\mathrm{N_{legs}}\times 1} \\ diag(\frac{1}{\boldsymbol{C}_F}) & \mathbb{O}_{\mathrm{N_{legs}}\times 1} & \mathbb{O}_{\mathrm{N_{legs}}\times 1} \\ \mathbb{O}_{\mathrm{N_{legs}}\times\mathrm{N_{legs}}} & \mathbb{O}_{\mathrm{N_{legs}}\times 1} & \mathbb{O}_{\mathrm{N_{legs}}\times 1} \\ \mathbb{O}_{1\times\mathrm{N_{legs}}} & -1/C_1 & 0 \\ \mathbb{O}_{1\times\mathrm{N_{legs}}} & 0 & 1/C_2 \end{bmatrix}$	$\begin{bmatrix} diag\left(\frac{1}{\boldsymbol{L}_G}\right) & \mathbb{O}_{\mathrm{N_{legs}}\times 1} & \mathbb{O}_{\mathrm{N_{legs}}\times 1} \\ \mathbb{O}_{3\mathrm{N_{legs}}\times\mathrm{N_{legs}}} & \mathbb{O}_{3\mathrm{N_{legs}}\times 1} & \mathbb{O}_{3\mathrm{N_{legs}}\times 1} \\ \mathbb{O}_{1\times\mathrm{N_{legs}}} & 1/C_1 & 0 \\ \mathbb{O}_{1\times\mathrm{N_{legs}}} & 0 & -1/C_2 \end{bmatrix}$
3L-CHB	$\begin{bmatrix} diag(\frac{1}{\boldsymbol{L}_F}) & \mathbb{O}_{\mathrm{N_{legs}}\times 1} & \mathbb{O}_{\mathrm{N_{legs}}\times 1} \\ \mathbb{O}_{\mathrm{N_{legs}}\times\mathrm{N_{legs}}} & diag(\frac{1}{2\boldsymbol{C}}) & diag(-\frac{1}{2\boldsymbol{C}}) \end{bmatrix}$	$\begin{bmatrix} \mathbb{O}_{\mathrm{N_{legs}}\times\mathrm{N_{legs}}} & \mathbb{O}_{\mathrm{N_{legs}}\times 1} & \mathbb{O}_{\mathrm{N_{legs}}\times 1} \\ diag\left(\frac{1}{\boldsymbol{C}_F}\right) & \mathbb{O}_{\mathrm{N_{legs}}\times 1} & \mathbb{O}_{\mathrm{N_{legs}}\times 1} \\ \mathbb{O}_{\mathrm{N_{legs}}\times\mathrm{N_{legs}}} & diag(\frac{1}{2\boldsymbol{C}}) & diag(-\frac{1}{2\boldsymbol{C}}) \end{bmatrix}$	$\begin{bmatrix} diag(\frac{1}{\boldsymbol{L}_G}) & \mathbb{O}_{\mathrm{N_{legs}}\times 1} & \mathbb{O}_{\mathrm{N_{legs}}\times 1} \\ \mathbb{O}_{2\mathrm{N_{legs}}\times\mathrm{N_{legs}}} & \mathbb{O}_{2\mathrm{N_{legs}}\times 1} & \mathbb{O}_{2\mathrm{N_{legs}}\times 1} \\ \mathbb{O}_{\mathrm{N_{legs}}\times\mathrm{N_{legs}}} & diag(\frac{1}{2\boldsymbol{C}}) & diag(-\frac{1}{2\boldsymbol{C}}) \end{bmatrix}$

6 Validation of the obtained models

To validate the models presented above, a Simscape Power System™ simulation model has been used with the configuration illustrated in Fig. 2.7. The AC grid considered is modeled by means of a balanced ideal star-connected three-phase generator, whereas the DC link is portrayed as a voltage generator associated to a resistance. Fig. 2.7 shows a generic overview of the modeled system, where the passive LCL filter block is selected from Fig. 2.6 and the converter legs are chosen among the ones described in Fig. 2.3, Fig. 2.4, or Fig. 2.5. The illustration shows a FC leg.

To be consistent with the topologies, in the NPC and FC cases, the DC side voltage generator is lone and connected in parallel to the three DC sides of the converter legs, while in the CHB case a different generator is connected to each leg. The 9 combinations of topology and filter can be implemented with this same structure, minding the property explained previously. The electrical parameters considered for the overall system are displayed in Table 10.

TABLE 2.10
NUMERICAL VALUES OF THE PARAMETERS

Parameter	Value	Unit
R_{Fj}	10	Ω
R_{Gj}	10	Ω
L_{Fj}	30	mH
L_{Gj}	30	mH
C_{Fj}	1	mF
C_j	1	mF
C_1	3.3	mF
C_2	3.3	mF
V_{Gj}	230	V (rms)
i_{DC}	10	A
T	100	µs

The capacitors of the DC link of the CHB topology are chosen equal to C_1 and C_2. In the present case, the i_{DC} value from the previous table is applied for i_{DC1} and $-i_{DC2}$. For the case of CHB, the three DC generators are identical to the one used for NPC and FC.

Aiming at assessing the accuracy of the SSSR, its continuous and discrete-time versions are compared to each other as well as to the aforementioned Simscape Power Systems™ model (SPSM). All three models —SPSM, continuous SSSR (CSSSR) and discrete SSSR (DSSSR)— undergo identical disturbance inputs and are driven by the same switching sequence. The sequence has been chosen to cover a large spectrum of possible switching positions and is not relevant in terms of control. Fig. 2.8, Fig. 2.11 and Fig. 2.14 present the switching sequences used for the different topologies. An important number of transitions are performed, with a representative diversity. This is crucial to draw a conclusion on the accuracy of the models: they have to be confronted to a maximal number of cases.

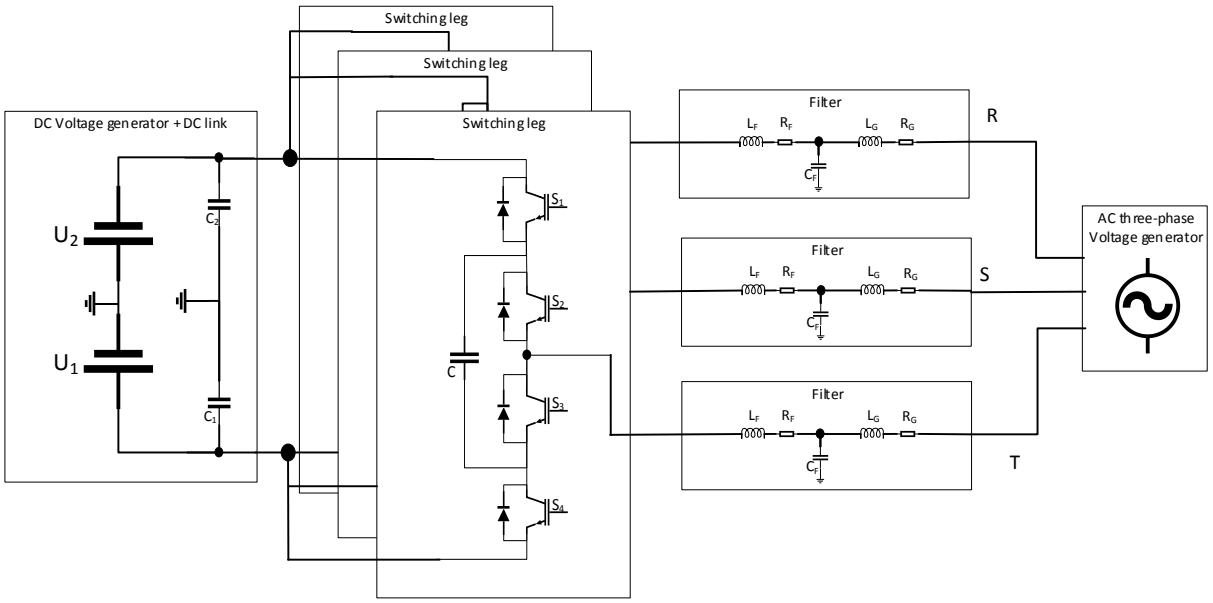

Fig. 2.7. Overview of the context of the study, particularized for the example of 3L-FC with LCL filter

For the evaluation test, only a 30-millisecond window of the 1-second test performed is displayed, during which a particularly high number of all the possible switching states takes spontaneously place. Among the state variables, only the interface ones are shown here. The current flowing through the inductance closest to the grid is one of them, the other one is the voltage across the terminals of the DC link capacitors. Each topology is associated to the three different filters, so three sets of data are extracted for each topology. To gain clarity, those sets are generated with the exact same inputs, both the control and the uncontrolled ones. Contrary to the uncontrolled inputs, which are defined by external elements, found in Table IX, the control sequence has to be topology-specific. Therefore, the same control sequence is used for the three applications of each topology, but different ones are generated for the different topologies.

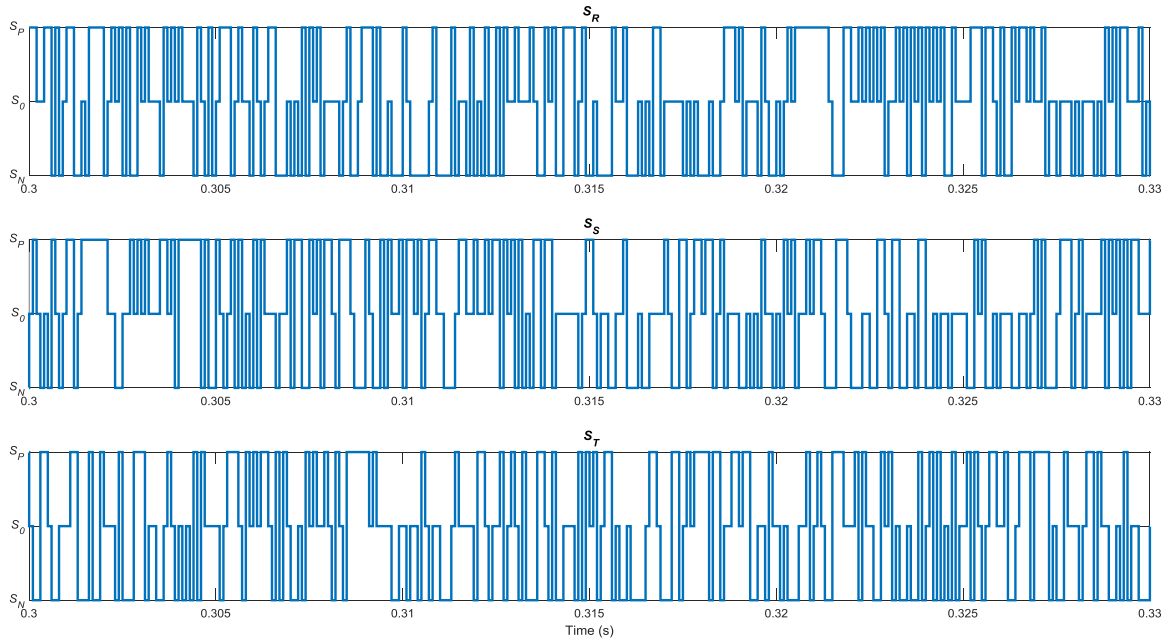

Fig. 2.8. Switching sequence applied to the 3L-CHB model

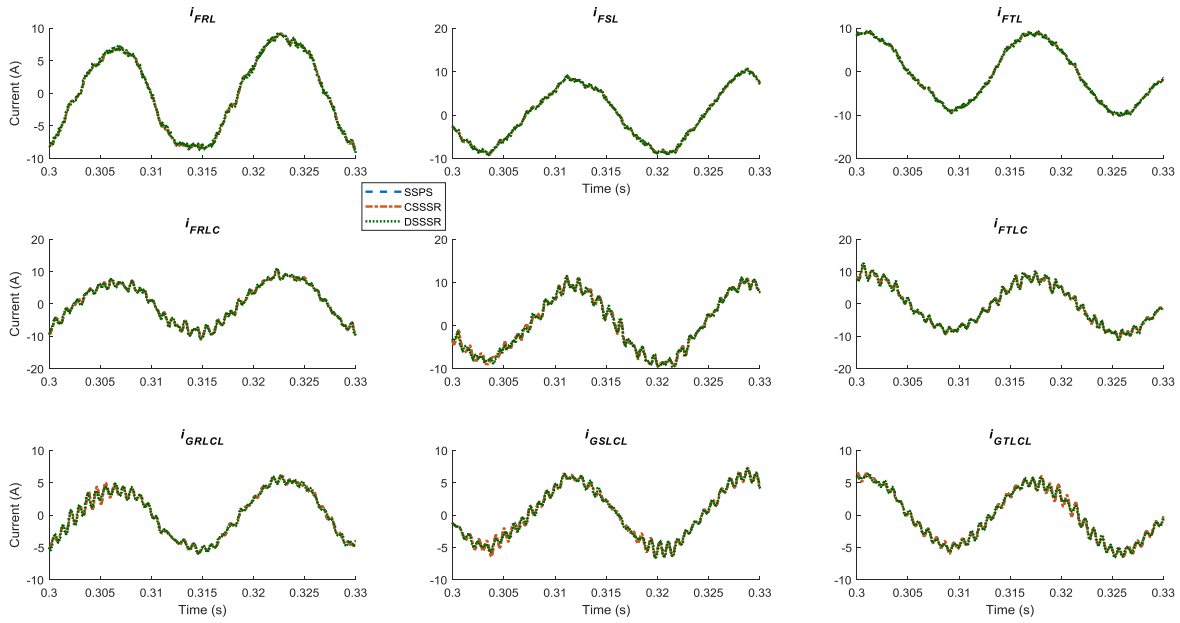

Fig. 2.9. Currents flowing through the connection point between the AC side and the associated filters, 3L-CHB

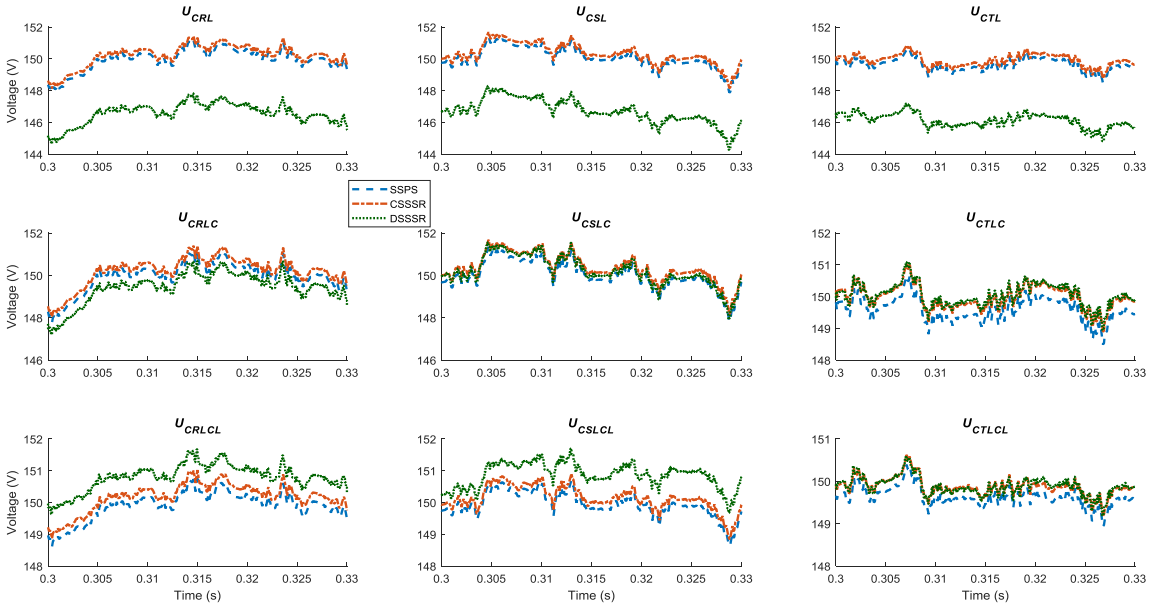

Fig. 2.10. Voltages at the terminals of the DC capacitors, 3L-CHB

The states are displayed in parallel: horizontal lines show the results for one filter, L at the top, LC in the middle and LCL at the bottom, while the rows exhibit the different phases of the converter, R, S and T from left to right, corresponding to the notations used in Fig. 2.7.

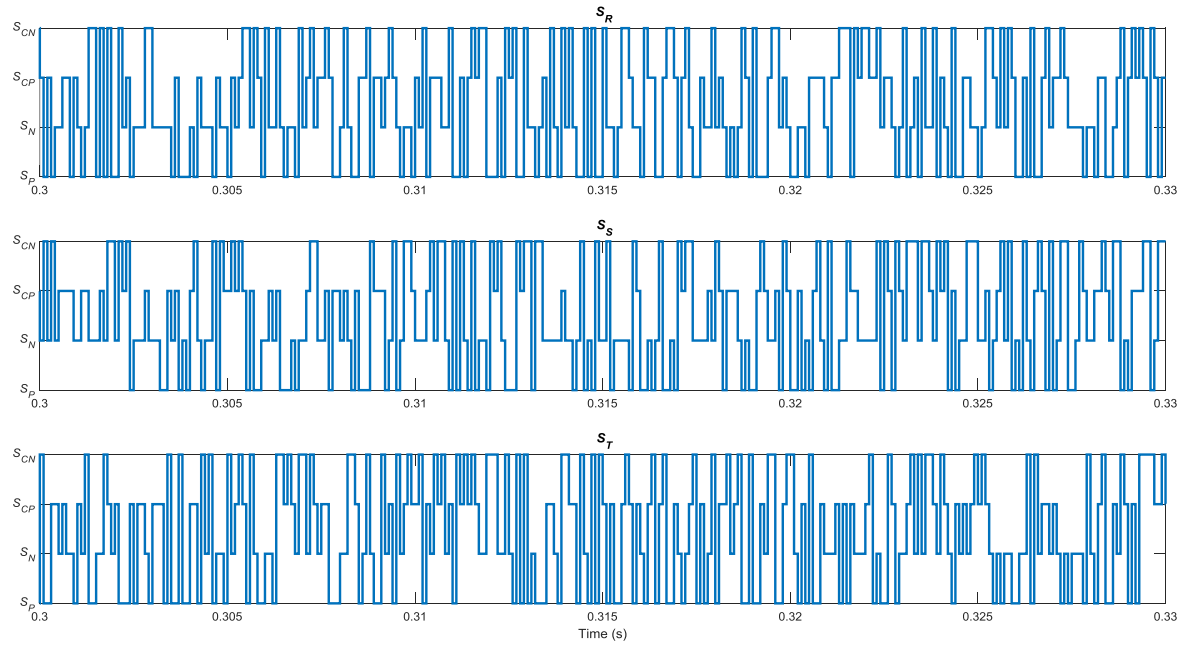

Fig. 2.11. Swithcing sequence applied to the 3L-FC topology

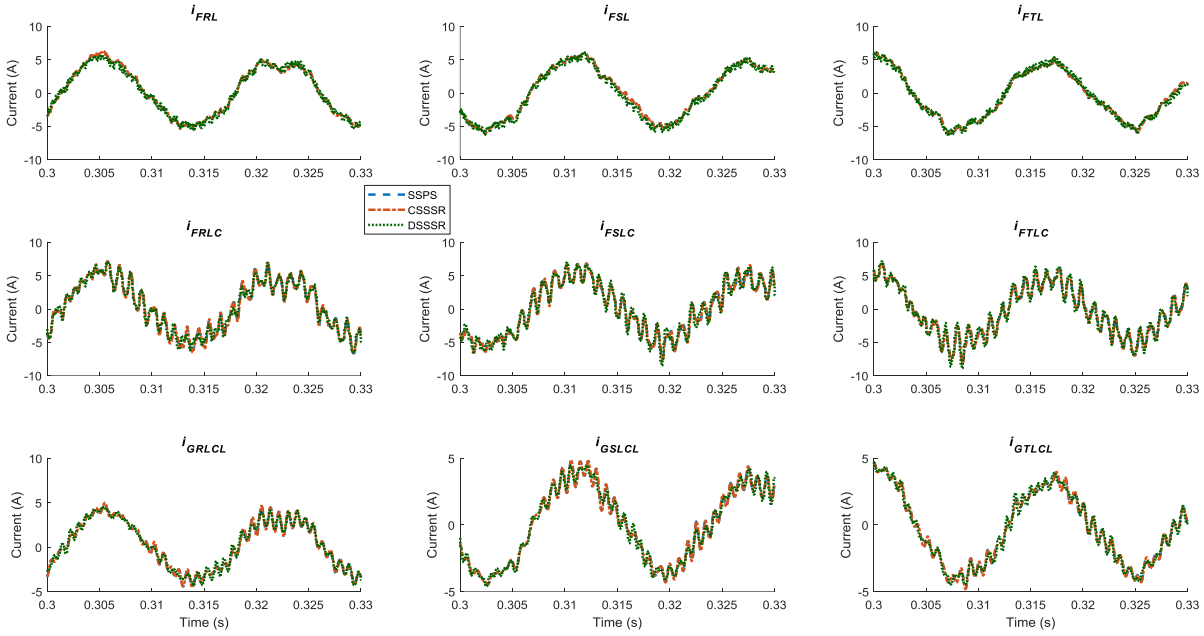

Fig. 2.12. Currents flowing through the connection point between the filter and AC side of the 3L-FC topology

The information is disposed with the same scheme for all topologies: first the control sequence, then the currents at the interface with the grid, and finally the voltages across the DC-link. The 3L-CHB topology is presented in Figs. 8-10, the 3L-FC is shown Figs. 11-13, and the 3L-NPC in Figs. 14-16.

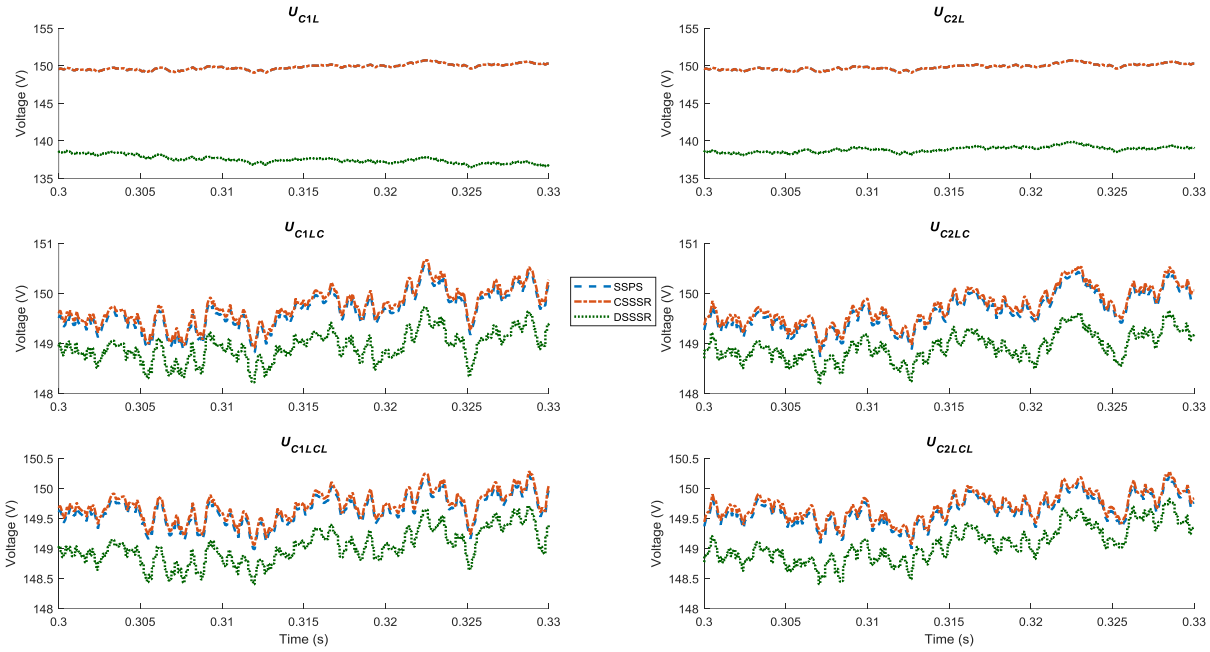

Fig. 2.13. Voltages at the terminals of the DC side capacitors of the 3L-FC topology

For each topology, the proximity between the performances of the three models is highlighted. The juxtaposition in Figs.9, 10, 12, 13, 15 and 16 and each of their subfigures of the signals coming from all three simulation models allows validating the proposed modeling technique. It also corroborates the suitability of the discretization method selected, as the discrete and continuous systems are coherently obeying the same dynamics.

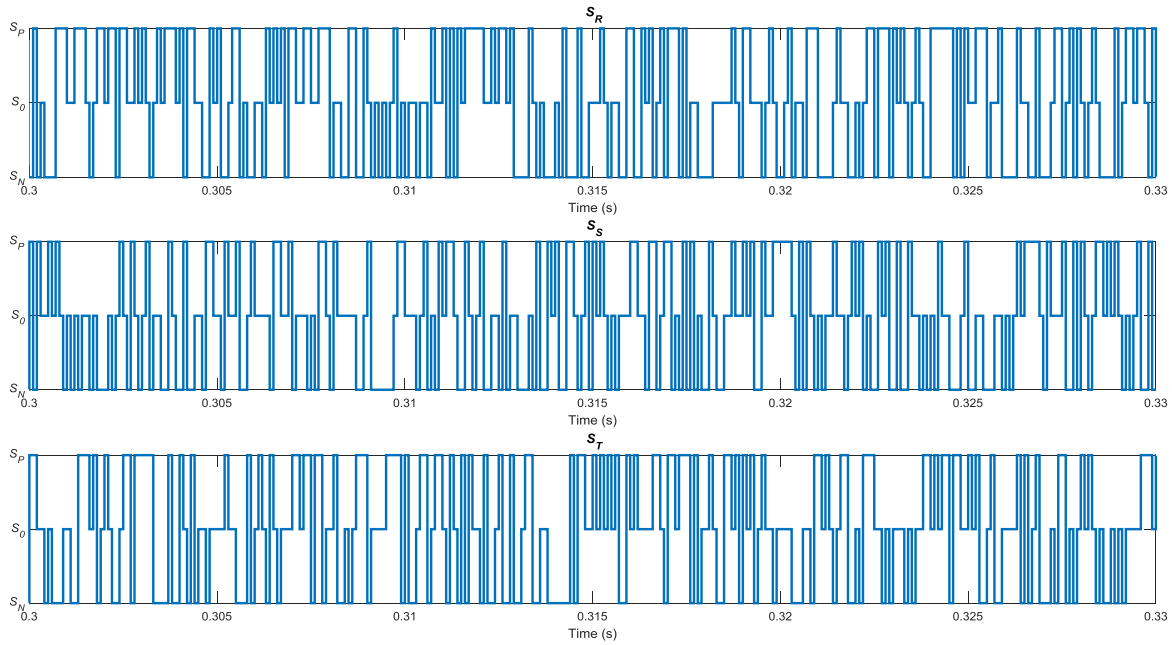

Fig. 2.14. Switching sequence applied to the 3L-NPC topology connected to the different filters

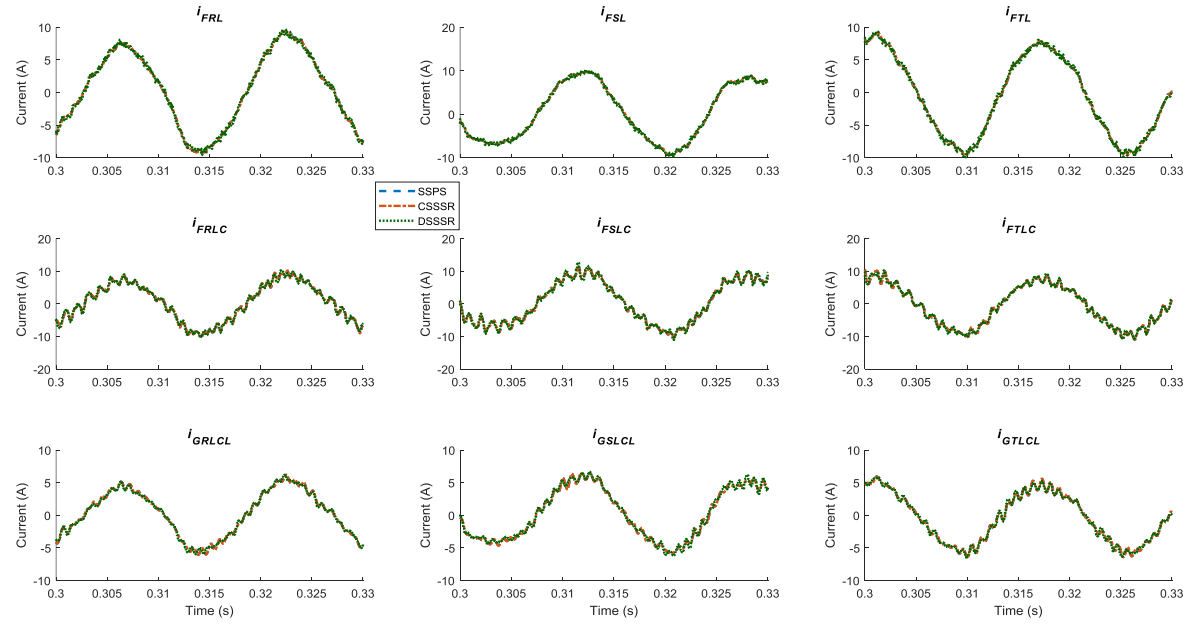

Fig. 2.15. Currents flowing trhough the connection point between the AC side and the filters for the 3L-NPC topology

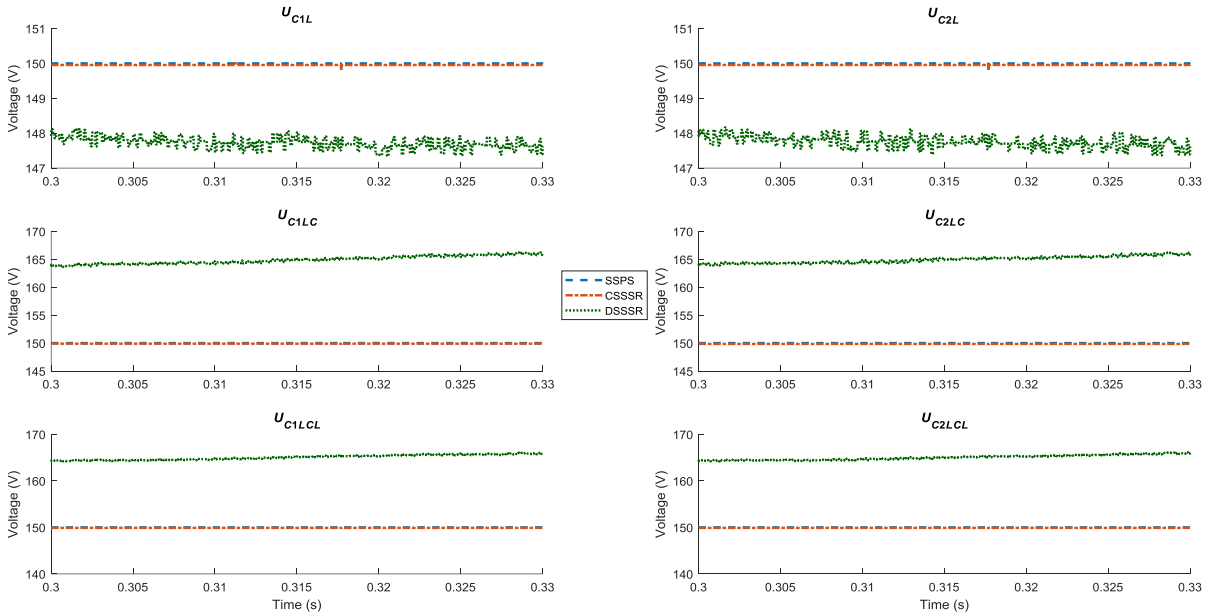

Fig. 2.16. Voltages across the terminals of the capacitors of the DC side, 3L-NPC

However, certain inconsistencies also appear. The currents presented in Fig. 2.9, Fig. 2.12 and Fig. 2.15 behave identically, independently from the model used. A close examination shows small neglegible differences, always inferior to a half percent. However, the voltages, presented in Fig. 2.10, Fig. 2.13, and Fig. 2.16, highlight a more concerning behavior. First, the continuous and discrete models differ from one another. The CSSSR is closer to the SPSM, while a bias seem to have formed on the DSSSR. Actually, the difference between the CSSSR and SPSM grows for the whole duration of the simulation, but keeps at sufferbale amounts, inferior to a percent, even after 4s of it. The discrete model behaves similarly but the

differences are much more outstanding, growing up to 10 percent in only 1s in the case of CHB topology and L filter. For both the FC and CHB topologies, the error on the L filter is much more considerable than for the two other filters, while the exact opposite is shown Fig. 2.16 in the NPC case.

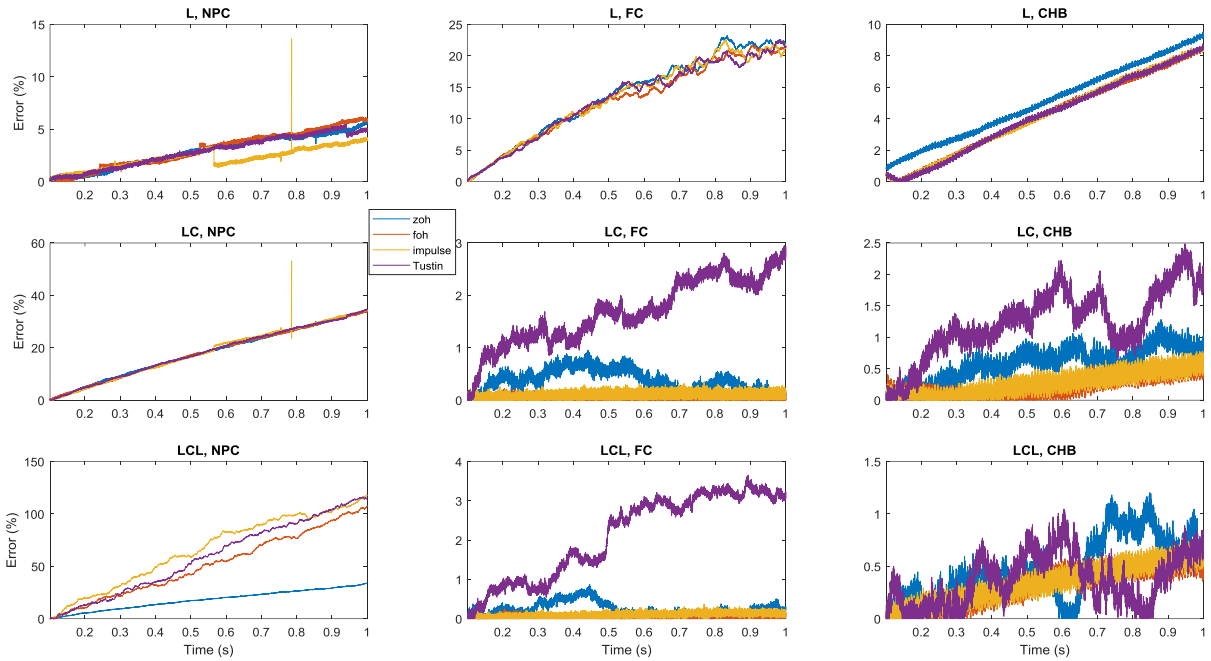

Fig. 2.17. Absolute values of the relative errors for different discretizing strategies for all the topologies and filters

A plausible explanation for the difference between the continuous and the discrete models could be an incorrect choice of discretizing method. Remembering Section 3, the zero-order hold method has been preferred because it matches with the operation of discrete controllers. However, tests with other methods such as first-order hold, impulse method or Tustin method led to no noticeable improvement. This result is presented in Fig. 2.17, where the absolute values of the relative errors of the four methods evoked are superimposed for the voltage of one of the DC-link capacitors, and so for all three topologies, on the lines, and the three filters, along the columns. Even though they do not provide the exact same results, none of the strategies appears to be better than the others. The use of ZOH method is then maintained.

The hypothesis of a wrongful discretizing method is ruled out by Fig. 2.17. Another explanation comes from the very nature of the model. When the system switches from a subsystem to a new one, the possible differences between the model and the reality at the switching moment entail different initialization points for the new subsystems. These variations can not be corrected and can both add up or cancel one another. The closer the sample period considered is to the switching frequency, the more impact these errors have. This explains why the continuous model, which has a virtually infinite sample frequency, suffers much less from this issue than the discrete model, whose sampling time is equal to the minimal period between

two change of the switching variables. There is no appropriate answer to this phenomenon apart from reducing the sample period of the model, which is not coherent with the operation of the controller.

Nonetheless, the results presented in the different figures show that the models are fitting for prediction for low time ranges. The NPC case (Fig. 2.14, Fig. 2.15 and Fig. 2.16) is the only one presenting less fitting results for the LC and LCL filters in comparison to the L filter. The evolution of the bias is crescent, slightly limiting the validity of the model presented. Nevertheless, the discrepancy evolution shown here is extremely slow from the switching point of view, and thus from the controller's point of view: it takes several thousands of sample period steps to notice this gap, which is an astronomical number compared to the realistic objectives of the controller. In the case of a computationaly costless optimization, hence an infinite horizon optimization, the models might need some tuning to be acceptable. However, for more plausible values, under a dozen switching orders per call of the controller, the precision seen in the different figures is amply sufficient.

7 Conclusion

In this chapter, the necessity of designing a new pair of model and optimization algorithm has been highlighted, and a canonical model was selected. Based on Switched State-Space Representation, this definition describes any power converter application down to the state of its switching devices. Such a description means that an algorithm dedicated to solve optimization problems based on this particular canonical approach can be implemented to any power conversion system. The design of this algorithm is described in the next chapter.

8 Bibliography

[1] E. F. Camacho et C. Bordons, *Model predictive control*. London ; New York: Springer, 2004.

[2] S. Kouro, M. A. Perez, J. Rodriguez, A. M. Llor, et H. A. Young, « Model Predictive Control: MPC's Role in the Evolution of Power Electronics », *IEEE Ind. Electron. Mag.*, vol. 9, nº 4, p. 8‑21, déc. 2015.

[3] T. Geyer, G. Papafotiou, et M. Morari, « Model Predictive Control in Power Electronics: A Hybrid Systems Approach », in *Proceedings of the 44th IEEE Conference on Decision and Control*, 2005, p. 5606‑5611.

[4] R. A. Decarlo, M. S. Branicky, S. Pettersson, et B. Lennartson, « Perspectives and results on the stability and stabilizability of hybrid systems », *Proc. IEEE*, vol. 88, nº 7, p. 1069‑1082, juill. 2000.

[5] B. Lennartson, B. Egardt, et M. Tittus, « Hybrid systems in process control », in *Proceedings of 1994 33rd IEEE Conference on Decision and Control*, 1994, vol. 4, p. 3587‑3592 vol.4.

[6] L. Tavernini, « Differential automata and their discrete simulators », *Nonlinear Anal. Theory Methods Appl.*, vol. 11, nº 6, p. 665‑683, janv. 1987.

[7] P. Sindareh-Esfahani, S. S. Tabatabaei, et J. K. Pieper, « Model predictive control of a heat recovery steam generator during cold start-up operation using piecewise linear models », *Appl. Therm. Eng.*, vol. 119, p. 516‑529, juin 2017.

Chapter III: Model Predictive Control Algorithm

1. Finite Control Set MPC

As stated in the previous chapter, time is the most important constraint for the MPC controller. Indeed, to eliminate the modulation stage, the control algorithm should be able to directly output the switching states by updating its command signal at the switching frequency of the power converter, on the scale of 100 μs. This technique implies very short time to perform the required control computations. Thus, the main limitation of MPC is the computation time; as it performs optimization, it requires more computation time compared to classical controllers. The Finite Control Set MPC (FCS-MPC) [1], [2] is often implemented for solving optimization problems due to its ability to take advantage of the limited number of switching states of the power converter. It relies on a look-ahead strategy —prediction of system behaviour— to virtually gain at least a full sample period to finish computing the solution.

The algorithm is depicted in Fig. 3.1. When called, it receives the current state of the system and the optimal control sequence planned to be applied at the previous call of the controller. They are used to predict the state of the same system after application of said control sequence. Let us define N_{pred} as the horizon of prediction related to this operation, applied prior to any optimization step. The computation effort associated with such prediction is low, which means that the $t_1 - t_0$ time needed to perform these N_{pred} predictions is small in comparison to the advance in time it actually permits. Instead of having to deliver the control sequence to be applied immediately, the optimization block focuses on selecting the optimal control sequence required N_{pred} sample times later. The former approach would imply solving the optimization problem in an as short as possible fraction of the sample time, while the proposed strategy gives the controller more time to perform computations. The pressure on the computation time of the algorithm is significantly reduced with this strategy. This look-ahead approach is similar to walking, where the next step is planned while the previous one is still mid-air.

The bigger N_{pred} is, the more time is gained. However, this growth also entails a modification of the period between two consecutive calls of the controller: although it generates control signals with a sample period of T_s, it actually updates these orders on a $N_{pred}T_s$ basis. This implies a delay on the reaction to variations from the exterior, and requires posing an operational hypothesis: the dynamics of the plant and its uncontrolled inputs have to be much slower than $N_{pred}T_s$ instead of in comparison with just the sample time. In the case of power converters, this property is verified, as the dynamics considered, from the grid or the various possible loads, are on a scale of a few tens of Hz, while the power switches operate at a frequency of kHz. This means that the uncontrolled inputs can be considered as constants for all the estimations made by the controller until the next call. Such property may prove to be false if the horizon is

chosen too big, over a hundred, for example. This is not the case for this application, and so the impact of large prediction horizons will not be discussed further, though it might be interesting for a different application.

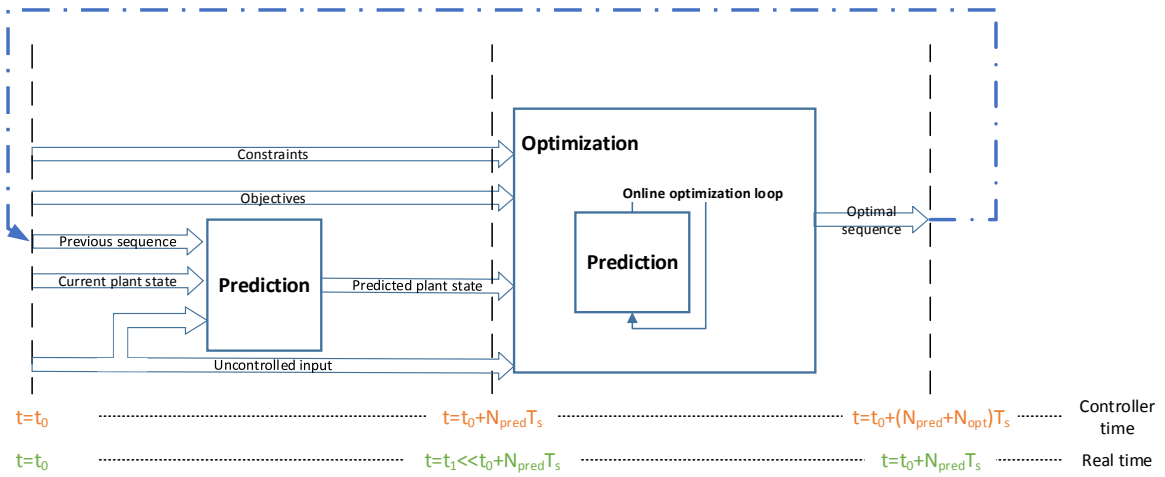

Fig. 3.1: Operation of Finite Control Set Model Predictive Algorithm

FCS-MPC is initially planned to present a one-step optimization and prediction, but it is also extendable to further optimization and prediction algorithms. It often designates the whole MPC algorithm, but it is closer to an internal strategy to enable complex computations. This way, it is possible to acknowledge developing more advanced algorithms and, for example, include further control considerations, with longer prediction and optimization horizons. Let us define the optimization horizon, N_{opt}, as the length of the optimal control sequence, and the control horizon, sum of the prediction and optimization horizons, representative of the depth of prediction of the complete algorithm. In the first implementations of FCS-MPC, both the optimization and prediction horizons were unitary, showing limits in the treatment of the data and of the constraints.

Because the algorithm relies on the control sequence previously computed to perform its look-ahead predictions, the optimization horizon has to be greater than the prediction horizon for the FCS strategy to operate. Indeed, would the length of the optimal sequence be shorter than the prediction depth desired, it would not be possible to properly predict the behavior of the system all the way to the wished horizon. Therefore, the control sequence computed has to be compatible with the prediction length, leading to the following equation:

$$N_{opt} \geq N_{pred}. \tag{3.1}$$

The bigger N_{pred} is, the more time is allotted to the optimization algorithm. However, it also entails longer computations for the optimization algorithm because of (3.1). The interest of increasing the optimization horizon is mainly to enhance the performance of the MPC. From a theoretical point of view,

precision and results grow accordingly to N_{opt}. Because the computation also follows the same tendency, it is necessary to find an adequate balance between the optimization horizon and the computation time. This balance is what helps to decide the values of the various horizons. So far, because of the complexity of the optimal problems considered and the infinitesimal time to solve them, the control horizon is usually of 2 to 5 steps, 2 being the most simple case where both the prediction and the optimization horizons are unitary. The results obtained show an important progress from a unitary control horizon (therefore without the FCS-MPC) to a double one, but less interest when going from two to three. However, enabling higher levels can only be beneficial, whether by improving overall hardware performances or by enhancing the control algorithm's efficiency.

2. Optimization algorithms

2.1 Consequences of the model and tree definition

A canonical converter model has been defined in the previous chapter. This model brings about a linear by piece definition of converters. Therefore, from a given state at a given time, the model linearly predicts the upcoming state by considering that the control applied is constant during the whole sample period. The hybrid nature of the converters and the finite number of combinations for the switching entail a limited number of possible different linear predictions. Possible states branch out of an initial state, defined by the sample period and the switch inputs applied during such period.

This vision leads to a graph definition, or a tree: from any given state, all the accessible switching positions form a tree of possibilities. The nodes of this tree are the different accessible states, and its edges the corresponding switching inputs required to reach them. It is easy to associate a cost to the change of state resulting from the control input, i.e. to weight the edges of the graph. The canonical model proposed in Chapter II intrinsically leads to a graph definition of the system, as depicted in Fig. .

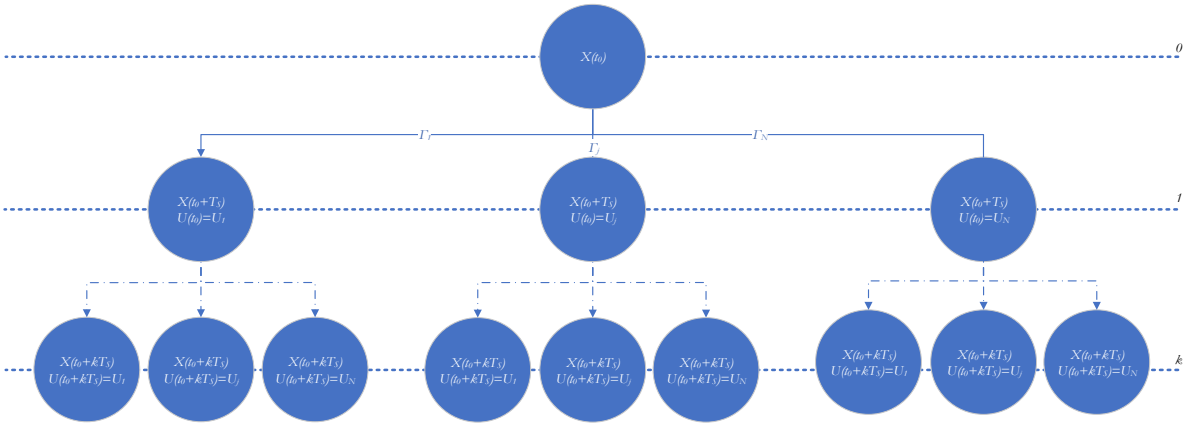

Fig. 3.2: Tree depiction of the model

The general objective of the optimization algorithm is to find $[U(t_0) \dots U(t_0 + N_{opt}T_S)]$, the sequence that best agrees with the control objectives and constraints. Note that the t_0 used here is not necessarily the one of Fig. 3.1, according to which this initial time would actually be $t_0 + N_{pred}$ when the complete algorithm is in operation. Finding such a switching sequence is equivalent to reaching the appropriate N_{opt}th layer of the tree. Considering that the weights associated to the edges of the graph are images of the control objectives and constraints —built so that moving away from such requirements increases the weight—, the goal of the optimization algorithm becomes to find the path to the N_{opt}th layer, or the control sequence, that minimizes the total wieght. Therefore, the canonical model defined in Chapter II underlies the use of a shortest path algorithm for the optimization block of the MPC displayed in Fig. 3.1. The model and the algorithm are closely related: would it be a different kind of model, the choice of the optimization algorithm would change, and vice versa.

There are no structural limitations on the cost function from the definition of the optimization problem. Contrarily to quadratic or linear problems that force the cost function to be itself quadratic or linear to properly apply the solvers, the pathfinding approach does not require any particular trait. Different such algorithms exist, and they may demand certain traits, such as positive costs, but there is no constraint on linearity at all. It enables some flexibility concerning the implementation of the control objectives and constraints. As such, this property is already very interesting for control design and will be discussed more in-depth later on.

The causality implies that the edges are oriented: it is not possible to progress backwards, henceforth against the flow of time. For the same reason, the graph is not cyclic: there is no way to create a loop or interconnections without breaking the laws of causality. The plane graph developed is much wider than long: the relation between $N_{vertex}(k)$ the number of nodes at the level k, N_{poss} and N_{legs}, as presented in Chap.II, for any power converter is given by

$$N_{vertex}(k) = N_{poss}^{N_{legs}{}^{k}} . \tag{3.2}$$

This expression is exponential, leading to a very large graph, in which accessing deeper levels is exponentially difficult. Numerical values are provided in Table 3.1 for the particular case of $N_{legs} = 3$, to highlight how the topologies strongly impact the complexity of control.

TABLE 3.1
NUMERICAL VALUES OF $N_{vertex}(k)$

3L-NPC	3L-FC	3L-CHB
27^k	64^k	27^k
4L-NPC	4L-FC	4L-CHB
81^k	256^k	81^k

It appears that the Flying Capacitor topology, because it proposes more distinct switching positions, leads to wider trees, which are much more difficult to develop. This property is generalized to the levels of the topology: higher levels imply a more diverse set of switching positions, which in turns entails a much more explosive growth of the tree. The graph to be explored expands quickly when considering a large optimization horizon and when the controlled topology allows more switching possibilities. The difficulty of finding the optimal control sequence in such a tree evolves similarly. Coincidentally, the applications relying on a more diverse set of possibilities are often those that offer the best control options and require advanced intelligent control. The most interesting targets for optimal control and direct switching sequence generation are also the less simple to adapt to.

2.2 Shortest path algorithms

Due to the unitary horizons used and because the number of possibilities to explore was reasonable, a *brute force algorithm* was deployed in the first iterations of FCS-MPC. However, since the number of nodes grows exponentially with the value of the optimization horizon, leading to a similar expansion of the time needed to compute the optimal path, brute force can not be relied on for non-unitary horizons. The brute force is often the most intuitive way to solve finite optimization problems: it consists in exploring the entirety of the possibilities before taking an informed decision. This strategy ensures the discovery of the global optimal solution of the problem, but the number of operations and thus the time required to solve the problem grow as fast as the number of possibilities. From the previous subsection, the graphs generated quickly expand: their growth is exponential, as evidenced by (3.2). Consequently, while it is relevant for small N_{opt} values, brute force is an non-adapted solution for higher figures. In fact, for an optimization horizon of 3, the number of possibilities is already close to twenty thousand —precisely 19683— for the simplest application considered so far, which yields an expansion rate of 27 per node, as stated in Table 3.1.

Another common solution is the *greedy algorithm*. This strategy is the polar opposite of the brute force. While the latter explores all potentialities indiscriminately, the greedy algorithm jumps to the first best visible solution and never looks back. This behavior signifies a fast pace in the graph solution. It is the most cost-effective way to proceed through such a graph, as the number of steps required to solve the shortest path problem is exactly equal to the depth or the horizon desired. This performance is unbeatable. Nevertheless, it does not guarantee finding of the global optimal path. This is because it only selects the immediate best answer: and, consequently, it does not have access to other alternative ones that may prove to be more satisfying afterwards.

Thankfully, other approaches to solve shortest path problems in oriented graphs exist. The best-known ones are the *Bellman-Ford* algorithm [3] and the *Dijkstra* algorithm [4].

Described in 1958 by Richard Bellman, this algorithm is meant to find the shortest path between any two given nodes of a weighted oriented graph. It was initially devised for route planning between cities. To do so, it computes the shortest distance between all vertices iteratively: at the beginning, the total distance

to all nodes is set as infinite, then iteratively updated with the smallest weight accessible. This method, called relaxation, is based on the definition of the distance between two nodes. Any given graph is characterized by its vertices, forming the set V, and its edges defined by their weight. The notation $w(u, v)$ designates the weight of the edge bridging the vertices u and v, nodes belonging to the set V. This variable is inherent to the graph and can not change. Hence the introduction of the distance $d(u, v)$ between two nodes. This distance is not relevant to an individual edge but to a path, potentially passing by several nodes and edges. Admiting that the distance $d(u, u)$ is null, let us define $d(u)$ as the distance from the source vertex to the node u. The objective of the optimization is to minimize this distance for u, the destination node, linked to all the nodes of the N_{opt}th layer with weightless edges. As pointed out in Fig. 3.2.3(a), the relaxation step is repeated as many times as there are elements in V. This value is demonstrated as sufficient by Bellman to define and minimize all the $d(u, v), (u, v) \in V^2$. Though sufficient, the condition is not necessary and other variants exist to try and decrease the number of incrementations of the distance necessary. An interesting property of the algorithm is the potential to handle negative weights and to detect cycles with negative costs[3]. This aspect is not specifically important for the application described earlier, as it does not present any cycle, but it can be critical for many other cases.

Described in 1959, the Dijkstra algorithm is slightly faster than its predecessor, but it does not support negative weights and negative cycles. This algorithm divides the graph into two sets, S and F, the first one referring to a visited set, and the second one to a yet-to-be-explored set. These two sets are mutually exclusive and complementary in V: their intersection is empty, and their union forms the total set nodes of the graph. It is impossible for a vertex to be both visited and unexplored. Initially, the set S only contains the source node, s. For a generic application, this initial node can be chosen randomly, but here it corresponds to the level 0 of Fig. . Then, the different paths exiting from that node are considered and the shortest one is selected. The corresponding node is then extracted from F and added to S. The operation is then repeated: all the paths exiting from S to F are considered, the best node selected, extracted from its initial set and added to the other one. This operation is repeated until the destination node has been reached, as portrayed in Fig. 3.2.3(b).

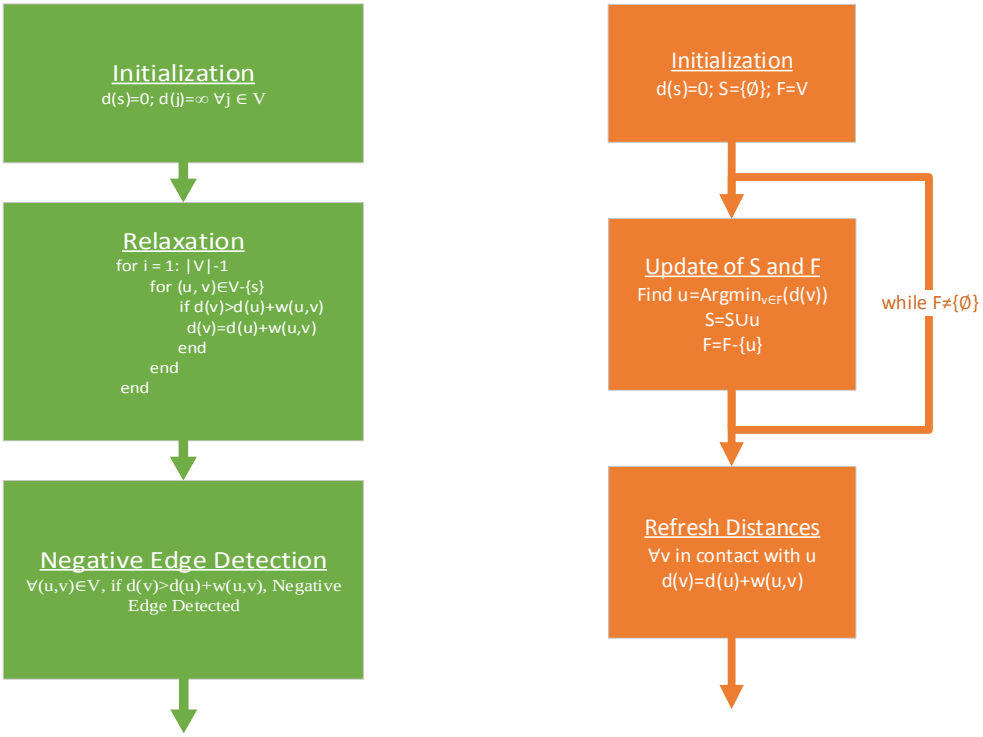

Fig. 3.2. Bellman (a) and Dijkstra (b) algorithms

To illustrate the algorithms described earlier, let us consider a clarifying example on the tree described in Fig. 3.3. It is a simplified situation where the objective is to select the optimal input among a set {1, 2, 3} of possible choices at every step, three steps in advance, which is equivalent to $N_{poss} = 3$ and $N_{opt} = 3$. Another way of illustrating the optimization horizon is to consider a destination node linked to all the nodes at the desired depth —confounded with the horizon in this case—, with edges of null weight, as previously suggested. Therefore, once it reaches the wished depth, the algorithm automatically reaches its destination. The algorithm should provide the sequence with the smallest overall cost on the time period considered.

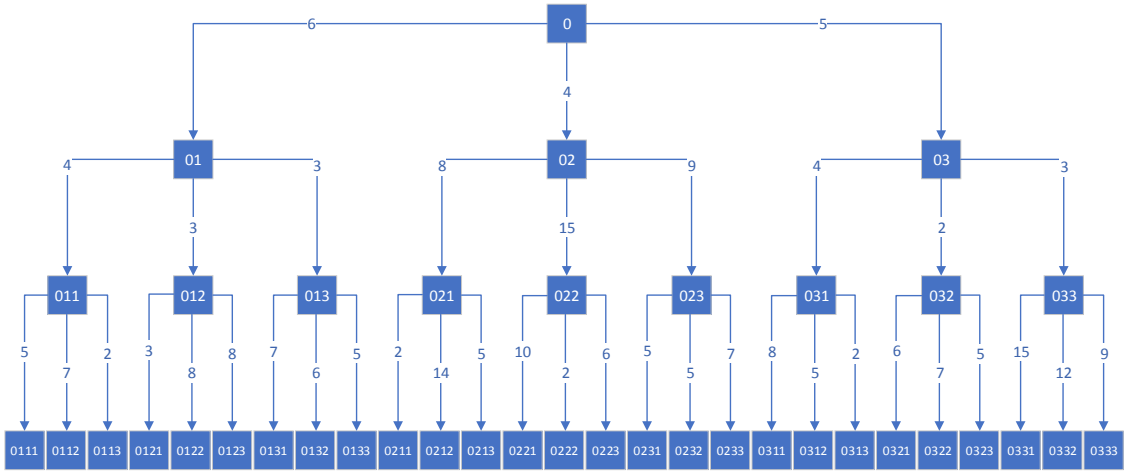

Fig. 3.3: Weighted tree

First of all, the brute force *algorithm* will determine the distance separating each node from the initial vertex. This amounts to summing up the weights of the edges leading to the nodes. By doing so, all the paths leading to the desired layer are known. The only thing left is to select the lesser one, revealing in this example that the sequence [313] is the best, with a total cost of 11. The algorithm computed all sums, hence 39 counting the initial three weights, summed with 0. This approach is summarized in Fig. 3.4, with the weights $w(u, v)$ in blue and the distances $d(u)$ in red. This strategy is often used for simple applications involving only a low number of possibilities. It is extremely simple to program and to implement. As evoked earlier, if the graph is exponentially big, the algorithm quickly shows its limits.

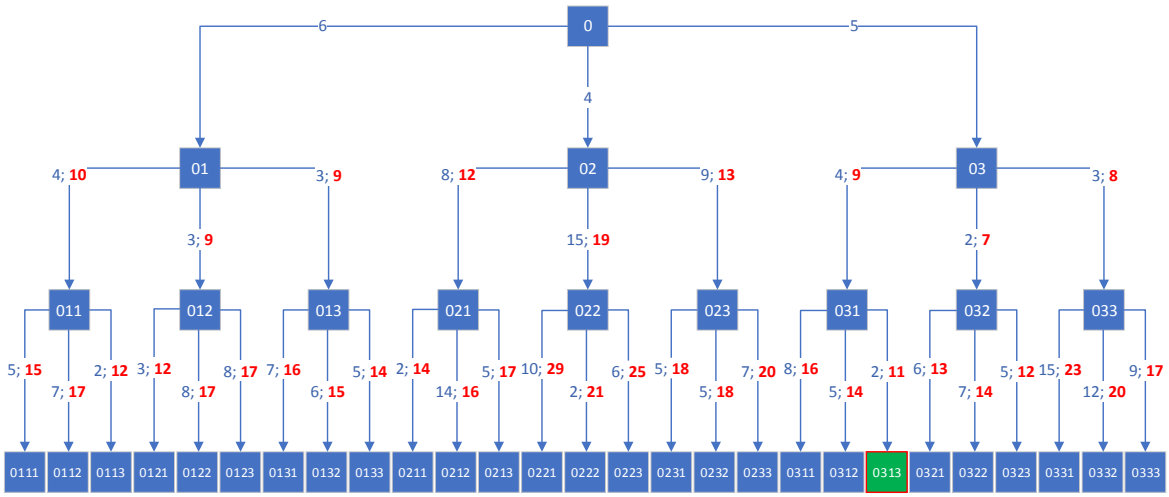

Fig. 3.4: Application of brute force

The greedy algorithm, depicted in Fig. 3.5, proceeds differently and progresses in the graph much faster than the brute force. It is the fastest possible algorithm. This is similar to not developing the tree and computing one step ahead three times in a row. Because it never considers previous possibilities again, it may miss better solutions. This algorithm selects local optima in the hope of reaching the global optimum at the end. The example illustrates this property: the algorithm explored only 9 edges, meaning more than 75% economy compared to the previous case. However, it delivered path [211] as solution, with a total cost of 14. This route is less interesting than the [313] and its 11 final distance. In addition, this example perfectly illustrates the advantages of increasing the optimization horizon, as it mitigates the risks of choosing local optimal solutions as opposed to global ones. It is the equivalent of applying several low-horizon optimizations in a row, while the other strategies discussed actually perform a long-horizon optimization. This aspect is important for the controller: implementing this strategy is fast, but changing the value of the horizons does not entail any difference. Indeed, in this situation, the optimization loop behaves the same as the controller loop from Fig. 3.1.

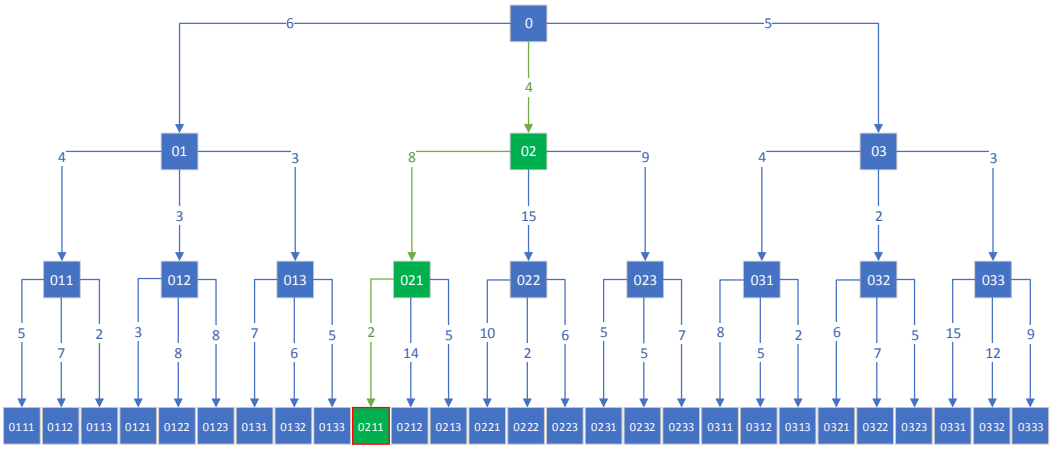

Fig. 3.5: Application of the greedy algorithm

The Dijkstra algorithm is a compromise between the two previous strategies. It does not necessarily explore the entirety of the possibilities, but always provides the global optimal solution. Fig. 3.6 traces the path followed by the algorithm. Ten iterations are required here to solve the graph. At the first iteration, the closest node is 02. From the set {[0] [02]}, the most satisfying destination is [03], which is therefore added to the set. Then, [01] is the closest node from the set {[0] [02] [03]}, and so on. The initial node is represented in red, while the nodes added to the visited set are encased in red, and coloured in contrast according to the order they were reached, darker shades amounting to earlier addition. The green hues depict the 3 first extensions, while the orange ones portray the next 6. The nodes whose edges were considered but were not put in the visited set are encased in yellow. Overall, 30 edges were considered out of the total 39, therefore implying a 23% economy compared to brute force. This indicator is more interesting than the simple number of nodes added to the set, which would give 75% of economy, because it thoroughly exposes the real computation cost of the algorithm. A detrimental aspect is the impossibility to quantify the number of steps needed to solve the problem: a different weight repartition would mean a different number of steps, either smaller or bigger. It can never be higher than what brute force proposes, and never smaller than what greedy algorithm offers.

The *Bellman-Ford algorithm* follows similar steps, without defining sets, and adjusting the distance exactly 38 times. The economy is not as consequent as wished, because the distance has been computed and relaxed for all paths: the nodes are all accessible via only one other node, case in which the interest of the algorithm is slighter.

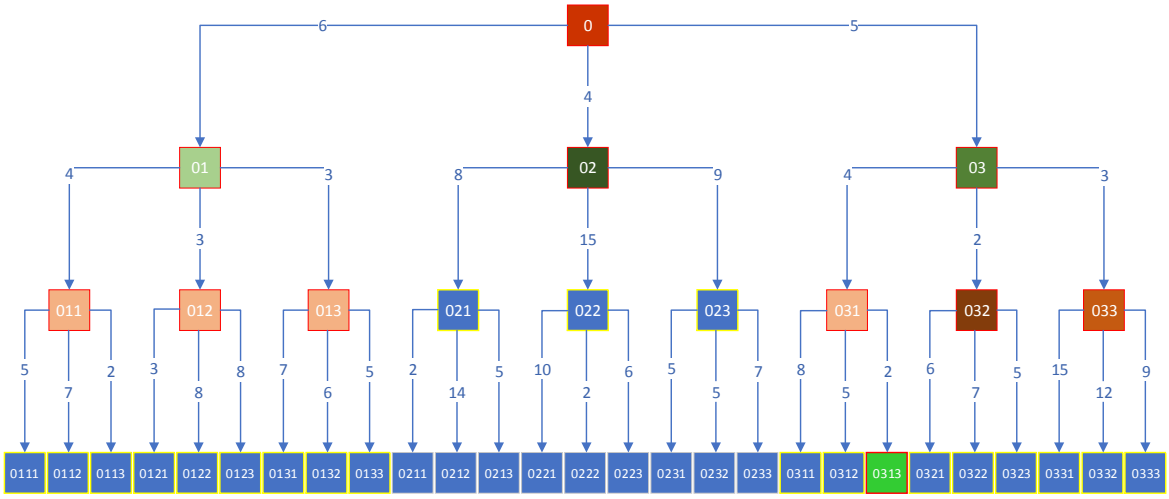

Fig. 3.6: Application of Dijkstra algorithm

Only a few algorithms have been described here. It could be possible to define the optimization problem differently and to solve it with other approaches. The main idea here is to exploit graph theory and operational research as a logical consequence to the piece-wise linear definition that comes naturally from the hybrid nature of all power converters.

The advantages and limitations of the four algorithms introduced are listed in Table 3.2.

TABLE 3.2
LIMITS AND INTERESTS OF THE ALGORITHMS

Algorithm	Number of operations	Global optimal solution
Brute Force	Maximal: size of V	YES
Greed	Minimal: $N_{opt} + 1$	NO
Bellman-Ford	High: $\|V\| - 1$	YES
Dijkstra	Undefined number	YES

3 Algorithm deployed

The developed MPC algorithm is based on the canonical model described in Chapter II, on the step ahead strategy explicated in Section 1 of this chapter and on a variation of the Dijkstra algorithm adapted to dynamic graph. Indeed, underlying the previous subsection is the difficulty to compute the complete tree of possibilities, and specifically to weight its edges. The weights are computed using predictions which, thanks to the linearity, are cost-efficient, but their quantity tends to overcharge the computations. The main advantage of the Dijkstra algorithm for the present application is that it does not need to know the entirety of the graph to perform accurately. The greedy algorithm does not either, but it brings no advantage whatsoever compared to one-step optimization, which is already well-established. As a matter of fact, the

algorithm adopted is the A* algorithm, developed in 1968 based on the Dijkstra algorithm for path searching applications [5]. It increments the visited set very similarly to the Dijkstra algorithm, but it also uses a function to estimate the weights of the edges outside of the visited known set. In the present case, this function can be a prediction and a cost function associated with the states or the change of states. It is the principle of the branch and bound algorithms, which could all be fitting for the application under consideration. The chosen implementation is very light code-wise and can be improved at any time.

The final algorithm relies on four main steps. At the very beginning, it starts by predicting the state of the plant after N_{pred} sample periods. To do so, it needs the initial state and the control sequence planned to be applied during the first N_{pred} steps. This sequence of orders is supposed to have been initially computed at the previous execution of the controller.

The second step is the optimization, as shown in Fig. 3.1. This block uses the tree definition and the principles of the Dijkstra algorithm described in the previous subsection. Practically, the graph is built progressively as the algorithm explores it. The goal of the pathfinder is to reach a certain level, a certain depth characterized by N_{opt}. The progression of the tree is in fact done by incrementing the number of vertices known to the controller, similar to the visited set of the Dijkstra algorithm. These nodes are defined as structures whose fields are summed up in Table 3.3, where N_{states} designates the dimension of the state vector for any node.

TABLE 3.3
FIELDS DEFINING THE NODE'S STRUCTURE

Name of the field	Initial value
Level/depth	0
Accessible nodes	$\mathbb{O}_{N_{vertex}(1)\times 1}$
Cost to reach	0
State of the node	$\boldsymbol{x}(t_0)$
Costs to reach the accessible nodes	$\mathbb{O}_{N_{vertex}(1)\times 1}$
Control sequence to reach the node	$\boldsymbol{u}_0$
States of the destination nodes	$\mathbb{O}_{N_{vertex}(1)\times N_{states}}$
Flag on complete predictions	0

The most fundamental fields for the controller are, of course, the cost and the control sequence to reach the node, along with the state of the vertex. The depth indicator's purpose is to manage the optimization horizon and to stop the algorithm when this objective is reached. The states of all the nodes accessible are computed and stored to progress in the tree. Finally, a flag on completion of the predictions is used to ensure the correct operation of the algorithm.

The tree is initialized with a source node, whose fields are filled as summarized in Table 3.3. From this only node, the tree is expanded until the desired level is reached, at which a node presents the correct value on its depth field, as presented in Fig. 3.7. The expansion of the tree consists in three steps: first extract the possible destinations from the known set of nodes, then select the best one amongst them and, finally, update the tree. This last step allows creating a new node and ensures a path can not be crossed twice, as it could lead to an infinite loop. This is the function that actually implements mathematically the graph aspect of the problem.

Identifying destinations can be done in various ways. First of all, it is necessary to note that the latest node to have been integrated to the graph is not complete: as the initial node does not contain the predicted possibilities, the actualization block does not compute anything and thus leaves the predicted destinations uncompleted. Henceforth, the heavy work of the calculations is performed in the "Identify the destinations" block. This solution diminishes the total computation time by compartmenting the operations.

Another cost-effective measure is to store only the best destination from each node instead of keeping them all. This greatly reduces the size of the elements handled by the algorithm. The economy depends on how many times the algorithm crosses a same node and follows a different edge. In the ideal case, where all nodes considered are passed only once, the economy is of $N_{poss}^{N_{legs}}$-the number of potential nodes not stored if the algorithm only crosses one node once-, but in a situation where the same vertices are solicited numerous times, though the storing economy is still real, the need to find again and again the best destination from each node counterbalances this profit.

Ultimately, the objective is to make the algorithm as light as possible. The identification block thus verifies for each known node that the possible destinations have been computed, calculates them if necessary, and finally stores the best destination to send it to the next step, as depicted in Fig. 3.8, where the number of known nodes is described by N_{sit}. In order to know if it is necessary to compute the predicted states from a given node, a flag is implemented. At the creation of the node, this flag is determined as 0, meaning that no prediction has been performed from this node yet. Once it has been performed, the flag takes a 1 value and the computation is not repeated.

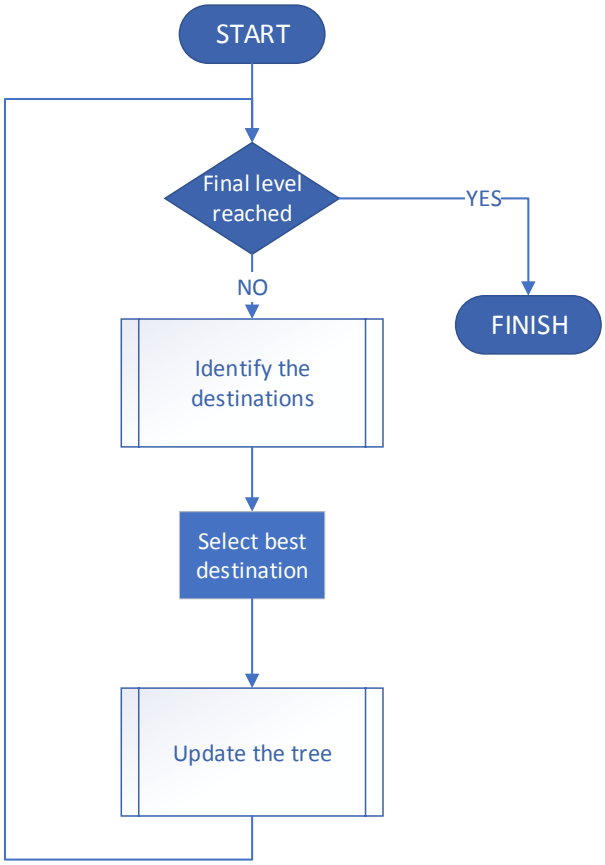

Fig. 3.7: Algorithm deployed

The selection block consists in a searching function that finds the smallest element of the vector of best destinations given by the precedent function, therefore delivering a decision on the optimal node to be added to the graph. Finally, the most important step of the algorithm is the updating block. So far, the navigation compass of the algorithm has not been implemented yet. The update is the most critical function of the algorithm, as it decides of the strategy of the algorithm. To be more precise, the task is double: first create a new node and complete it with the appropriate information, from the preceding vertex, but also and above all, update this previous node. Depending on how the vertices are updated, the shortest-path algorithm implemented differs.

For example, in order to implement a greedy strategy, it is sufficient to force to an infinite value the weights of all the edges starting from the node predating the new more optimal one. This way, only the ultimate vertex can propose finite-weight edges, therefore banishing the algorithm from exploring different paths from the previous iterations. As explained earlier, this implies a very low number of visited nodes before reaching an optimal solution, but does not guarantees finding the global optimal path. In order to implement a Dijkstra roadmap, the idea is to prevent browsing the exact same control sequence twice but to allow backtracking in search of better options. Therefore, forcing an infinite value to the followed path and only to this path entails implementing the Dijkstra algorithm.

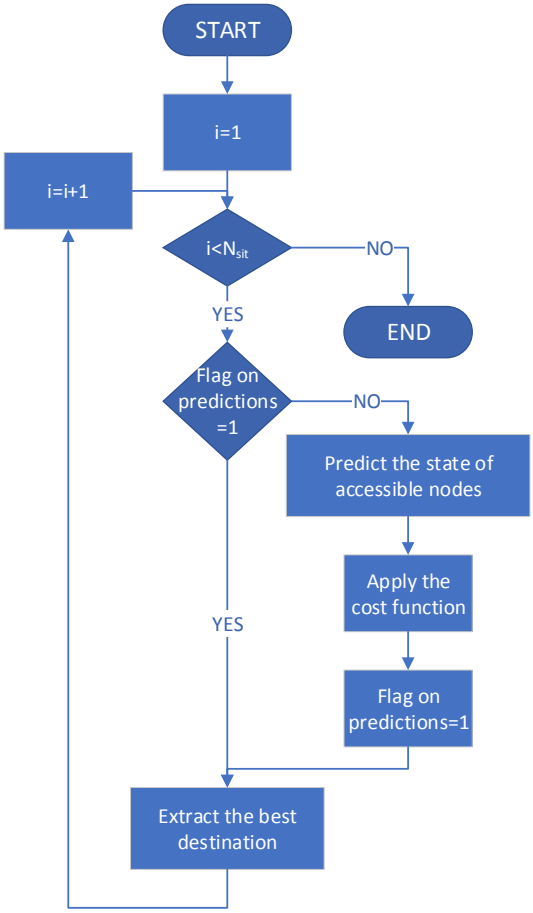

Fig. 3.8: "Identify the destinations" block details

4 Evaluation of the algorithm performance

In order to properly quantify the interest of the algorithm in terms of computation economy, it is pushed to solve random trees, i.e. graphs in which the weights of the edges are randomly generated. The objective is to highlight the computation cutbacks enabled by this algorithm. To begin with, it stands out that the algorithm proposed does not guarantee a fixed number of visited nodes. It highly depends on the proximity of the nodes cost-wise: the bigger the cost difference, the better the algorithm navigates the graph. In contrast, if edges share very similar values, the algorithm has to visit a greater number of nodes to sink deeper in the tree. The fastest progress is made when a path similar to the greedy algorithm one is possible, and the slowest one corresponds to the brute force case, where all nodes have to be considered prior to finding the optimal path. From there, N_{nodes}, the number of nodes added to the visited set of the algorithm, obeys to:

$$N_{opt} + 1 < N_{nodes} < 1 + \sum_{k=0 \dots N_{opt}-1} N_{vertex}(k), \tag{3.3}$$

as the left-hand side of the equation represents the minimal number of visited nodes, i.e. one by level plus the initial one, counted as level 0 as portrayed in Fig. , while the right-hand side displays the total

number of vertices of the graph when all the nodes prior to the aimed-at level have been completely explored.

The size of the visited set is an important mark of the efficiency of the path searching algorithm. However, in terms of computational effort, the most important aspect is in fact the number of predictions and cost computations. From the way the algorithm operates, the same number of predictions and cost evaluations takes place for each node added to the set, except for the last one, as it signals the end of the tree. Therefore:

$$N_{computation} = (N_{nodes} - 1) * N_{vertex}(1), \tag{3.4}$$

where $N_{computation}$ represents the number of predictions and cost function evaluations performed to reach the end of the graph and thus select the optimal control sequence. $N_{computation}$ must not be confused with N_{pred}, the optimization horizon, as they do not pertain to the same block of the general algorithm; the former is a quantitative criterion assessing the operation of the shortest-path algorithm, while the latter defines the depth of prediction performed before reaching such optimization step.

The algorithm has been confronted with ten thousand (10000) random trees. Such trees are obtained when deploying a random cost function: according to the operation of the algorithm, the weights of the edges are randomly affected once the algorithm first meets the corresponding edge. The value of a given edge does not change once it has been attributed, but each value allotted is randomly generated, leading to a random tree. Such an operation is repeated thousands of times to generate as many different trees. Those trees are all designed and solved for $N_{opt} = 3$ and $N_{vertex}(1) = 27$, corresponding to a 3L-CHB or 3L-NPC application.

The resulting number of predictions and of cost evaluations is displayed in Fig. 3.9. The minimum found is 81, which is the theoretical best, while the maximum is 459, much smaller than the 20411 derived from (3.3) and (3.4). In fact, the mean value is close to 150 calls of the prediction and cost functions. These values show a rather polynomial tendency, instead of the exponential feared one. This allows a deeper progress in the tree and, thus, a more enlightened sequence selection.

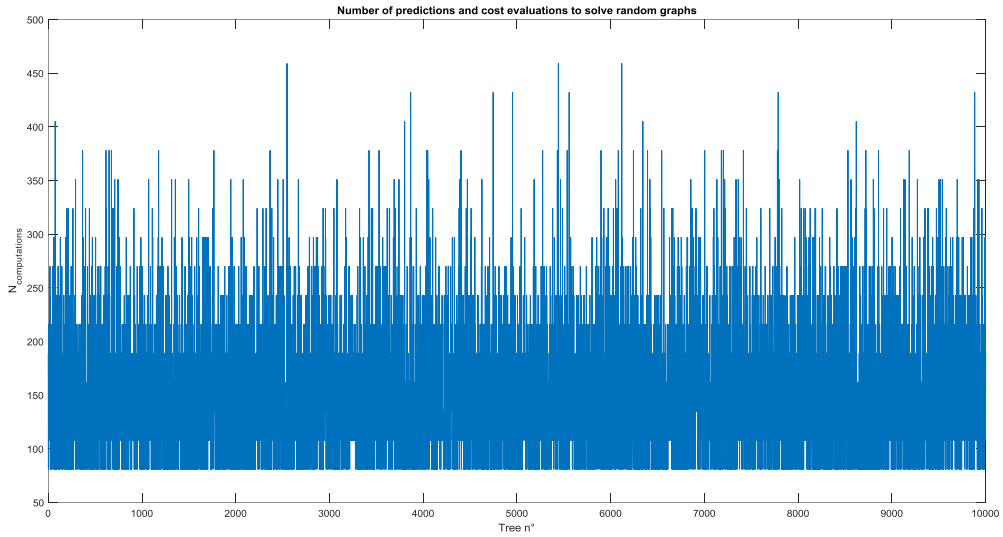

Fig. 3.9: Number of calls to the prediction and cost blocks for 10000 random trees

These results are highly satisfactory, as they are heavily linked to the total computation time of the optimization algorithm, which consumes most of the computation time of the complete MPC program.

The algorithm is now tested on a differently generated random tree. In this case, the costs are made of two components: a first random one and a second one depending on the change of control applied. The repartition of the cost for this second part is focused on a specific path, equivalent to never changing the control signal. A tree designed with only this second part is solved in exactly 4 visited nodes, hence 3 steps and 81 predictions, which is, as expected, the strict minimum possible. When a random behavior is added to this cost evaluation, it leads to a much more difficult tree to explore, where the two components of the cost may contradict each other. The distribution is expectedly different: the number of nodes that need to be visited before reaching the destination point rises consequently, from an average of 150 to 371. Likewise, though the minimum value is similarly capped at 81 envisioned possibilities, the maximum number of predictions explodes from 459 to 1350. The results are illustrated in Fig. 3.10.

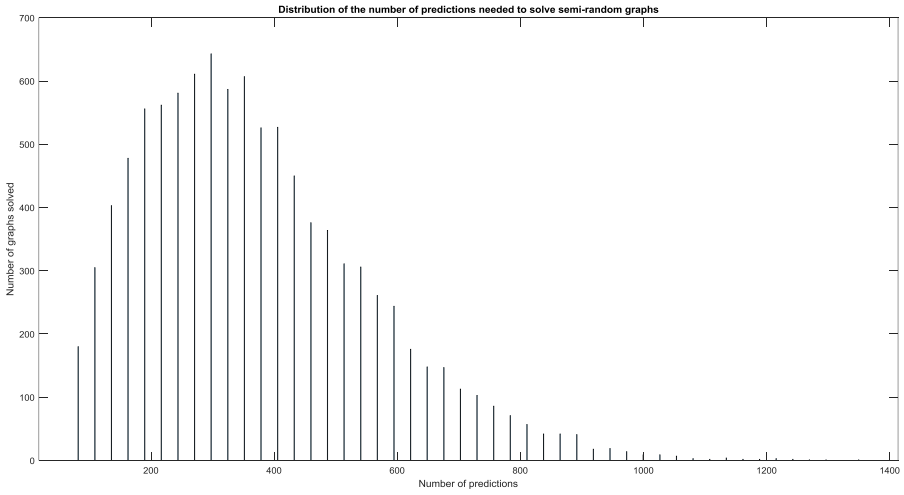

Fig. 3.10: Distribution of the number of predictions needed to solve random graphs with contradictory objectives

Though still satisfactory, it highlights the impact of the cost function on the algorithm. Another interesting note is that the prediction and cost evaluation functions are still called quite often by the algorithm, even in the most optimistic cases. In fact, since the time allotted to the controller to perform its computations is very limited, around 100 µs, these functions have to be very effective. In terms of time consumption, the prediction step is a low-cost call thanks to the state-space representation. The complexity augments quickly with the number of states modeled. The last computationally heavy block left is the cost evaluation. It is important not to make it too complex, which will be discussed in the next chapter.

5 Conclusion

This chapter described in detail the operation of the algorithm used to solve the optimization problem of the Model Predictive Controller. The desire to generate the switching orders down to the level of the switches directly by the controller led to the canonical model from Chapter II, which, in turn, conducted to the domain of graph theory for the optimization. Several algorithms were compared, and the most satisfying one in terms of depth of prediction has been selected, as it stands out from the other algorithms found in the state of the art. The final algorithm is based on the Dijkstra and A* algorithms, and it is specially adapted to the model definition described in Chapter II with the aim of proposing a fast graph exploring optimization. The controller proposed is therefore designed to tackle any power conversion system and application, as well as to handle longer horizons than what is mostly found in the literature. However, specificities concerning control aspects, such as control design, stability and robustness are still to be discussed.

6 Bibliography

[1] J. Rodriguez *et al.*, « State of the Art of Finite Control Set Model Predictive Control in Power Electronics », *IEEE Trans. Ind. Inform.*, vol. 9, nº 2, p. 1003‑1016, mai 2013, doi: 10.1109/TII.2012.2221469.

[2] C. Xia, T. Liu, T. Shi, et Z. Song, « A Simplified Finite-Control-Set Model-Predictive Control for Power Converters », *IEEE Trans. Ind. Inform.*, vol. 10, nº 2, p. 991‑1002, mai 2014, doi: 10.1109/TII.2013.2284558.

[3] R. Bellman, « ON A ROUTING PROBLEM », nº 1, p. 87‑90, 1958.

[4] E. W. Dijkstra, « A Note on Two Problems in Connexionwith Graphs », *Numer. Math.*, vol. 1, nº 1, p. 269‑271, 1959.

[5] P. Hart, N. Nilsson, et B. Raphael, « A Formal Basis for the Heuristic Determination of Minimum Cost Paths », *IEEE Trans. Syst. Sci. Cybern.*, vol. 4, nº 2, p. 100‑107, 1968, doi: 10.1109/TSSC.1968.300136.

Chapter IV: Control aspects

1. Model properties

The modelling method presented in Chapter II, SSSR, is a useful technique allowing the definition of piecewise linear state-space representation. This description is particularly valuable when considering the case of power converters, and especially multi-level power converters. This method separates and articulates the non-linearities caused by the hybrid nature of switching systems. These systems are definitely not linear, but demonstrate linear traits nonetheless. For example, in the case of power conversion, the plant is divided into strictly linear sub-systems characterized by one value of the control input each. When the control is constant, the system is linear; the control is considered as a parameter of the system representation. This is undoubtedly a direct way to include the hybrid nature of power converters in the model, then to control it with a single controller, without any intermediary modulation. This original practical requirement has heavy consequences on the end result. The objective of this chapter is to study those repercussions on three levels. The first level concerns the properties of the model and the transposition of results on stability and controllability from linear state-space representation. The second level is related to the qualification and quantification of the opportunities brought by the algorithm proposed to perform optimization. Finally, the third level is connected to the general performance of the complete MPC algorithm.

1.1 Extension of the model

A strength of the modeling method presented is the possibility to combine its result to more classical state-space representations. Quite often, the objectives of control of the power converter are deeply connected to those of the equipment to which it is connected. For example the generators are controlled using power converter according to the application, while impacting the behavior of the currents and voltages at their interface. This situation is very common, and the opportunity to add the dynamics of the loads and sources to the power conversion model brings intelligence to the control. However, this systematically implies rendering the final model non-linear. Also, judging from the short range of the predictions this type of system entails, separating levels of control can be preferred, applying a variety of hierarchical structure to combine different scales of interest.

1.2 Stability and stabilisability

The stability of a system is a property linked to its behavior when unsolicited. Several definitions are given, with different levels of strictness, with for example the asymptotic, exponential and Lyapunov stabilities. These definitions are valid for any given system, linear or not. For the rest of the discussion, stability will designate the asymptotical stability, which states that a system is stable if and only if it converges to a point of equilibrium from any given point. In the case of linear systems, the study of their eigenvalues is sufficient to demonstrate the stability or instability. The representation of multi-level power converters is

linear by piece but overall non-linear. Therefore, the criteria of stability for the global system have to be adapted and cannot be used as such. To begin with, the statement of no application of inputs to the system is irrelevant to the case of power converters, as the control is already included in the definition of the matrices of the system. From this declaration, the notion of stability already has to be defined differently for SSSRs.

Because they are linear, the stability of each subsystem can be determined by studying the eigenvalues of its corresponding submatrix: if and only if all the eigenvalues of the $\boldsymbol{A}$ matrix own strictly negative real parts, then the system described by the said matrix is asymptotically stable. In contrast, if one or more eigenvalues exhibit strictly positive real parts, the system turns out to be unstable. Finally, if one or more eigenvalues are placed on the imaginary axis and the rest show strictly negative real parts, stability cannot be determined.

However, establishing the stability of each subsystem is not sufficient to demonstrate the stability of the overall system [1]. In fact, even if all submatrices correspond to asymptotically stable subsystems, it may exist a sequence that renders the global system unstable. Similarly, even if a system is comprised only of unstable submatrices, there might be a series of commutation stabilizing it [2], [3].

Therefore, two definitions of stability for SSSRs are found. The first one deals with the existence of a stabilizing sequence, whereas the second focuses on stability for any commutation sequence. The latter definition is close to the definition given earlier and requires all subsystems to be asymptotically stable, though this condition alone is not sufficient. The case of filter-connected power converters leads to just a few stable subsystems because of the different oscillatory phenomena they generate and the consequences on the model, so this first definition is judged obsolete for power converters. However, it is interesting to demonstrate the existence of a sequence stabilizing the system, as if such a sequence does not exist, it is useless to consider applying control. This notion is stabilisability: from any given initial state there exists a sequence that lets the system converge to a stable state. This definition is less demanding and is included in the first stability proposition, but is nevertheless critical.

According to Lyapunov's theorem, finding a convex linear combination of the subsystems is sufficient to prove the existence of a commutation sequence that stabilizes the overall system [4], [5]. This amounts to finding

$$\alpha_i > 0; \ \sum_{i=1}^{N} \alpha_i = 1, \tag{4.1}$$

with N being the total number of subsystems, such that the equivalent system represented by matrix

$$\boldsymbol{A}_{eq} = \sum_{i=1}^{N} \alpha_i \boldsymbol{A}_i \tag{4.2}$$

is stable. Accordingly, proving that such an equivalent system is stable is sufficient to demonstrate the existence of a switching sequence stabilizing the system. However, this method does not provide the said commutation sequence. A numerical approach can be employed by generating various combinations and testing them, brute-forcing the problem. The stability results for the topologies and filters studied in Chapter II are presented in Table 4.1. For each case, the number of stable, unstable and undecided subsystems is given, in both the continuous and discrete models, as well as if a coefficients' vector has been found to demonstrate the existence of a stabilizing sequence. This combination has to generate a stable equivalent matrix in the continuous and the discrete realms.

TABLE 4.1
ANALYSIS OF STABILITY ON THE DIFFERENT TOPOLOGIES AND FILTERS

Topology	Filter	Continuous			Discrete			Stability proved
		Stable	Unstable	Undecided	Stable	Unstable	Undecided	
NPC	L	12	0	15	12	0	15	YES
	LC	6	14	7	4	7	16	YES
	LCL	12	0	15	12	0	15	YES
FC	L	1	17	46	4	6	54	YES
	LC	0	49	15	0	48	16	NO
	LCL	0	18	46	2	9	53	YES
CHB	L	8	0	19	8	0	19	YES
	LC	0	24	3	0	12	15	YES
	LCL	8	0	19	8	0	19	YES

The results presented in this table are obtained with the parameters described in Table 2.10. The results are destined to change with different values, preventing from generalizing them directly. However, certain properties and interesting traits can be extracted.

From Table 4.1, the LC filters systematically entail reduced stability, with much more subsystems being unstable or undecided for this filter than for the other two filters, and so for all three topologies studied. Another remark concerns the difference between the continuous and discrete subsystems. According to the table, stable subsystems are well preserved by the discretization method, as their number stays the same, and so for all topologies and filters. However, the unstable and undecided systems are not conserved the same way. Some subsystems unstable in continuous representation are undecided in the discrete one, and some undecided ones either fall in the stable or the unstable category. Logically, the repartition varies slightly between the continuous and discrete representations of the same model.

The table also shows that the NPC topology presents more stable subsystems than any other topology shown. For L and LCL filters, 44% of its subsystems are stable, while FC has less than 2% and CHB about 30%. These numbers can be compared with the number of capacitors in the topologies: ignoring the ones from the filters, NPC contains 2, FC 5 and CHB 3. The LCL case presents a few more unstable systems than the L case. The difference is nevertheless, minimal when compared to the LC situations. Finally, in spite of a million vain attempts, no coefficient vector was found obeying (1) and implying (2) for the combination of the LC filter and the FC topology. This does not ensure that there is no sequence stabilizing this system, but it appears very unlikely, especially considering that the other topologies required a maximum of 5 attempts.

1.3 Controllability

The controllability of a system is a fundamental characteristic, defined by the possibility to reach any given state of the system from any other state, using the right control sequence. Incidentally, it does not necessarily mean that the destination state can be maintained, simply reached. For continuous Linear Time-Invariant (LTI) systems (3), it is possible to define a controllability matrix, defined by (4), where N_{states} is the number of states defining the state-space representation of the system.

$$\dot{\boldsymbol{x}} = \boldsymbol{A}\boldsymbol{x} + \boldsymbol{B}\boldsymbol{u} \tag{4.3}$$

$$\boldsymbol{R} = [\boldsymbol{B}\ \boldsymbol{A}\boldsymbol{B}\ \ldots.\ \boldsymbol{A}^{N_{states}-1}\boldsymbol{B}] \tag{4.4}$$

If the rank of this matrix is full, henceforth equal to N_{states}, the system is controllable. This definition is applied to both continuous and discrete LTI systems. Given that the input vector is included in the $\boldsymbol{A}$ matrix by the definition of the SSSR (5), it is impossible to leave the zero state. Considering the uncontrolled inputs as null, the system is defined by (6).

$$\dot{\boldsymbol{x}} = \boldsymbol{A}(\boldsymbol{u})\boldsymbol{x} + \boldsymbol{E}\boldsymbol{d} \tag{4.5}$$

$$\dot{\boldsymbol{x}} = \boldsymbol{A}(\boldsymbol{u})\boldsymbol{x} \tag{4.6}$$

If $\boldsymbol{x} = 0$, then $\dot{\boldsymbol{x}} = 0$ for all u, which in turn means that $\boldsymbol{x}(\boldsymbol{u}) = 0$ for all $\boldsymbol{u}$. This result contradicts the definition of controllability. The systems defined by the model from Chapter II are therefore not controllable. However, the situation where both $\boldsymbol{d}$ and $\boldsymbol{x}$ are null is not sensible in the case of power conversion: if the current and voltages flowing through a converter are equal to zero, it means that the converter is not in operation. Consequently, the converter is unable to control the power flow, or anything else. It is not judicious to apply the definition given earlier for the controllability of such a system as power converters.

In the case of power converters, the study of the system separated from all inputs, be it the states of the switches or the currents and voltages provided by the different sources and loads, is physically unfit. These two inputs are separated from the control point of view, as the first one corresponds to the control

input and the second one to disturbances, or uncontrolled input. This uncontrolled input is not irrelevant. From there, another approach rises: determine the controllability regarding both $\boldsymbol{u}$ and $\boldsymbol{d}$. This definition revisits the original one, considering the two inputs as relevant control-wise: the system described by (6) is controllable if for any given initial state $\boldsymbol{x_0}$ some inputs $\boldsymbol{u}$ and $\boldsymbol{d}$ exist such that their application leads to any state $\boldsymbol{x_f}$. In other words, what was previously a disturbance is considered as a proper input, as it is physically. For a given control position, the situation is then brought back to the LTI situation, and the controllability matrix can be expressed.

The logic behind the controllability matrix is the definition of a base in the vector space of the state-space representation. If the vector family defined by $\boldsymbol{R}$ is full, then it forms a base of the space, proving any position in this space can be reached with the proper input. While this family is only defined around the input $\boldsymbol{u}$ from (3), it has to include both $\boldsymbol{u}$ and $\boldsymbol{d}$ from (5) to properly express the reachable space in the chosen SSSR by application of these inputs. The matrix family results from the combinatory logic of the inputs: it is formed by the concatenation of the combinations of the controllability matrices from (4). In order to illustrate this concatenation, let us define first

$$\boldsymbol{\Pi}_c(\boldsymbol{k}) = \prod_{i=1}^{c} \boldsymbol{A}\big(\boldsymbol{k}(i)\big), \tag{4.7}$$

the product of the matrices described by the vector of combinations $\boldsymbol{k}$, representative of the sequence that is applied to the system. The resulting matrix is of the same size as all $\boldsymbol{A}(\boldsymbol{u})$, square matrix defined by the number of states in the SSSR. These matrices are combined as follows:

$$\boldsymbol{R} = \begin{bmatrix} \boldsymbol{E} & \boldsymbol{\Pi}_1(1)\boldsymbol{E} & \boldsymbol{\Pi}_2(1,1)\boldsymbol{E} & \cdots & \boldsymbol{\Pi}_{N_{states}-1}(1,1,\dots,1)\boldsymbol{E} \\ \boldsymbol{E} & \boldsymbol{\Pi}_1(1)\boldsymbol{E} & \boldsymbol{\Pi}_2(1,1)\boldsymbol{E} & \cdots & \boldsymbol{\Pi}_{N_{states-1}}(1,1,\dots,2)\boldsymbol{E} \\ \vdots & \vdots & \vdots & \vdots & \vdots \\ \boldsymbol{E} & \boldsymbol{\Pi}_1(1)\boldsymbol{E} & \boldsymbol{\Pi}_2(1,1)\boldsymbol{E} & \cdots & \boldsymbol{\Pi}_{N_{states}-1}(1,1,\dots,N_V)\boldsymbol{E} \\ \vdots & \vdots & \vdots & \vdots & \vdots \\ \boldsymbol{E} & \boldsymbol{\Pi}_1(1)\boldsymbol{E} & \boldsymbol{\Pi}_2(1,2)\boldsymbol{E} & \cdots & \boldsymbol{\Pi}_{N_{states}-1}(1,2,\dots,1)\boldsymbol{E} \\ \vdots & \vdots & \vdots & \vdots & \vdots \\ \boldsymbol{E} & \boldsymbol{\Pi}_1(1)\boldsymbol{E} & \boldsymbol{\Pi}_2(1,2)\boldsymbol{E} & \cdots & \boldsymbol{\Pi}_{N_{states}-1}(1,2,\dots,N_V)\boldsymbol{E} \\ \vdots & \vdots & \vdots & \vdots & \vdots \\ \boldsymbol{E} & \boldsymbol{\Pi}_1(N_V)\boldsymbol{E} & \boldsymbol{\Pi}_2(N_V,N_V)\boldsymbol{E} & \cdots & \boldsymbol{\Pi}_{N_{states}-1}(N_V,\dots,N_V)\boldsymbol{E} \end{bmatrix}, \tag{4.8}$$

where the notation N_V is chosen to abbreviate the $N_{vertex}(1)$ value introduced in Chapter III. The size of this new controllability matrix is determined by the number of possible combinations, namely $N_V^{N_{states}-1} N_{states} \times N_{states} N_d$, with N_d the number of elements in the disturbance vector. The size of the matrix is then very large, and the objective is to determine whether the rank of this matrix is equal to the number of states or not. This operation is hardly performed, and though sufficient and necessary, this criterium does not seem easy to apply on systems such as power converters, where the size of this controllability matrix quickly gets too big for computations. However, the discrepancy between the size of the matrix and the desired rank is enormous and corroborates in a way the intuition that such systems are always controllable, because of the multitude of dynamics they propose.

Another approach consists in studying each subsystem. If even one of them is, then the global system is controllable: if there is at least one subsystem designated by $\boldsymbol{u}$ for which for any initial state an input $\boldsymbol{d}$ exists leading to any destination state when applied, then the same property can be transmitted to the global system formed by the different subsystems. This condition is sufficient but not necessary: the same way transposition of the properties of stability is not as direct as they may seem, it is not possible to affirm that because none of its subsystems is controllable, then the general system is not either. Especially because the combination and sequencing of the subsystems is the actual control input. This new condition can then be used to quickly prove that if one of its subsystems is controllable by $\boldsymbol{d}$ then the general system is controllable by $\boldsymbol{d}$ and $\boldsymbol{u}$.

The definition used is strong and not quite adequate. The disturbances, though crucial to the system behavior, are still uncontrolled and deducing the controllability regarding them is not exactly fitting. The perfect situation would be to fully determine the disturbances and demonstrate the existence of a control input leading from any initial state to any final state in finite time under this disturbance profile, finding a middle point between the different definitions introduced earlier.

2 Cost Function Design

2.1 General expression

The aim of the cost function is to accurately represent the different control objectives in the optimization block of the controller. From a theoretical point of view, the expression of this function to minimize is strongly related to the algorithms used. For example, a quadratic programming algorithm requires a quadratic cost function to operate properly. This quadric also has to be a paraboloid with a minimum, leading to various criteria on the expression of the cost function when dealing with quadratic programming.

This limitation is different from the situation described in Chapter III. Indeed, there is no restriction on the format of the costs, thanks to the graph definition of the optimization problem. The only relevant rule is the need to have a limited number of minima. It is preferable to show only one minimum, guaranteeing any local minimum encountered to be the global minimum of the function. However, this condition is difficult to implement strictly in the definition. For this reason, according to the way the function is defined, it may lead to several local minima.

Critically, the cost function discussed here is not the cost function of the controller like it could be for a common MPC algorithm, but the function used to determine the weight of the edges of the graph solved by the shortest path algorithm described in the previous chapter. For clarification issues, let us note Γ_{cont} the cost function eventually solved by the algorithm and Γ the one used to predict the weights of the edges. The relation between these two costs is the same than the one linking the distances and the weights

of the graph, as explained in Chapter 3. As such, the controller's cost function is the sum of the N_{opt} edges selected as optimal to reach the destination node from the source node:

$$\Gamma_{cont} = \sum_{k_{opt}=1}^{N_{opt}} \Gamma(k). \tag{4.9}$$

This sum is presented as independent of the advancement of the algorithm in the graph, meaning that the costs of all layers have the same impact on the total distance. It is not impossible to moderate the influence of the furthest depths of progress in the tree, in order to emphasize on different phases of the control. For example, if the costs to reach a vertex from the k^{th} level to the $(k+1)^{th}$ layer of the tree are mitigated in comparison to the previous levels, the algorithms may be inclined to progress faster in-depth than without mitigation. Similarly, if a layer transition holds more weight than the others, the algorithm will have to focus more on this particular passage. The interest of this method can be discussed but does not seem relevant here. For this reason, (9) is applied onwards.

The edge function is extracted from the requirement specifications of the system. Each stipulation leads to a sub-cost. All sub-costs are scalars, as well as all the cost functions discussed here should be. The general function is a linear combination of these elements:

$$\Gamma = \sum_m \alpha_m \Gamma_m. \tag{4.10}$$

Defining the sub-costs Γ_m and balancing them is the main task of the control designer. The weights associated with the different elements of the total cost must be managed in relation to each other. There are no imperative rules on their attribution, but out of two sub-costs, the one with a higher α coefficient will be treated prominently, as the same correction, or the same reduction of Γ_{m1} and Γ_{m2}, leads to a bigger decrease in the global Γ function if α_{m1} is superior to α_{m2}. In consequence, the minimum of Γ is more interesting if the correction on Γ_{m1} is applied instead of the one on Γ_{m2}.

There is no point in reasoning with absolute values of weights. Only relative values hold interest. There is no immediate generic method to properly balance the coefficients apart from the heuristic approach, keeping in mind the principles enounced earlier. Adjusting the weights becomes harder with the accumulation of sub-functions, even more so when these sub-functions contradict one another or entail multiple local minima when combined.

2.2 Different sub-costs

The most generic control specifications can be categorized in four categories. First, tracking objectives on states, then tracking objectives on other variables, operational recommendations and, finally, system constraints. The first group is the most intuitive one, where an ideal value is expressed and compared to the current state of the system, as depicted in (5), where $\boldsymbol{x}^*$ represents the desired value of $\boldsymbol{x}$. In order to minimize the resulting error, the algorithm will select the states that get the system closest to the desired reference. The reference can be a fixed point, time-independent, or a trajectory, a line of time-bound points.

$$\Gamma_{\boldsymbol{x}} = \|\boldsymbol{x}^* - \boldsymbol{x}\| \tag{4.11}$$

The second group is similar to this one, but with a broader definition. It allows defining complex objectives, functions of the different data elements available to the controller. The most generic definition is

$$\Gamma_{\boldsymbol{y}} = \left\|\boldsymbol{y}^* - \boldsymbol{f}_{\boldsymbol{y}}(\boldsymbol{x}, \boldsymbol{u}, \boldsymbol{d}, t)\right\| \tag{4.12}$$

where $\boldsymbol{f}_{\boldsymbol{y}}$ is a function of the past and current states of the system, of the control input, of the time and the different uncontrolled inputs. The image of this function is also called $\boldsymbol{y}$ and compared to a desired value $\boldsymbol{y}^*$. Not specifying such a value implies an objective of zero. $\boldsymbol{f}_{\boldsymbol{y}}$ can illustrate a large variety of goals, from simple combinations of the states and inputs to variations of those, as well as more complex definitions. From a purely theoretical point of view, almost any interesting variable can be expressed with such a function. In the case of power converters, a common use is the computation of the active and reactive powers and could be, with extremely powerful hardware and longer optimization horizon, the retrieval of the frequency and harmonics induced by the system. The main restriction lies in the computational effort. These functions cannot afford to be too computationally demanding, as it hinders the operation of the controller more than tolerable.

The third group specializes in the control input. Because the controller directly acts on the states of the switches, various stipulations that would otherwise be managed by the modulation block are included via this class of costs. For example, the switching frequency is an important aspect, closely related to the switching losses of the converter and thus to its efficiency. Expressing the need to reduce the number of commutations is, therefore, a priority. This can be done by counting the number of state shifts induced by the control considered.

As often found in the literature, another typical kind of cost is found on the input of the system. Since the control input is of discrete nature, the costs associated with it are necessarily different from the ones in continuous nature. An interesting value to monitor is the number of changes of state implied by the control. For example, for a 3L-NPC topology, applying the S_P command from an initial S_0 position, two switches change state, while from the S_N it implies 4 state modifications and from the S_P position no changes are made. The switching frequency is an important factor of efficiency for power converters. Each switching modification implies an energy loss. The characterization of these losses is a subject of research by itself and was not incorporated into the models described in the second chapter. However, the switching losses can be implemented in the cost function somehow. The switching losses can be estimated as proportional to the number of state changes, and counting those is sufficient to indirectly monitor these losses. Adding the number of switching actions to the cost function is an efficient way to control the efficiency of the power converter. The function counting the switches can be implemented with a look-up table or by associating to the switching positions manipulated by the algorithm a value: for the case raised up earlier, Table 4.2 illustrates this possibility.

TABLE 4.2
CORRESPONDENCE BETWEEN THE SWITCHING POSITIONS AND THEIR COST

Switching position	States of the switches	Value given	Distance calculated with	
			Real States	Affected Value
S_P	[1 1 0 0]	1	$\rightarrow S_P: 0$ $\rightarrow S_N: 4$ $\rightarrow S_0: 2$	$\rightarrow S_P: 0$ $\rightarrow S_N: 2$ $\rightarrow S_0: 1$
S_N	[0 0 1 1]	-1	$\rightarrow S_P: 4$ $\rightarrow S_N: 0$ $\rightarrow S_0: 2$	$\rightarrow S_P: 2$ $\rightarrow S_N: 0$ $\rightarrow S_0: 1$
S_0	[1 0 1 0]	0	$\rightarrow S_P: 2$ $\rightarrow S_N: 2$ $\rightarrow S_0: 0$	$\rightarrow S_P: 1$ $\rightarrow S_N: 1$ $\rightarrow S_0: 0$

Table 4.2 explains how to simplify the counting of the switching actions for the case of 3L-NPC. It shows that a coefficient of proportionality of 2 appears here. As long as this coefficient is the same for all transitions, the transformation is satisfying. This exercise becomes more difficult with more switching positions. It is interesting to affect the values in a bijective manner to conserve the properties of the designations of the switching positions. This bijectivity cannot be achieved for the 3L-FC topology: the only way to fulfill the condition of constant proportionality is to give the two switching positions S_{CP} and S_{CN} the same value, which contradicts bijectivity. The look-up table can be implemented with a fairly low cost for the algorithm and is here preferred.

Including such a cost leads automatically to an inaction influence: if it is the only one taken into consideration, this cost prevents any change of position of the system switches from occurring. Defining $\boldsymbol{f_u}$ a function of the control input $\boldsymbol{u}$ properly representing the control specifications on the switching patterns, the input cost is of the form:

$$\Gamma_{\boldsymbol{u}} = \boldsymbol{f_u}(\boldsymbol{u}, t) \tag{4.13}$$

The function $\boldsymbol{f}_u$ can present various properties. A critical illustration is its sign: taking the state switching count function, assigning it a positive sign orientates the algorithm to an economy of switches, while a negative sign directs it towards an extravagance of them.

Finally, the algorithm developed is able to manage constraints. Constraints are hard limitations and rules, unlike the previously introduced objectives, considered as directions by the algorithm. Constraints permanently block branches in the tree of possibilities. The correct way to do so is to implement an infinite cost of transition on an edge when the node it leads to does not respect the constraints. This way, the algorithm is strictly incapable of proposing control sequences leading to the non-respect of the constraints.

It leads to a definition of a constraint cost, either null when all conditions are respected or infinite as soon as one is not.

2.3 Evaluation of the performances of the algorithm

The design of the cost function is difficult and there is no generic strategy other than trial and error. Some principles can be kept in mind to manipulate the different sub-costs cleverly. But first of all, it is necessary to define performance criteria. Two kinds of criteria emerge: first, the performance of the controller according to the specifications, and then, the internal factors such as the behavior of the optimization algorithm. The first category illustrates the quality of the cost function and its weighing, and is quantified by studying the tracking results and, overall, the decrease of the cost. The first two sub-costs presented, Γ_x and Γ_y naturally have a global minimum at zero, a situation where the real value is strictly equal to the desired reference. The other cost (13) may not have such a behavior. Either way, if the optimization problem is well-posed, meaning the cost function is well defined, then the optimal cost determined by the algorithm decreases over time. The only situation in which an increase in the cost is acceptable is when references undergo sudden variations, such as steps of reference.

The shortest path algorithm always provides the best path according to the cost function. If the cost increases, it can only mean two things: either the global cost function does not lead to a clear minimum or one of the sub-costs is not properly controlled. To put it simply, the latest possibility is the sign of a wrongly defined sub-function that prevents the existence of a minimum stable in time, such as what a random sub-cost would imply, and the first case corresponds to an equilibrium that cannot be reached. Perfectly accessible objectives can contradict one another and prevent the system from properly achieving any of them. The criterion is the first qualifier of success, and can also be used as a quantifier of success, as the faster it decreases, the better the performances are. However, the general cost is not always sufficient to properly evaluate the behavior of the control. Observing the objectives separately is also interesting, as, like in a tug-of-war, a compromise can be found in which neither of the objectives is attained and a middle point is selected instead. This is rarely an interesting situation control-wise.

The second category rates the feasibility of the cost function and its impact on the internal operation of the MPC algorithm. The main limitation is computation. The cost function affects the total computation time in two ways. To begin with, it is the most called upon element of the algorithm, with the prediction. The complexity of the determination of the cost strongly impacts the complete MPC computation effort. The other aspect is linked to the behavior of the graph. Because it is defined by the cost function, the explored graph and the number of steps needed to solve it both depend on the cost function. To quantify the first aspect, measuring the operating time is sufficient. It is better to perform a high number of measures and mean the results. Concerning the second aspect, the most efficient way is to retrieve the number of nodes crossed by the algorithm before solving the optimization problem.

As a reminder, the best graph in terms of steps necessary is the one where edges are clearly discriminated with distant weights. Indeed, different paths with similar costs have to be travelled the same way: if several routes exhibit identical or close total costs, they will all be considered by the algorithm the same way. This trait is what gives the power to the algorithm to always find the global optimal, but it is also a cause of longer computation times. To put it shortly, the cost function has to be chosen to trim the tree.

An example of the three performance evaluations described is developed onward on the choice of the norm used to measure the distance between the reference and the current state of the system. So far, the norm in (11) and (12) has not been defined. There are three mainly used norms: the taxicab norm, the Euclidean norm and the infinity norm. Mathematically, they correspond to the L^1, L^2 and L^∞ norms. The first one is given by the absolute value as

$$\|\boldsymbol{x}\|_1 = \sum_i |x_i|, \tag{4.14}$$

the second is obtained by the square root of the square product, i.e.

$$\|\boldsymbol{x}\|_2 = \sqrt{\boldsymbol{x}'\boldsymbol{x}}, \tag{4.15}$$

and finally, the ultimate one is determined by the maximum value, as given next:

$$\|\boldsymbol{x}\|_\infty = \max(\boldsymbol{x}). \tag{4.16}$$

These norms are metrics used to determine how close two comparable elements are. Judging from the way they are defined, these distances are not strictly equivalent. An illustration of this is the "circle" of unitary radius, i.e. the set of points defined by (17) in the 2D plane and presented in Fig. 4.1.

$$\|x\| = 1 \tag{4.17}$$

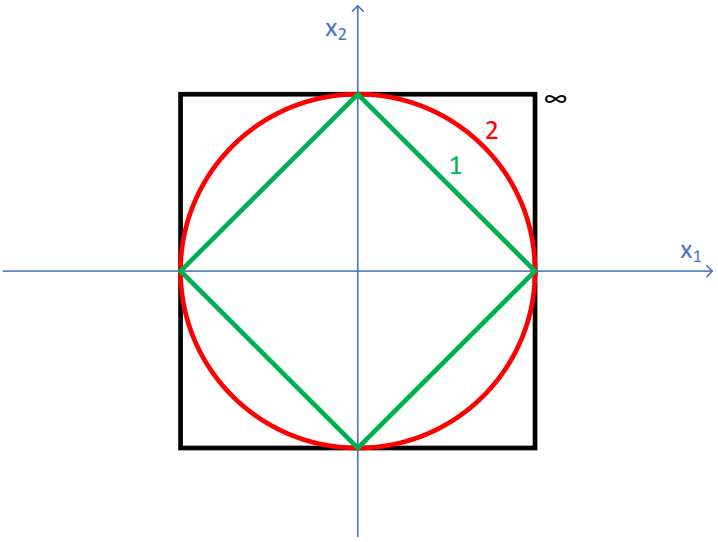

Fig. 4.1. Unity circle with the 1, 2 and ∞ norms

Intuitively, computing absolute values and summing them seems more economical than computing the square root of a cross product. Finding the maximum value of a vector being different from ordering it, this calculation should not require too much effort either. This affirmation is not necessarily true. For

example, many graphic cards consider the Euclidean norm operations as basic operations, rendering all three norms very similar when it comes to computation time.

To illustrate this observation, all three norms where computed and timed in MATLAB. The three norms were all computed in meantime of 3 µs when using the built-in norm function, while the application of the direct expressions put the taxicab norm and the infinite norm slightly faster than the Euclidean norm, with respectively 4, 3 and 7 µs to completion. Though minuscule, this difference implies a 100% increase in the time needed. The first conclusion is that the existence of a fastest norm depends on the hardware implementation and has to be considered when defining the cost function.

In order to test the second criterium, the controller is put in a situation similar to that studied in Chapter II, for 3L-FC converter associated with an LCL filter. The controller receives references to control the voltages of the inner capacitors of the topology, and instates a cost function of the form

$$\Gamma = \|\boldsymbol{U}_{\boldsymbol{C}}^{*} - \boldsymbol{U}_{\boldsymbol{C}}\|, \tag{4.18}$$

where $\boldsymbol{U}_{\boldsymbol{C}}^{*}$ represents the voltage references and $\boldsymbol{U}_{\boldsymbol{C}}$ the current state of the inner capacitors' voltages. The norm is not given expressly in (18) as the objective is to implement all three of them and check if the number of nodes or the number of calls to the cost function is influenced by the norm selected. The algorithm is used with $N_{opt} = 2$. Therefore, the number of nodes explored is contained between 3 and 757 by numerical application of (3.3) from Chapter III.

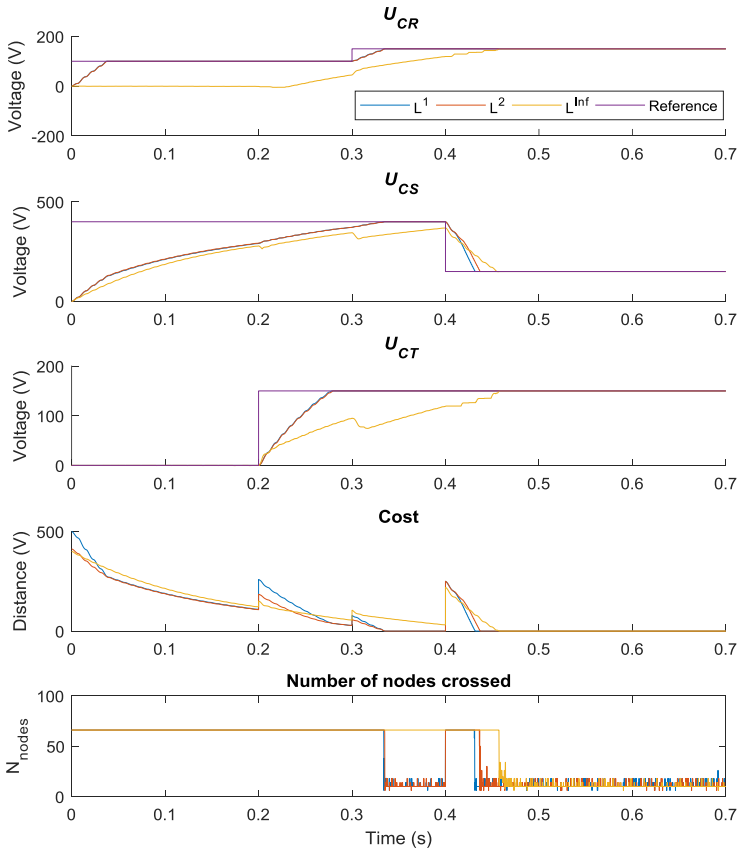

Fig.4.2. Comparison of the impact of the choice of the norms on the performance of the algorithm

From the simulation results presented in Fig.4.2, it is difficult to properly establish a preference between the L^1 and L^2 norms. This figure first shows the objective $\boldsymbol{u}^*$ on the three phase-capacitor voltages and the behavior of the controlled voltages. This first part illustrates an interesting property: the signals generated by the first two norms are quite similar. It is actually difficult to distinguish them. The infinite norm behaves strangely, as it seems to neglect one of the voltages for a while before finally acting after 0.2 s. This is coherent with the definition of the norm: this timestamp corresponds to the moment when the error on U_{CS}^* becomes smaller than the one on U_{CR}^*, which coincides with the definition of the infinite norm: the algorithm ends up focusing its attention on only one of the three references at a time, instead of treating them altogether as do the other two norms. For this reason, this norm is not well adapted to the aspirations of the controller, particularly the one concerning balancing multiple objectives.

It is also possible to see on Fig.4.2 the evolution of the cost and of the number of steps needed by the research algorithm to find the optimal control sequence. The first conclusion from these is that the three costs are following very similar evolutions: even though the tracking behavior appears very different, the costs do not. The second conclusion is that all three norms require the same number of steps (66 in the situation presented) to solve the trees they form as long as the cost is strictly superior to zero. In consequence, it is possible to claim that the norms discussed previously do not impact the difficulty to solve the optimization problem. However, though the three norms entail the same effort profiles, the duration of this effort varies. The L^1 norm shows slightly superior performances than the L^2 norm, while the L^∞ performs poorly in comparison. For this reason, it is wise to prefer the first two to the last one. Otherwise, no element suffices to push away any of the other two possibilities. Therefore, all objectives on references, or rather on errors, can be expressed with any of them.

The previous figure also illustrates the specific situation where the cost is already equal to zero. The number of nodes needed to solve the shortest path problem appears then random, between 7 and 18 nodes crossed. This corroborates the affirmation that a graph with several identical paths is solved in a random number of steps. In the present situation, 18 is the number of paths all conserving the cost at its null state, and the algorithm solves the tree in a number of steps only constrained by this value.

3 Controller traits

The particularities of the MPC methods used so far accumulate themselves when considering the higher point of view of the controller and the controlled plant. A critical aspect resulting from this harvest is the difficulty to study the behavior of the strategy developed based on theory. The open and closed-loop stability of the system combined with the MPC controller are very difficult to characterize and study. Even though the Lyapunov methods are still applicable, the graph-oriented optimization is particularly difficult to adapt to. Various techniques can be used when the switching sequence is known, as sometimes found for modulation-based controllers [6] [7]. How difficult the theoretical approach may be, nothing prevents

heuristic study and methods, as well as applicative results. For example, the robustness and sensitivity of the controller can be determined and exposed from practical results.

3.1 Robustness

The robustness of a controller is its capacity to conserve performances when the system varies. A typical situation where this property is interesting is for aging systems: with time, the values of the parameters of the system are bound to change slightly. The question is whether the controller, left unchanged and therefore attempting to control a different system, still performs its control correctly or not. It is not easy to properly qualify or quantify this property for a generic case, but will be observed and scrutinized for a specific situation, the same as the one described in Subsection 2.3 of this chapter. As a reminder, the controller uses the model of a 3-legged FC topology associated with an LCL filter to control the voltages of its inner capacitors. The objective in this part is to employ a degenerated model for the MPC where the different variables show a certain error and to see how the performances evolve. The results are presented in the following figure, where the control results are superposed for ten different percentage errors on the parameters.

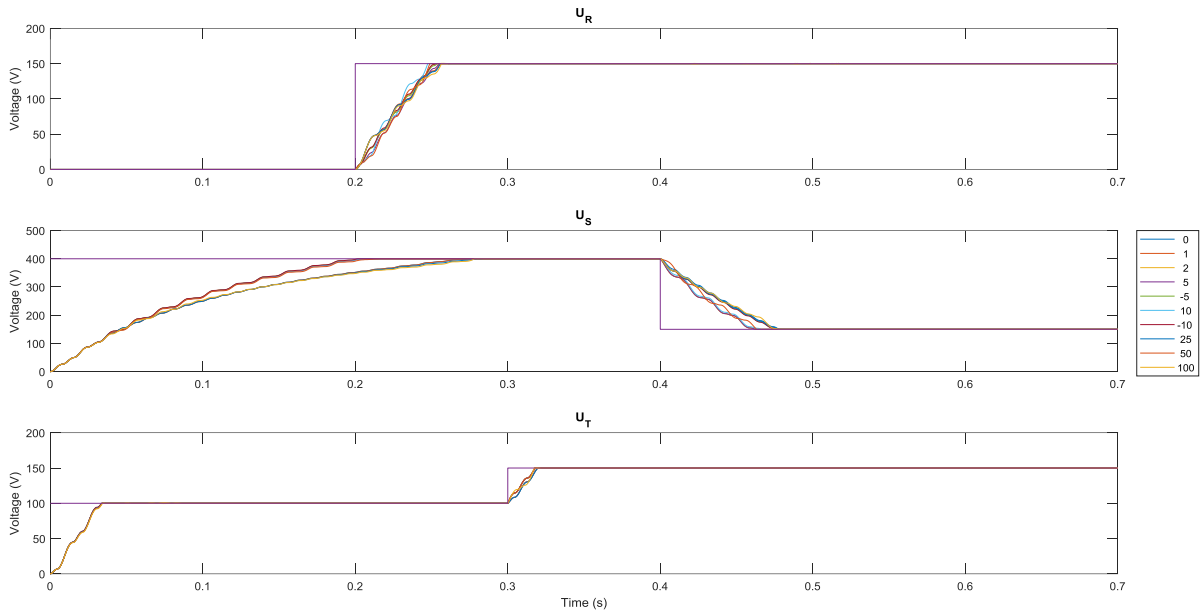

Fig. 4.3. Comparison of tracking performances with model errors, reference in purple, error given in %

Figure 4.3 shows optimistic results: the controller displays strong robustness, managing to perform its objectives even with an inner model in which all values were the double of the parameters of the controlled plant. MPC is often praised for leading to very robust controllers, thus making this result not necessarily surprising. As long as the dynamics are respected and somewhat similar to real behavior, the controller is able to steer the system in the right direction. The figure shows that the performances are not identical, which is to be expected, with lower errors leading to better tracking speedtime-independentfor example. However, this difference is only substantial.

The conclusions from the simplified situation used have to be moderated: the control objectives are simplistic and do not use all the states and all the dynamics of the model. For a more complex situation, where several objectives combine and form a much more demanding control problem; the impact may well be much more visible.

3.2 Sensitivity

The sensitivity of a controller is parallel to its robustness: where the latter designates the ability to keep operating with a different system like the one originally planned. Sensitivity evaluates the impact of changes internal to the controller. For PI controllers, this means modifying the different gains of the control transfer function. This is actually crucial for analogue controllers, as the components responsible for these parameters are physical components prompt to fatigue and deterioration, where their value change, therefore modifying the controller's parameters. In the MPC case, the control aspects and characterization are all found in the cost function. Variations of the values of the coefficients can entertain miscellaneous consequences in the resulting controlled system. These changes may occur "naturally" with errors of communication between blocks of the controller, or in the case of communications with an external component, potentially another controller in a hierarchical or distributed control structure. These events are represented by modified values for the coefficients of the cost function (10). The impact of changes on these values has already been qualified in previous subsections. The quantification is a harsher task: numerous sub-costs steering the controller in different directions leads to a specific equilibrium. Observing the impact of the change of one coefficient out of 2 is already subject to skepticism, as the nature of the two sub-functions associated has to be considered before any conclusion: if the two pull the system towards the same state, the sensitivity will be very different from when they lead towards opposite or misaligned directions. With two sub-functions, the logic is rather easy to fathom, but when their number increases, it quickly becomes difficult to properly study the sensitivity of the controller.

From there, the sensitivity question can only be answered from a practical point of view, based on a specific set of objectives, constraints and requirements. So far, no analytical approach has been found to determine the best coefficients for the cost function, leaving the heuristic method as the only applicable one. This property is transposed directly to the study of sensitivity: only heuristic results can be extracted and only for specific situations.

4 Conclusion

In this chapter, various traits and properties of the controller were studied theoretically and in practice, particularly the stability and the controllability of the models deployed, the quantification and qualification of the algorithm performance with the method to affect them for the control designer, and finally the behavior of the controller under certain modifications of its environment. Now that the general behavior of the controller is known, we propose to confront it to applications we judge fit to reveal its

capacity and interests in the domain of power conversion and especially weak grids and distributed generation.

5 Bibliography

[1] F. El Hachemi, « Analyse de stabilité des systèmes à commutations singulièrement perturbés », PhD Thesis, Université de Lorraine, 2012.

[2] R. A. Decarlo, M. S. Branicky, S. Pettersson, et B. Lennartson, « Perspectives and results on the stability and stabilizability of hybrid systems », *Proc. IEEE*, vol. 88, nº 7, p. 1069‑1082, juill. 2000.

[3] D. Liberzon, « Switched Systems: Stability Analysis and Control Synthesis », p. 71.

[4] M. A. Wicks, P. Peleties, et R. A. DeCarlo, « Construction of piecewise Lyapunov functions for stabilizing switched systems », in *Proceedings of 1994 33rd IEEE Conference on Decision and Control*, 1994, vol. 4, p. 3492‑3497 vol.4.

[5] M. Wicks, P. Peleties, et R. DeCarlo, « Switched Controller Synthesis for the Quadratic Stabilisation of a Pair of Unstable Linear Systems », *Eur. J. Control*, vol. 4, nº 2, p. 140‑147, janv. 1998.

[6] A. Babiarz, T. Grzejszczak, A. \Lęgowski, et M. Niezabitowski, « Controllability of discrete-time switched fractional order systems », in *2016 12th World Congress on Intelligent Control and Automation (WCICA)*, 2016, p. 1754–1757.

[7] Z. Sun, S. S. Ge, et T. H. Lee, « Controllability and reachability criteria for switched linear systems », *Automatica*, vol. 38, nº 5, p. 775‑786, mai 2002.

Chapter V: Case studies

1. Introduction

The controller presented in the previous chapters is developed to control any power converter down to its power switches. The main purpose of this characteristic is to add flexibility and polyvalence to the controller, but also and mostly to the control structure. In fact, with the control scheme proposed in Chapter III, the same MPC controller can theoretically tackle a wide range of different situations, provided that an adaptation of the models and of the cost function is carried out, with no other impact on the structure. Several questions have already been tackled theoretically, about controllability, stability or robustness, but the validation of the proposed controller both in simulation and experimentation is still pending. The objective of this chapter is to address the question of validation in simulation, and particularly to illustrate and demonstrate the abilities of the developed MPC controller.

This demonstration will be performed in three stages, corresponding to four different cases of study. The first one has a vocation to illustrate the polyvalence of the controller, by confronting it to multiple objectives in a simplified, yet relevant, control situation. The chosen example is a standalone application. The second and third ones explore more specific situations, which highlight the flexibility and intelligence of the controller, focusing respectively on a grid-connected inverter associated with power objectives and on a rectifier mode, with unbalanced loads. Finally, the fourth example aims to investigate a more complete situation, with an isolated grid and a combination of the two previous applications, where the controller has to manage objectives from both the AC side and the DC side of the converter.

For all the applications cited above, the MPC controller used is described in Chapter III, with the A* search algorithm, $N_{pred} = 1$ and $N_{opt} = 2$. The models used for prediction and optimization are the switched state-space models presented in Chapter II, chosen among the ones presented in function of the application studied. The elements of the cost functions and their coefficients change with the cases and are therefore discussed separately for each of them.

2. Inverter stand-alone case study

2.1. Context

To begin with, the controller is confronted to an isolated inverter. The controlled system consists of an AC load connected to a multi-level converter through an LCL filter, converter fed by a DC voltage source, as illustrated in Fig. 5.1. As presented in Chapter II, the three studied topologies have different DC links. In particular, for the CHB topology, three isolated DC voltage sources are connected to the converter, leading to a different scheme for the DC-side, similar to the ones displayed in Chapter I. The parameters

used for simulation, taken from [1], are given in Table 5.1, where R_{dc} designates almost negligible resistances added to the DC sources to allow parallel connection with the capacitors.

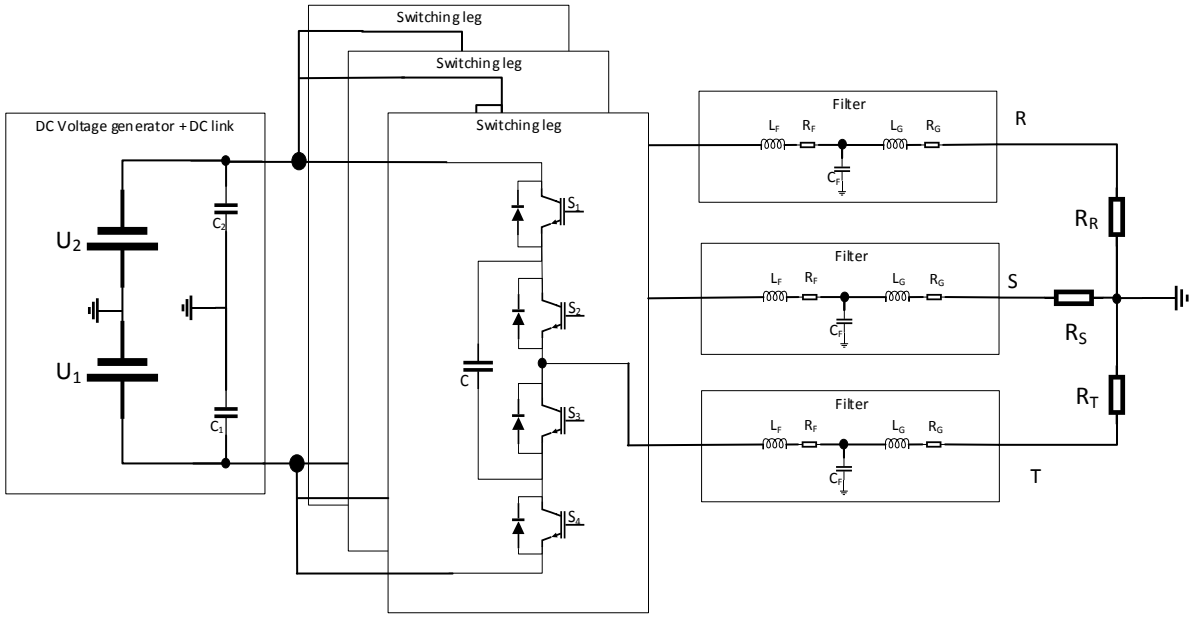

Fig. 5.1. Controlled system: stand-alone inverter, example with 3L-FC

The objective of the controller is to generate appropriate switching orders so that the currents of the AC branches follow the given references. This case study allows investigating three operating conditions: first, the ideal situation, with balanced load and common references, then, an unbalanced case or unusual references, and finally, a study of the impact of the weights of the cost functions. Additionally, the controller is evaluated using the three topologies presented in the previous chapters.

TABLE 5.1
NUMERICAL VALUES OF THE PARAMETERS

Parameter	Value	Unit
R_{Fj}	10	μΩ
R_{Gj}	10	μΩ
L_{Fj}	30	mH
L_{Gj}	30	mH
C_{Fj}	1	mF
C_j	1	mF
$C_1 = C_2 = C_3$	3.3	mF
$R_R = R_S = R_T$	100	Ω
R_{dc}	10	μΩ
U_1, U_2 for NPC & FC	600	V (rms)
U_1, U_2, U_3 for CHB	400	V

2.2. Scenarios, objectives and associated cost functions

Three scenarios are to be tackled, according to the complexity they address. The first case study is ideal, involving a balanced load and classical instructions for three-phase systems. The second one goes further by considering the case of an unbalanced load, and, consequently, of more complex objectives to reach. Finally, the third situation focuses on the impact of the weighting of the cost function to study the sensitivity of the controller.

Remarkably, the choice of the objectives has to be made according to the model of the system present in the MPC controller. To begin with, it is not causal to try and control an uncontrolled input of the modelled system. As evoked in Chapter II, the uncontrolled inputs when considering LCL filters are the AC phase-voltages, as well as the DC side currents. Consequently, these variables cannot be controlled directly by the MPC algorithm developed. Accordingly, the cost function is chosen with controllable states, as stated below:

$$\Gamma = \alpha_i \|\boldsymbol{i}^* - \boldsymbol{i}\| + \alpha_{switch}\Gamma_{switch} \quad (1)$$

where α_i represents the coefficient allocated to the objective on the error on the currents, $\boldsymbol{i}$**.** In this equation, $\boldsymbol{i}^* = [i_R^* \; i_S^* \; i_T^*]^T$ and $\boldsymbol{i} = [i_R \; i_S \; i_T]^T$. The norm used in the simulations to follow is the quadratic norm, but others can be selected. The switching sub-cost function is the one described in Chap. IV.

In the first two situations, the α_{switch} coefficient is chosen negligible compared to the α_i one. The current references are chosen in order to ensure various properties of the grid voltage, such as its amplitude and frequency. It appears that the control of the voltages is jeopardized, though it usually is the main objective in such a situation. However, knowledge of the load can be injected into the controller in two ways. The first approach consists in generating intelligent references, computed according to the loads and to the different quality properties sought for. The second solution provides this information directly to the controller, technically expanding the internal prediction model to incorporate the dynamics of the load. In the case of a simple resistive load, the relation between the current and the voltage is extracted from the Ohm's law. This relation is transcribed in the cost function by changing the reference. For example, if the main objective of control is to follow voltage references, a new cost function can be

$$\Gamma = \alpha_U \|\boldsymbol{U}^* - \boldsymbol{R}\boldsymbol{i}\| + \alpha_{switch}\Gamma_{switch}. \quad (2)$$

where $\boldsymbol{R} = \boldsymbol{diag}(R_R, R_S, R_T)$ is a diagonal matrix representing the phase resistances of the three-phase load and $\boldsymbol{U}^* = [U_R^* \; U_S^* \; U_T^*]^T$. For different load profiles, it is possible to adapt the expression (2) to include the impedance of the load instead of limiting it to its resistive aspect. This formula requires knowledge of the load and can be extended to other load profiles, but it inherently damages the robustness of the controller.

Both of these solutions rely on the same principle: injecting additional knowledge to the controller, directly or indirectly. Neither of them stands above the other: the choice of one approach instead of the other is philosophical, depending on the level of autonomy desired for the controller. If the identification of the load is correct, the results are identical for both methods. The main difficulty resides in this identification: this operation requires an observation of the behaviour of the grid. Even though the operation itself is not necessarily complex or difficult, as it is performed by analysing the relation between the currents and the voltage of the component. An identification can thus be performed according to the time scale of the dynamics of said component. This time scale is systematically much larger than the sampling time of the controller, which means the controller designed so far is not adapted to perform a load identification, therefore favouriting an external approach. This indirect method is close to the hierarchical command's principles, where different controllers handle different time scales of the system and of the control objectives.

Overall, the most important difference between the balanced and unbalanced load case studies is the reference profiles fed to the controller: if the inverter feeds an unbalanced load with the objective of keeping a balanced voltage, the currents are modified accordingly. Since the currents are ultimately the states on which the controller acts, managing the balanced and unbalanced cases only means managing different current references on the three phases. This exercise is then stretched by imposing unrealistic trajectories, not related to any particular application or case study, in order to further emphasize the potential of the controller.

2.3. Results

2.3.1. Balanced load

The objective in this subsection is to generate a balanced 50-Hz sinusoidal voltage signal. The load is considered to be known and, therefore, the cost function described in (2) is preferred. The values of the load resistances are integrated into the MPC controller via the cost function, as depicted earlier. The same cost function, with $\alpha_U = 1$ and $\alpha_{switch} = 0.01$, is employed for the three topologies. The results are presented in Figs. 5.2 to 5.4.

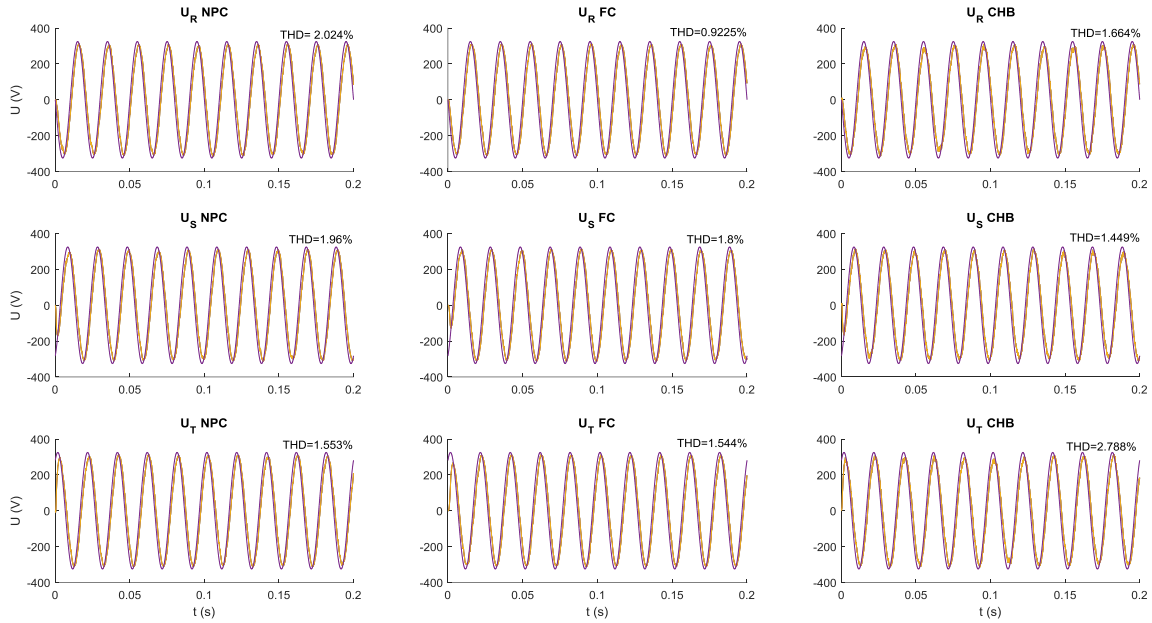

Fig. 5.2. Voltage tracking performances, inverter mode, balanced AC load for NPC, FC and CHB

Fig. 5.2. presents the tracking performance of the controller, with the sinusoidal reference presented in red in each graph. The figure is built so that each column is associated with a topology and each row to a phase of the AC load. The left column corresponds to the NPC topology, the centred one to the FC, and the right to CHB. Similarly, the top row illustrates the R phase, while the centre and lower lines picture respectively the S and T phases, as shown in Fig. 5.1. This format for the repartition of the signals and topologies is repeated throughout all the chapter.

This figure highlights the ability of the controller to follow the given references, and thus its capacity to generate the appropriate switching signals, presented in Fig. 5.3. This last figure emphasizes the difficulty to design a controller operating for any topology without incorporating specific models, as the switching profiles are clearly distinct for identical references. The switching actions are correlated to the frequency and phase of the desired references, but they differ from one topology to another. This has to be put in front of the complexity of the modulation techniques briefly described in Chapter I.

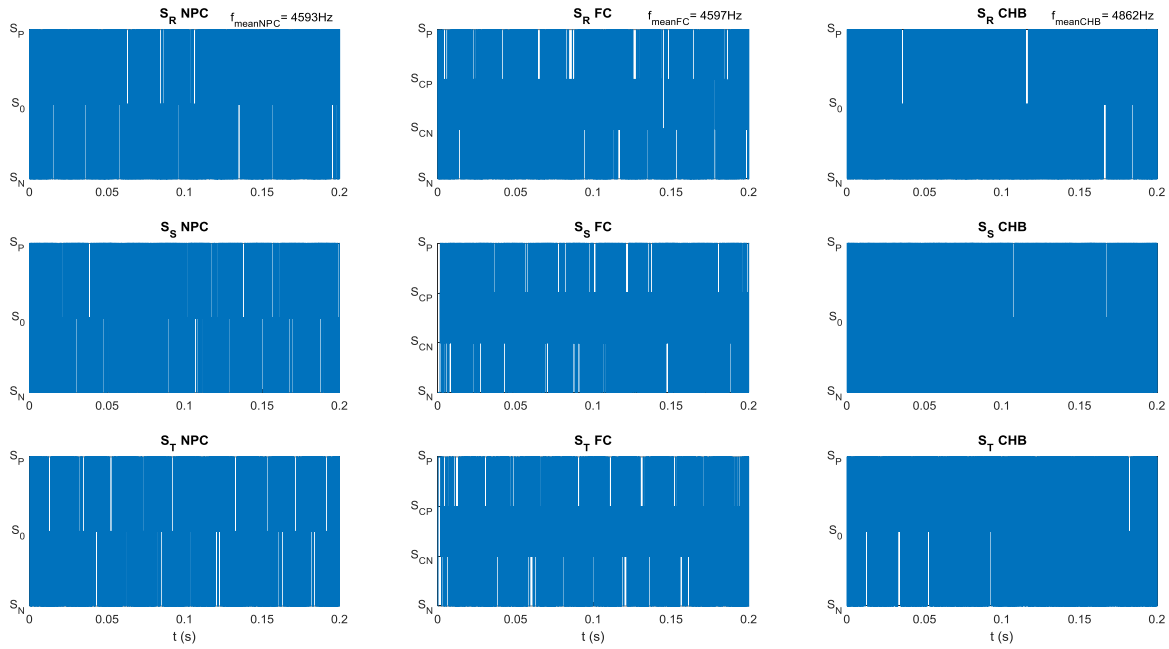

Fig. 5.3. Switching orders for each leg of each topology: NPC, FC and CHB

Fig. 5.4. shows the frequency spectra of the produced currents. This figure helps to evaluate the accuracy of the tracking results. As expected, the fundamental frequency is at 50 Hz. The other harmonics are caused by the switching operation, around 2 kHz, and the nature of the filter. Overall, the harmonic content provided is according with the standards. The reference norm used in this study is [2], for both harmonic characteristics, voltage falls and frequency qualification. The Total Harmonic Distortion (THD) for all topologies is lower than 2% and even smaller than 1% for the FC topology, as explicitly displayed in Fig. 5.2. The difference in performance between the NPC and FC topologies and the CHB one is related to the different DC sources. It must be noted that this quality aspect obeys the same laws as more common modulation methods: higher desired amplitudes or frequencies lead to poorer harmonic content, depending on the converter's maximum switching frequency and the DC side source.

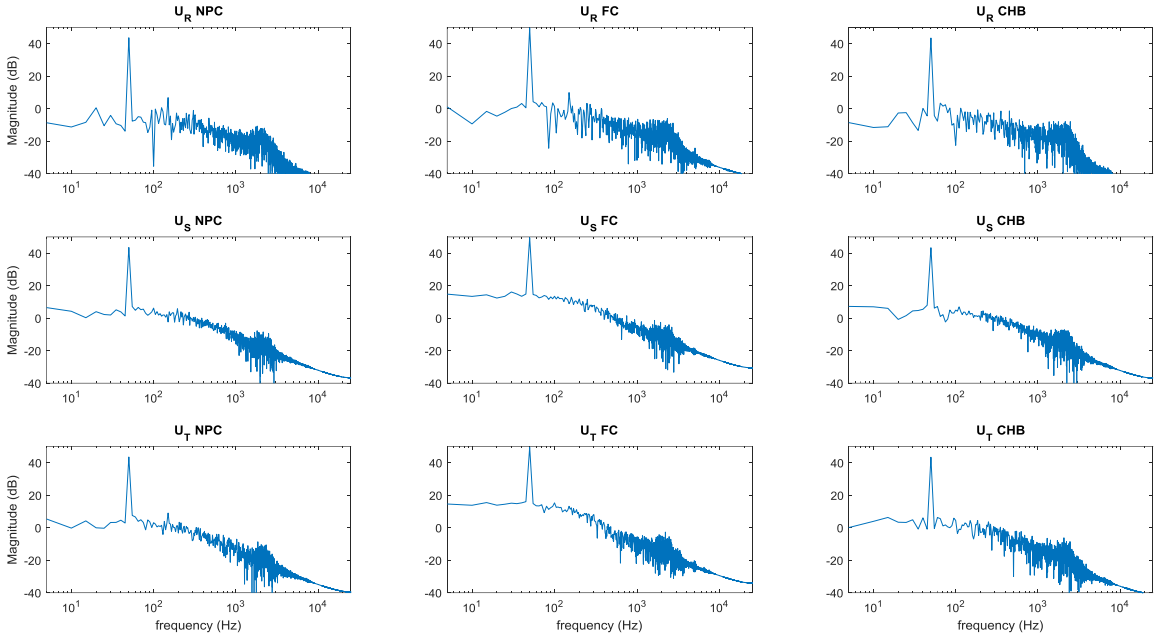

Fig. 5.4. Frequency performance for balanced AC load: NPC, FC and CHB

2.3.2. Unbalanced load

In this second case, the values of the resistive loads are not balanced, as described in Table 5.2. The relationship between the currents and the voltages is treated by an external block, not described. This block is considered as an external intelligence, actually performing the same computations as previously used in the balanced load case. The difference is that, in this case, this outsider possesses the knowledge of the values of the resistances, by identification for example. In fact, identifying such a value over time is not necessarily difficult, but cannot be done in the time scale in which the MPC controller evolves. As a matter of fact, tasks such as parameter identification, frequency and harmonics study or mean values control require long time scales, compared to the refreshing frequency of the MPC controller, and are therefore performed better when delegated to the outside of the controller.

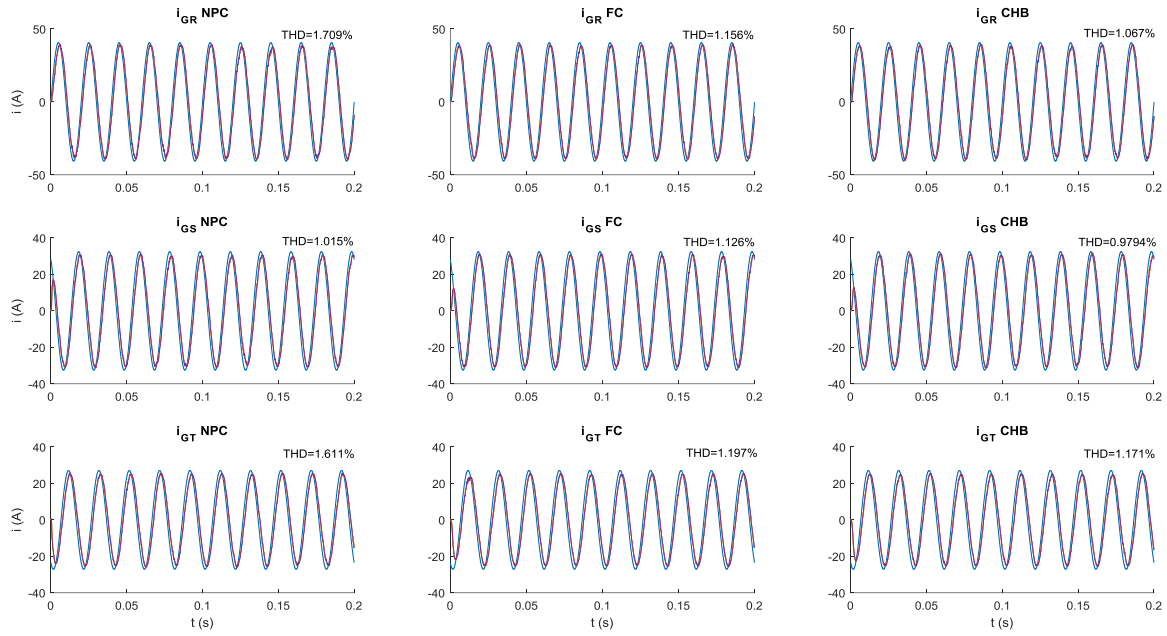

Fig. 5.5. Current tracking performances for the three topologies: NPC, FC and CHB, reference in blue.

Figs. 5.5 to 5.7 present the results obtained when trying to balance an unbalanced system. Fig. 5.5 shows the tracking of the current reference and Fig. 5.6 illustrates the consequences on the voltages. Finally, Fig. 5.7 shows the switching orders generated by the controller and sent to the converter's power switches, for each topology. These figures respectively demonstrate the ability of the controller to follow different current references on each phase, the possibility to use this capability to balance the voltages of an unbalanced system and the aptitude to generate coherent switching signals for different topologies.

TABLE 5.2
NUMERICAL VALUES OF THE PARAMETERS

Parameter	R	S	T	Unit
R	8	10	12	Ω
P	6.613	5.290	4.408	kW
I	28.75	23	19.16	A

The unbalance chosen between each phase is of 20% impedance-wise, leading to around 1 kW difference between phases R and S and phases S and T, as summarized in Table 5.2, where P represents the powerflowing through the phase and I the current. Fig. 5.5 illustrates the consequences on the controlled system. The THD values are slightly different between each phase, and the CHB topology offers the lowest THDs of the three topologies studied.

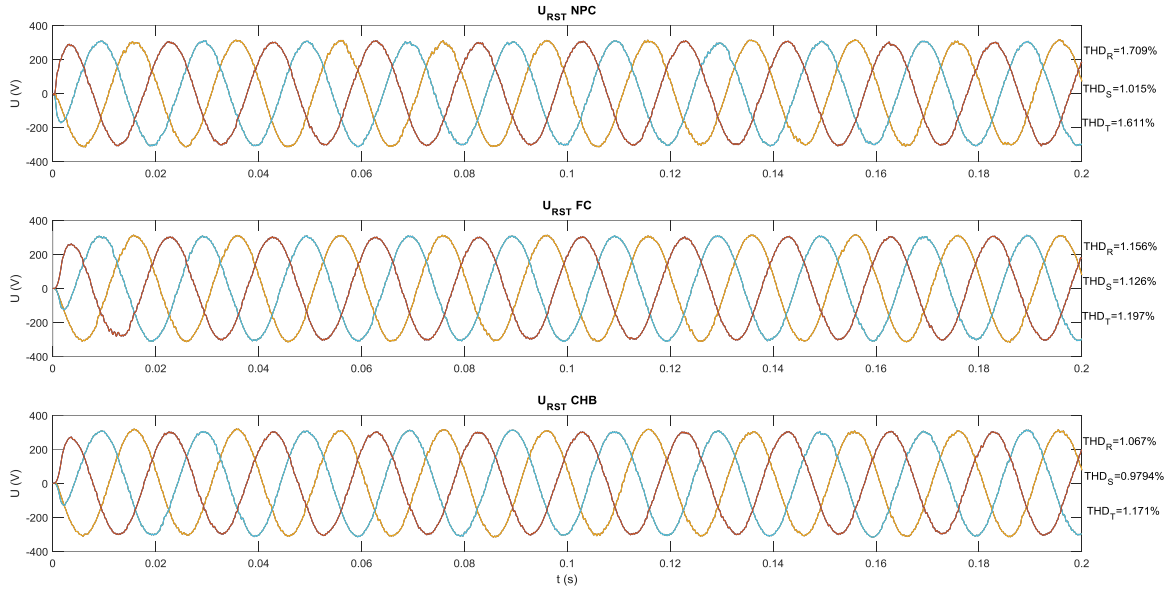

Fig. 5.6. Voltage balance: NPC, FC and CHB

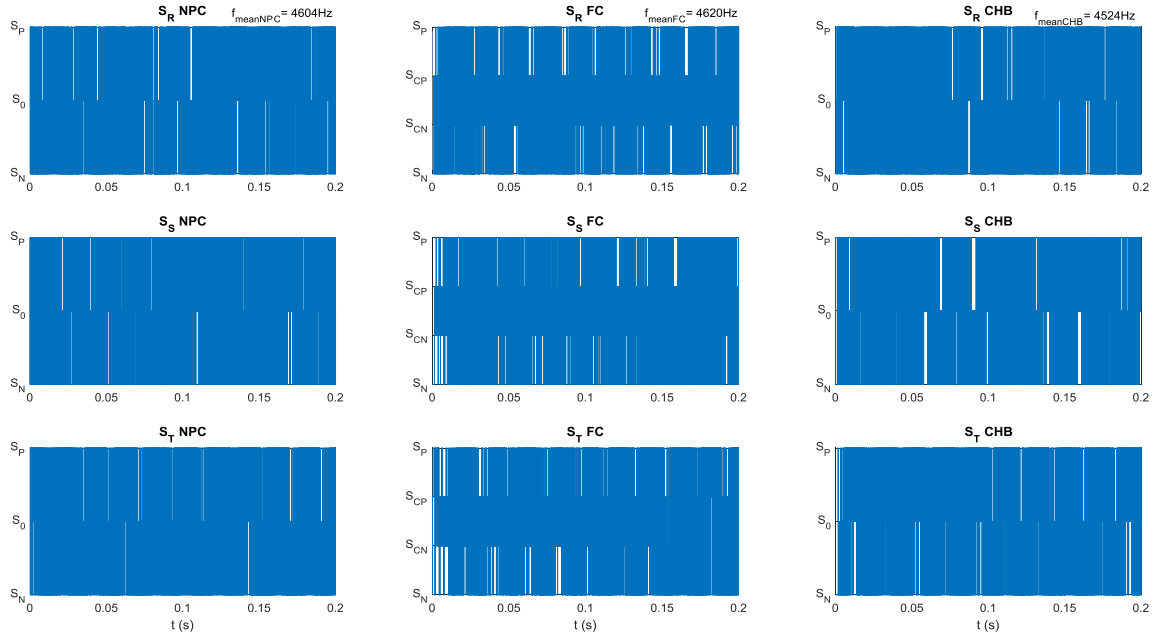

Fig. 5.7. Switching orders: NPC, FC and CHB

The set of results displayed in Figs. 5.5 to 5.7 confirms the adaptability of the converter to deal with unbalance loads. The THDs presented in Fig. 5.6 demonstrate the potential of the controller, as they are comparable to the ones obtained in the balanced case in Fig. 5.2. Obtaining these results did not require any modification of the MPC algorithms or of the modulation laws: the adaptation was completed by modifying the set-points, the references and the cost function. The exact same state-space model is used for both the balanced and unbalanced case-studies. It is crucial to note that the state variables define the realm of possibilities of the controller. If the objective is to control a variable seen as an uncontrolled input by the model, an adaptation will be necessary. This difficulty remains for all filters and models, but it is transferred to different variables. For example, for the LCL and L filters and their corresponding models, the grid

voltages are uncontrolled inputs and necessitate arrangement, but for the LC filter, the difficulty comes from the control of the grid currents instead, without any difficulties concerning the voltages, as they are state variables of the model for that particular case.

In order to further demonstrate the versatility of the developed controller, it is now asked to follow uncommon current references, with different phases, frequencies, biases and amplitudes for each phase. This example was not designed for a specific load profile, as it is meant to highlight the diversity of possibilities and to insist on the ability of the MPC controller to generate complex switching sequences for complex objectives. The properties of the signals inputted as references are summed up in Table 5.3, and the tracking performances are presented in Figs. 5.8 and 5.9. The parameters describing the signals in Table 5.3 are based on:

$$i_j^* = A_j \sin\left(2\pi f_j t + \phi_j\right) + B_j\,,\ \ j = R,S,T. \tag{3}$$

TABLE 5.3
REFERENCE CHARACTERISTICS FOR FIG. 5.8

Parameter	Value		Unit
	$0 \le t < 0.2$	$0.2 \le t \le 0.4$	
A_R	30	15	A
A_S	30	30	A
A_T	30	15	A
f_R	50	50	Hz
f_S	50	50	Hz
f_T	20	75	Hz
ϕ_R	0	0	rad
ϕ_S	0	0	rad
ϕ_T	$2\pi/3$	$2\pi/3$	rad
B_R	0	0	A
B_S	0	-5	A
B_T	0	0	A

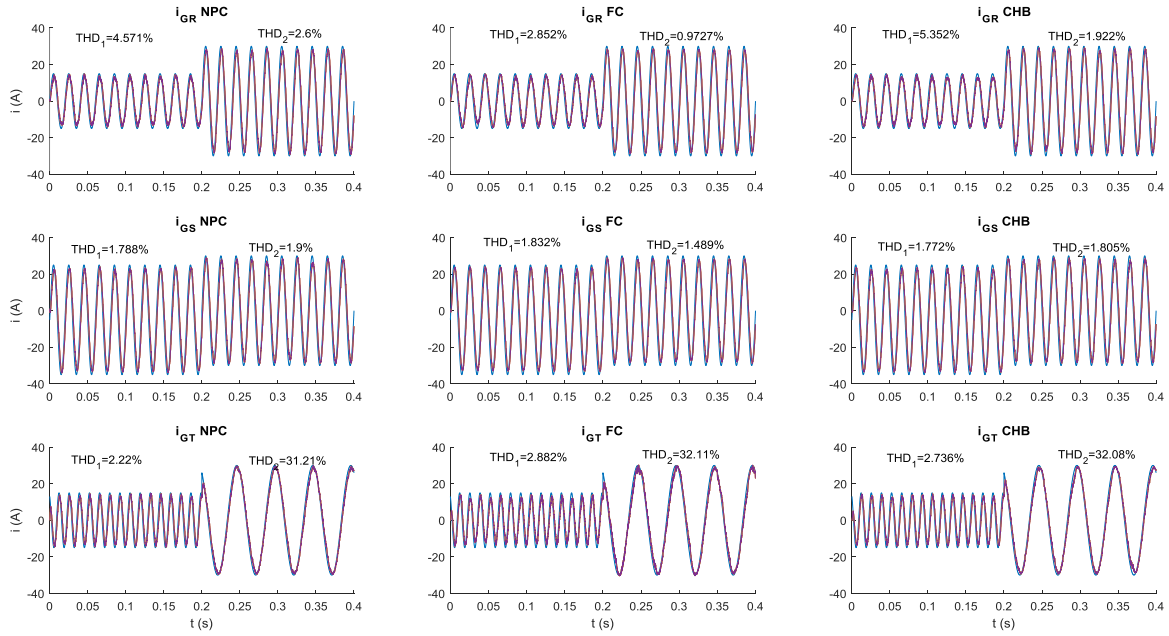

Fig. 5.8. Tracking performance with unusual reference profiles: NPC, FC and CHB, reference in blue

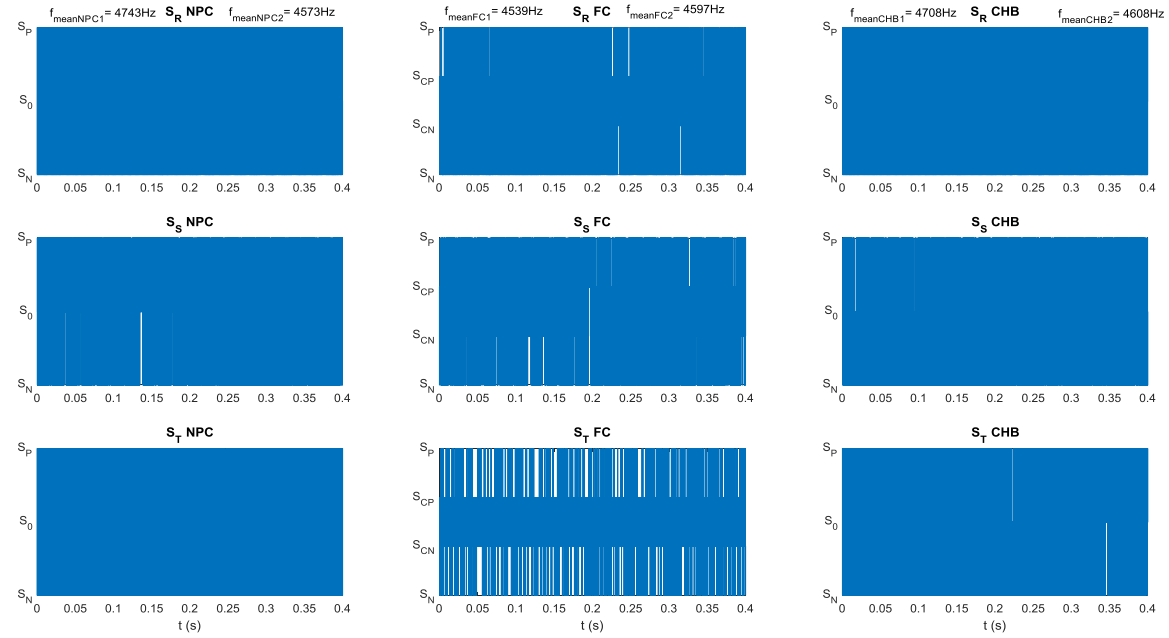

Fig. 5.9. Switching orders for each topology: NPC, FC and CHB

The results presented in Figs. 5.8 and.9 match with the theoretical conclusions: the MPC controller is able to generate complex switching patterns for different topologies, to comply with complex objectives. This specific situation highlights the advantage of the developed MPC controller in comparison to conventional control architectures relying on modulation, as the generated switching sequence is too unusual and specific for most common modulation strategies. The switching frequencies displayed in Fig. 5.9 show little no variations, with a mean frequency around 4.5kHz for each topology, half of the maximal predicted switching frequency. This value changes slightly to accommodate the change of reference but the difference

is minimal. The THDs presented within Fig. 5.8 are not exactly the same for each topology, but none of them stands out more than the others. This result further demonstrates the power of the MPC algorithm proposed, as it manages effortlessly these three very different topologies, with complex tracking objectives.

2.3.3. Sensitivity

In order to study the sensitivity of the controller, the situation investigated in Section 2.3.1 is reproduced with 20 values of α_{swich}. The values implemented are chosen to portray an evolution from a very high importance towards the tracking of the reference to higher priority given to the number of switching actions, and follow the law given in (4). Indubitably, the preference for one or the other sub-cost is only relative: it is not the value of α_{switch} that matters, but the ratio α_{switch}/α_i. Because the coefficient related to tracking the current references remains unchanged, the evolution of the ratio and the switching sub-cost's weight are equivalent.

$$\alpha_{switch}(i) = 10^{-2+\frac{i}{5}}, \quad i = 1 \dots 20 \tag{4}$$

The results are presented by means of Figs. from 5.10 to 5.12. First, Fig. 5.10 displays the superposition of the tracking performances for three different values of α_{switch}, one extremely in favor of the tracking objective, one overriding it for the benefit of switching economy goal, and another one in between. The current reference is a 50-Hz and 25-A sinusoidal wave.

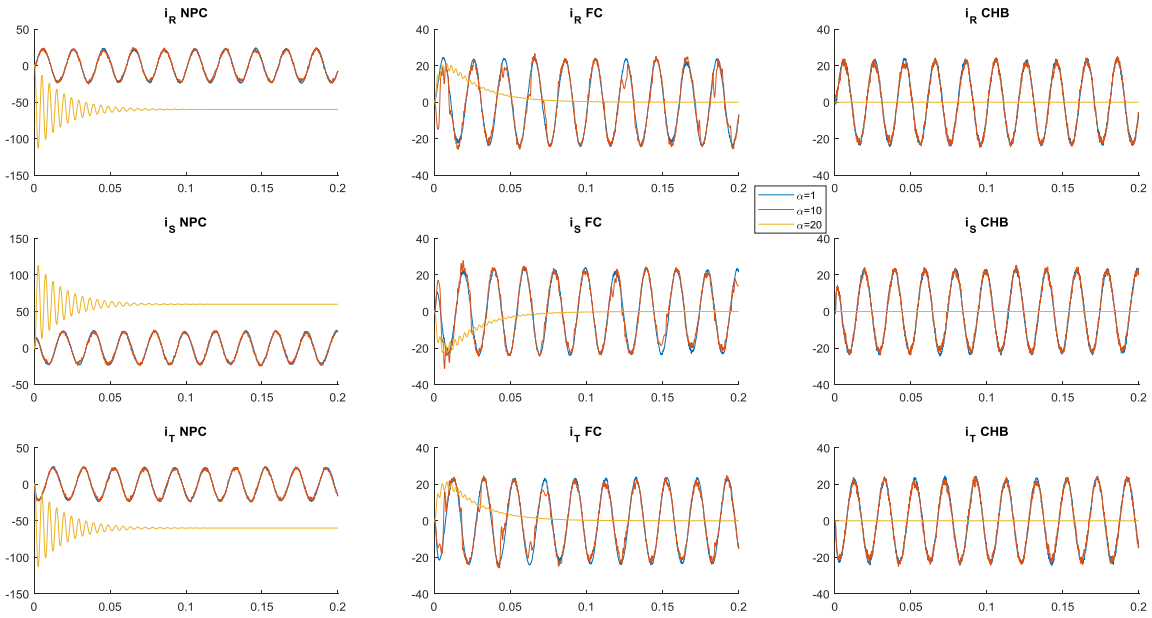

Fig. 5.10. Impact of α_{switch} on the current tracking performance: NPC, FC and CHB

This figure underscores the importance of properly balancing the different sub-costs, as it shows harmonic deterioration of the signal, caused by the will of the controller to minimize the number of

switching actions. An even more extreme value of α_{switch} leads to an absence of commutation. In this case, since many of the sub-systems are unstable, as described in Chapter IV, it is possible to render the system unstable. This is an extreme case and should not happen in the normal operation of the algorithm, but it once again highlights the necessity to properly design and weigh the cost function. It is interesting to notice that the deterioration rate is different for the topologies, as it is much more pronounced for the FC case than for the CHB one in the example provided in Fig. 5.10, with identical values of α_{switch}.

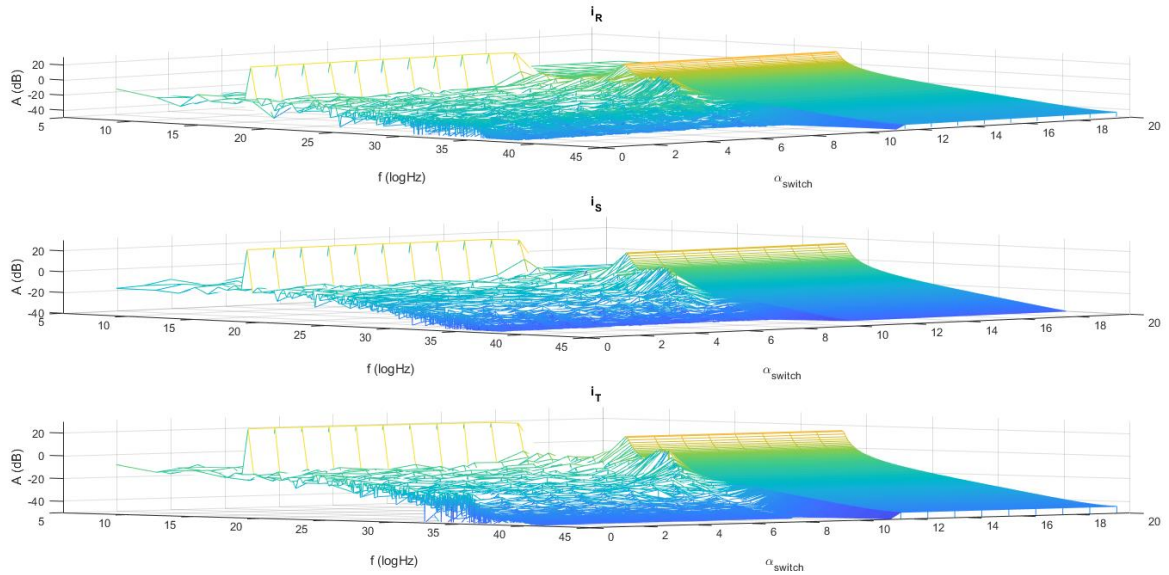

Fig. 5.11. Evolution of the harmonic content of the currents for NPC in function of α_{switch}

Fig. 5.11 shows the evolution of the harmonic content of the currents with the coefficients' ratio, via Fourier transforms. It brings to light the appearance of new harmonics when diminishing the importance of the tracking objective. To counterbalance this figure, it is important to actually perceive the other consequence from this sub-cost balance. To that end, the number of switching actions is presented in Fig. 5.12. As expected, this number falls when α_{switch} increases. The evolution is divided in three parts. First, the case studied here shows a decrease of the number of switching actions, with irregularities demonstrating that the influence of this coefficient alone is not necessarily obvious. After a while, the line collapses rapidly to 0 switching actions, remaining at $N_{switch} = 0$ for all higher values of α_{switch}. It is interesting to see that the three topologies have a very similar qualitative and quantitative behaviour. Considering the switching losses proportional to the number of switching actions, this figure shows the ability of the controller to reduce these losses, therefore increasing the overall efficiency. This is particularly interesting when watching the deterioration of the harmonic quality of the signal, as, for certain values of the weight, the signal is still following very closely its references with lower energy losses. However, the tuning of this ratio is difficult, as the graph shows a less linear behaviour than expected.

Fig. 5.12 displays the evolution of the number of switching actions performed in function of the weight attributed to Γ_{switch}. The three topologies show the exact same trend, an expected fall leading to no switching actions at all after a certain value for α_{switch}. This value can change for different topologies, and the collapse does not happen at the same speed either. For example, the FC topology falls slightly faster

than for the other topologies, while the CHB topology reaches the zero actions point later than the other two.

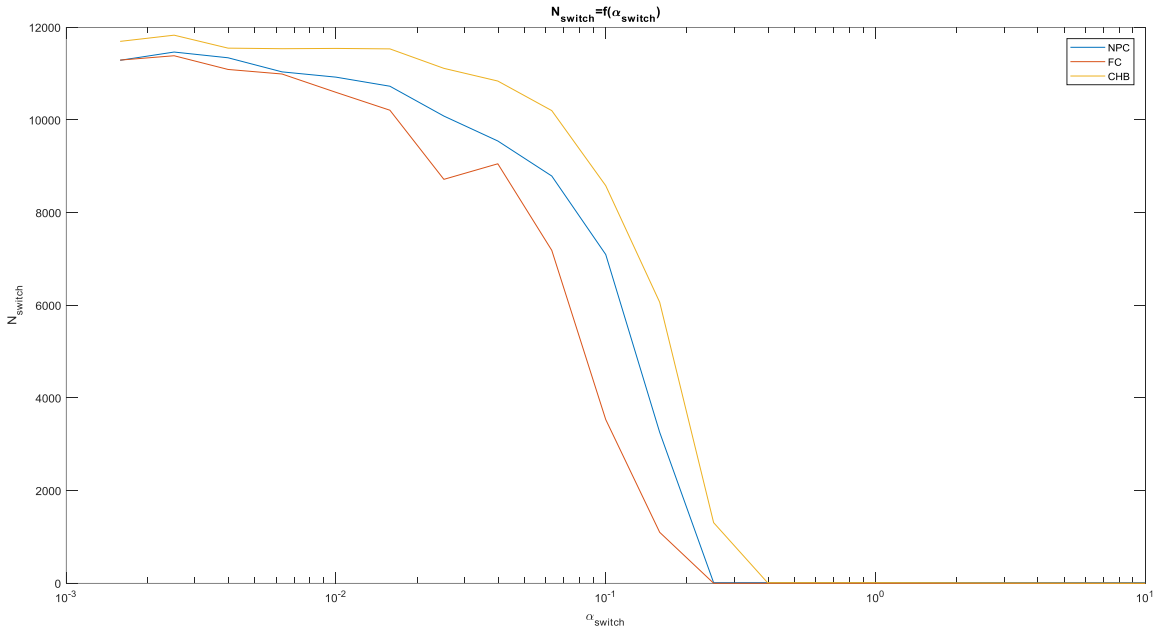

Fig. 5.12. Number of switching actions in function of α_{switch}

This sensitivity study was performed for only two competing sub-costs. The conclusions are simple to draw for such a low number of competing objectives, but become much more complicated to generalize for high numbers. The competition between the different objectives is not necessarily uncoupled: the ratio between two sub-costs may impact a third one. Consequently, the heuristics method is often the only operating method.

2.4. Discussion

This second section illustrates the efficacy of the developed controller when dealing with state references. It has been proved that the controller is able to generate the switching sequences for a large variety of such references, with unrelated objectives for each phase. Its ability to follow complex references and to compose a different input sequence when asked to minimize the energy losses has also been shown, adding more depth to its capabilities. However, this section highlighted a few limitations as well. Mainly, not all phenomena are treated equally by the controller, for various reasons. The most common one is the absence of knowledge: MPC, as a control methodology, is very powerful, but relies heavily on its ability to model and thus predict the behaviour of the controlled system. De facto, when the objectives concern unmodeled aspects of a larger system comprising the modelled one, as is the case with the AC voltage in the example tackled here, the algorithm must be fed with the missing information and rely on external resources. The case studied earlier shows that there are several ways to inject knowledge into the MPC controller without modifying its inner operation and models. One approach consists in procuring

"intelligent" references on the states, determined by an external element, while the other approach prefers including the expression of the objective directly into the cost function.

The difference between the two approaches is thin, yet critical. The second point of view simplifies the control structure, but increases the tasks of the MPC. The first option does the opposite: by relocating part of the intelligence outside of the controller, it makes the control architecture more complex, but can enhance the overall intelligence of the control. This leads to a second limitation: the time scale and prediction depth of the controller. With the algorithms developed and the physical computational limitations, it is unrealistic to even consider a millisecond of depth of vision for the controller. Many phenomena happening in grid systems have much larger time scales than this, starting from the frequency analysis. Consequently, it is difficult for the controller to identify the frequency of any variable, if not impossible. It becomes then useless to propose frequency-based objectives. Similarly, determining the amplitude of an alternative signal is impossible for the controller as is, and has to be either given up upon or delegated to an external identifier.

This prediction depth limitation is, as that regarding external variables, solved by adding another block to the control architecture, whose time scale is much larger than the MPC one. Such a module generates appropriate references to fulfil the objectives the MPC controller is unable to master, similar to what was done here when feeding the algorithms with already sinusoidal signals as references, with the right frequency, phase and amplitude. Another looming limitation of the controller is the balance of the weights, seeing how strongly they impact the general behaviour and performance of the controlled system. Once again, it is possible to propose an external unit managing this equilibrium. This can become indispensable when considering important modifications of the environment, such as grid connection/disconnection, load modification, or swap of inverter mode to rectifier or bidirectional mode.

3. Grid-connected inverter case study

3.1. Grid-connected operation

This next study sees the addition of the grid to the previous context of work, as presented in Fig. 5.13. The grid is considered infinite, without line impedance. It thus imposes the phase voltages, with a 230-V and 50-Hz sinusoid. The filter implemented is of *L* type. The different parameters, also from [1], are gathered in Table 5.4. In this situation, various objectives can be encountered. It is common to find requirements related to ancillary services, such as harmonics filtering, voltage and frequency quality. Handling of potential faults from the grids, such as unbalance or momentaneous disruption of the service, can be added. Some of these aims are directly linked to the active and reactive powers transmitted from the DC sources to the grid through the power converter. Therefore, power regulation becomes primordial when considering grid-connected case studies. Apart from the power related objectives, the grid synchronization is another critical aspect of the control of grid connected power converters. Several kinds of aims are found: ones related to the powers exchanged and others involving the voltages and currents alone.

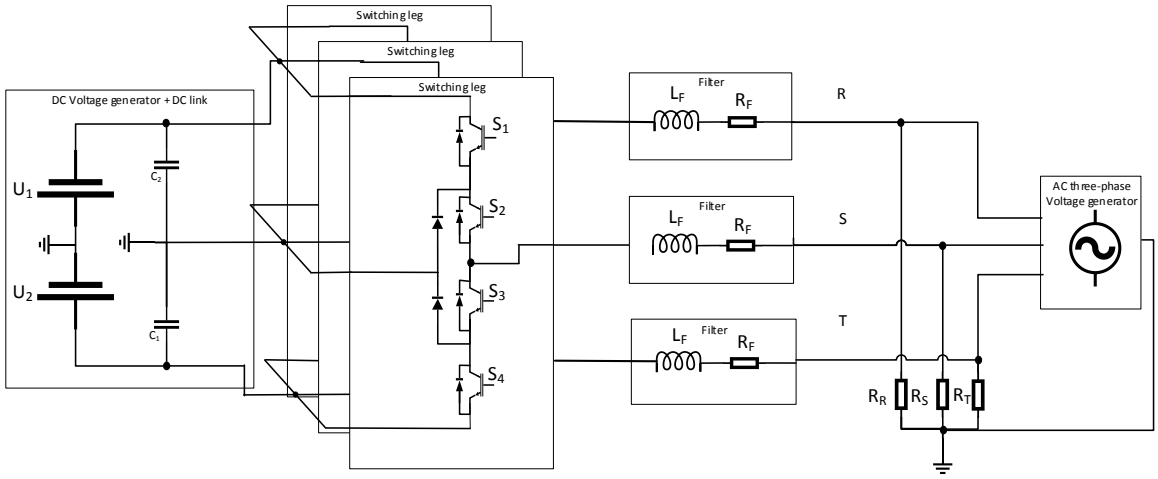

Fig. 5.13. Grid-connected inverter, example with 3L-NPC

TABLE 5.4
PARAMETERS USED IN THE CASE STUDY REPRESENTED BY FIG. 5.13

Parameter	Value	Unit
R_{Fj}	10	mΩ
L_{Fj}	1.2	mH
$C_1 = C_2 = C_3$	3.3	mF
C_j	3.3	mF
f_{grid}	50	Hz

In order to handle all these different objectives and requirements, two approaches can be applied. The first one, unrealistic, directly states all of them and includes them into the cost function. As discussed in Section 2, many objectives are impossible to incorporate into the cost function, especially the ones requiring long time spans to observe and/or influence. For example, all energy related objectives are too slow for this controller to perceive, let alone control. Similarly, it is difficult for a controller with such a short control horizon to tackle system identifications, making it impossible to include any consideration related to the grid model and parameters.

The model used in this MPC algorithm is entirely focused on the power converter itself and has no understanding of what it is connected to: all AC loads/sources are perceived as uncontrolled inputs, whatever may their profile be. Similarly, a DC voltage source is seen the same way as a resistive load, or a complex one, or a storage element… This means that modifications of the environment of the controlled system do not necessarily have consequences on the operation and structure of the controller. This can be advantageous, as the controller is then supposed to behave the same way with all possibilities (under conditions of feasibility), but it also limits specific adaptation to these possibilities, for which the control can be very different depending on the case. The MPC algorithm developed in these works does not model the behaviour of the grid or of the different components the converter is connected to. This is meant to enable operation under any disposition, but it also reduces the specialization of the controlled system.

Another approach consists in delegating part of the intelligence to a different layer of control, more adapted. Depending on the quantity of intelligence diverted, the type of references set to the controller is bound to change. Typically, two kinds are dominant: active and reactive power references, or current and voltage references. That last one essentially brings the cost function back to the one used in Section V.2. For the first case, it is necessary to adapt the cost function.

3.2. Translation into the cost function

The multiple objectives related to grid integration can be translated into either power or current references. The philosophical difference between these two possibilities resides in the location and type of intelligence of the control architecture. The second approach receives current or voltage objectives computed beforehand, considering various elements, such as the uncontrolled inputs or other measures. In this case, most of the knowledge and intelligence is situated in an external controller, which provides the reference values to the MPC controller. In the other case, a different controller is still needed, to consider energy-related problems for example, but an important part of the computations, the intelligence and the responsibilities are transmitted to the developed controller.

Considering the situation where the references are currents, or any states of the prediction models, the situation is equivalent to the one discussed and studied in Section 2 of this chapter. However, the power references infer adaptation of the cost function. Computation of both the active and reactive powers is required, and, even though it can be performed in several ways, only those which are instantaneous can be used by the MPC controller. For this reason, either the stationary *a-β* or the synchronous *d-q* reference frames could be used to compute the power. However, given that transformation to the *d-q* reference frame requires information on the angle of the grid voltage vector, the *a-β* representation has been selected. Because this decision is entirely based on the power expression, the matrix used to translate the instantaneous three-phase variables to the *a-β* reference frame is the Concordia matrix, given in (5). The expression of this translation is also presented in (6), with x representing either the currents or the voltages.

$$T_c = \sqrt{\frac{2}{3}} \begin{bmatrix} 1 & -1/2 & -1/2 \\ 0 & \sqrt{3}/2 & -\sqrt{3}/2 \\ 1/\sqrt{2} & 1/\sqrt{2} & 1/\sqrt{2} \end{bmatrix} \tag{5}$$

$$\begin{bmatrix} x_\alpha \\ x_\beta \\ x_0 \end{bmatrix} = T_c \begin{bmatrix} x_R \\ x_S \\ x_T \end{bmatrix} \tag{6}$$

The active and reactive powers exchanged with the grid are then expressed as follows:

$$P = u_\alpha i_\alpha + u_\beta i_\beta \tag{7}$$

$$Q = u_\alpha i_\beta - u_\beta i_\alpha. \tag{8}$$

With this formulation, both the current and predicted powers can be included in the cost function with two sub-costs such as in (9) and (10). The final cost function is given in (11).

$$\Gamma_P = \|P^* - P\| \tag{9}$$

$$\Gamma_Q = \|Q^* - Q\| \tag{10}$$

$$\Gamma = \alpha_P \Gamma_P + \alpha_Q \Gamma_Q + \alpha_{switch} \Gamma_{switch} \tag{11}$$

The cost function (11) leads to satisfying results concerning the three objectives, but does not include any information or restriction concerning grid synchronization. In consequence, the controller is not constrained to generate sinusoidal or balanced currents. An illustration of the aftereffects is shown in Figs. 5.14 and 5.15, portraying respectively the tracking performance for the active and reactive powers, and the currents profile obtained. These results were produced with $\alpha_P = \alpha_Q = 1$ and $\alpha_{switch} = 0.01$ The behaviour is not the same for the three topologies considered, but the NPC and FC cases clearly evidence a shortcoming: the resulting currents are not sinusoidal and, what is worse, they are not stable, which is absolutely inacceptable.

In such context, it is possible to add sub-costs such as (12) and (13) to include the angle estimation and angle synchronization to the cost function (14), as well as the balance of the currents. Both aspects were not acknowledged by the controller yet, as they did not appear anywhere in the previous cost function.

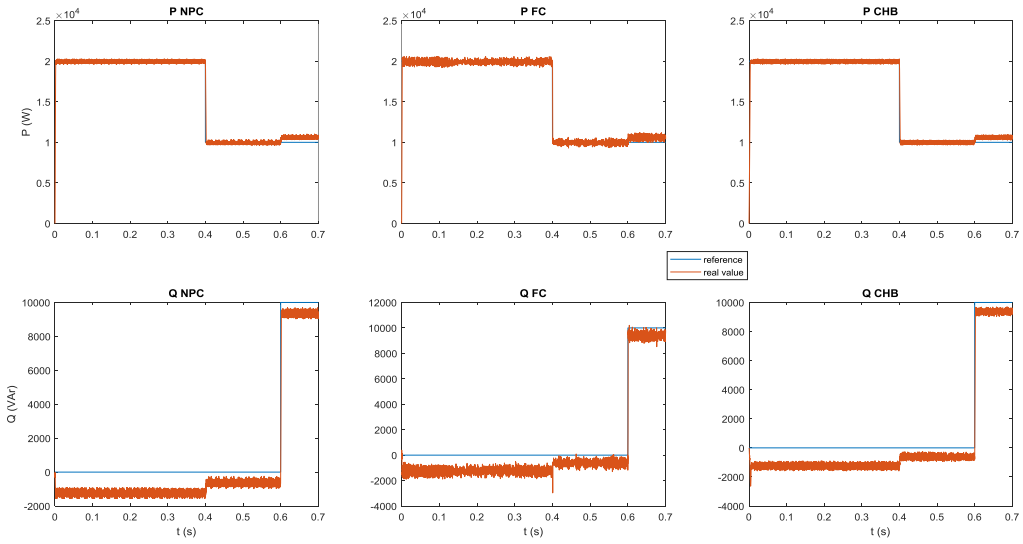

Fig. 5.14 Power tracking obtained with cost function (11)

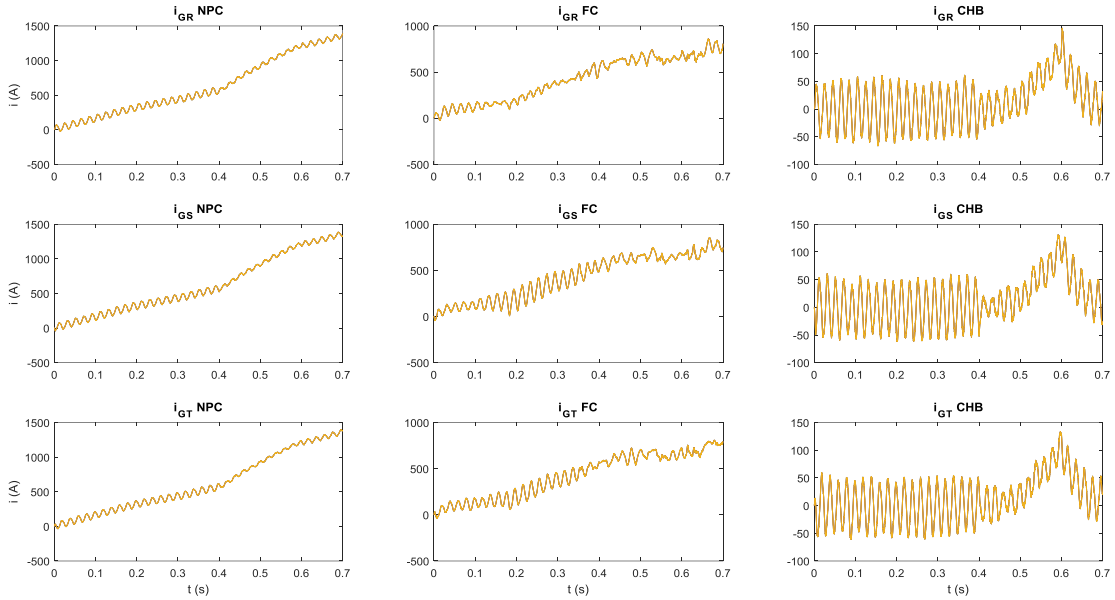

Fig. 5.15 Currents produced when using cost function (11)

$$\Gamma_{balance} = \|i_R + i_S + i_T\| \tag{12}$$

$$\Gamma_\theta = \left\| \arctan\left(\frac{U_S - U_T}{\sqrt{3}U_R}\right) - \arctan\left(\frac{i_S - i_T}{\sqrt{3}i_R}\right) \right\| \tag{13}$$

$$\Gamma = \alpha_P \Gamma_P + \alpha_Q \Gamma_Q + \alpha_{bal} \Gamma_{balance} + \alpha_\theta \Gamma_\theta + \alpha_{switch} \Gamma_{switch} \tag{14}$$

Equation (13) is based on Phase-Locked Loop (PLL) considerations, and its objective is to synchronize the angle of the currents with that of the grid voltages. This expression is not correct unless the system is balanced, which justifies the need for the sub-cost provided in (12). The sub-cost from (13) leads to an absolute synchronization of the voltage and the current, which is generally not the objective, except if $Q = 0$ is sought. For this reason, its coefficient in (14) must be selected carefully: strong enough to enforce a sinusoidal waveform to the currents, yet sufficiently small not to hinder the power-related costs, more important control-wise.

3.3. Results

The first results displayed in Fig. 5.16 are obtained by feeding the MPC controller with externally computed current references to fit the desired active and reactive powers. The currents and their respective references are illustrated in Fig. 5.17. Similar to the previous results, the current tracking shows very slight error. A close-up is presented in Fig. 5.18 to corroborate this statement. Consequently, the powers are well controlled.

Two parameters have a major effect on the variance of the powers: the inductance used in the filter on the one hand, and the α_{switch} ratio on the other. For Fig. 5.16 to Fig. 5.18, the cost function is (5.1), with $\alpha_{switch} = 0.01$. This value is meant to prioritize the quality of tracking of the current over the number of switching actions, and its influence over the power and its variance can be complex: both over switching and under switching have consequences on the powers. For example, an overly chopped signal can lead to oscillations on the active and reactive powers, while the opposite situation will lead to poor tracking performance. The balance between these two poles has to be performed carefully.

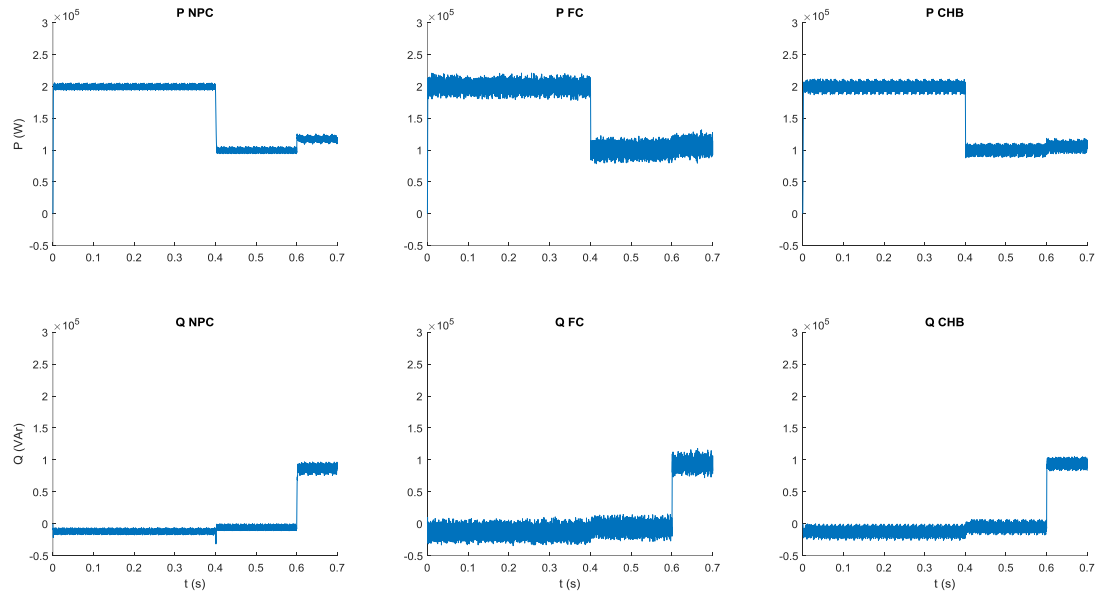

Fig. 5.16. Active and reactive powers obtained with precomputed current references

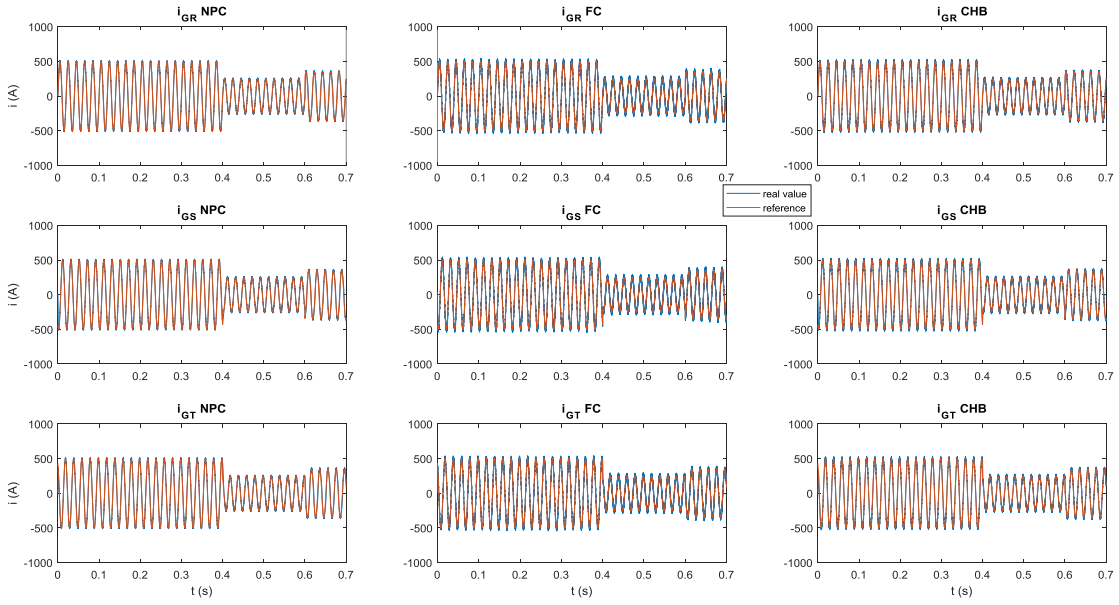

Fig. 5.17. Current references and tracking performance for power control

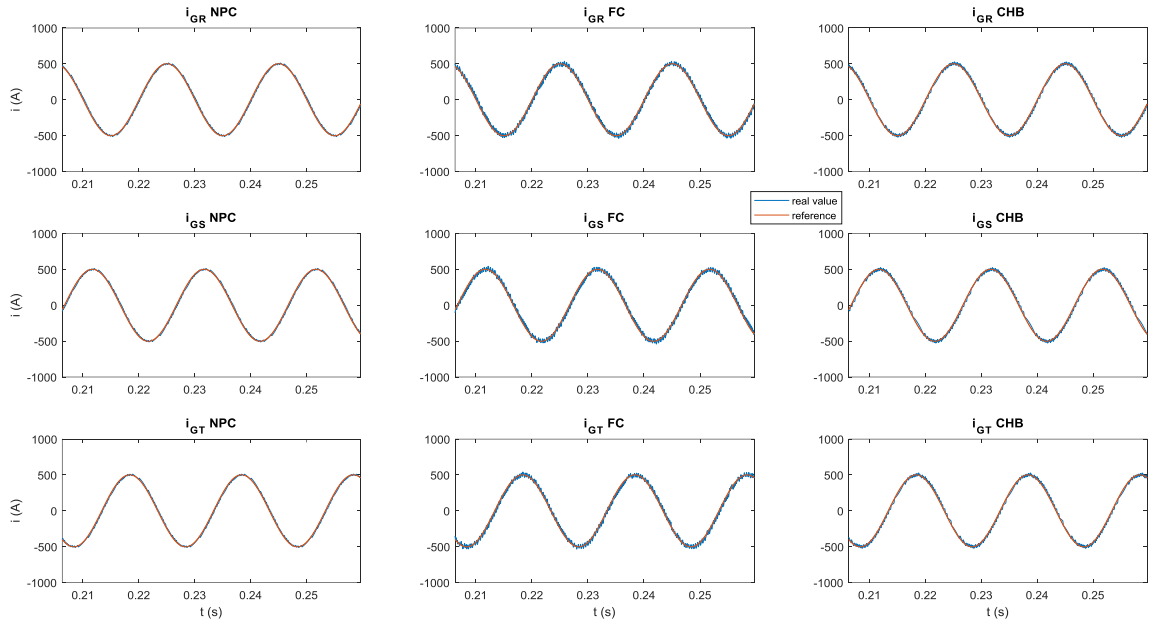

Fig. 5.18. Close-up of the current waveforms

The results obtained with the cost function described in (14) are compiled in Fig. 5.19 and Fig. 5.20, for $\alpha_P = 1$, $\alpha_Q = 1$, $\alpha_{switch} = 0.01$, $\alpha_{bal} = 10$ and $\alpha_\theta = 10$. They match the ones obtained with the previous method, with slightly improved performances for the FC topology, as the chatter is slightly less important. This is related to the current profiles, which vastly differ, in spite of the cost function. They can also be compared to the ones presented in

Fig. 5.15, in which the currents were not considered in the optimization process. Different current profiles can therefore lead to the same powers when applying the expressions in (7) and (8), which emphasizes the need to include other terms to the cost function for grid synchronization, where these profiles are paramount. Another distinctive feature in these last figures is the coupling between the active and reactive powers, the value of one affecting the other.

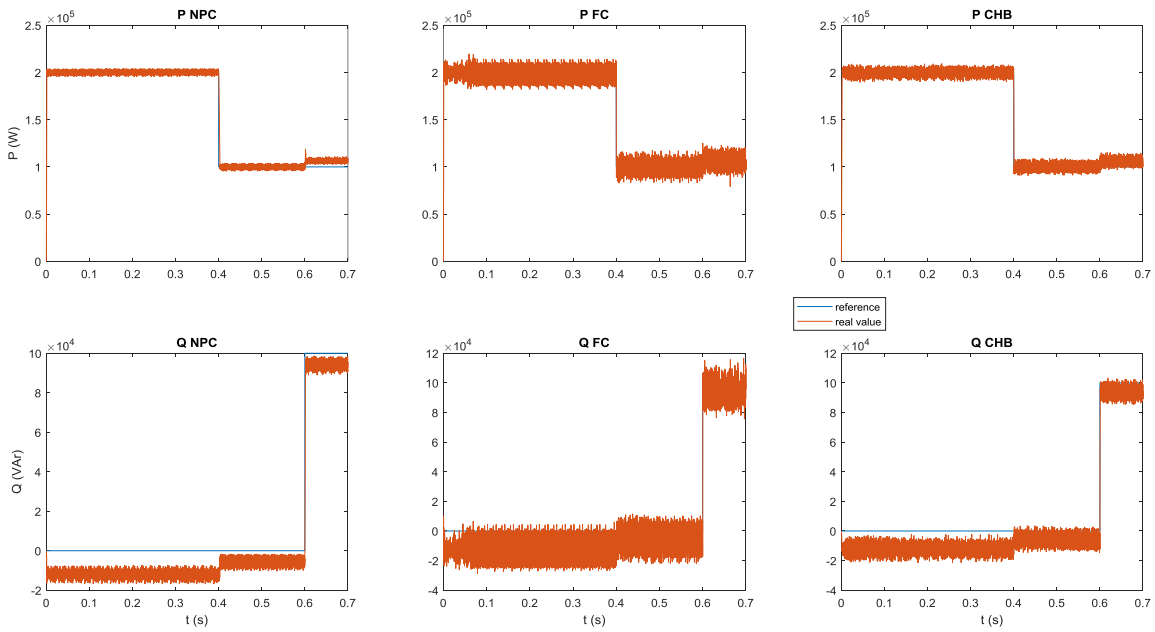

Fig. 5.19. Power tracking with cost function (14): NPC, FC and CHB

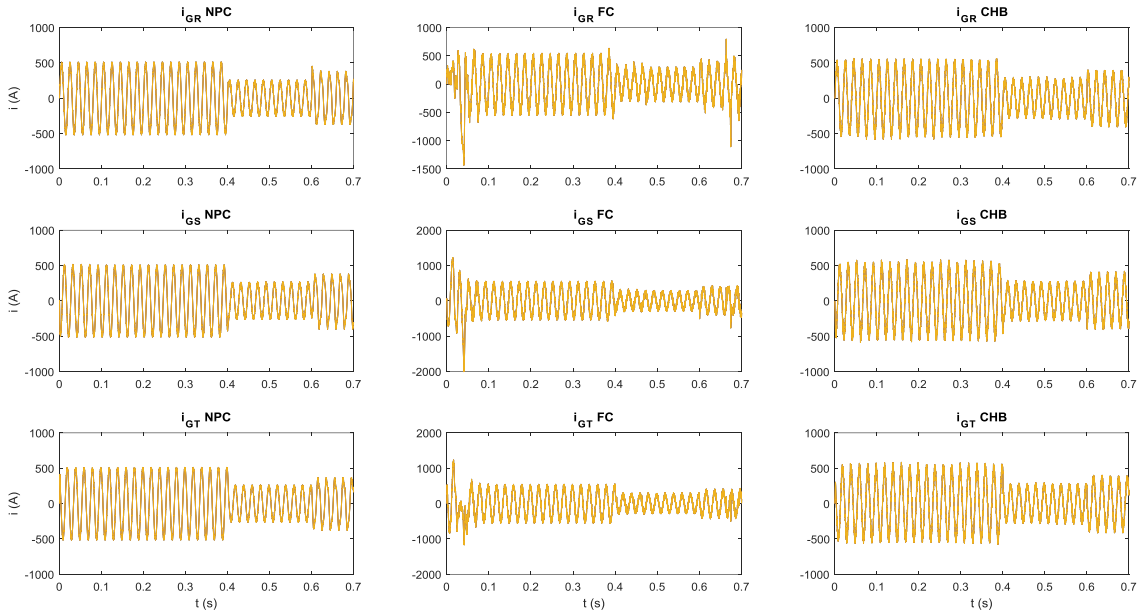

Fig. 5.20. Current profiles with cost function (14): NPC, FC and CHB

This coupling effect is not exactly related to the cross-coupling voltage terms depending on ωL, as the resulting coupling values do not coincide with those due to such terms. Furthermore, different values of the grid filter inductance deeply changed the levels of chatter un active and reactive power, but did not affect this coupling factor in any way. This issue appears to be related to the inner operation of the MPC controller developed, and needs further consideration. In any case, a corrective coefficient is applied to compensate for the noticed coupling effect, according to (15) and (16).

$$P = u_\alpha i_\alpha + u_\beta i_\beta + 0.06\left(u_\alpha i_\beta - u_\beta i_\alpha\right) \tag{15}$$

$$Q = u_\alpha i_\beta - u_\beta i_\alpha - 0.06\left(u_\alpha i_\alpha + u_\beta i_\beta\right) \tag{16}$$

The value of the coefficient is deduced from the measures and observations made previously. This value does not vary with either frequency or grid filter inductance modifications, highlighting a phenomenon deserving deeper investigation. However, the results obtained with this countermeasure are corrected, as illustrated in Fig. 5.21.

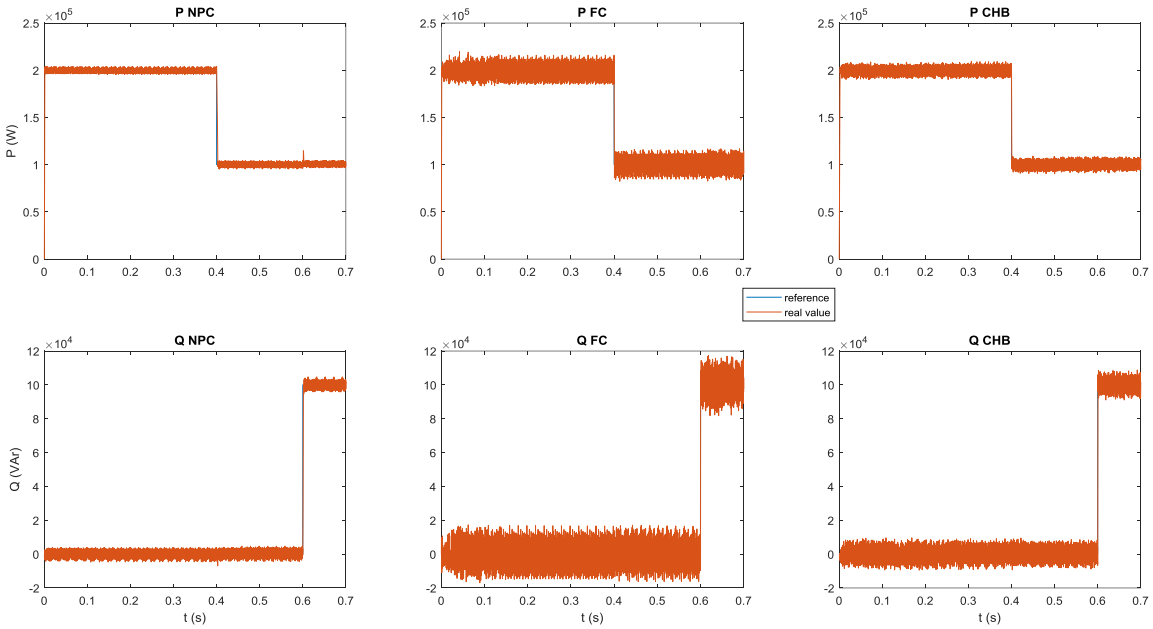

Fig. 5.21. Power tracking with coupling compensation from (15)-(16): NPC, FC, CHB

4. Rectifier mode operation

So far in this document, the converters have only been studied operating as inverters. This section focuses on the rectifier and four-quadrant operation of the converters with MPC control. The scheme of the context is presented in Fig. 5.22. In this situation, the AC side is once again considered to be infinite. The DC side, however, can be interpreted in different ways. The DC-link is considered as two pure loads for the NPC and FC topologies, three for the CHB one. These loads are theoretically separate and do not necessarily share their properties. This is precisely the case when considering that the converter manages two different storage devices. A critical example that combines storage systems with significantly different time constants, such as supercapacitors and batteries, is addressed.

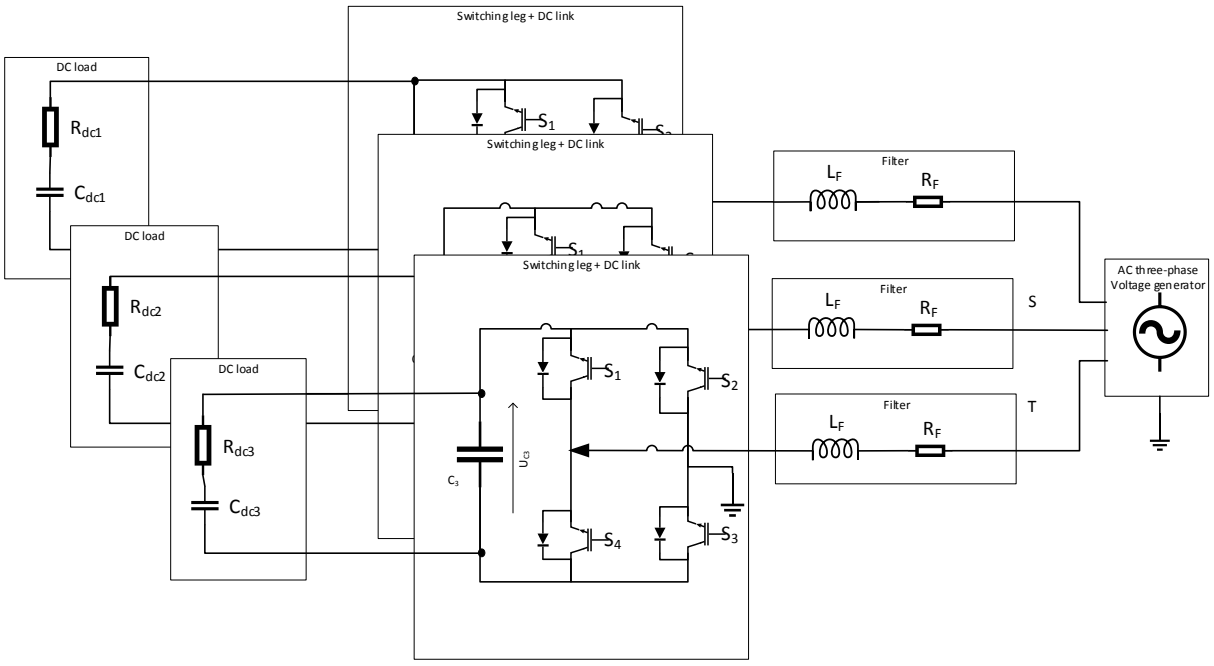

Fig. 5.22. Context of study, rectifier mode, example with 3L-CHB topology

From the MPC controller's point of view, the dynamic differences between the storage devices are unperceived, as they are not contemplated by its inner model. Furthermore, the dynamics of these elements are still very slow compared to the sampling time of the models used by the MPC controller, meaning they can be seen as constants from the latter's perspective. This hypothesis may prove false for specific applications such as supercapacitors, for example, and needs to be verified case by case. With these hypotheses, the rectifier control objectives concern the separate control of the DC-link and/or the DC power exchange for each DC element. In order to demonstrate the effectiveness of the MPC controller, two sub-costs are introduced, related to the sum of the voltages of the DC-link and to their difference; namely:

$$\Gamma_{\Sigma DC} = \|\Sigma^* - \sum_i U_{Ci}\| \tag{17}$$

$$\Gamma_{\Delta DC} = \|\Delta^* - (U_{C2} - U_{C1})\| \text{for NPC and FC; } \Gamma_{\Delta DCi} = \left\|\Delta_i^* - \left(U_{Ci} - U_{C(i-1)}\right)\right\| \text{ for CHB} \tag{18}$$

TABLE 5.5
PARAMETERS USED IN THE CASE STUDY REPRESENTED BY FIG. 5.22

Parameter	Topology	Value	Unit
R_{Fj}	all	10	μΩ
L_{Fj}	all	3	mH
$C_1 = C_2$	NPC, FC	3.3	mF
$C_1 = C_2 = C_3$	CHB	3.3	mF
C_j	FC	3.3	mF
f_{grid}	all	50	Hz
R_{dc1}	NPC; FC CHB	100 150	Ω
C_{dc1}	all	0	mF
R_{dc2}	all	50	Ω
C_{dc2}	all	50	μF
R_{dc3}	CHB	100	Ω
C_{dc3}	CHB	0	mF

While the results were so far similar for the studied topologies, they are fairly different when it comes to rectifier mode. The first distinction comes from the difference of the DC-links, as the CHB topology presents a very different one from the two others. As a result, the cost function is not exactly the same for the three topologies. An additional term is used for CHB to include all the differences between voltages. Another result is the need to adjust the weight factors. So far, the weighting had been the same for the different converters, but experience shows that it is not the case here.

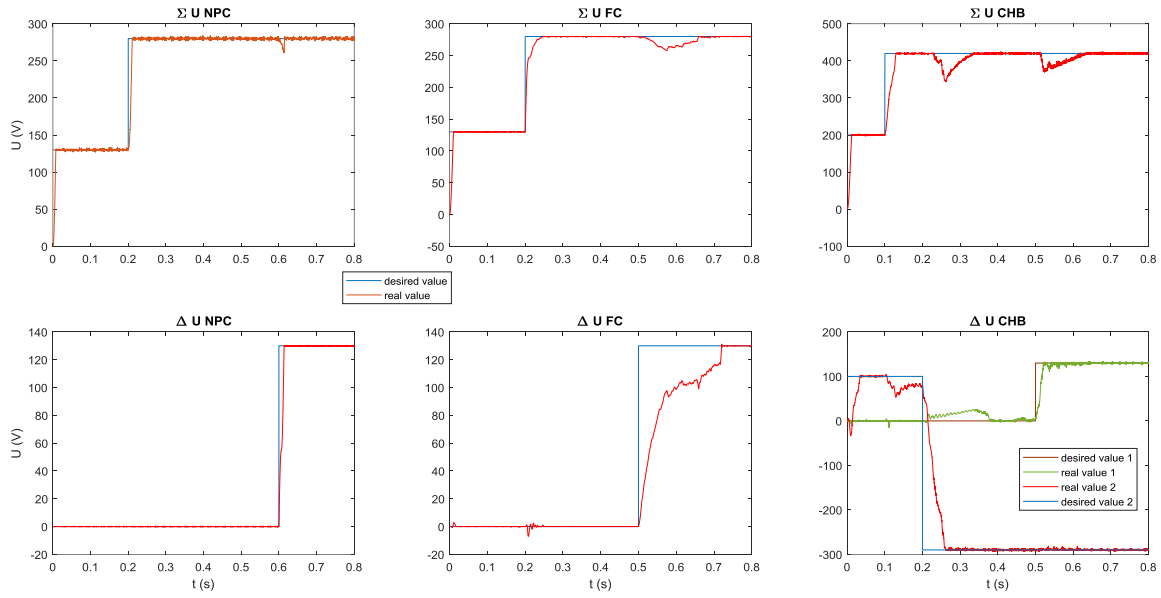

Fig. 5.23. Tracking results in rectifier mode for NPC, FC and CHB

Fig. 5.23 shows that the control of the different DC elements, related to the topology and the number of levels, can be performed independently. The cost function adopted has to change accordingly, with different sub-costs and different weights. The results shown in Fig. 5.23 have been obtained with the

three cost functions described in (19), (20) and (21) respectively for the NPC, FC and CHB topologies. First experimental results revealed a phenomenon similar to the previous issue with the power: in the case of the NPC topology, simply including a cost on the primary objectives led to highly disturbed current profiles. in order to address this issue, the same solution was used, with the addition of subcosts (12) and (13). No evidence of this issue was found for the other two topologies and as such no such modification was performed, resulting in (20) and (21). The cost function used for the CHB topology contains two subcosts related to the difference between the DC voltages in order to align with the three DC voltages.

$$\Gamma_{NPC} = 2000\Gamma_{\Delta DC} + 5\Gamma_{\Sigma DC} + 100\Gamma_{balance} + 50\Gamma_{\theta} \quad (19)$$

$$\Gamma_{FC} = \Gamma_{\Delta DC} + \Gamma_{\Sigma DC} \quad (20)$$

$$\Gamma_{CHB} = \Gamma_{\Sigma DC} + \Gamma_{\Delta DC_2} + \Gamma_{\Delta DC_3} \quad (21)$$

The dynamics portrayed in the results are fast compared to other modulation-based methods, especially for the NPC topology, which shows only 10 ms between the change of reference and its tracking. This is made possible by the switching decisions made by the controller, exploiting the redundancy and the depth of modulation.

5. Grid forming application

This next case-study aims to further challenge the controller developed with a more complex and realistic situation. A multi-level converter is used as a voltage generator feeding an isolated grid containing two 2-MW resistive loads, a 15-kVAr inductive load and a 25-kVAr capacitive load. The converter is connected to the grid via a LC filter, and controlled by the MPC algorithm developed. Concerning the DC side of the converter, it is modeled as current sources in series with resistors. The configuration is depicted in Fig. 5.24. The parameters, gathered in Table 5.6, are extracted from similar cases depicted in Simulink's demonstrative case studies, namely "250-kW Grid-Connected PV Array" and "Power SVPWM 3-Level".

TABLE 5.6
PARAMETERS USED IN THE CASE STUDY REPRESENTED BY FIG. 5.24

Parameter	Value	Unit
R_{Fj}	5	mΩ
L_{Fj}	500	µH
C_{Fj}	50	µF
C_j	3.3	mF
f_{grid}	50	Hz
C_{dc1}	50	µF
C_{dc2}	50	µF

In order to challenge the controller and the controlled system, several events are scheduled. One of the resistive loads is always connected to the AC bus. However, at the very beginning, the DC side voltage is not initialized at a value permitting the power exchange between the DC and AC sides. During this period, the converter brings the voltages of the DC-link's capacitors to the adequate value, while managing as well

as possible to generate a sinusoidal waveform. Next, the different loads are added one at a time, then disconnected from the AC bus. The results discussed next are all obtained with the NPC topology, but can be extended to the two other topologies, CHB and FC, also investigated in the previous case studies.

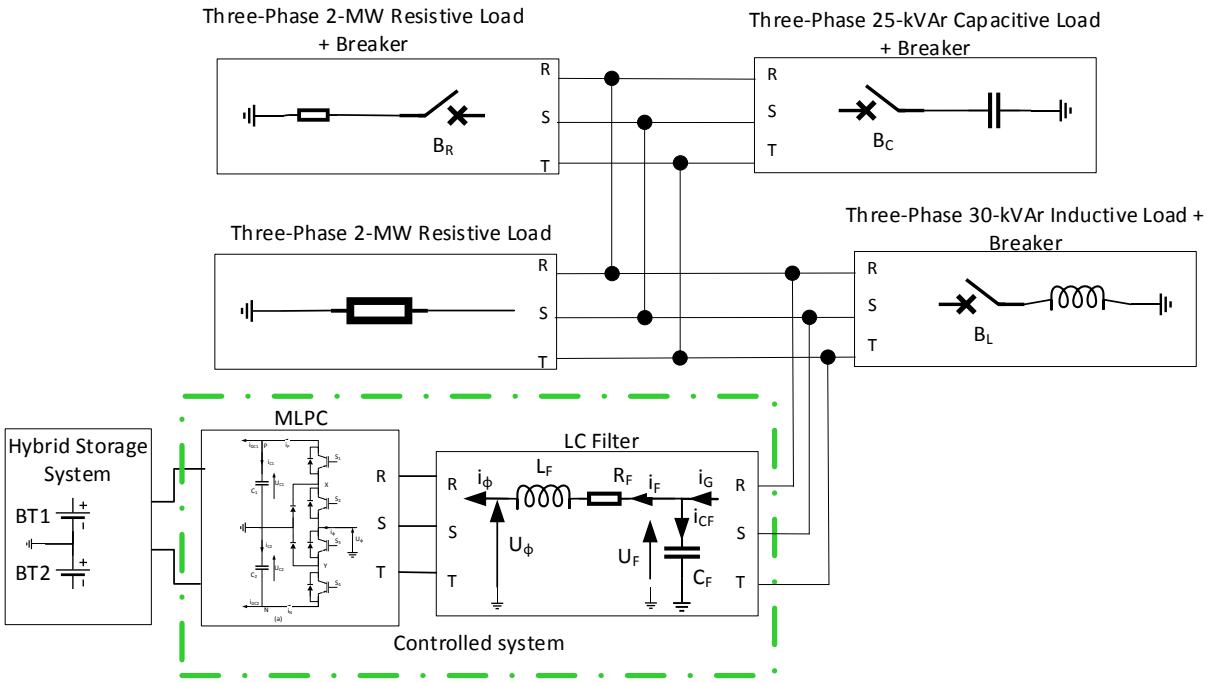

Fig. 5.24. Final case-study: isolated-grid application

This generates eight time periods, each separated by 0.2 s, where the different combinations of the loads are made, as summarized in Table 5.7. In this table, $B_X = 1$ means that the breaker of element X, which can be the resistive one R, the capacitive one C or the inductive one L, is closed. A value of 0 for the same parameter means it is open. All the possibilities are considered, leading to a large variety of events. The objective of the controller concerning the AC side is to generate a 1.5-kV (rms) balanced three-phase sinusoid at the Point of Common Coupling. This objective translates as the following sub-cost, which can be linked to the ones discussed in the first part of this chapter:

$$\Gamma_{AC} = \|\boldsymbol{U}_F^* - \boldsymbol{U}_F\|, \tag{22}$$

where $\boldsymbol{U}_F^* = [U_{FR}^* \quad U_{FS}^* \quad U_{FT}^*]^T$ and $\boldsymbol{U}_F = [U_{FR} \quad U_{FS} \quad U_{FT}]^T$. In addition, the quadratic norm is adopted for the calculation of the sub-cost in (22). The desired characteristics of the AC voltage are directly included into the references.

TABLE 5.7
EVENTS AND CONNECTION TABLE

t (s)	0.2	0.3	0.4	0.6	0.8	0.9	1	1.2	1.3	
B_R	0	1	1	1	1	0	0	0	0	0
B_C	0	0	0	1	1	1	1	0	0	1
B_L	0	0	0	0	1	1	1	1	0	0
P^*(MW)	2	4	4	4	4	2	2	2	2	2
β	0.5	0.5	0.515	0.515	0.515	0.515	0.475	0.475	0.475	0.5

When it comes to the DC side, the objective is bipartite: the first part is related to the total power extracted from the different DC sources, and the second expresses the desired repartition between these sources. Contrarily to the case studied in Section 4 of this chapter, the cost function has been unified as shown in (23), where the total power P^* and the coefficient β are references received directly from the exterior of the converter.

$$\Gamma_{DC} = \|P^* - (1-\beta)U_{C2}i_{DC2} - \beta U_{C1}i_{DC1}\| \tag{23}$$

The different inputs and references provided to the cost function of the MPC controller are summarized in Fig. 5.25. The form of the sub-cost (23) is only one of the ways to implement such a control requirement, as it also may translate as two separate objectives related to the different sources. This illustrates the possibility to create a hierarchy of sub-costs, with base sub-costs that cannot be reduced, intermediary sub-costs similar to (23) that congregate several elementary sub-costs and, finally, the cost function itself. The interest of this classification is to ease the balancing of the coefficients, as it can prove difficult whenever the number of requirements translates in more than three sub-costs. These intermediate sub-costs must make sense: here, the AC objectives and the DC objectives are gathered together, but a random grouping could lead to an over complexification of the cost balancing.

The final cost function used to obtain all the following results is of the form

$$\Gamma = \alpha_{AC}\Gamma_{AC} + \alpha_{DC}\Gamma_{DC} + \alpha_{switch}\Gamma_{switch}, \tag{24}$$

with $\alpha_{AC} = 1$, $\alpha_{DC} = 18$ and $\alpha_{switch} = 0.001$. At a first glance, this coefficient's arrangement greatly favours the AC side objectives. Nonetheless, the impact of one cost over the other is not necessarily simple, and having equal coefficients on two costs doesn't mean that those sub-costs have the same impact on the total cost, as the cost functions discussed here are not normalized.

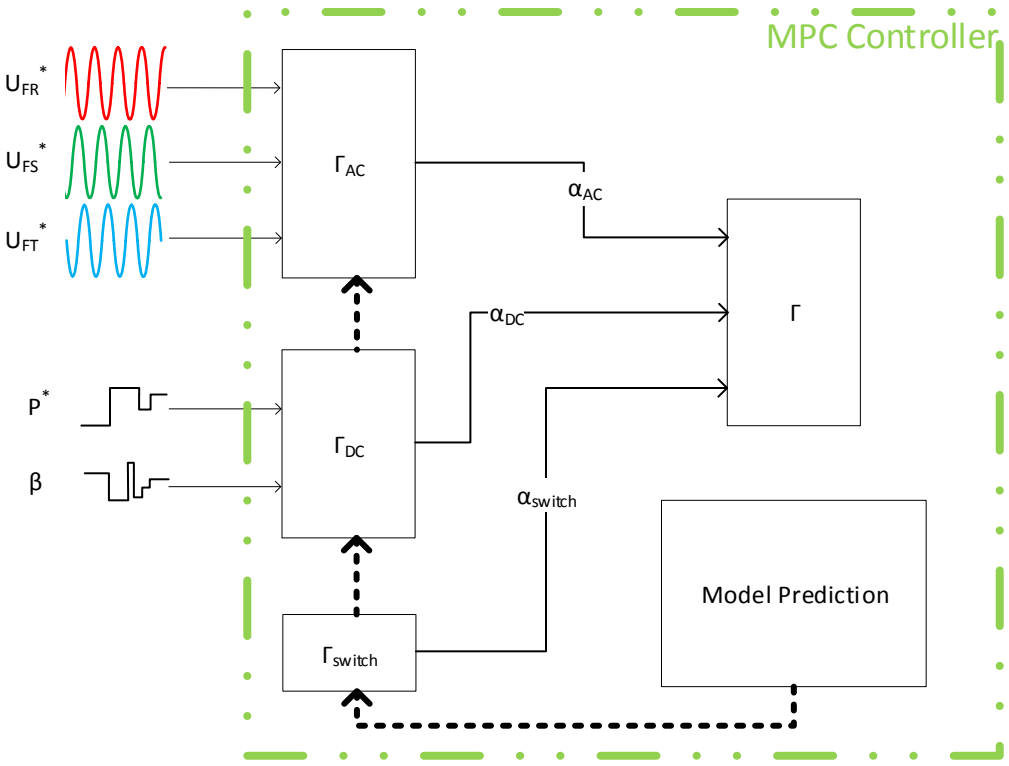

Fig. 5.25. Cost function inputs

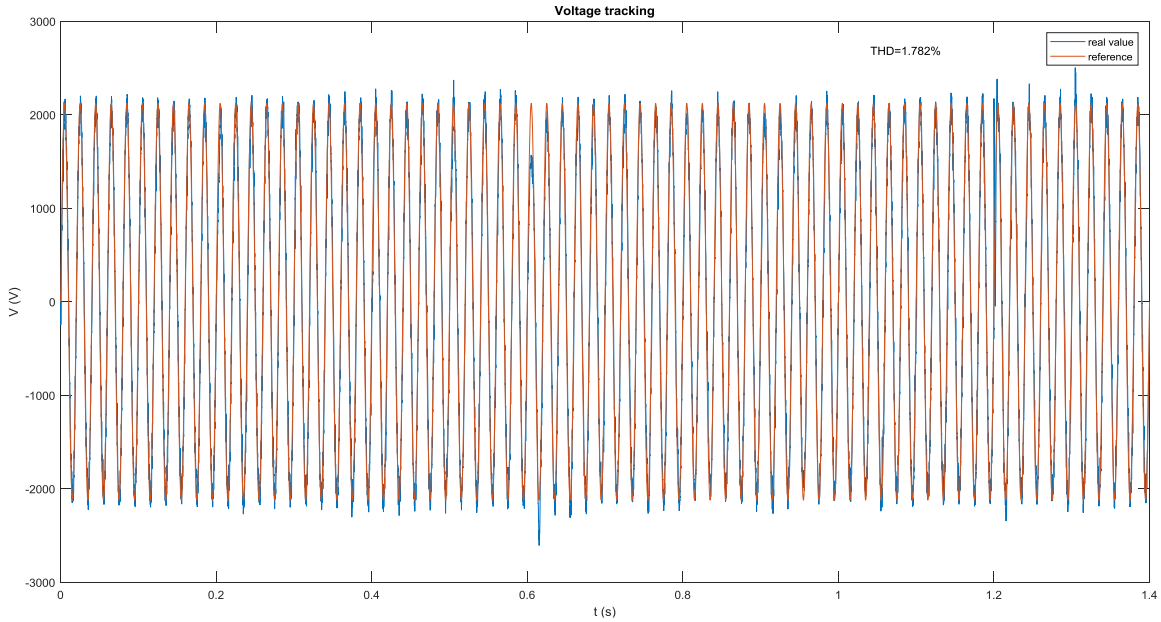

Fig. 5.26. Voltage at the PCC on phase R

The results displayed in Fig. 5.26 highlight the ability of the controller to effectively control the voltage at the Point of Common Coupling (PCC) under various circumstances. Two major events have a temporary consequence on the voltage's waveform: at 0.6s the addition of the inductive load and at 1.2s its removal. An immediate voltage fall is shown in Fig.5. 27, corresponding to when the inductive element is included. This fall is mitigated after 0.02s. Inversely, the disconnection of the inductive load leads to a

voltage surge, completely erased after a 0.003s period, as highlighted in Fig. 5.28. In spite of these dynamics, the overall THD is still of 1.782%, as displayed on Fig. 5.26, which is satisfying for isolated grid applications.

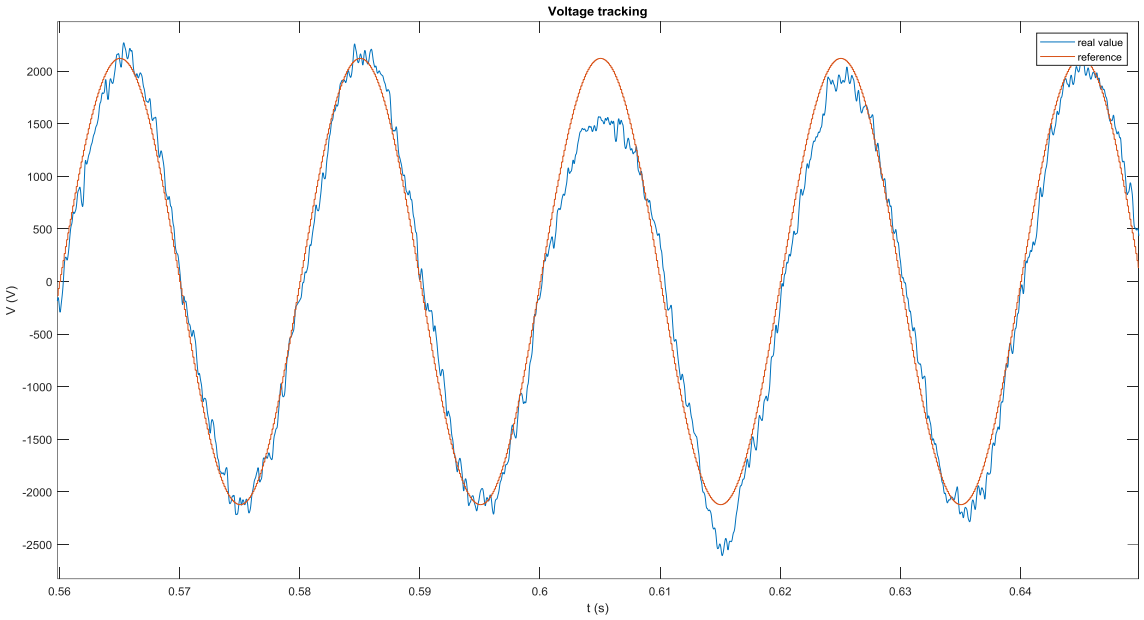

Fig.5. 27. Voltage tracking at the PCC, phase R, focus on the time of inclusion of the inductive load

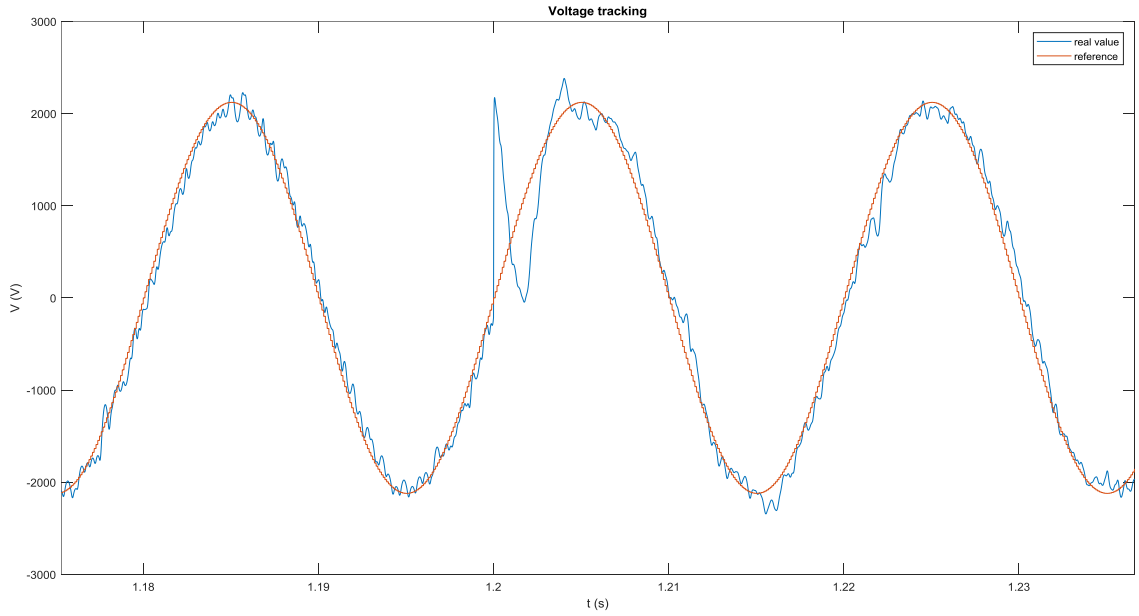

Fig. 5.28. Voltage tracking at the PCC, phase R, focus on the time of disconnection of the inductive load

Fig. 5.29 highlights the different events described in Table 5.7, as the addition of the resistive loads appears on the active power and the capacitive and inductive loads are put in evidence on the reactive power. The transitions and the events related to the AC objectives are clearly shown thanks to these two graphics.

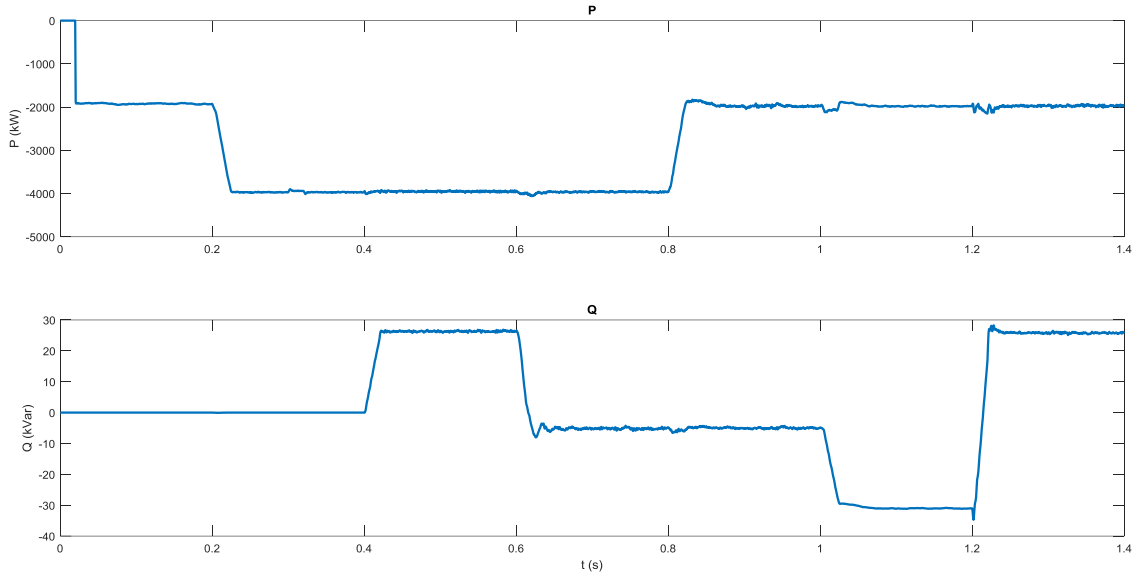

Fig. 5.29. Active and reactive powers received by the converter

Both Fig. 5.29and Fig. 5.30illustrate the compliance of the controlled system to the context and objectives defined earlier. The DC sources behave in synchronization with P^*: the current output changes at the same time the power objective does, which explains how the system is able to generate such fast power variations with close to no dynamics. The power variations are performed accurately, without impacting the total power.

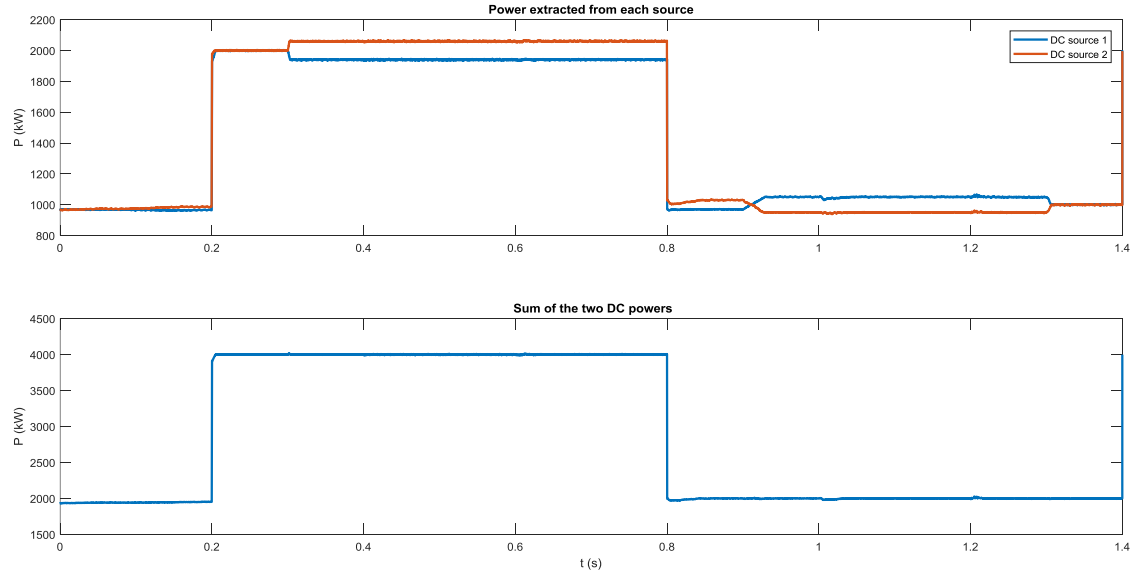

Fig. 5.30. DC objectives: total power and power repartition between the sources

The effect of the coefficients of the cost function would be especially apparent on Fig. 5.26 and Fig. 5.30, with in the best case longer transition periods after events and in the worst case the strict failure to reach the control target. For example, if the cost related to the AC voltage tracking is too high in comparison to α_{DC}, the voltages at the DC-link would be left free. The controller then let these values grow

endlessly, which in turn seriously deteriorates the harmonic content of the AC phase voltages. The opposite leads to similar results: if α_{AC} is too small, the power exchange is not sensible, which prevents the controller from reaching the operating point defined by the DC objectives. This in turn leads to an important consideration: the AC and DC objectives have to be compatible, coherent and, most of all, combined. In fact, the controller is unable to fix by itself the AC operating point enabling its DC objectives and vice-versa. To summarize, if given reasonable and feasible objectives properly expressed through its cost function, the controller developed is capable of managing both the AC and DC sides of any converter, in four quadrants.

6. Conclusion

The MPC controller presented in the previous chapters has been confronted with a variety of situations to demonstrate and trial its operation. The controller shows great polyvalence by handling a variety of different issues for different topologies, accurately generating switching orders to comply with various control objectives and requirements. A few possible sub-costs have been presented and used to reach certain goals and performance. Three operations have been treated separately extensively, namely inverter, rectifier and four-quadrant operation, leading to satisfying results and important considerations concerning the definition of the cost function. No constraints were used here as no objective was seen as needing such a hard limitation. This kind of requirements translates as conditioned infinite costs, which does not impact any of the conclusions and results already drawn. Overall, the tasks enquired to the controller have been performed satisfyingly. The role of the control designer is still paramount to the good operation of the controller and the controlled converter. Among the main difficulties arisen from these simulation results are the sub-costs coefficients and the localization of the intelligence, as limitations concerning the amount of cleverness that can be incorporated directly into the MPC controller have been highlighted. The main reason to these limitations is the fact that the controller operates at a very fast time step and with very short time to perform longer computations.

The fact that the same MPC controller was used for the three studied topologies underlines the universality of the algorithm proposed, while the different applications, case studies and cost functions developed showed the versatility and the potency of the designed controller.

7. Bibliography

[1] J. Scoltock, T. Geyer, et U. Madawala, « Model Predictive Direct Current Control for a grid-connected converter: LCL-filter versus L-filter », in *2013 IEEE International Conference on Industrial Technology (ICIT)*, Cape Town, Feb. 2013, p. 576‑581, doi: 10.1109/ICIT.2013.6505735.

[2] *Voltage characteristics of electricity supplied by public electricity networks*, EN 50160:2010, 2010

Conclusion and perspectives

1. Conclusion

The main objective of this thesis has been to develop a universal modulation-less solution aimed at controlling power converters to comply with the control requirements brought by the integration of RES in the energy mix. The algorithms and methods proposed have been subject to a theoretical analysis as well as to a simulation validation.

A review of the power conversion technologies, applications and their associated control strategies carried out in Chapter I revealed several issues. First of all, power conversion and power electronics are omnipresent in all current electricity distribution paradigms, and their evolution and maturation impose many new control objectives. Second, these requirements are met thanks to a large array of specialized control strategies. Finally, these strategies generally get around the non-linear nature of power converters by separating the control in two phases: a modulation block managing the objectives related to efficiency and performance of the converter itself, and a linear structure handling its interfacing function.

Because many of the new requirements are related to the deepest operation of the converters and their function altogether, it was decided to develop a controller able to handle both of these levels of control. To do so, the MPC family of strategies was chosen, for its potential in robustness, non-linear control and handling of multi-objective control problems through optimization. Two necessary elements are intertwined to form such a MPC controller: the model, used for prediction, and the optimization algorithms used to solve the control problem. This thesis proposes a possible pair of model and algorithm, which is not necessarily the only one.

The modelling aspect has been detailed in Chapter II, in which a method based on Switching State-Space Representation is formalized for all power converters and applied to three common multi-level topologies (NPC, FC and CHB) and three different filters (L, LC and LCL). The obtained results were validated through a comparison using MATLAB/Simulink models. The hypotheses used in the SSSR model considered the power switches as ideal: they have no impedance. Other interesting results may emerge from the incorporation of these dynamics, potentially to study in-depth the conduction and switching losses caused by the power switches. Though only three topologies were expressed, many others deserve to be.

Then, Chapter III introduces the FCS-MPC algorithm and reveals that the optimization problem described with the prediction model discussed in Chapter II is equivalent to a graph theory problem. Therefore, several methods from this domain are compared, and the A* algorithm, based on the Dijkstra one, is selected. The complete algorithm is then described thoroughly, and several performance criteria are proposed and evaluated, yielding promising results. Graph theory is a vast domain of research, and many other algorithms, more advanced, emerged from it and may present an interest for this specific MPC application.

Chapter IV approaches theoretical consequences concerning the prediction method described in Chapter II, the optimization algorithm defined in Chapter III and the controller resulting from their association. The problem of stability leads to new definitions, more adapted to the particular form of the models used: the stabilizability, property determining the existence of a control sequence that can bring stability to the system. A simple method is provided to evaluate the stabilizability of any model expressed with the canonical form established in the second chapter. The controllability is a problematic issue, and a numerical method is devised to evaluate it for the canonical form used. The question of observability was not addressed. The design of the cost function is another central aspect of this chapter, as several types of cost are defined to represent as many control objectives as possible, and as the balancing of the cost function is discussed. Finally, this chapter concludes on the questions of the robustness and sensitivity of the MPC controller developed, suggesting a practical post-design evaluation rather than a theoretical tool to design the controller according to these categories. With the experience accumulated during this thesis, an automatic weighing tool seems unattainable, except maybe using complex advanced algorithms such as artificial intelligence.

Chapter V illustrates the results obtained by investigating the operation of the proposed controller, with four different case studies: a standalone application, an inverter operation connected to the grid with and without load unbalances, a rectifier operation, and a complete case of study, with a four-quadrant operation of a converter in an isolated grid. The different examples are conducted for three topologies, with different filters and different control objectives. The same controller is used, with adjustments on the models and the terms of the cost function. These applications and the results obtained serve to demonstrate the universality, polyvalence and potential of this controller for future use in medium- to high-power applications with RES. A few issues appeared, such as the need to specify various operating objectives such as grid synchronization to the controller: the optimization sometimes does not respect this requirement, often considered as a given with other controllers. Another issue concerns objectives related to frequency: because of the short horizon of optimization and prediction, it was not possible in this work to implement such objectives, and a variety of other goals with more extended dynamics. Even with this limitation, the MPC controller developed is well adapted to mid-to-low levels of control and poses as a particularly interesting intermediary directly between energy management systems and power converters.

2. Perspectives

The experimental validation of the controller could not be performed, for various reasons, in the timeframe of this thesis work and represents a future priority line of research. Other perspectives listed below have been identified and will be investigated to improve the presented results:

- Investigate different shortest path algorithms to eventually enhance the speed of resolution and the control horizon of the MPC controller. This would also expand the possibilities of control, including frequency analysis, more precise power quality, and

inclusion of ancillary services and failure management.

- Analyze, evaluate and enhance the effect of the algorithm on power losses, with precise models of the power switches. This efficiency property is extremely important for current advances in power electronics, and the controller resulting from this thesis work shows promising abilities.
- Validate the models and the controller on other power converters and/or on other case studies. The diversity of topologies and applications of power converters is massive and, even though the principles and the validity of the proposed method stay the same with other topologies, only a few of them were explicitly expressed in this thesis. The modular converters, for example, and their applications are both very interesting considering the current evolution of the grid paradigms and has similar demands for universality, efficiency and flexibility of control that motivated this thesis work. The MPC strategy devised seems to have a high potential for theoretically all power conversion problems, and it would be interesting to demonstrate further and exploit this potential.
- Investigate the behaviour of the MPC controller when associated with more complete control structures, with different control loops, and especially when used in hierarchical control. This structure shows high potential for many applications of power converters, and the algorithms could form a layer of the hierarchy, bringing further intelligence and flexibility to it.
- Study the limits of the MPC controller: this thesis presents the controller under its best light, and various dimensions could not be investigated. For example, the controller does not require any modelling of the grid or any other component to perform its interfacing task, specifically between these two undescribed elements. This dimension is extremely interesting and deserves an in-depth study.
- Other modelling methods could also be considered, such as port-Hamiltonian approaches, which seem to be another viable take on the modelling issues evoked in Chapter II. Different optimization algorithms may rise to cooperate with such modelling methods.

3. Publications

During the course of this thesis, a journal paper was published in Electric Power Systems Research, insisting on the theoretical results described in the course of Chapter IV, with conclusions on the controllability, stability with a validation on a four-legs three-level FC topology.

- S. Jupin, I. Vechiu, and G. Tapia-Otaegui, «Universal switched state-space representation for model predictive control of power converters,» *Electr. Power Syst. Res.*, vol. 180, p. 106120, March 2020, doi: 10.1016/j.epsr.2019.106120.

This work also led to three publications in conferences, in IECON 2017, ICIT 2018 and SGE 2018. The papers form IECON and SGE are focused on the MPC algorithm developed and its early results- described in chapters II, III and V -, while the one from ICIT focuses on energy management.

- S. Jupin, I. Vechiu, and G. Tapia, "Direct state-space model for model predictive control of multi-level power converters," in *Proc. IECON 2017 - 43rd Annual Conference of the IEEE Industrial Electronics Society*, Beijing, 2017, pp. 7759–7764.
- R. H. L. Rodriguez, I. Vechiu, S. Jupin, S. Bacha, Q. Tabart and E. Pouresmaeil, "A new energy management strategy for a grid connected wind turbine-battery storage power plant," in *Proc. 2018 IEEE International Conference on Industrial Technology (ICIT)*, Lyon, 2018, pp. 873–879, doi: 10.1109/ICIT.2018.8352293.
- S. Jupin, I. Vechiu, and G. Tapia, "Représentation d'état directe pour le contrôle prédicitf de convertisseurs de puissance multi-niveau," in *Proc. 2018 Symposium de Génie Electrique (SGE)*, Nancy, 2018.

ANNEXES

Annexe 1: Detailed modelling of 3L-NPC with LCL filter

This annexe aims to develop the progression to express the SSSR model of the 3L-NPC topology associated with a LCL filter. The electronic scheme of the topology for the different switching positions is reminded in Fig. 1, and the filter is recalled in Fig. 2.

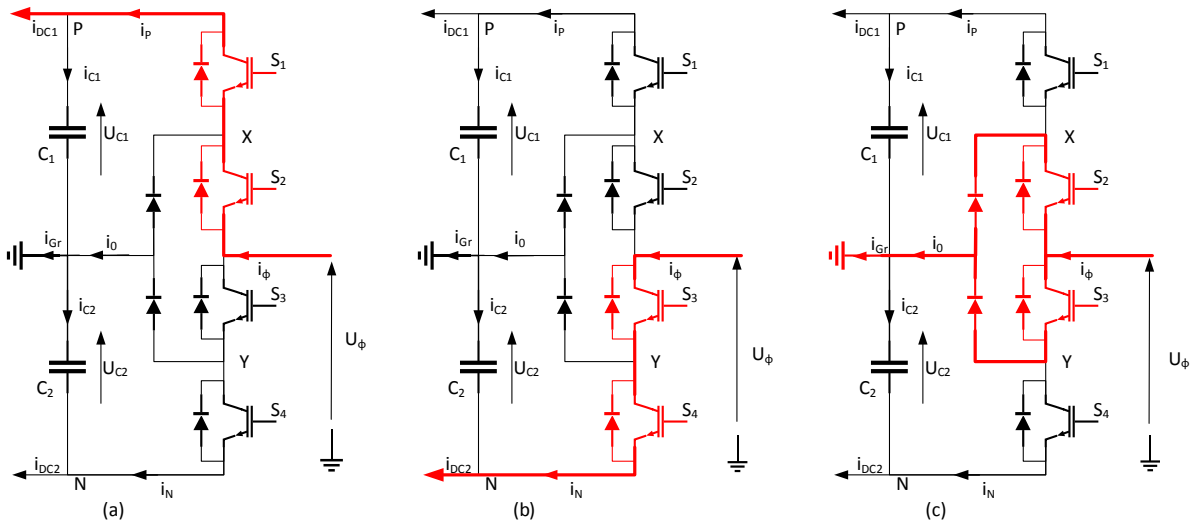

Fig. 1. Switching positions for one phase of a 3L-NPC converter

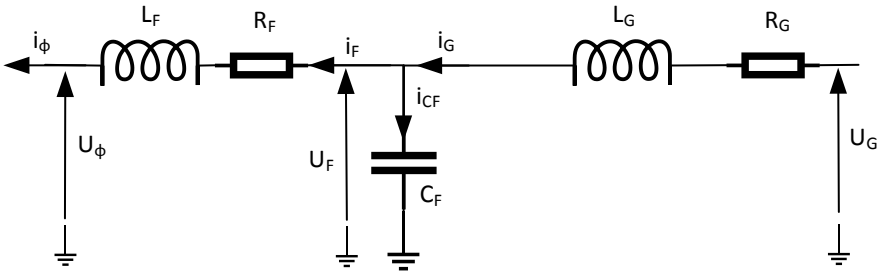

Fig. 2. LCL filter

The equations used are extracted from Sections 4.1 and 5.1 of Chapter II, describing the behaviour of the topology and the dynamics of the filter respectively. The equations describing the 3L-NPC topology and the impact of the states of the power switches are recalled as follows:

$$U_{\phi j} = S_{jP}U_{C1} - S_{jN}U_{C2};\ \ \forall\, j \in \Psi \tag{An1.1}$$

$$i_{C1} = i_P - i_{DC1};\ \ i_P = \sum_{j\in\Psi} S_{jP} i_{\phi j} \tag{An1.2}$$

$$i_{C2} = -i_N + i_{DC2};\ \ i_N = \sum_{j\in\Psi} S_{jN} i_{\phi j} \tag{An1.3}$$

$$i_0 = \sum_{j\in\Psi} S_{j0} i_{\phi j}. \tag{An1.4}$$

The equations regarding the filter are those given below:

$$U_{Gj} - L_{Gj}\frac{di_{Gj}}{dt} - R_{Gj}i_{Gj} - U_{Fj} = 0;\ \forall\, j \in \Psi \tag{An1.5}$$

$$U_{Fj} - L_{Fj}\frac{di_{Fj}}{dt} - R_{Fj}i_{Fj} - U_{\phi j} = 0;\ \forall\, j \in \Psi \tag{An1.6}$$

$$i_{Gj} - i_{Fj} - C_{Fj}\frac{dU_{Fj}}{dt} = 0;\ \forall\, j \in \Psi. \tag{An1.7}$$

The dynamics of the capacitors of the DC-link can be represented by

$$C_1\frac{dU_{c1}}{dt} = i_{c1} \tag{An1.8}$$

$$C_2\frac{dU_{c2}}{dt} = i_{c2}. \tag{An1.9}$$

Some useful intermediate parameters and variables can be created to lighten the equations. Let us define (An.10).

$$\left.\begin{aligned}\tau_{Gj} &= \frac{R_{Gj}}{L_{Gj}}\\ \tau_{Fj} &= \frac{R_{Fj}}{L_{Fj}}\end{aligned}\right\};\quad \forall j \in \Psi. \tag{An1.1}$$

Solving for di_{Gj}/dt in (An.5) gives rise to the following first set of four state equations:

$$\frac{di_{Gj}}{dt} = -\tau_{Gj}i_{Gj} - \frac{1}{L_{Gj}}U_{Fj} + \frac{1}{L_{Gj}}U_{Gj};\quad \forall j \in \Psi. \tag{An1.1}$$

Moreover, replacing (An.1) into (An.6), and subsequently solving for di_{Fj}/dt, produces

$$\frac{di_{Fj}}{dt} = -\tau_{Fj}i_{Fj} + \frac{1}{L_{Fj}}U_{Fj} - \frac{1}{L_{Fj}}S_{jP}U_{C1} + \frac{1}{L_{Fj}}S_{jN}U_{C2};\quad \forall j \in \Psi. \tag{An1.1}$$

The last set of four state equations arising from the LCL filter is derived from (An.7) as follows:

$$\frac{dU_{Fj}}{dt} = \frac{1}{C_{Fj}}i_{Gj} - \frac{1}{C_{Fj}}i_{Fj};\quad \forall j \in \Psi. \tag{An1.1}$$

Finally, the last two state equations provided next are derived by substituting (An.2) and (An.3) into, respectively, (An.8) and (An.9):

$$\frac{dU_{c1}}{dt} = \frac{1}{C_1}\sum_{j\in\Psi} S_{jP} i_{Fj} - \frac{1}{C_1} i_{DC1} \tag{An1.14}$$

$$\frac{dU_{c2}}{dt} = -\frac{1}{C_2}\sum_{j\in\Psi} S_{jN} i_{Fj} + \frac{1}{C_2} i_{DC2}. \tag{An1.15}$$

From (An.11)–(An.15), the adequate state vector as described in Section 5.3 of Chapter II is

$$\boldsymbol{x}_A^T = \left[i_{G\Psi_1} \dots i_{G\Psi_{N_{legs}}} i_{F\Psi_1} \dots i_{F\Psi_{N_{legs}}} U_{F\Psi_1} \dots U_{F\Psi_{N_{legs}}} \right] \tag{An1.16}$$

$$\boldsymbol{x}_{con}^T = \emptyset; \;\; \boldsymbol{x}_B^T = [U_{C1}\; U_{C2}], \tag{An1.17}$$

and the input vector is given by

$$\boldsymbol{d}_A^T = \left[U_{G\Psi_1} \dots U_{G\Psi_{N_{legs}}} \right]; \;\; \boldsymbol{d}_B^T = [i_{DC1}\; i_{DC2}]. \tag{An1.18}$$

For any topology and any phase-repeated parameter or variable, $\lambda_j; j \in \Psi$, let us also define

$$\boldsymbol{\lambda} = \begin{bmatrix} \lambda_{\Psi_1} \\ \vdots \\ \lambda_{\Psi_{N_{legs}}} \end{bmatrix}; \;\; diag(\boldsymbol{\lambda}) = \begin{bmatrix} \lambda_{\Psi_1} & \cdots & 0 \\ \vdots & \ddots & \vdots \\ 0 & \cdots & \lambda_{\Psi_{N_{legs}}} \end{bmatrix}. \tag{An1.19}$$

From there on, the submatrices defined in Section 3 of Chapter II can be deduced for the 3L-NPC case associated to an LCL filter as follows:

$$\boldsymbol{A}_{AA} = \begin{bmatrix} diag(-\boldsymbol{\tau}_G) & \mathbb{O}_{N_{legs}\times N_{legs}} & diag(-\frac{1}{\boldsymbol{L}_G}) \\ \mathbb{O}_{N_{legs}\times N_{legs}} & diag(-\boldsymbol{\tau}_F) & diag(\frac{1}{\boldsymbol{L}_F}) \\ diag(\frac{1}{\boldsymbol{C}_F}) & diag\left(-\frac{1}{\boldsymbol{C}_F}\right) & \mathbb{O}_{N_{legs}\times N_{legs}} \end{bmatrix} \tag{An1.20}$$

$$\boldsymbol{A}_{AB} = \begin{bmatrix} \mathbb{O}_{N_{legs}\times 1} & \mathbb{O}_{N_{legs}\times 1} \\ \frac{-\boldsymbol{S}_P}{\boldsymbol{L}_F} & \frac{\boldsymbol{S}_N}{\boldsymbol{L}_F} \\ \mathbb{O}_{N_{legs}\times 1} & \mathbb{O}_{N_{legs}\times 1} \end{bmatrix}; \; \boldsymbol{A}_{Acon} = \emptyset \tag{An1.21}$$

$$\boldsymbol{A}_{BA} = \begin{bmatrix} \mathbb{O}_{1\times N_{legs}} & \boldsymbol{S}_P^T/C_1 & \mathbb{O}_{1\times N_{legs}} \\ \mathbb{O}_{1\times N_{legs}} & -\boldsymbol{S}_N^T/C_2 & \mathbb{O}_{1\times N_{legs}} \end{bmatrix} \tag{An1.22}$$

$$\boldsymbol{A}_{BB} = \mathbb{O}_{2\times 2};\ \ \boldsymbol{A}_{Bcon} = \boldsymbol{A}_{conB} = \boldsymbol{A}_{concon} = \boldsymbol{A}_{conA} = \emptyset. \tag{An1.23}$$

Similarly, the $\boldsymbol{E}$ matrix is stated thereafter:

$$\boldsymbol{E} = \begin{bmatrix} diag(\frac{1}{\boldsymbol{L}_G}) & \mathbb{O}_{N_{legs}\times 1} & \mathbb{O}_{N_{legs}\times 1} \\ \mathbb{O}_{2N_{legs}\times N_{legs}} & \mathbb{O}_{2N_{legs}\times 1} & \mathbb{O}_{2N_{legs}\times 1} \\ \mathbb{O}_{1\times N_{legs}} & \frac{1}{C_1} & 0 \\ \mathbb{O}_{1\times N_{legs}} & 0 & -\frac{1}{C_2} \end{bmatrix}. \tag{An1.24}$$

Annexe 2: Detailed modelling of 3L-CHB with LCL filter

This annexe aims to develop the progression to express the SSSR model of the 3L-CHB topology associated with a LCL filter. The schemes used are summarized in Fig. 1 and Fig. 2.

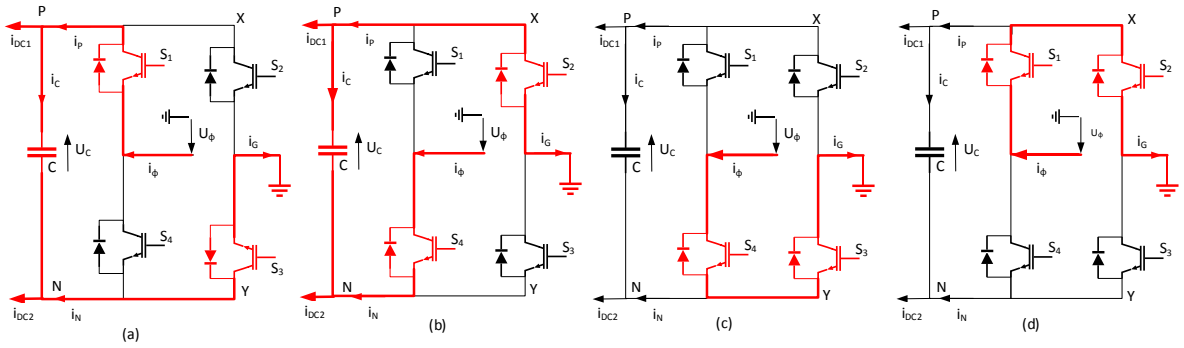

Fig. 1. Switching positions for one phase of 3L-CHB

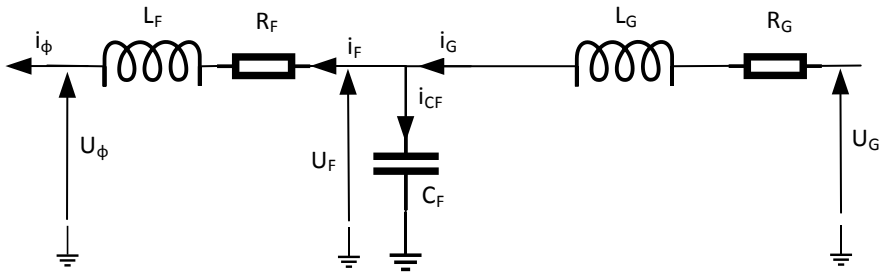

Fig. 2. LCL filter

The equations used are extracted from Chapter II subsection 4.3 and subsection 5, describing the behavior of the topology and the dynamics of the filter respectively. The equations describing the 3L-NPC topology and the impact of the states of the power switches are recalled as follows:

$$U_{\phi j} = (S_{jP} - S_{jN})U_{Cj}; \quad \forall j \in \Psi \tag{An2.1}$$

$$i_{Cj} = \frac{(S_{jN} - S_{jP})i_{\phi j}}{2} + \frac{i_{DC1j}}{2} - \frac{i_{DC2j}}{2} \quad \forall j \in \Psi \tag{An2.2}$$

$$i_G = \sum_{j\in\Psi} i_{\phi j} - i_{DC1j} - i_{DC2j}. \tag{An2.3}$$

The equations regarding the filter are given below.

$$U_{Gj} - L_{Gj}\frac{di_{Gj}}{dt} - R_{Gj}i_{Gj} - U_{Fj} = 0; \ \forall j \in \Psi \tag{An2.4}$$

$$U_{Fj} - L_{Fj}\frac{di_{Fj}}{dt} - R_{Fj}i_{Fj} - U_{\phi j} = 0; \ \forall j \in \Psi \tag{An2.5}$$

$$i_{Gj} - i_{Fj} - C_{Fj}\frac{dU_{Fj}}{dt} = 0;\ \forall\, j \in \Psi. \tag{An2.6}$$

The dynamics of the capacitors of the DC-link can be represented by:

$$C_j \frac{dU_{cj}}{dt} = i_{cj};\ \forall\, j \in \Psi \tag{An2.7}$$

Some useful intermediate parameters and variables can be created to lighten the equations. Let us define (An.8)

$$\left.\begin{aligned}\tau_{Gj} &= \frac{R_{Gj}}{L_{Gj}}\\ \tau_{Fj} &= \frac{R_{Fj}}{L_{Fj}}\end{aligned}\right\};\quad \forall j \in \Psi, \tag{An2.8}$$

as well as (An.9):

$$\Delta_j = S_{jP} - S_{jN}\ . \tag{An2.9}$$

Solving the di_{Gj}/dt in (An.4) gives rise to the following first set of four state equations:

$$\frac{di_{Gj}}{dt} = -\tau_{Gj} i_{Gj} - \frac{1}{L_{Gj}} U_{Fj} + \frac{1}{L_{Gj}} U_{Gj};\quad \forall j \in \Psi. \tag{An2.10}$$

Moreover, replacing (An.1) into (An.5), and subsequently solving for di_{Fj}/dt, produces

$$\frac{di_{Fj}}{dt} = -\tau_{Fj} i_{Fj} + \frac{1}{L_{Fj}} U_{Fj} - \Delta_j U_{Cj}\quad \forall j \in \Psi. \tag{An2.11}$$

The last set of four state equations arising from the LCL filter is derived from (An.6) as follows:

$$\frac{dU_{Fj}}{dt} = \frac{1}{C_{Fj}} i_{Gj} - \frac{1}{C_{Fj}} i_{Fj};\quad \forall j \in \Psi. \tag{An2.12}$$

Finally, the last set of state equations provided next is derived by substituting (An.2) into (An.7):

$$\frac{dU_{cj}}{dt} = \frac{1}{C_j}\left(\left(S_{jCN} - S_{jCP}\right) i_{\phi j} + \frac{i_{DC1j}}{2} - \frac{i_{DC2j}}{2}\right)\quad \forall j \in \Psi \tag{An2.13}$$

From (An.10)–(An.13), the adequate state vector as described in Chapter II Subsection 3 is

$$\boldsymbol{x}_A^T = \left[i_{G\Psi_1} \dots i_{G\Psi_{Nlegs}} i_{F\Psi_1} \dots i_{F\Psi_{Nlegs}} U_{F\Psi_1} \dots U_{F\Psi_{Nlegs}}\right] \tag{An2.14}$$

$$\boldsymbol{x}_{con}^T = \emptyset; \;\; \boldsymbol{x}_B^T = \left[U_{C\Psi_1} \dots \; U_{C\Psi_{Nlegs}}\right], \tag{An2.15}$$

and the input vector is given by

$$\boldsymbol{d}_A^T = \left[U_{G\Psi_1} \dots U_{G\Psi_{Nlegs}}\right]; \;\; \boldsymbol{d}_B = \left[i_{DC1\Psi_1} \dots i_{DC1\Psi_{Nlegs}} \; i_{DC2\Psi_1} \dots i_{DC2\Psi_{Nlegs}}\right]. \tag{An2.16}$$

For any topology and any phase-repeated parameter or variable, $\lambda_j; j \in \Psi$, let us also define

$$\boldsymbol{\lambda} = \begin{bmatrix} \lambda_{\Psi_1} \\ \vdots \\ \lambda_{\Psi_{N_{legs}}} \end{bmatrix}; \;\; diag(\boldsymbol{\lambda}) = \begin{bmatrix} \lambda_{\Psi_1} & \cdots & 0 \\ \vdots & \ddots & \vdots \\ 0 & \cdots & \lambda_{\Psi_{N_{legs}}} \end{bmatrix}. \tag{An2.17}$$

From there on, the submatrices defined in Chapter II, Subsection 3 can be deduced for the 3L-CHB case associated with an LCL filter as follows:

$$\boldsymbol{A}_{AA} = \begin{bmatrix} diag(-\boldsymbol{\tau}_G) & \mathbb{O}_{\mathrm{N_{legs}}\times\mathrm{N_{legs}}} & diag\left(-\frac{1}{\boldsymbol{L}_G}\right) \\ \mathbb{O}_{\mathrm{N_{legs}}\times\mathrm{N_{legs}}} & diag(-\boldsymbol{\tau}_F) & diag\left(\frac{1}{\boldsymbol{L}_F}\right) \\ diag\left(\frac{1}{\boldsymbol{C}_F}\right) & diag\left(-\frac{1}{\boldsymbol{C}_F}\right) & \mathbb{O}_{\mathrm{N_{legs}}\times\mathrm{N_{legs}}} \end{bmatrix} \tag{An2.18}$$

$$\boldsymbol{A}_{AB} = \begin{bmatrix} \mathbb{O}_{\mathrm{N_{legs}}\times\mathrm{N_{legs}}} \\ \mathrm{diag}\left(\frac{\boldsymbol{\Delta}}{\boldsymbol{L}_F}\right) \\ \mathbb{O}_{\mathrm{N_{legs}}\times\mathrm{N_{legs}}} \end{bmatrix}; \; \boldsymbol{A}_{Acon} = \emptyset \, . \tag{An2.19}$$

$$\boldsymbol{A}_{BA} = \begin{bmatrix} \mathbb{O}_{\mathrm{N_{legs}}\times\mathrm{N_{legs}}} & diag(-\frac{\boldsymbol{\Delta}^T}{2\boldsymbol{C}}) & \mathbb{O}_{\mathrm{N_{legs}}\times\mathrm{N_{legs}}} \end{bmatrix} \tag{An2.20}$$

$$\boldsymbol{A}_{BB} = \mathbb{O}_{\mathrm{N_{legs}}\times\mathrm{N_{legs}}}; \;\; \boldsymbol{A}_{Bcon} = \boldsymbol{A}_{conB} = \boldsymbol{A}_{concon} = \boldsymbol{A}_{conA} = \emptyset \tag{An2.21}$$

Similarly, the $\boldsymbol{E}$ matrix is stated thereafter:

$$\boldsymbol{E} = \begin{bmatrix} diag(\frac{1}{\boldsymbol{L}_G}) & \mathbb{O}_{\mathrm{N_{legs}}\times 1} & \mathbb{O}_{\mathrm{N_{legs}}\times 1} \\ \mathbb{O}_{2\mathrm{N_{legs}}\times 1} & \mathbb{O}_{2\mathrm{N_{legs}}\times 1} & \mathbb{O}_{2\mathrm{N_{legs}}\times 1} \\ \mathbb{O}_{\mathrm{N_{legs}}\times\mathrm{N_{legs}}} & diag(\frac{1}{2\boldsymbol{C}}) & diag(-\frac{1}{2\boldsymbol{C}}) \end{bmatrix} \tag{An2.22}$$